

“Assessing the role of Piccolo and Bassoon Zinc Finger domains on Synapse Vesicle Recycling and Maintenance”

**Dissertation
zur Erlangung des akademischen Grades**

**doctor rerum naturalium
(Dr. rer. nat.)**

genehmigt durch die Fakultät für Naturwissenschaften
der Otto-von Guericke-Universität Magdeburg

von

Biochemist Sergio Alejandro Leal Ortiz

geb. am

11.10.1973 in Rio Bueno, Chile

**Gutacher: Prof. Dr. Eckart D. Gundelfinger
Prof. Dr. Christian Rosenmund (PhD)**

eingereicht am: 15.09.2012

verteidigt am: 07.02.2013

*Dedicated to my lovely wife,
Ximena Esparza
without her support,
I would have never achieved all what I have done.*

Acknowledgements

I want to sincerely thank Prof. Eckart D. Gundelfinger for giving me the opportunity to perform part of my thesis in his department and support me during all these years of work.

I would like to thank to my supervisor and friend Prof. Craig Garner who has direct my career development from the very beginning. Craig's valuable guidance, constructive criticism, creative suggestions, and constant encouragement during the course of my work inspired me to continue working in science and enabled me to complete this thesis.

I also would like to thank a very special friend and colleague Dr. Clarissa Waites who has helped and supported me during the time we worked together, her focus, tenacity orientation and way to solve problems gave me the necessary tools to finish my thesis and the base for my future career. I cannot find words to thank her for all her contribution and discussion

I also want to thank all the people who have contributed, in one way or another, to make the best of the situation. I should thank, as well, Dr. Sally Kim, without her help, I would have found difficult to finish the thesis. I am grateful to Dr. Dhananjay Wagh, Dr. Christoph Maas, Dr. Nathan Okerlund, Dr. Pedro Zamorano, Magali Arons, Jacqueline Rodriguez, Madeleine Geisheker, Loren Garner, Pureshka Maharaj and Monica James for their technical help, helpful discussions and their sincere friendship, it made life easier.

Many thanks to Dr. Noam Ziv for developing a wonderful and simple program for image and digital analysis.

Lastly, I would like to extend special thanks to my parents Sabino and Isabel for always being there for me. Also I want to give thanks to my wife Ximena and my daughter Allison for their understanding and support during this time.

Summary:

The present study investigates the function of two large presynaptic proteins, Piccolo and Bassoon, in regard to synapse formation and regulation. Synapses are sites of neurotransmission between neuronal cells. The presynaptic compartment of each synapse is filled with 50-nm clear centered synaptic vesicles (SV) that dock and fuse in an activity dependent manner with a specialized region of plasma membrane, called the active zone. Fusion of SV with the active zone releases the neurotransmitters, which generate a new signal at the postsynaptic site by binding to neurotransmitter receptors. Piccolo and Bassoon are high molecular-weight components of the cytoskeletal matrix assembled at the active zone (CAZ), and are hypothesized to participate in active zone formation and the regulated release of neurotransmitter. However, most evidence supporting this hypothesis remains circumstantial in part due to the apparent redundancy between these molecules and challenges associated with knocking out all of the alternatively splice isoforms of Piccolo and Bassoon. In the present study, interference RNAs were developed and used to eliminate the expression of Bassoon and/or Piccolo from cultured hippocampal neurons.

Primary cultures of rat hippocampal neurons elaborate synaptic active networks that are invaluable for studying the molecular, cellular, and physiological mechanisms underlying neuronal morphogenesis, nascent synapse formation and synaptic function. To further facilitate the study of any presynaptic proteins in these cultures, new technologies were developed for delivery and expression of recombinant molecules at near endogenous levels. This was accomplished in part by developing methodologies to cryopreserve and store stocks of glial cells and neurons for months that had been genetically manipulated. In addition, a range of plasmid, lentiviral, and adenoviral vectors were created allowing the expression of fluorescent protein (XFP)-tagged synaptic reporter proteins as well as several short-hairpin RNAs (shRNAs) eliminating expression of the AZ proteins Piccolo and Bassoon. Together these technologies permit the cell autonomous and synapse specific assessment of collections of synaptic proteins using high-resolution fluorescent and electron microscopy and allow collaborators to more efficiently share reagents.

Interference RNAs targeting all Piccolo isoforms revealed that while this active zone protein is not required for glutamatergic synapse formation, it plays a fundamental role in the translocation, docking and fusion of SVs at active zones. Mechanistically, Piccolo was found to negatively regulate neurotransmission by modulating the dispersion kinetics of Synapsin1a and the recruitment of CamKII by regulating the activity dependent assembly of presynaptic F-Actin. These data demonstrate that Piccolo functions primarily within presynaptic boutons to coordinate the dynamic assembly of F-Actin during SV cycling. This function is not shared by the highly homologous protein Bassoon, indicating that Piccolo has a unique role in coupling the mobilization of SVs in the reserve pool to events within the active zone.

To uncover redundant functions of Piccolo and Bassoon, short-hairpin RNAs were used to knockdown the expression of both of these two large AZ proteins (by >95%) from cultured hippocampal neurons. Results of these studies show that these proteins are essential for maintaining SV pools within presynaptic boutons and synapse integrity. Mechanistically, Bassoon and Piccolo were found to maintain SV pool size by negatively regulating the activity of the E3 ubiquitin ligase Siah1, and thus the ubiquitination and degradation of SV-associated proteins. These findings demonstrate a novel role for Bassoon and Piccolo as regulators of presynaptic ubiquitination and proteostasis.

Taken together these studies provide fundamental insights into how presynaptic CAZ proteins are central organizers of presynaptic boutons performing functions that not only direct the activity dependent fusion of SVs but also more global facets of presynaptic function which include the maintenance, efficient delivery, and recycling of SVs at the active zone.

Zusammenfassung

Im Zentrum der vorliegenden Arbeit stehen die Fragen, ob und inwieweit die beiden präsynaptischen Proteine Piccolo und Bassoon an der Entstehung und Regulation neuronaler Synapsen beteiligt sind. Synapsen sind Orte der Reizübertragung zwischen Neuronen. Hierfür befinden sich auf der präsynaptischen Seite einer Synapse 50 nm große synaptische Vesikel (SV), die in Reaktion auf einen elektrischen Reiz mit der Aktiven Zone (AZ), einer spezialisierten Region der präsynaptischen Plasmamembran, fusionieren können. Durch die Fusion der SV mit der AZ wird Neurotransmitter in den synaptischen Spalt freigesetzt, um auf der postsynaptischen Seite durch Aktivierung von Neurotransmitterrezeptoren einen neuen elektrischen Reiz zu generieren. Piccolo und Bassoon sind Bestandteile der Cytomatrix an der Aktiven Zone (CAZ), und es wird vermutet, dass sie eine Rolle bei der Entstehung von Aktiven Zonen und der Regulation der Neurotransmitterausschüttung spielen. Allerdings beruht diese Hypothese vorwiegend auf indirekten Hinweisen, da Piccolo und Bassoon offensichtlich eine große Redundanz in ihren Funktionen besitzen und sich Knockout-Experimente, bei denen alle alternativen Spleißvarianten von Piccolo und Bassoon eliminiert werden, bisher als schwierig erwiesen. Für diese Arbeit wurden daher neue RNA-Interferenzvektoren und lentivirale Expressionsvektoren zur Eliminierung der Expression von Piccolo und/oder Bassoon in kultivierten hippocampalen Neuronen entwickelt. Diese Vektoren erlaubten nicht nur die Identifizierung und Charakterisierung von Funktionen, die spezifisch für Piccolo sind, sondern auch von solchen, die sowohl von Piccolo als auch von Bassoon erfüllt werden.

Für die Experimente, die in dieser Arbeit beschrieben werden, wurden primäre Kulturen hippocampaler Neuronen von Ratten genutzt. Die Neuronen in diesen Kulturen bilden aktive Netzwerke, anhand derer die molekularen, zellulären und physiologischen Mechanismen neuronaler Morphogenese, Synaptogenese und synaptischer Aktivität untersucht werden können. Um die Verwendbarkeit neuronaler Zellkulturen zur Untersuchung präsynaptischer Proteine wie Piccolo und Bassoon weiter zu verbessern, wurden im Rahmen dieser Arbeit neue Techniken entwickelt, die eine Expression rekombinanter Proteine auf endogenem Niveau gewährleisten. Außerdem sollte die Eignung dieser Art von Zellkulturen für Kooperationen zwischen verschiedenen Arbeitsgruppen erhöht werden. Letzteres wurde zum Teil durch die Entwicklung neuer Methoden zur Kryopräservierung und Langzeitlagerung von genetisch manipulierten Neuronen und Gliazellen erreicht. Darüber hinaus wurden verschiedene Plasmide sowie lenti- und adenovirale Vektoren konstruiert. Mit ihrer Hilfe wurden präsynaptische Reporterproteine mit Molekulargewichten von 15kD (VAMP2) bis zu 420kD (Bassoon) in Neuronen exprimiert und mit fluoreszierenden Proteinen fusioniert. Außerdem konnten sie genutzt werden, um mittels shRNA (short-hairpin RNA) die Expression von endogenem Piccolo und Bassoon zu eliminieren. Diese neuen Techniken erlauben zellautonome und Synapsen-spezifische Untersuchungen mit hochauflösender Fluoreszenz- und Elektronenmikroskopie.

Untersuchungen mit shRNAs gegen alle Isoformen von Piccolo ergaben, dass Piccolo auf der einen Seite nicht essentiell für die Synaptogenese ist, auf der anderen Seite jedoch eine fundamentale Rolle bei Translokation, Anlagerung und Fusion von synaptischen Vesikeln an der Aktiven Zone spielt. Dabei konnte gezeigt werden, dass der dieser Funktion von Piccolo zugrundeliegende Mechanismus auf einer Regulation des aktivitätsabhängigen Aufbaus präsynaptischen F-Aktins beruht. Hierdurch wird sowohl die Dispersionskinetik von Synapsin1a als auch die Rekrutierung von CaMKII an die Präsynapse reguliert. Diese Ergebnisse zeigen, dass die primäre Funktion von Piccolo in Präsynapsen in der Koordination des Aktinzytoskeletts während des Kreislaufes synaptischer Vesikel besteht. Diese Funktion wird nicht vom homologen Protein Bassoon geteilt und Piccolo spielt daher

eine besondere Rolle bei Kopplung synaptischer Vesikel des Reservepools mit Ereignissen an der Aktiven Zone.

Um mögliche gemeinsame Funktionen von Bassoon und Piccolo zu ermitteln, wurden shRNAs eingesetzt, die die Expression beider Proteine in hippocampalen Neuronen um mehr als 95% verringern. Ergebnisse dieser Experimente belegen, dass beide Proteine nötig sind für die Erhaltung verschiedener Untergruppen von synaptischen Vesikeln und für die synaptische Integrität. Dabei konnte gezeigt werden, dass der Mechanismus für die Erhaltung verschiedener synaptischer Vesikelpools auf einer negativen Regulierung der E3 Ligase Siah1 und damit der Ubiquitinierung und Degradation von SV-assoziierten Proteinen beruht. Diese Daten zeigen eine neue Funktion von Bassoon und Piccolo als Regulatoren präsynaptischer Ubiquitinierung und Proteostasis.

Die vorliegende Arbeit konnte damit neue fundamentale Erkenntnisse zur Rolle von CAZ Proteinen als zentrale Organisatoren von Präsynapsen liefern. Dabei umfassen ihre Funktionen nicht nur die Regulation der aktivitätsabhängigen Fusion synaptischer Vesikel mit der Plasmamembran sondern auch der Erhaltung, Translokation und Recycling von synaptischen Vesikeln an der Aktiven Zone.

Contents

Contents	8
Figures and tables	11
1. Introduction	12
1.1 Neuronal structure	13
1.2 Synapse structure	15
1.3 The post-synaptic specialization	15
1.4 Presynaptic Structure and Function	17
1.5 Active Zones	18
1.6 RIMs	19
1.7 Munc13	20
1.8 CAST/ELKS	21
1.9 Liprin-α	22
1.10 Bassoon and Piccolo	23
1.11 Aims	26
2. Materials and methods	27
2.1 Materials	27
2.1.1 Chemicals	27
2.1.2 Bacterial cells	27
2.1.3 Bacterial culture media and antibiotics	27
2.1.4. Molecular biology reagents, buffers and kits	27
2.1.5 Cells lines and media	28
2.1.6 Primary antibodies	28
2.1.7 Secondary antibodies	29
2.1.8 Immunocytochemistry	29
2.1.9 Biochemistry	30
2.1.10 Animals	30
2.1.11 Plasmid transfections	30
2.1.12 Live cell imaging reagents and solutions	30
2.2 Methods	30
2.2.1 Molecular biological methods	30
2.2.1.1 <i>Genotyping of Pclo mutant mice</i>	31
2.2.1.1a <i>DNA extraction for genotyping Pclo mutant mice</i>	31
2.2.1.1b <i>Polymerase chain reaction (PCR) for genotyping</i>	31
2.2.1.2 <i>Bacterial transformations</i>	31
2.2.1.3 <i>Growing bacterial colonies for plasmid minipreps</i>	32
2.2.1.4 <i>Plasmid DNA minipreps</i>	32
2.2.1.5 <i>Preparing endotoxin-free maxiprep plasmid DNA</i>	32
2.2.1.6 <i>Separating DNA fragments using agarose gel electrophoresis</i>	33
2.2.1.7 <i>DNA purification from gel slices</i>	33
2.2.1.8 <i>DNA restriction enzyme digestion</i>	33
2.2.1.9 <i>Removal of phosphate from DNA using calf intestine alkaline phosphatase CIP</i>	33
2.2.1.10 <i>Ligation of DNA fragments</i>	34
2.2.1.11 <i>Annealing oligonucleotides</i>	34
2.2.1.12 <i>Phosphorylation of oligonucleotides</i>	34
2.2.1.13 <i>PCR amplification</i>	34
2.2.2 Design and generation of vectors	35
2.2.2.1 <i>Generation of the pZOff vector</i>	35
2.2.2.2 <i>Design and cloning of shRNAs</i>	35
2.2.2.3 <i>Generation of FUGW H1 vector</i>	35
2.2.2.4 <i>Generation of EGFP::Syn1a, SV2::EGFP and Vamp::HRP constructs as well as the Pclo28 and Bsn16 shRNAs</i>	36
2.2.2.5 <i>Creation of tricistronic lentiviral vectors</i>	36
2.2.2.6 <i>Creating an shRNA-resistant (Bsn16) full-length Bassoon</i>	37
2.2.2.7 <i>Construction of an adenoviral vector expressing mRFP-BsnSM16</i>	37
2.2.2.8 <i>Creating mCherry-tagged Piccolo and Bassoon zinc finger domains</i>	38
2.2.3 Biochemical methods	38
2.2.3.1 <i>Preparation of cellular lysates</i>	38
2.2.3.2 <i>Separating proteins via SDS-polyacrylamide electrophoresis</i>	38

2.2.3.3	<i>Western blotting</i>	39
2.2.3.4	<i>Immunoblot detection of protein bands</i>	39
2.2.4	Heterologous cell culture techniques	39
2.2.4.1	<i>Growth and passage of mammalian cell lines</i>	39
2.2.5	Hippocampal and glial primary cultures	40
2.2.5.1	<i>Coverslip preparation</i>	40
2.2.5.2	<i>Glial culture preparation</i>	40
2.2.5.3	<i>Sub-culturing rat glial cells</i>	40
2.2.5.4	<i>Hippocampal neuronal culture preparation</i>	41
2.2.6	Gene transfer into cells	41
2.2.6.1	<i>Cell transfections with Lipofectamine 2000</i>	41
2.2.6.2	<i>Cell transfections by electroporation</i>	42
2.2.6.3	<i>Lentivirus production</i>	42
2.2.6.4	<i>Lentivirus infection of neurons</i>	42
2.2.7	Immunocytochemistry and electron microscopy	43
2.2.7.1	<i>Lorene's fixative solution</i>	43
2.2.7.2	<i>Immunohistochemistry</i>	43
2.2.7.3	<i>Image acquisition for immunocytochemistry</i>	43
2.2.7.4	<i>Electron microscopy of VAMP2-HRP expressing neurons</i>	43
2.2.8	Live cell microscopy and analysis	44
2.2.8.1	<i>Live imaging of XFP-tagged synaptic proteins</i>	44
2.2.8.2	<i>FM loading/destaining of neuronal synapses</i>	44
2.2.8.3	<i>Calculating the size of the readily releasable pool (RRP) of SVs as well as neurotransmitter release probability (Pr)</i>	45
2.2.8.4	<i>Fluorescent recovery after photobleaching (FRAP), acquisition and analysis</i>	45
2.2.8.5	<i>Defining EGFP::Syn1a dispersion kinetics</i>	46
2.2.8.6	<i>Quantification of EGFP::Syn1a dispersion and FM destaining kinetics</i>	47
2.2.8.7	<i>Image analysis of live cell experiments</i>	47
3. Results		48
3.1 Optimization and characterization of cryopreserved astrocyte cultures and hippocampal neuronal cultures		48
3.1.1	Cryopreservation of glial cells	48
3.1.2	Viability of cryopreserved dissociated hippocampal neurons	50
3.1.3	Morphological characterization of cryopreserved neurons	50
3.1.4	Characterization of lentiviral use in cryopreserved neurons	52
3.1.5	Electrophysiological characterization of cryopreserved neurons	55
3.2 Development of vectors for the effective expression of recombinant protein and shRNA in cultured hippocampal neurons		57
3.2.1	Custom design of a short hairpin RNA expression vector for the efficient knockdown of multiple synaptic proteins	57
3.2.2	Design of shRNAs for selective and efficient knockdown of Piccolo and Bassoon	58
3.2.3	Assessment of shRNAs for selective and efficient knockdown of Piccolo and Bassoon	59
3.2.4	Harnessing viruses for the efficient expression of shRNAs and recombinant proteins in cultured neuronal cells	62
3.2.5	Expressing recombinant proteins at endogenous levels with lentivirus	62
3.2.6	Development of a bicistronic lentiviral vector for the down-regulation of presynaptic proteins	64
3.2.7	Design of a tricistronic lentiviral vector for the down-regulation of multiple synaptic proteins	66
3.2.8	Expressing full-length Bassoon for rescue experiments using a helper-dependent adenoviral vector (HDAd)	69
3.3 Assessing the role of Piccolo in presynaptic assembly and function		71
3.3.1	Loss of Piccolo does not affect synapse formation or morphology	71
3.3.2	Synapses lacking Piccolo exhibit faster rates of SV exocytosis	75
3.3.3	Piccolo modulates the dispersion kinetics of Synapsin1a	77
3.3.4	Changes in SV exocytosis and Synapsin dynamics are not observed at synapses lacking Bassoon	80
3.3.5	Loss of Piccolo enhances the CaMKII sensitivity of Synapsin 1a	82
3.3.6	Synapsin1a is hypophosphorylated in the absence of Piccolo	84

3.3.7 Altered Synapsin phosphorylation does not mediate the Piccolo LOF phenotypes	84
3.3.8 Activity-dependent F-actin assembly is disrupted in the absence of Piccolo	85
3.3.9 CaMKII dynamics are altered in axons lacking Piccolo	89
3.3.10 Pclo Δ Ex14 $-/-$ mice exhibit normal F-actin assembly	89
3.4 Assessing the role of Bassoon and Piccolo on the maintenance of Synaptic Vesicle Pools	93
3.4.1 Characterization of synapses lacking Bassoon and Piccolo	93
3.4.2 Decreased SV pool size in the absence of Bassoon and Piccolo	95
3.4.3 SV pool size is rescued by the expression of full-length, shRNA-resistant, Bassoon	97
3.4.4 Ultrastructure of boutons lacking Bassoon and Piccolo	99
3.4.5 SV degradation is enhanced in the absence of Bassoon and Piccolo	101
3.4.6 Bassoon and Piccolo zinc finger domains mediate synaptic vesicle elimination in DKD neurons	103
4. Discussion	107
4.1 Cyropreserving hippocampal neurons	107
4.2 Assessing the role of Piccolo and Bassoon in the assembly, function and integrity of excitatory hippocampal synapses	109
4.3 Roles of CAZ proteins at presynaptic boutons	110
4.4 Changes in the rates of SV exocytosis in neurons lacking Piccolo can be linked to altered Synapsin dynamics	111
4.5 Altered phosphorylation of Synapsin in boutons lacking Piccolo cannot account for Piccolo dependent changes in SV exocytosis and Synapsin dispersion.	112
4.6 Piccolo is an essential regulator of activity dependent presynaptic F-actin assembly	113
4.7 Piccolo dependent presynaptic phenotypes are not exhibited by neurons cultured from Pclo Δ Ex14 mice	114
4.8 Bassoon and Piccolo regulate of SV proteostasis	115
4.9 ZnF domains in Bassoon and Piccolo modulate SV pool size	117
4.10 Ubiquitination in presynaptic structure and function	118
4.11 Ubiquitination and neurodegeneration	119
5. General conclusions	119
6. Bibliography	121
7. Abbreviations	132
8. Curriculum Vitae	135

Figures and Tables

Table 2.1. Bacterial cells	27
Table 2.2. Bacterial culture media and antibiotics	27
Table 2.3. Molecular biology reagents, buffers and kits	28
Table 2.4. Cells line and medias	28
Table 2.5. Primary antibodies	29
Table 2.6. Secondary antibodies	29
Table 2.7. Immunocytochemistry reagent	30
Table 2.8. Biochemistry reagent	30
Table 2.9. Animals	30
Table 2.10. Transfection reagents	30
Table 2.11. Live cell imaging reagents	30
Table 2.12. Primer Sequence for PCR for genotyping wildtype and Pclo KO	31
Table 2.13: Thermocycling set up program for genotyping	31
Table 2.14: PCR amplification process time and temperature cycles	34
Fig. 3.1 Cryopreserved glia support the growth and differentiation of rat hippocampal neurons	49
Fig. 3.2 Viability of cryopreserved neurons and normal differentiation	51
Fig. 3.3 Synaptic contacts and lentiviral infections of cryopreserved hippocampal neurons	53
Fig. 3.4 Infected cryopreserved neurons form normal numbers and functional synapses	54
Fig. 3.5 Cryopreserved hippocampal neurons exhibit normal electrophysiological properties	56
Fig. 3.6 Schematic flow diagram used to create the pZoff shRNA expression vector	58
Fig. 3.7 shRNA mediated knock down of EGFP-Piccolo	59
Fig. 3.8 shRNA mediated knockdown of Piccolo and Bassoon with the pZoff vector in cultured hippocampal neurons	61
Fig. 3.9 Lentiviral expression of EGFP::Synapsin1a at endogenous levels and schematic diagram of the lentiviral vector (FUGW) used to express XFP-tagged proteins and shRNA	63
Fig. 3.10 Lentivirus mediated knockdown of Piccolo with interference RNAs	64
Fig. 3.11 Lentivirus mediated knockdown of Piccolo and Bassoon	65
Fig. 3.12 Schematic diagrams of double knock down vectors	67
Fig. 3.13 Western analysis of Piccolo and Bassoon doubleknockdown (DKD)	68
Fig. 3.14 Expressing full-length mRFP tagged Bassoon via Adenovirus	70
Fig. 3.15 Piccolo is not essential for the clustering of key pre and postsynaptic proteins	72
Fig. 3.16 Ultrastructural characterization of excitatory synapses with Horseradish peroxidase (HRP) tagged VAMP2	73
Fig. 3.17 Ultrastructural characterization of excitatory synapses lacking Piccolo	74
Table 3.1 Quantitative ultrastructural analysis of synapses with or without Pclo28	75
Fig. 3.18 Synapses lacking Piccolo have functional boutons	76
Fig. 3.19 Loss of Piccolo enhances the rate and does not affect the size of the readily releasable pool of synaptic vesicles	77
Fig. 3.20 Loss of Piccolo increases the solubility and exchange kinetics of synapsin1a within presynaptic boutons	79
Fig. 3.21 Loss of Piccolo increases Synapsin1a dispersion and FM5-95 destaining kinetics	81
Fig. 3.22 Loss of Piccolo but not Bassoon from presynaptic boutons alters the dispersion kinetics of Synapsin1a and the destaining kinetics of FM5-95	82
Fig. 3.23 CaMKII inhibition rescues Pclo28 phenotypes and synapsin1a is hypo-phosphorylated in the absence of Piccolo	83
Fig. 3.24 Aberrant Synapsin1a phosphorylation does not cause the Pclo28 phenotypes	86
Fig. 3.25 Inhibiting F-actin assembly with Jasplakinolide rescues the Pclo28 phenotypes	87
Fig. 3.26 Presynaptic localization of EGFP::Actin markers	88
Fig. 3.27 CaMKII α recruitment to presynaptic boutons is impaired in Piccolo knockdown neurons	90
Fig. 3.28 Piccolo isoform expression in Pclo Δ Ex14 mice and rat hippocampal neurons expressing Pclo28 shRNA	91
Fig. 3.29 Pclo Δ Ex14 mice exhibit normal presynaptic F-Actin assembly	92
Fig. 3.30 Double knockdown of Bassoon and Piccolo reduces the expression of synaptic vesicle proteins but not hippocampal neuronal differentiation, made smaller synapses but does not affect synapse density	94
Fig. 3.31 Loss of Piccolo and Bassoon reduces SV pool size in presynaptic boutons	96
Fig. 3.32 Expression of mRFP::Bsn-SM16 rescues SV pool size at DKD boutons	98
Fig. 3.33 Quantification of synaptic ultrastructure in boutons lacking Bassoon and Piccolo	100
Fig. 3.34 Protein degradation drives SV loss in the DKD background	102
Fig. 3.35 Bassoon and Piccolo interact with Siah1 and modulate its activity	104
Fig. 3.36 Zinc finger domains in Piccolo and Bassoon regulate SV loss in DKD neurons	106

1. Introduction.

Interest in how our brains work began long ago, in fact the ancient Egyptians are responsible for the oldest written record using the word "brain" and have provided the first written accounts of the anatomy of the brain, the meninges and cerebrospinal fluid. The word "brain" appears on a papyrus written around the year 1700 BC, but is based on text that go back to about 3000 BC. This document is considered to be the first medical document in the history of mankind. Teaching in Athens ~387 BC, Plato states that he “believes the brain is the seat of mental process”. Galen, 130-200 AD, puts forth the idea that the brain receives sensory information and is responsible for motor control, using the mechanism of fluid energies. René Descartes, 1596-1650, states that nerves contain fluids, or "animal spirits", which are responsible for the flow of sensory and motor information in the body. Johannes Purkinje, 1787-1869, was the first to describe a nerve cell, contributing extensively to the field of experimental psychology through his work on sensory and visual experience after stimulation, e.g. by applying pressure and electrical current to the eyeball. He also discovered the large nerve cells in the cerebellum, "Purkinje Cells" which have the most beautiful dendrites' arbors in the brain. Korbinian Brodmann, 1868-1918, was the first to categorize the brain into 52 distinct regions based on the cellular organization of neuronal networks in the cortex, thus providing support to the “Localist” view, which was already very strong. This was accomplished through histological tissue stains to visualize the different cell types. This also led to the concept that neurons have sub-regions, called “cytoarchitectonics”, that define their cellular architecture. Camillo Golgi, 1843-1956, was the first to develop a silver stain that permitted the full visualization of single neurons, revolutionizing our understanding of the cellular organization of the brain. However, he interpreted his images to conclude that the brain was a continuous mass of tissue that shares a single cytoplasm. This concept was challenged by Santiago Ramón Y Cajal, 1852-1934, who used Golgi's silver stain technique to show that neurons were discrete unitary entities, and that they might conducted electrical signals in only one direction. Importantly, Cajal established the “Neuron Doctrine” of the brain, which is the fundamental organizational and functional principle of the nervous system, stating that the neuron is the anatomical, physiological, genetic and metabolic unit of the nervous system. In 1897, Sir Charles Scott Sherrington introduces the term Synapse (from the Greek “Clasp”) to define the cellular junction formed between nerve cells. In 1938, the concept defined by the Neuron Doctrine was further refined by Fulton stating that the neuron is the anatomical, physiological, genetic and metabolic unit of the nervous system. There are three main parts of this doctrine namely, a) neurons are discrete and autonomous cells that

can interact, b) synapses are gaps that separate neurons, c) information is transmitted in one direction from dendrites (input) to the axon (output).

Studies over the last half-century have sought to refine our understanding of how neurons function within neuronal networks to define cognitive function and behavior. Important open questions remain such as where are neurons born, how do they reach their final position in the brain and what governs their differentiation. Other include, how do neurons form functional synaptic connections and how does this affect neuronal network function. All of these issues are influenced by genetics, the dynamic properties and life times of individual molecules, and cellular programs that regulate the removal of mis-folded or functionally inactive proteins, RNAs etc. Emerging data indicate that dysfunctions at all of these levels contribute to neuropsychiatric disease, developmental disorders, cognitive function and neuro-degeneration. In my thesis work, I have tried to contribute core information on how synapses in the developing nervous system form and function. Much of my work has focused on two molecules, Piccolo and Bassoon, of the presynaptic active zone (AZ), and their role in regulating the docking and fusion of synaptic vesicles (SVs) at the AZ and the release of neurotransmitter substances in an activity dependent manner. My data show that Piccolo and Bassoon are large multidomain proteins that regulate the functional assembly of the presynaptic AZ and modulate the activity dependent assembly and dynamics of Filamentous Actin (F-actin) as well as the machinery involved in the docking, fusion and recycling of SVs and their proteins. Particularly exciting, I have discovered that Piccolo and Bassoon also regulate the local ubiquitination of presynaptic molecules by regulating the activity of an E3 ubiquitin ligase, Siah. Importantly, loss of function of Piccolo and Bassoon, leads to local imbalances of poly-ubiquitination resulting in the degradation of SV proteins and synaptic degeneration. Below I provide an overview of neuronal differentiation and the molecular mechanisms thought to underlie synaptogenesis and synaptic degeneration.

1.1 Neuronal structure.

The nervous system is comprised of many different kinds of cells. The two principle classes of cells include nerve cells (neurons), and glial cells (glia). Neurons are the minimal cellular unit for information acquisition and processing in the nervous system, while glial cells are thought to primarily serve a supporting role including: physical protection, guidance for cell/neuron migration, separating and insulating axons, buffering extracellular ions, clearance of neurotransmitters and providing synaptotrophic factors that facilitate neuronal differentiation and synaptogenesis.

Although glia are interesting in their own right, it is the formation of neuronal networks that are crucial for sensory perception, information acquisition and processing, motor control, cognition and behavior. Thus understanding how neurons establish, maintain, modulate and eliminate selective connections is essential for elucidating how neuronal networks carry out their diverse functions. Critical to addressing this fundamental question is a clear understanding of the cellular mechanisms that guide neuronal differentiation and function.

Neurons are polarized and highly specialized cells designed to rapidly and reliably transmit signals to other neurons, muscles and glands. Neurons contain three morphologically distinct regions: the cell body (or soma) where a majority of cellular metabolism occurs, dendrites a highly differentiated set of processes designed for receiving and processing neurotransmitter signals and axons highly differentiated processes involved in conducting electrical signals known as action potentials as well as the regulated release of neurotransmitters from presynaptic boutons beaded along their length (Kandel, Klein et al. 1986; Siegelbaum and Kandel 1991). Generally, neurons extend several dendrites and one axon from the cell body. Dendrites are relatively large in diameter, taper over their length and usually have extensive branches. The main function of dendrites is to receive and process inputs from other neurons. In contrast, axons are generally thin caliber processes that can also be highly branched yet capable of being very long, e.g. 1m in length (Banker and Goslin 1988; Banker and Goslin 1998). The main function of an axon is to initiate and propagate action potential from the cell soma/axon-hillock to distal sites of cell-cell contact called synapses. Synapses can either be electrical, passing current directly through gap junctions between nerve cells or chemical. Chemical synapses are much more common in vertebrates converting electrical signals to chemical signals through the regulated release and reception of small molecules or peptide referred to as neurotransmitters. Generally neurons produce and release only one neurotransmitter e.g. glutamate, acetylcholine, dopamine, serotonin, nor-epinephrine, glycine or gamma-amino-butyric acid (GABA), and/or neuropeptides.

Synaptic connections between neurons or other excitable cells (e.g. a muscle cell) or glands are highly specific both with respect to the cells they form contacts as well as in the transmitter released (Hill-Eubanks, Werner et al. 2011). Synapses are highly evolved neural processors that ensure rapid and efficient communication between neurons. They are the building blocks of learning and memory, cognition, behavior and consciousness (Cline 1998). This accurate and regulated neural transmission requires a complex and highly ordered structural organization. A typical chemical synapse is composed of a presynaptic bouton, where neurotransmitters and neuropeptides are stored in discrete membrane packets called SVs and released via SV fusion with the plasma membrane. Presynaptic boutons are situated

juxtaposed to postsynaptic cells, which receives signals in the form of neurotransmitters released from the pre-synaptic terminal (Jessell and Kandel 1993). Between these pre- and post-synaptic compartments lies the synaptic cleft, a narrow space 20-50nm consisting of cell-adhesion and extracellular matrix molecules.

1.2 Synapse structure.

It was not until the advent of high-resolution electron microscopy (EM) that the synapses could be classified on the basis of their morphological characteristics. For example, Gray, in 1959, was the first to describe the two main types of synapses. Type I, or asymmetric synapses, are typically found along dendritic arbors and are characterized by a pronounced electron-dense thickening of postsynaptic membrane, referred to as the postsynaptic density (PSD). The PSD is situated juxtaposed to the presynaptic bouton. Type II or symmetric synapses were observed along the soma or dendrites of neurons. These had roughly equal amount of electron-dense material associated with the pre and postsynaptic plasma membranes. Generally, excitatory synapses are asymmetric, with a pronounced PSD, while inhibitory synapses are associated with symmetric type II synapses (Garner and Kindler 1996).

The presynaptic boutons of type I and type II synapses exhibit similar structural features. These include a large pool of SVs, filled with neurotransmitter, clustered at a specialized region of the pre-synaptic plasma membrane, juxtaposed to the PSD, referred to as the Active Zone (AZ). SVs dock, fuse and release their cargo into the synaptic cleft at the AZ. The speed and efficiency of synaptic transmission requires precise formation of these specialized compartments. Several subtypes of SVs are found within presynaptic boutons: one is approximately 30-50 nm in diameter and appears to have clear centers. These are filled with fast-acting neurotransmitters like amines and amino acids. The second is larger in diameter (from 80 to 200 nm) has an electron dense core and contains slower-acting neuropeptides (Burns and Augustine 1995).

1.3 The post-synaptic specialization.

The postsynaptic plasma membrane is specialized for the reception and processing of information transmitted by neurotransmitters released from presynaptic boutons. At excitatory synapses, the PSD was originally defined ultrastructurally by its electron-dense thickening associated with the cytoplasmic side of the postsynaptic plasma membrane (Gray 1959; Gray 1959; Kim and Ko 2006). This is a region with a high concentration of neurotransmitter receptors, ion channels, scaffolding proteins as well as regulatory proteins,

kinases, phosphatases etc (Boeckers 2006; Gundelfinger, Boeckers et al. 2006). Biochemically the PSD is rather insoluble in nonionic detergents, allowing it to be isolated and characterized (Montgomery, Zamorano et al. 2004; Baron, Boeckers et al. 2006). To date over 500 distinct proteins have been identified, including receptors, scaffolding proteins, cytoskeletal elements, kinases and adhesion molecules among other, (Langnaese, Seidenbecher et al. 1996; Ziff 1997; Beresewicz 2007). (Maas, Torres et al. in press).

At excitatory synapses, glutamate receptors are key signaling components of the PSD, comprised of both metabotropic and ionotropic receptors. Metabotropic receptors appear to be localized peri-synaptically around the PSD (Lujan, Roberts et al. 1997; Nusser, Lujan et al. 1998; Awatramani and Slaughter 2001). In contrast, ionotropic receptors, like N-methyl-D-aspartate (NMDA) and α -amino-3-hydroxy-5-methyl-4-isoxazole propionic acid (AMPA) receptors are localized and concentrate at PSDs. These receptors can be inserted, tethered and removed independently from each other allowing for example immature synapses to contain primarily NMDA receptors (e.g. silent synapses) that acquire AMPA receptors only upon activation (Nusser, Lujan et al. 1998; Malenka and Nicoll 1999; Takumi, Ramirez-Leon et al. 1999; Malinow and Malenka 2002; Petralia, Sans et al. 2005; Citri and Malenka 2008) The subsynaptic and functional segregation of metabotropic and ionotropic glutamate receptors suggest the existence of specific intracellular scaffolding proteins important for forward trafficking and immobilization of neurotransmitter receptors within synaptic subdomains (Montgomery, Zamorano et al. 2004; Jeyifous, Waites et al. 2009; Waites, Specht et al. 2009).

Of the many PSD proteins thus far identified, those with multidomain structures have emerged as key regulators in the assembly of the PSD and in defining receptor specific signaling complexes (Montgomery, Zamorano et al. 2004; Okabe 2007; Sheng and Hoogenraad 2007). Of these, members of the MAGUK family of membrane associated guanylate kinases (MAGUK) have been shown to play pivotal roles in the assembly of the PSD and the clustering and targeting of glutamate receptors to their synaptic sites (Xu 2011). These proteins are characterized by the presence of one or more PDZ domains, an SH3 domain, and a guanylate kinase-like (GK) domain, all of which are actively involved in protein-protein interactions (Cho, Hunt et al. 1992; Kistner, Wenzel et al. 1993; Kornau, Schenker et al. 1995; Muller, Kistner et al. 1995; Kim, Cho et al. 1996; Muller, Kistner et al. 1996; Montgomery, Zamorano et al. 2004).

These prototypically multidomain proteins do more than just cluster and localize receptors to the PSD. For example, they also scaffold specific signaling and regulatory protein complexes in the vicinity of NMDA receptors and AMPA receptors, which allow the regional and rapid modulation of synaptic function and plasticity (Montgomery, Zamorano et

al. 2004; Okabe 2007; Sheng and Hoogenraad 2007; Jeyifous, Waites et al. 2009; Waites, Specht et al. 2009; Xu 2011). Although further studies are needed, it is clear that the MAGUKs proteins are important for the assembly of the PSD (Montgomery, Zamorano et al. 2004).

1.4 Presynaptic Structure and Function.

Although pre-synaptic boutons emerge from the end of axons as at the neuromuscular junction (NMJ), most exist as varicosities/boutons along the length of axons forming synapses *en passant* with thousands of postsynaptic targets. Intriguingly, presynaptic boutons/terminals contain all the machinery necessary for the regulated release of neurotransmitters. These include trans-synaptic cell-cell adhesion molecules that maintain registry between the presynaptic AZ and PSD as well as molecules involved in the docking and calcium regulated fusion of SVs with the AZ plasma membrane (Garner, Kindler et al. 2000; Dresbach, Qualmann et al. 2001; Garner, Zhai et al. 2002; Ziv and Garner 2004; Waites, Craig et al. 2005; Fejtova and Gundelfinger 2006).

Although aldehyde fix specimens have provided tremendous insights into the ultrastructure of synapses, Electron Microscopy (EM) tomography combined with high pressure freezing has revealed remarkable details of the fine architecture of presynaptic boutons (Peters 2007; Hoopmann, Rizzoli et al. 2012; Robert, Cloix et al. 2012; Zhao, Studer et al. 2012). The most remarkable feature is the AZ, a region of the plasma membrane where SVs dock and fuse (Landis 1988; Landis, Hall et al. 1988; Oswald and Sigrist 2009; Sigrist and Schmitz 2011). Typically, hundreds of SVs are localized in the vicinity of AZs. These can be functionally divided into a) a readily releasable pool (RRP) that are physically docked at the AZ plasma membrane, b) a recycling pool that readily undergo fusion with synaptic activity and c) a reserve pool that largely remains quiescent. The latter two pools represent most of the SVs within presynaptic boutons and are generally situated far from the AZ plasma membrane (100 nm) (Galli and Haucke 2004; Kuromi and Kidokoro 2005; Cheung and Cousin 2011). Docked vesicles are surrounded by a network of cytoskeletal and structural proteins (Garner, Kindler et al. 2000; Kuromi and Kidokoro 2005; Schoch and Gundelfinger 2006; Sigrist and Schmitz 2011). Most are multidomain proteins similar to the MAGUK family that function to organize the SV docking and fusion machinery (Garner, Kindler et al. 2000; Waites, Craig et al. 2005; Oswald and Sigrist 2009; Robert, Cloix et al. 2012)(see also below).

One of the best-studied presynaptic proteins is Synapsin. It has been shown to associate and cross-link SVs within the reserve and recycling pools (Greengard, Valtorta et al. 1993;

Ryan, Li et al. 1996; Jovanovic, Czernik et al. 2000; Jovanovic, Sihra et al. 2001). Studies on the biochemical properties of Synapsin have shown that it also binds F-actin providing a potential link for SVs with the Actin-based cytoskeleton. Importantly, Synapsin undergoes activity dependent phosphorylation and dephosphorylation that regulates its cross-linking activity and thus the availability of SVs in the reserve and recycling pools to translocate to the AZ where they dock and fuse (Rosahl, Geppert et al. 1993; Bloom, Evergren et al. 2003; Gitler, Xu et al. 2004; Evergren, Benfenati et al. 2007; Bykhovskaia 2011). Synaptic activity also regulates the dynamic assembly of F-actin from monomeric Globular-Actin (G-actin). Together with Synapsin, this dynamics is crucial for regulating three aspect of presynaptic function (Cole, Villa et al. 2000; Colicos, Collins et al. 2001; Bloom, Evergren et al. 2003; Dillon and Goda 2005; Cingolani and Goda 2008). For example, F-actin assembled at the plasma membrane is thought to create a barrier that restrains SV fusion at the AZ, thus reducing SV release probability (Pr) (Morales, Colicos et al. 2000; Cingolani and Goda 2008). In concert with Synapsin, F-actin also plays a role in maintaining the reserve pool and through the actions of myosin the translocation of SVs to the RRP (Greengard, Benfenati et al. 1994; Cingolani and Goda 2008). Intriguingly, the dynamic assembly of F-actin also regulate SV endocytosis and the recycling of synaptic proteins through endosomal pathways (Shupliakov, Bloom et al. 2002; Bloom, Evergren et al. 2003; Engqvist-Goldstein and Drubin 2003; Fenster, Kessels et al. 2003; Dillon and Goda 2005; Evergren, Benfenati et al. 2007). Each of these steps greatly facilitates SV fusion and recycling, ensuring that sufficient numbers of SVs are available for fusion even under periods of high neuronal activity.

A fundamental questions regarding presynaptic function is how SVs fusion is restricted to the presynaptic AZ. Knowledge gained over the last few decades have shown that a complex network of multidomain scaffold proteins assembled at the AZ plasma membrane are extremely important for defining and regulating the activity dependent recruitment and recycling of SVs pools (Garner, Kindler et al. 2000; Dresbach, Qualmann et al. 2001; Garner, Zhai et al. 2002; Fejtova and Gundelfinger 2006; Schoch and Gundelfinger 2006).

1.5 Active Zones.

The Active Zone (AZ) is a site of SV docking and fusion where neurotransmitter is release into the synaptic cleft (Garner, Kindler et al. 2000; Dresbach, Qualmann et al. 2001; Garner, Zhai et al. 2002; Fejtova and Gundelfinger 2006; Schoch and Gundelfinger 2006). The regulated fusion of SVs, e.g. exocytosis requires a number of specialized proteins. Those involved in SV docking with the AZ plasma membrane are known as SNAREs (Soluble NSF (N-ethylmaleimide-sensitive factor) Attachment Protein Receptor). These include

SynaptobrevinII/VAMP2 located on vesicle membrane, Syntaxin-1 and synaptosome-associated protein 25 kDa (SNAP-25) both located on the plasma membrane, which form a complex and represent the minimal machinery for fusion (Jahn and Sudhof 1999; Galli and Haucke 2004; Pobbati, Stein et al. 2006). Progressive zippering of the four helix bundle that comprise the SNARE complex drives fusion of SVs with the plasma membrane. Syntaxin I and SNAP-25 are localized to the plasma membrane at AZ, but neither of them is solely concentrated at AZs (Garcia, McPherson et al. 1995; Sigrist and Schmitz 2011). This suggests that other proteins present within the AZ cytoskeletal matrix (or CAZ) are responsible for regulation of SV exocytosis. A growing number of studies have begun to characterize the core CAZ proteins. These include member of the RIM, Munc13, CAST/ELKS, Liprin, RIM-BP and Piccolo families (Garner, Kindler et al. 2000; Dresbach, Qualmann et al. 2001; Garner, Zhai et al. 2002; Fejtova and Gundelfinger 2006; Schoch and Gundelfinger 2006; Oswald and Sigrist 2009).

1.6 RIMs.

RIM was first identified in a screen for effectors of the SV-associated proteins, Rab3A and Rab3C. These Rab Interacting Molecules (RIM) are highly enriched in synaptic junctional preparations and tightly associated with AZs. Immuno-EM studies of the most abundant isoform RIM1 demonstrate that it is concentrated within presynaptic boutons at the AZ (Wang, Okamoto et al. 1997). RIM1 is a 180kDa protein that contains an N-terminal zinc finger domain, a PDZ domain, and two calcium/phospholipid binding C2 domains. Intriguingly, the C2A and C2B domains in RIM1 lack the five consensus charged amino acid residues (aspartate or glutamate) that are essential for Ca^{2+} binding. This suggests that these domains do not bind Ca^{2+} but instead serve as sites of protein-protein interaction (Sudhof and Rizo 1996; Wang, Okamoto et al. 1997). This is supported by studies showing that the C2 domains of RIM1 do not bind calcium but do bind with high affinity the C2 domains of Synaptotagmin 1. Importantly, Synaptotagmin 1 is a known calcium sensor at the AZ and is critical for SV fusion in an activity dependent manner, implying that RIM1 may indirectly control of SV fusion (Coppola, Magnin-Luthi et al. 2001). Further support for this concept come from studies showing that RIM1 forms a tripartite complex via its Zinc Finger (ZF) domains with Munc13 and Rab3, both of which are important for priming of SV with the AZ (Dulubova, Lou et al. 2005). Furthermore, RIM1 uses its multidomain structure to form a complex with several other AZ proteins including ELKS, RIM-Binding Protein 1 (RIM-BP1) and the cytoplasmic domains of presynaptic N- and P/Q-type voltage gated Ca^{2+} channels (VGCC) (Wang, Okamoto et al. 1997; Wang, Sugita et al. 2000; Betz, Thakur et al. 2001;

Hibino, Pironkova et al. 2002; Ohtsuka, Takao-Rikitsu et al. 2002; Schoch, Castillo et al. 2002; Wang, Liu et al. 2002; Ko, Na et al. 2003; Lu, Li et al. 2005; Andrews-Zwillling, Kawabe et al. 2006; Kaeser, Kwon et al. 2008; Kaeser, Deng et al. 2011). These interactions are thought to mediate the clustering of VGCC at AZs, thus facilitating activity dependent SV fusion (Han, Kaeser et al. 2011). RIM1 loss of function studies are consistent with this concept revealing that RIM1 is necessary for efficient neurotransmitter release from AZ (Schoch, Castillo et al. 2002; Kaeser, Deng et al. 2011). Finally, RIM1 has been found to be a substrate for Protein Kinase A (PKA) phosphorylation, a modification that is associate with presynaptic forms of long-term potentiation (preLTP) increasing, for example, SV release probability (Castillo, Schoch et al. 2002; Lonart, Schoch et al. 2003)

1.7 Munc13.

Munc13 is the mammalian homolog of the *C. elegans* unc-13 protein that was originally identified as member of an uncoordinated (*unc*) group of mutant phenotypes in worms (Brenner 1974; Brose, Hofmann et al. 1995). Interestingly, Munc13-1 and its isoforms, ubMunc13-2, and Munc13-3, are enriched at presynaptic AZs (Betz, Ashery et al. 1998). Munc13-1 is a 200 kDa protein that contains three C2 domains and a C1 domain similar to that found in protein kinase C (PKC) (Kazanietz, Lewin et al. 1995; Betz, Ashery et al. 1998). As mentioned previously, disruption of the *C. elegans* and *Drosophila* *unc-13* (*dunc-13*) as well as the mouse *unc13* (*Munc13-1*) genes dramatically suppresses both spontaneous and evoked release of neurotransmitter (Aravamudan, Fergestad et al. 1999; Augustin, Betz et al. 1999; Augustin, Rosenmund et al. 1999; Richmond, Davis et al. 1999). This is likely due to a loss of vesicle priming which precludes fusion of docked vesicles with the plasma membrane.

Munc13 family members appear to regulate SV priming at AZs (Rosenmund, Sigler et al. 2002; Rosenmund, Rettig et al. 2003). For example, in mouse, the absence of Munc13.1 completely blocks SV fusion and transmitter release (Varoqueaux, Sigler et al. 2002; Varoqueaux, Sons et al. 2005). Munc13 proteins are regulated by a variety of proteins, making SV priming and release a complex and highly dynamic regulated process (Rosenmund, Rettig et al. 2003). Intriguingly, Munc13-1 can form a homodimer that can switch to a heterodimer with RIM1 proteins. This molecular switch is thought to be a key step regulating SV priming and presynaptic forms of short-term plasticity (Lu, Machius et al. 2006). Importantly, Munc13-1 homodimerization inhibits its priming function, leading to the concept that RIM1 activate priming by disrupting Munc13-1 homodimerization (Deng, Kaeser et al. 2011).

1.8 CAST/ELKS.

Both CAST and ELKS α are structurally related proteins of ~120 kDa containing four coiled-coil (CC) regions and a unique C-terminal amino acid motif, IWA. In *C. elegans* and *Drosophila*, CAST/ELKS is encoded by a single gene, CeCAST and Bruchpilot, respectively (Deken, Vincent et al. 2005; Kittel, Wichmann et al. 2006; Wagh, Rasse et al. 2006). In vertebrates, CAST belongs to a protein family that also includes ELKS (Nakata, Kitamura et al. 1999; Monier, Jollivet et al. 2002; Wang, Liu et al. 2002; Deguchi-Tawarada, Inoue et al. 2004) and importantly, the genes for CAST and ELKS are located on different chromosomes in mice, rats and humans (Nakata, Kitamura et al. 1999). ELKS α is predominantly expressed in the brain (Deguchi-Tawarada, Inoue et al. 2004) and shows a relatively high homology with CAST at the protein level (~70% identical). Similar to CAST, RIM1, Munc13 and Bassoon, ELKS α is localized in the vicinity of the presynaptic plasma membrane in the mouse cerebellum (Ohtsuka, Takao-Rikitsu et al. 2002). Immuno-EM of photoreceptor cell ribbon synapses have shown that CAST is localized at the base of the ribbon near the archiform density where SV dock and fuse, whereas ELKS α is localized more peripherally around the ribbon (Deguchi-Tawarada, Inoue et al. 2006). These observations suggest that CAST and ELKS have distinct functions at synapses in spite of their high degree of homology. CAST and ELKS can directly interact with Bassoon, Piccolo and RIM1, and indirectly to Munc13-1, forming a large molecular complex at AZ (Ohtsuka, Takao-Rikitsu et al. 2002). The subsynaptic localization of CAST and ELKS and their interactions with other AZ proteins suggest that the CAST/ELKS family is involved in the formation and/or maintenance of AZs. This conclusion is supported by genetic studies in *Drosophila* (Kittel, Wichmann et al. 2006; Wagh, Rasse et al. 2006), where EM studies of neuromuscular junctions (NMJs) revealed that null mutations in *bruchpilot* cause the loss of the electron-dense T-bar structures and the declustering of VGCCs (Kittel, Wichmann et al. 2006; Wagh, Rasse et al. 2006). Intriguingly, while evoked synaptic transmission is profoundly impaired, spontaneous neurotransmitter release is unaffected, indicating that the fundamental mechanism of exocytosis is still preserved in these mutants. Consistent with a role in regulating VGCC, Bruchpilot was recently shown to directly interact with the α -subunit of Ca²⁺ channels in *Drosophila* (Fouquet, Oswald et al. 2009).

In vertebrates, the inhibition of CAST–Bassoon binding significantly impairs neurotransmission (Takao-Rikitsu, Mochida et al. 2004). In contrast to Bruchpilot loss of function in *Drosophila*, no gross changes in the size or morphology of AZs is seen in CAST knockout mice (Kaeser, Deng et al. 2009), a finding similar to CeCAST loss of function in *C.*

elegans (Deken, Vincent et al. 2005). One reasonable explanation for this phenomenon is that ELKS may be somewhat functionally redundant with CAST at central nervous system synapses in mice. Functionally, CAST loss of function in mice has no effect on excitatory synaptic transmission, though the release of neurotransmitter from inhibitory synapse is increased as is the size of the RRP of SVs (Takao-Rikitsu, Mochida et al. 2004). A particular confound in these studies is that the deletion is not a null and shorter isoform of CAST (~95 kDa) are still expressed in these mice (Kaeser, Deng et al. 2009). Thus, it remains unclear whether CAST plays a direct role in the regulated release of neurotransmitters, as seen for Bruchpilot, Munc13 and RIM1 or whether its role is more indirect by e.g. efficiently scaffolding other AZ proteins.

1.9 Liprin- α .

The Liprin- α family of proteins was first characterized by their ability to bind to the cytoplasmic domains of LAR (the receptor protein tyrosine phosphatase (RPTP) leukocyte common antigen-related) (Serra-Pages, Kedersha et al. 1995) in a yeast two-hybrid screen. Liprin- α and LAR can influence one another's subcellular distribution. For example, LAR mislocalization is sufficient to change the distribution of Liprin- α (Serra-Pages, Kedersha et al. 1995), and Liprin- α can localize LAR to the proximal edges of focal adhesions (Serra-Pages, Kedersha et al. 1995). Vertebrate genomes generally encode four Liprin- α (Liprin α 1-4), whereas *Drosophila* and *C. elegans* each have one (Liprin- α and Syd-2, respectively) (Stryker and Johnson 2007).

The interaction between LAR and Liprin α is also conserved in *Drosophila* (Kaufmann, DeProto et al. 2002). Fly *liprin- α* mutants display dramatic reductions in the size and branch complexity of NMJs. LAR mutants in *Drosophila* have a nearly identical phenotype (Kaufmann, DeProto et al. 2002), which is consistent with a model in which Liprin- α and LAR work together to control synapse formation. Pre-synaptic overexpression of LAR is sufficient to increase synaptic size. This effect depends on the presence of Liprin- α , demonstrating that LAR requires Liprin- α to function at the NMJ (Stryker and Johnson 2007). Both *Liprin- α* and *LAR* mutants have reduced evoked synaptic responses and a nearly 50% reduction in quantal content (Kaufmann, DeProto et al. 2002), which suggests a defect in the function of the SV fusion machinery in both mutants.

Liprin- α interacts with a diverse array of proteins that regulate the formation of AZs (Zhen and Jin 2004). They are essential for regulated SV release and interact with the SV trafficking protein Rab3A. CAST/ELKS family members form large oligomeric complexes

with other known AZ proteins and influence the subcellular localization of both Liprin- α (Ko, Na et al. 2003) and RIM1 (Ohtsuka, Takao-Rikitsu et al. 2002), targeting these proteins to presynaptic sites. Liprin- α is essential for active zone localization of RIM1 (Dai, Taru et al. 2006; Stigloher, Zhan et al. 2011)

Liprin- α also binds the MALS/Veli-Cask-Mint1 scaffolding complex, a ternary complex of PDZ-domain-containing proteins that regulates the replenishment of SVs in the RRP from the reserve SV pool (Olsen, Moore et al. 2005). Although MALS mutants have no visible defects in Liprin- α localization, they do have larger synaptic areas and decreased excitatory post-synaptic currents, which is similar to *Liprin- α* mutants in *C-elegans* (Olsen, Moore et al. 2005). Given that *Liprin- α* mutants have defects in evoked responses (Kaufmann, DeProto et al. 2002), that RIM1 α regulates SV release, it is conceivable that Liprin- α , RIM1 α and the MALS/Veli-Cask-Mint1 complex functions to facilitate SV priming and neurotransmitter release at AZs (Stryker and Johnson 2007).

Liprin- α colocalizes with Piccolo clusters at the AZ, presumably via interactions with RIM1 and CAST/ELKS (Ko, Kim et al. 2003). Invertebrates lack both Piccolo and Bassoon, leading to the suggestion that Bruchpilot may assume some of their functions during AZ morphogenesis. The phenotypic differences between *bruchpilot* and *liprin- α* mutants suggest that, although both proteins regulate AZ formation, they likely function in distinct pathways. Nevertheless, the observation that the localization of Bruchpilot to the AZ is reduced almost 30% in *liprin- α* mutants (Miller, DeProto et al. 2005) suggests some kind of functional interaction between Bruchpilot and Liprin- α during active zone assembly.

1.10 Bassoon and Piccolo.

Piccolo and Bassoon are two high-molecular-weight (520 and 420 kDa) structurally related vertebrate specific AZ proteins that are specifically concentrated at AZs (Cases-Langhoff, Voss et al. 1996; tom Dieck, Sanmarti-Vila et al. 1998; Fenster, Chung et al. 2000; Garner, Kindler et al. 2000; Gundelfinger and tom Dieck 2000; Dresbach, Qualmann et al. 2001; Zhai, Vardinon-Friedman et al. 2001; Fenster and Garner 2002). In addition to being some of the first synaptic proteins to cluster at nascent synapses, immunoreactivity for Piccolo and Bassoon is observed within the presynaptic boutons of nearly all neurotransmitter types, including glutamatergic, GABAergic, cholinergic, dopaminergic and serotonergic among others, implying a core set of functions for these AZ proteins (tom Dieck, Sanmarti-Vila et al. 1998; Richter, Langnaese et al. 1999; Zhai, Olias et al. 2000). Structurally, Piccolo and Bassoon share a great deal of homology that is concentrated in a

series of ten Piccolo-Bassoon homology (PBH) domains that are scattered along their length (Fenster, Chung et al. 2000; Fenster and Garner 2002). Several PBH domains contain identifiable region such as Zinc Finger (ZF) and coiled-coil (CC) domains. In addition, Piccolo also contains a C-terminally localized PDZ, C2A and C2B domains (Fenster, Chung et al. 2000; Garner, Kindler et al. 2000; Gundelfinger and tom Dieck 2000; Dresbach, Qualmann et al. 2001; Zhai, Vardinon-Friedman et al. 2001).

Piccolo and Bassoon use their multidomain structure to interact with a large number of synaptic proteins. For example, the central region of Piccolo and Bassoon, critical for their synaptic localization, interacts with Ribeye/CtBP1 (tom Dieck, Altmann et al. 2005), CAST/ELKS (Takao-Rikitsu, Mochida et al. 2004), RIM-BP1 (Davydova, Fejtova, Gundelfinger, in preparation), Dynein Light Chain (Fejtova, Davydova et al. 2009) and each other (Maas, Torres et al. in press). Piccolo also engages in a set of unique interactions that suggest a role in the regulation of F-actin. For example, its N-terminal Poly-Q domain interacts with Abp1 (Fenster, Kessels et al. 2003), its central regions with GIT1 (Kim, Ko et al. 2003), Profilin1/2 (Wang, Kibschull et al. 1999) and Daam1 while its C-terminal domains interact with Trio and cAMP-GEFII (Personal communication). Intriguingly, the PDZ, C2A and C2B domains of Piccolo interact with RIM2 and L-type VDCC, respectively (Fujimoto, Shibasaki et al. 2002; Shibasaki, Sunaga et al. 2004). Not surprisingly, these interactions permit Piccolo and Bassoon to indirectly interact with a broader range of proteins that likely affects their common recruitment to Piccolo/Bassoon transport vesicles (PTVs) (Zhai, Vardinon-Friedman et al. 2001) (Maas, Torres et al. in press). and/or differential localization, e.g. along photoreceptor ribbon synapses (tom Dieck, Altmann et al. 2005).

Of the two, the functions of Bassoon have been characterized in the most detail. For example, in Bassoon knockout mice, the ribbons of photoreceptor cell are no longer tethered to the archiform density (Dick, tom Dieck et al. 2003). Morphological defects at central synapses have not been detected though a greater proportion of hippocampal synapses are silent implying a role for Bassoon in synaptic transmission (Altmann, tom Dieck et al. 2003). This concept is consistent with recent studies showing that short-term synaptic depression occurs during sustained high-frequency trains at hippocampal mossy fiber synapses (Hallermann, Fejtova et al. 2010) and abnormalities in the organization and function of calcium channels at photoreceptor ribbon synapses (Frank, Rutherford et al. 2010). Intriguingly, Bassoon and CAST have been found to have direct interactions with $\beta 1b$ or $\beta 4$ subunits of the VGCC. Moreover, in double knock-out mice for P/Q- and N-type VGCCs, synapses are normal in size but have significantly reduced numbers of AZs and docked vesicles (Chen, Billings et al. 2011). At present, little is known concerning how each of the

fore-described interactions is regulated. Recent mass-spectrometry studies have shown that both Piccolo and Bassoon are extensively modified by post transduction modification like phosphorylation and O-GlcNAC (Skorobogatko, Deuso et al. 2011).

Other than the growing number of binding partners, our understanding of Piccolo and its functions at synapses is rather limited. Conceptually, based on its structural similarity with Bassoon, one would expect that many functions of Piccolo are redundant with Bassoon, yet the presents of domains unique in Piccolo indicate it provides novel functions to synapses as well (Fenster, Chung et al. 2000; Fenster and Garner 2002; Fenster, Kessels et al. 2003). Regions unique to Piccolo are scattered along its length, many of which appear to be modified by alternative splicing (Fenster, Chung et al. 2000; Fenster and Garner 2002; Fenster, Kessels et al. 2003). One such region is the C-terminus of the longest Piccolo isoforms, which contain the PDZ, C2A and C2B domains. This region has been found to interact with L-type VGCC, RIM2 and dopamine transporters (DAT) (Garcia, Gerber et al. 2004; Cen, Nitta et al. 2008). The latter implies a novel function for Piccolo in dopaminergic neurons. Consistent with this concept, the expression of Piccolo was up regulated in the nucleus accumbens (NAc) in response to methamphetamine. Reducing Piccolo expression in the NAc augmented methamphetamine induced behavioral sensitization, as well as the accumulation of dopamine (Cen, Nitta et al. 2008). Studies in PC12 cells revealed that the C2A domain of Piccolo negatively regulates the surface expression of DAT indicating that Piccolo may regulate plasmalemmal DAT levels in dopaminergic presynaptic boutons (Cen, Nitta et al. 2008). Intriguingly, single nucleotide mutations in the C2A domain of Piccolo have been linked to major depressive disorders (Choi, Higgs et al. 2011), a behavior that can be elicited by the overexpression of the C2A domain of Piccolo in transgenic mice (Furukawa-Hibi, Nitta et al. 2010).

Unfortunately, unraveling the role of Piccolo at synapses has been complicated by the size complexity of the Piccolo gene (Fenster, Chung et al. 2000; Fenster and Garner 2002; Fenster, Kessels et al. 2003). Initial studies aimed at removing exon14 (Pclo Δ Ex14), had no effect on synaptic transmission or synapse formation (Mukherjee, Yang et al. 2010), yet only affected the expression of a subset of Piccolo isoforms (Waites, Leal-Ortiz et al. 2011). Injecting antisense oligonucleotides against Piccolo into the mouse hippocampus were found to affect both learning as well as the establishment of LTP (Ibi, Nitta et al. 2010). However, detailed electrophysiological studies were not performed. Finally, using neurons prepared from the Pclo Δ Ex14 mice and a short-hairpin RNA (shRNA) that reduces Bassoon expression by ~60%, Mukherjee and colleagues have explored potential redundant function of Piccolo and Bassoon (Mukherjee, Yang et al. 2010). In these studies, no change in

electrophysiological characteristics of either GABAergic or glutamatergic synaptic transmission was detected, though a small but significant reduction in SV pool size by electron microscopy was observed (Mukherjee, Yang et al. 2010). Taken together, it remains unclear whether Piccolo and Bassoon have only minor roles in presynaptic function and/or whether the ongoing expression of alternative spliced isoforms perform redundant/masking function.

1.11 Aims:

Based on published studies, the most intriguing and yet enigmatic presynaptic AZ proteins are Piccolo and Bassoon. Their large size, early arrival at nascent synapses and capacity to interaction with a growing number of both structural and regulatory proteins suggest that they perform fundamental roles in the initial assembly and function of vertebrate peripheral and central nervous synapses. In this thesis, I have sought to address the core functions of Piccolo and Bassoon by developing alternative strategies and technologies to inactivate all Piccolo and Bassoon isoforms in a cell-autonomous and synapse specific manner. These strategies have allowed us to define not only Piccolo specific functions at hippocampal glutamatergic synapses but also functions shared with Bassoon.

The specific aims of this thesis are:

- 1) Establish cell culture cryopreservation methodologies that allow genetically modified neurons to be stored and shared with collaborators.
- 2) Develop plasmid and lentiviral based expression systems that support the simultaneous down regulation of multiple synaptic proteins, while co-express XFP-tag reporter molecules at or near endogenous levels.
- 3) Generate a set of shRNAs that efficiently eliminate the expression of Piccolo and/or Bassoon.
- 4) Define the functions performed by Piccolo at excitatory hippocampal synapses.
- 5) Define the synaptic functions shared by Piccolo and Bassoon.

2. Materials and methods

2.1 Materials

2.1.1 Chemicals

All chemicals used were of analytical grade purchased from the described companies. Special chemicals and solutions utilized are detailed in the corresponding method descriptions.

2.1.2 Bacterial cells

Item	Company
NEB 10-beta Competent <i>E. coli</i> (High Efficiency) Genotype: <i>araD139 Δ(ara-leu)7697 fhuA lacX74 galK (ϕ80 Δ(lacZ)M15)</i> <i>mcrA galU recA1 endA1 nupG rpsL (Str^R) Δ(mrr-hsdRMS-mcrBC)</i>	New England BioLabs

Table 2.1. Bacterial cells

2.1.3 Bacterial culture media and antibiotics

Bacterial culture media	Composition
LB Miller Media	5 g yeast extract, 10 g peptone from casein, 10 g sodium chloride per liter of H ₂ O
LB Miller Agar	5 g yeast extract, 10 g peptone from casein, 10 g sodium chloride, 12 g agar-agar (??) per liter of H ₂ O
LB Lennox Media	5 g yeast extract, 10 g peptone from casein, 5 g sodium chloride per liter of H ₂ O
SOC	2% tryptone, 0.5% yeast extract, 10 mM NaCl, 2.5 mM KCl, 10 mM MgCl ₂ , 10 mM MgSO ₄ , 20 mM glucose
Kanamycin	50 mg/ml stock solution (1000x)
Ampicillin	100 mg/ml stock solution (1000x)

Table 2.2. Bacterial culture media and antibiotics

2.1.4. Molecular biology reagents, buffers and kits

Items	Composition or Company
Agarose	Invitrogen
1X TAE	40 mM Tris-OH, 20 mM Acetic Acid, 10mM EDTA pH 7.8
Ethidium bromide	Bio-Rad
Endonucleases (restriction enzymes)	New England Biolabs
Taq DNA polymerase	Invitrogen
Ultra high-fidelity KOD Taq polymerase kit	Novagen
Alkaline Phosphatase, Calf Intestinal (CIP)	New England Biolabs
T4 DNA ligase	New England Biolabs
T4 Polynucleotide kinase (PNK)	New England Biolabs
EndoFree Plasmid Maxi kit	Qiagen
PureLink HiPure Maxi kit	Invitrogen
Gel extraction kit	Qiagen
1 kb DNA ladder	New England Biolabs
100 bp DNA ladder	New England Biolabs

Annealing buffer	100 mM potassium acetate, 30 mM HEPES-KOH, pH 7.4, 2 mM magnesium acetate
------------------	---

Table 2.3. Molecular biology reagents, buffers and kits

2.1.5 Cells lines and medias

Item	Composition and Companies
HEK293T (<u>H</u> uman <u>E</u> mbryonic <u>K</u> idney cells, SV40 large T antigen)	ATCC
COS-7 (CV-1 (simian) in Origin, and carrying the SV40) Kidney Fibroblast Cells from African green monkey	ATCC
HEK293T and COS-7 media	DMEM, 1X GlutaMAX, 10% Fetal Bovine Serum (FBS), 1X Penicillin /Streptomycin.
TrypLE™ Express (1x), phenol red All your text says that you use Trysin-EDTA	Invitrogen
Poly-L-Lysine	33 mg/l Poly-L-Lysine in 100 mM boric acid pH 8.5, sterile filtered
HBSS pH 7.4	Hank's balanced salt solution, Ca ²⁺ and Mg ²⁺ Free (Sigma), 10 mM HEPES pH 7.4
Neuronal media	Neurobasal media, B27, GlutaMAX (all from Invitrogen)
Neuronal plating media	Minimum Essential Media with Earle's salts, 10% Donor horse serum, 100 mM Sodium pyruvate, 20 mM glucose,
Glia media	Minimum Essential Media with Earle's salts, 20 mM glucose; 10% FBS, Antibiotic-Antimycotic (Invitrogen)
Glia-conditioned media	Minimum Essential Media with Earle's salts and glutamine-free, 10% FBS, 20 mM glucose, A/A conditioned with glial cultures

Table 2.4. Cells line and medias

2.1.6 Primary antibodies

Antibodies	WB dilution	ICC dilution	Company
rb Piccolo 44aII		1/500	Custom-made
ms Bassoon 7f		1/500	Custom-made
rb Map2a/b		1/500	Custom-made
ms Map2a/b		1/500	Custom-made
ms Beta-Actin	1/1000		Sigma
ms GFAP	1/1000		Millipore
ms vGlut1?		1/1000	Synaptic Systems
rb Homer 1		1/500	Synaptic Systems
ms Synaptophysin		1/1000	Synaptic Systems
ms EGFP	1/5000		Roche
ms Neomycin	1/1000		Millipore
ms Tubulin	1/10000		Sigma
rb Rim1		1/200	Synaptic Systems
rb Munc13-1		1/200	Synaptic Systems

ms PSD95		1/200	Sigma
ms NR1		1/500	Abcam
ms HRP		1/500	Abcam
ms Synapsin	1/5000		Synaptic Systems
rb Synapsin site 4/5	1/1000		PhosphoSolutions
rb Synapsin site 3	1/1000		PhosphoSolutions
rb GluRI (S831-P)	1/1000		PhosphoSolutions
rb Synaptotagmin (S309-P)	1/1000		PhosphoSolutions
rb Rabphilin (S234-P)	1/1000		PhosphoSolutions
rb GluRI (S831-P)	1/1000		PhosphoSolutions
rb Munc18 (S515-P)	1/1000		PhosphoSolutions
rb Dynamin (S774-P)	1/1000		PhosphoSolutions
rb Dynamin	1/1000		PhosphoSolutions
rb SV2	1/1000		Synaptic Systems
rb Rab3	1/1000		Synaptic Systems
rb Syntaxin	1/1000		Synaptic Systems
rb SNAP25	1/1000		Synaptic Systems

Table 2.5. Primary antibodies

2.1.7 Secondary antibodies

Antibodies	WB dilution	ICC dilution	Company
rb Alexa 488		1/750	Invitrogen
rb Alexa 568		1/750	Invitrogen
rb Alexa 647		1/750	Invitrogen
ms Alexa 488		1/750	Invitrogen
ms Alexa 568		1/750	Invitrogen
ms Alexa 647		1/750	Invitrogen
ms HRP	1/10000		Roche
mb HRP	1/10000		Roche

Table 2.6. Secondary antibodies

2.1.8 Immunocytochemistry

Item	Composition
Lorene's fixative solution	60 mM PIPES pH7.0, 25 mM HEPES pH 7.0, 10 mM EGTA pH 8.0, 2 mM MgCl ₂ , 0.12 M sucrose, 4% paraformaldehyde
Permeabilization solution	0.25% Triton X-100 in 1X PBS
Blocking solution (for immunostaining)	2% Bovine serum albumin (BSA), 2% glycine, 0.2% gelatin, 50 mM NH ₄ Cl

PBS pH 7.4	137 mM NaCl, 2.7 mM KCl, 8 mM Na ₂ HPO ₄ , 1.46 mM KH ₂ PO ₄
------------	--

Table 2.7. Immunocytochemistry reagent

2.1.9 Biochemistry

Item	Composition
TBS	50 mM Tris-Cl pH 7.5, 150 mM NaCl pH 7.5
TBS-T	TBS plus 0.5% Tween-20
Blocking solution (Western blot)	5% milk in TBS-T
Homogenization buffer	Ice-cold 1X-PBS supplemented with protease inhibitors and 1% Tween-20
2X Sample buffer	125 mM Tris-HCl pH 6.8, 20% Glycerol, 4% SDS, >0.02% Bromophenol Blue, 5% Beta-Mercaptoethanol

Table 2.8. Biochemistry reagent

2.1.10 Animals

Animal	Notes	Origin
B6:129SF1/J	Mus musculus (Wild type)	Jackson Laboratory
B6;129 S6-Pclo ^{tm1Sud} /J	Mus musculus (PcloΔEx14/Neo)	Jackson Laboratory
Sprague-Dawley TIMED pregnant dams	Rattus Norvegicus	Charles River

Table 2.9. Animals

2.1.11 Plasmid transfections

Item	Composition or Company
Lipofectamine 2000	Invitrogen
Calfectin	SignaGen
Gene Pulser Electroporation	BioRad

Table 2.10. Transfection reagents

2.1.12 Live cell imaging reagents and solutions

Item	Composition or Company
Tyrode's solution pH 7.4	25 mM HEPES, 119 mM NaCl, 2.5 mM KCl, 30 mM glucose, 2 mM CaCl ₂ , 2 mM MgCl ₂ , 50 μM CNQX, 10 μM APV,
High K ⁺ Tyrode's solution pH 7.4	25 mM HEPES, 31.5 mM NaCl, 90 mM KCl, 30 mM glucose, 2 mM CaCl ₂ , 2 mM MgCl ₂ , 50 μM CNQX, 10 μM APV,
FM 5-95	Invitrogen
FM 4-64	Invitrogen

Table 2.11. Live cell imaging reagents

2.2 Methods

2.2.1 Molecular biological methods

2.2.1.1 Genotyping of *Pclo* mutant mice

2.2.1.1a DNA extraction for genotyping *Pclo* mutant mice

Neonate pups from *Pclo*ΔEx14/Neo mutant mice litters (P0-P1) were decapitated, and samples were taken for DNA extraction. Cortical samples from each pup were incubated with 300 μl of 50 mM NaOH at 99 °C per 30 min. After this incubation, 30 μl of 10 mM Tris was added, and samples were maintained on ice for PCR.

2.2.1.1b Polymerase chain reaction (PCR) for genotyping

PCR was performed using 10 μl of master mix containing all components and primers for WT and KO samples plus 2 μl of DNA extract for genotyping. Final concentrations of the PCR reagents were: 1 μM forward primer WT, 1 μM reverse primer WT 1 μM forward primer KO, 1 μM reverse primer KO (see Table 12 for sequences), 2.0 mM MgCl₂, 0.03 units/μl Taq-polymerase, 0.2 mM dNTPs in 1x PCR buffer II.

Primer Name	5' primer	3' primer	Product size
wt	5'cgtagtcagactggaactcta	5'gctctggtacagaggtaaagcttgc	195 bp
<i>Pclo</i> KO	5'ccttgagggtcaatgtgatca	5'gccaagtctcaattccatcagaagctcgataccg	210 bp

Table 2.12. Primer Sequence for PCR for genotyping wildtype and *Pclo* KO.

Process	Time and temperature	Cycles
Initial Denaturation	4 min, 94 °C	1 time
Denaturation	30 sec, 94 °C	35 time
Annealing	1 min, 55 °C	
Extension	1 min, 72 °C	
Final Extension	7 min, 72 °C	1 time
Hold	∞ 4 °C	

Table 2.13: Thermocycling set up program for genotyping

2.2.1.2 Bacterial transformations

Transformations of chemically competent *E. coli* were accomplished as described by the manufacturer (New England Biolabs). Frozen aliquots of competent bacterial cells, stored at -80 °C, were thawed for approximately 10 min on ice. The desired plasmid (0.2 μg) was added to the competent cell suspension, gently swirled with a pipet tip and placed on ice for 5 min. Cells were then heat-shocked for 45 sec at 42 °C and placed back on ice for 5 min. SOC media (100 μl) was added to the cell suspension; the cells suspension was then placed in a 37°C shaking incubator at speed of 200 rpm for 45 min. Cells were plated on LB agar plates with the appropriate antibiotics. Inoculated plates were placed at 37 °C overnight and removed after approximately 16 h.

2.2.1.3 Growing up bacterial colonies for plasmid minipreps

Individual colonies were picked using sterile technique and used to seed a 4 ml Lennox Luria Broth (LB) culture with the appropriate antibiotics. Single colonies were grown in 15 ml round-bottomed plastic tubes with adjustable caps to allow for oxygenation in a bacterial shaker overnight at 37 °C.

2.2.1.4 Plasmid DNA minipreps

Plasmid DNA was generally isolated from 2 ml overnight bacterial cultures using a modified Sambrook molecular cloning protocol. In brief, bacterial cultures were collected and centrifuged in a microcentrifuge at 14,000 rpm at room temperature for 5 min. The supernatant was carefully removed by vacuum suction without disturbing the cell pellet. Cell pellets were then resuspended in 200 µl Resuspension Buffer and then lysed in 200 µl Lysis Buffer. Tubes were then inverted 6-10 times for full lysis. Reactions were allowed to proceed for approximately 2 min but no longer than 5 min before the addition of 200 µl Neutralization Buffer. Tubes were inverted again 6-10 times until the formation of a white precipitate was seen. Tubes were then placed for 5 min on ice. Cellular debris was then removed by centrifugation at 14,000 rpm for 5 min at 4 °C. Approximately 600 µl of supernatant from each tube was placed into a new 1.5 ml centrifuge tube and 900 µl of isopropanol was added and mixed well by continuously inverting the tube. Plasmid DNA was collected by centrifugation at 14,000 rpm for 15 min at 4 °C. The supernatant was carefully removed by vacuum suction, and the dried DNA pellet was resuspended in 50 µl nanopure water and stored at -20 °C.

2.2.1.5 Preparing endotoxin-free maxiprep plasmid DNA

Plasmid DNA was prepared in large quantities (~1-2 mg) and high purity using a maxiprep kit [EndoFree Plasmid Maxi Kit (Qiagen) or PureLink HiPure Maxiprep Kit (Invitrogen)] according to the manufacturer's instructions with the following modifications. In brief, LB (300 ml) was inoculated with 100 µl from a 3ml bacterial starter culture grown overnight for 14 to 18 hr at 37 °C in a bacterial shaker. DNA was purified as described by the manufacturer (Qiagen or Invitrogen). DNA pellets were resuspended in 500 µl of endotoxin-free H₂O. DNA concentrations were quantified using a spectrophotometer (BioSpec-nano) at 260 nm.

2.2.1.6 Separating DNA fragments using agarose gel electrophoresis

Separation of DNA fragments was accomplished using one-dimensional agarose gel electrophoresis. Analytic agarose gels (1% w/v) were prepared in 1X TAE buffer. This solution was heated in a microwave in 30 s intervals with swirling until the agarose solution began to bubble and then cooled in a cold-water bath. For visualization of the separated DNA fragments under UV light, ethidium bromide was added to a final concentration of 0.5 µg/ml. The agar solution was poured into a gel apparatus and allowed to solidify at room temperature in the hood for 20-30 min. For running gels, 1X TAE was added until the meniscus was approximately 1 cm above the agarose. Gels were run between 1 to 5 V/cm. Gels were visualized using a UV transilluminator and documented using the KODAK camera system.

2.2.1.7 DNA purification from gel slices

DNA fragments are isolated and purified from agarose gels as described by the manufacturer (Qiagen). In brief, DNA fragment(s) were excised from DNA agarose gels with a clean razor blade and solubilized with Buffer QG (using three times volume of the agarose mass). The mixture was heated at 42 to 50 °C until the agarose melted. The DNA fragments were purified using a QIAquick mini columns and eluted with 25 µl of nanopure water. Products were analyzed using a diagnostic 1% agarose gel to obtain a rough estimate of the concentration of each DNA fragment by comparing band intensities relative to 1.0 kb DNA ladder (NEB).

2.2.1.8 DNA restriction enzyme digestions

DNA plasmid digest were performed as described by the manufacturer (New England Biolabs). In brief, the reaction consisted of: 1 µl of 10X Buffer X, 0.1 µl of restriction enzyme X and 1 µg of plasmid or sample for a total reaction volume of 10 µl in nanopure H₂O. The reactions were gently mixed by pipetting up and down and were incubated at 37 °C for more than 30 min. DNA fragments were separated on a 1% agarose gel (see above).

2.2.1.9 Removal of phosphate from DNA using calf intestine alkaline phosphatase CIP

Phosphatase DNA was performed as described by the manufacturer (New England Biolabs). In brief, reactions consisted of: 1 µl of 10X Buffer X, 3 µg of DNA, and 0.5 units CIP/µg vector DNA. Reactions were incubated for 60 min at 37 °C and then purified by agarose gel purification.

2.2.1.10 Ligation of DNA fragments

Ligations are performed as described by the manufacturer (New England Biolabs). In brief, reactions were set up on ice in microcentrifuge tube and consisted of: 2 μ l of 10X T4 DNA ligase buffer (thawed and resuspended at RT), 50 ng of Vector DNA (3 kb), 50 ng insert DNA (1 kb), and 1 μ l T4 DNA ligase (added last) in a total reaction volume with nanopure H₂O of 20 μ l. Reactions were mixed by pipetting up and down and incubated at room temperature for 10 min and then chilled on ice. Ligation reaction product (10 μ l) was transformed into 50 μ l chemically competent cells.

2.2.1.11 Annealing oligonucleotides

Annealing reactions consisted of 5 μ l of the respective complementary oligonucleotides (100 pmol/ μ l) in a 50 μ l, total volume of annealing buffer. The reaction was denatured at 99°C for 4 min, annealed at 99°C for 10 sec with a decrease of 1°C every 10 sec until the reaction reached 4°C. The reactions were placed on ice until used.

2.2.1.12 Phosphorylation of oligonucleotides

Oligonucleotides were phosphorylated as described by the manufacturer (New England Biolabs). In brief, reactions consisted of: 1 μ l T4 Polynucleotide Kinase (PNK) Buffer, 1 μ l ATP (10 mM), 1 μ l T4 PNK, 5 μ l of H₂O and 2 μ l of annealed oligos (see above). Reactions were gently mixed by pipetting up and down, incubated at 37 °C for 30 min and then incubated at 70 °C for 10 min to heat inactivation PNK.

2.2.1.13 PCR amplification

Amplification of cDNA was done by PCR using specific primers. All primers were resuspended in ddH₂O at 100 pmol/ μ l. The PCR reaction consisted of: 1X Buffer#1 For KOD HiFi DNA Polymerase, dNTPs (final concentration 0.2 mM), MgCl₂ (final concentration 1 mM), 10 to 90 ng/ μ l of Template DNA, 5' primer (final concentration 0.4 μ M), 3' primer (final concentration 0.4 μ M), 0.4 μ l of KOD HiFi DNA Polymerase (2.5 U/ μ l) in 50 μ l final volume.

Process	Time and temperature	Cycles
Initial Denaturation	1 min, 94 °C	1
Denaturation	15-60 sec, 95 °C	35
Annealing	15-60 sec, 50-70 °C	
Extension	15-60 sec, 72 °C	
Final Extension	10 min, 72 °C	1
Hold	∞ 4 °C	

Table 2.14: PCR amplification process time and temperature cycles

2.2.2 Design and generation of vectors

2.2.2.1 Generation of the pZOff vector

The pZOff vector was built on the backbone of the pEGFP-C1 vector (Clontech). The vector was modified to eliminate the resident multiple cloning site by digesting with BglII and BamHI followed by re-ligation (note that BglII and BamHI are compatible enzymes). Subsequently, a pair of synthesized oligonucleotides were inserted between the MluI and DraIII sites. (Note: the Sall, PvuI, and BamHI restriction sites in these oligos destroy the MluI and DraIII sites.) To create pZOff 1.0 H1 and pZOff 2.0 U6 vectors, the H1 or U6 promoter from the pSuper plasmid (Oligoengine) was inserted into the Sall and BamHI sites, respectively, of this modified pEGFP vector. (Note: shRNA transcription is driven in the opposite direction from EGFP, which increases the chance of producing shRNAs without disrupting polymerase-II EGFP transcription.)

2.2.2.2 Design and cloning of shRNAs

Short hairpin RNAs (shRNAs) were designed corresponding to the 21mer target sites using Ambion's criteria, which specifies oligo duplexes with 5' AA overhangs. The target sequence for the two Piccolo shRNAs were: Pclo6 5'-AAGGGCGCAGGGGCTGCCCAA-3' based on nucleotides (332-353) and Pclo28 5'-AAGTGCTGTCTCCTCTGTTGT-3' based on nucleotides 638-659 of the *Rattus norvegicus* Piccolo gene (GenBank accession no. NM_020098). For Bassoon, the Bsn16 shRNA 5'-AACACCTGCACCCAGTGTCAC-3' was based on nucleotides 652-673 of *Rattus norvegicus* Bassoon gene (GenBank accession no. NM_0191416). Sense and antisense oligodeoxynucleotides were purchased from Sigma or Protein and Nucleic Acid (PAN) facility at Stanford University, containing looped overhangs for BglII and Hind III. The following oligos were used: Pclo28FW, Pclo28RV, Bsn16FW, Bsn16RV Pclo28SCFW, Pclo28SCRV, Bsn16SCFW, Bsn16SCRV (SC is for scramble). Corresponding complementary strands were annealed in annealing buffer, using a Thermocycler, 2 µl of the annealed oligos were use for phosphorylation with T4-nucleotide kinase before being ligated with 0.2 µg of the pZOff 1.0 or 2.0 vectors open with BglII and HindIII endonucleases.

2.2.2.3 Generation of FUGW H1 vector

The lentiviral plasmid FUGW (Lois, Hong et al. 2002) was modified in several steps for expression of shRNAs, thus creating a new shRNA silencing vector FUGW H1. This was accomplished by first eliminating the EcoRI site in the FUGW vector. Oligonucleotides

(FUGW PacI Oligo FW and FUGW PacI Oligo RV) were then used to introduce EcoRI and BstBI sites to create a new multi-cloning site. The final FUGW H1 vector was created by moving the H1 promoter and/or different shRNA sequences from the pZOff vector into the EcoRI and BstBI sites.

2.2.2.4 Generation of EGFP::Syn1a, EGFP::SV2 and VAMP2::HRP constructs as well as the Pclo28 and Bsn16 shRNAs

EGFP Synapsin1a (EGFP::Syn1a) was incorporated into the FUGW vector by first removing the EGFP cassette from the vector with XbaI and inserting the EGFP::Syn1a sequences taken from pEGFP::Syn1a with NheI and XbaI. EGFP::SV2 was incorporated into FUGW by removing the EGFP cassette from the vector with AgeI and XhoI and inserting EGFP::SV2 sequences taken from pEGFP::SV2 with AgeI and XhoI. The coding sequence of horseradish peroxidase (HRP) was fused to VAMP2 by initially amplifying the coding region of HRP with two oligonucleotides (HRP FW and HRP RV) using the polymerase chain reaction (PCR). This fragment was subcloned into the BamHI & BsrGI site in a VAMP2 expressing vector (pVAMP2::EGFP) creating pVAMP2::HRP. Sequences encoding VAMP2::HRP flanked by NheI and MfeI restriction sites were then subcloned into the FUGW vector by removing the EGFP cassette with XbaI and EcoRI.

The creation of bicistronic vectors expressing each of these reporter molecules as well as the shRNAs for Piccolo (Pclo28) or Bassoon (Bsn16) were created by subcloning the H1-Pclo28 or H1-Bsn16 expression cassette into each of the aforementioned vectors using the corresponding NdeI or MluI and PacI sites in these vectors.

2.2.2.5 Creation of tricistronic lentiviral vectors

Double knock-down (DKD) of Piccolo and Bassoon was accomplished by creating tricistronic lentiviral vectors that expressed both a reporter gene and two shRNAs, one under the control of the H1 and the other U6 polymerase III promoter. Variants of these vectors are shown in Figure 3.19, and details are provided below for the creation of the DKD and scrambled control (SC) lentiviral vector (FUGW/DKD and FUGW/SC). The Bsn16/Pclo28 DKD vector was created by modifying the FUGW Pclo28 vector (containing Pclo28 shRNA with H1 promoter) in two steps. First, a 750 nucleotide stuffer sequence containing 5' BsiWI, EcoRI and BstBI and 3' BsiWI sites were inserted into the FUGW/Pclo28 vector opened at the BsiWI site. Second, the sequence containing the U6 promoter and Bsn16 shRNA in pZOff 2.0 (pZoff2.0/Bsn16), flanked by EcoRI and AccI sites was subcloned at the EcoRI and BstBI sites. The resulting FUGW vector drives expression of the Pclo28 shRNA via the

H1 promoter and the Bsn16 shRNA via the U6 promoter. These elements were separated by 750 nucleotides, an arrangement that allows for efficient lentivirus production and simultaneous knockdown of both Piccolo and Bassoon using FUGW/DKD. An identical strategy was used to generate the FUGW SC expressing scrambled sequence of Pclo28 (Pclo28SC) and Bsn16 (Bsn16SC). Note, the SC sequences retain the capacity to form hairpins yet are unable to bind Piccolo or Bassoon mRNA sequences. The final tricistronic vectors were created by opening each of the lentiviral vectors expressing EGFP-Syn1a, EGFP-SV2, or VAMP2-HRP with NdeI or MluI and PacI. The DKD or SC expression cassettes were moved into these vectors by isolating the NdeI or MluI and PacI inserts from the FUGW/DKD or FUGW/SC vectors, respectively.

2.2.2.6 Creating an shRNA-resistant (Bsn16) full-length Bassoon

A plasmid expressing EGFP 95-3938-Bassoon (Dresbach, Hempelmann et al. 2003) (NM_019146.) was used as a template for PCR. A two-step PCR was performed. The initial 5' and 3' PCR products were generated with two primer pairs: a 5' PCR fragment (Bsn AccIII FW/ Bsn 16 Silence mut RV) and 3' PCR fragment (Bsn 16 Silence mut FW/ Bsn AflIII RV). After purification of these fragments, they were used in a third PCR using the most 5' and 3' oligonucleotide primers (Bsn AccIII FW/ Bsn AflIII RV). This new fragment was purified, digested with the restriction endonucleases AccIII and AflIII before subcloning back in to the AccIII and AflIII sites within pEGFP 95-3938-Bassoon. The new construct is referred to as pEGFP-Bsn/SM16 (SM = Silent Mutation).

2.2.2.7 Construction of an adenoviral vector expressing mRFP-Bsn/SM16

An adenoviral vector expressing mRFP-BsnSM16 was created from pEGFP-Bsn/SM16. As a first step, EGFP was replaced with mRFP creating pmRFP-Bsn/SM16. To facilitate cloning of mRFP-Bsn/SM16 into the adenoviral transfer plasmid pLPBL, the AseI site in pmRFP-BsnSM16 was replaced with a short nucleotide segment containing MfeI, BsiWI, PacI and AseI sites using the oligonucleotide pair AseI/MfeI FW and RV. This oligo inactivates the 5' AseI site. Using the MfeI sites, the mRFP-Bsn/SM16 fragment from this vector was subcloned into the adenoviral shuttle vector pLPBL-1, which was opened with EcoRI. The new vector called pLPBL mRFP-Bsn/SM16 was sent to our collaborator Phillip Ng (Baylor College of Medicine, Houston, Texas, USA) for adenoviral production. At his adenoviral production facility, his team subcloned the mRFP-Bsn/SM16 fragment using flanking AscI sites into their final adenoviral vector, pHDAd. The new vector, pHDAd

mRFP-Bsn/SM16, was subsequently used to generate high titer adenovirus (Palmer and Ng 2005; Brunetti-Pierri, Ng et al. 2006). Resulting virus had a 1×10^{13} $\mu\text{f/ml}$ titer.

2.2.2.8 Creating mCherry-tagged Piccolo and Bassoon zinc finger domains

The zinc finger domains (ZF) from Piccolo and Bassoon were subcloned into the pmCherry-N2 expression vector using PCR to amplify each sub-region of these two molecules. pEGFP-Bsn/SM16 was used as a template for amplifying the first and second ZF domains from Bassoon (BsnZF1; BsnZF2), using the following oligonucleotide primers (Bsn HindIII ZF1 MutTS16 FW and Bsn BamHI Zn1 MutTS16 RV to amplify ZnF domain 1; Bsn HindIII ZF2 FW and Bsn BamHI ZF2 RV to amplify ZF domain 2). Using a similar strategy the two ZF domains from Piccolo were amplified by PCR. Here, a plasmid encoding the N-terminus of Piccolo (p7f EGFP; Fenster et al., 2001) was used as a template. The first and second ZF domains from Piccolo (PcloZF1; PcloZF2) were amplified with the following oligonucleotide pairs (Pclo HindIII ZF1 FW and Pclo BamHI ZF1 RV for PcloZF1 and Pclo HindIII ZF2 FW and Pclo BamHI ZF2 RV for PcloZF2). All four fragments were purified, digested with the restriction endonucleases HindIII and BamHI and subcloned into the pmCherry-N2 opened with HindIII and BamHI, creating the following new plasmids: pmCh/BsnZF1, pmCh/BsnZF2, pmCh/PcloZF1, and pmCh/PcloZF2.

To express these ZF in neurons, each mCherry tagged construct was placed into the lentiviral vector FUGW. This was accomplished by subcloning the NheI and MfeI fragments from each into the XbaI and EcoRI sites in FUGW. The new vectors are called: FUmCh/BsnZF1W, FUmCh/BsnZF2W, FUmCh/PcloZF1W and FUmCh/PcloZF2W.

2.2.3 Biochemical methods

2.2.3.1 Preparation of cellular lysates

Cellular lysates were prepared from transfected HEK293. Cells were harvested into homogenization buffer [ice-cold 1X-PBS supplemented with a protease inhibitor cocktail (Complete Protease Inhibitor Tablet, EDTA-free; Roche Molecular Biochemicals)], and then placed directly into loading buffer. Cellular lysates from infected hippocampal neurons were harvested directly into loading buffer.

2.2.3.2 Separating proteins via SDS-polyacrylamide electrophoresis

Proteins from cellular lysates were separated on a one-dimensional 3-8% Tris-Acetate gels (NuPAGE; Invitrogen) as described by the manufacturer. This system provided excellent

separation of large molecular weight proteins (60-600 kD) with NuPAGE Tris-Acetate sodium dodecasulfate (SDS) running buffer (Invitrogen). Alternatively, proteins were separated using Mini-Protean TGX (Tris-Glycine extended; Biorad) precast gels with Tris/Glycine/SDS running buffer (Bio-Rad). This allowed for excellent separation of proteins in a lower range (10-200 kDa).

2.2.3.3 Western blotting

After separation by SDS gel electrophoresis, proteins were transferred onto polyvinylidene fluoride membrane (PVDF) as described by the manufacturer (Invitrogen or BioRad).

2.2.3.4 Immunoblot detection of protein bands

Specific proteins were detected on PVDF membranes using standard immunoblotting techniques. In brief, following transfer, PVDF membranes were rinse with distilled water and placed in blocking solution for 15 min at 30 °C. PVDF membranes were then incubated with primary antibody in blocking solution or Tris-buffered saline+0.5% Triton (TBS-T) for 1 hr at 30 °C or overnight at 4 °C. Membranes were then washed once for 15 min in TBS-T. After washing, secondary antibody coupled with horseradish peroxidase (HRP) in TBS-T was added to the membrane for 1 hr at 30 °C. Membranes were then washed with TBS-T three times, and immuno-detection was carried out with WesternBright ECL HRP substrate for 5 min and visualized using high sensitivity x-ray film (LucentBluein) with an automatic developing machine (All Pro Imaging 100plus).

2.2.4 Heterologous cell culture techniques

2.2.4.1 Growth and passage of mammalian cell lines

To passage both HEK293T and COS-7 cells, media was removed from the cells using a vacuum apparatus within a laminar flow hood. Cells were washed with sterile 1X phosphate-buffered saline (PBS) and incubated with 2 ml 0.05% trypsin-EDTA at 37 °C for 5-10 min. Cells were dissociated by pipetting the solution up and down until a homogenous cell suspension was obtained. Cells were transferred to a 15 ml conical tube with media. Cells were centrifuged at 1000 g for 2 min, and the cell pellet was resuspended in the appropriate volume of media for plating or passing.

2.2.5 Hippocampal and glial primary cultures

2.2.5.1 Coverslip preparation

The coverslips for E18 hippocampal neuronal cultures were prepared as described previously (Banker and Goslin 1988; Tanaka 2002; Meberg and Miller 2003; Kaech and Banker 2006) with the following modifications. Specifically, square (22x22 mm) No.1 coverslips were cleaned in ceramic holders in nitric acid for 2 h, washed with MilliQ water multiple time and air dried at room temperature for 2 h. Coverslips were then placed in a 100 mm Petri dish, and a small drop of melted paraffin wax was added to each corner. Coverslips were sterilized by a germicidal ultraviolet lamp FG30T8 for 30 min and then treated with poly-L-Lysine (25 µg/ml, vendor) overnight at 37 °C in the cell culture incubator. Finally, coverslips were rinsed three times with sterile MilliQ water and maintained in plating media until use.

2.2.5.2 Glial culture preparation

Preparation, plating and growth of astrocytes from the cerebral cortex of P1-2 rats (type) was identical to that described previously (Banker and Goslin 1988; Tanaka 2002). Dissections for glial cell culture preparations were performed in a laminar flow hood. Several (2-4) postnatal rat pups (P1 or P2) were sacrificed using decapitation. Brains were removed and transferred to a dish containing HBSS plus 10 mM HEPES pH 7.4. Cortical hemispheres were isolated and the meninges carefully stripped away using fine forceps. The tissue was then minced into small pieces using scissors. The pieces of cortex were transferred into a 50 ml centrifuge tube with 12 ml of HBSS with 1.5 ml each of 1% DNase and 2.5% Trypsin with EDTA and then incubated at 37 °C for 15 min. The trypsin reaction was stopped with 5% Fetal Bovine Serum (FBS) and perform the trituration step, the tissue was centrifuged at 1000xg for 5 min. Finally, the glial pellet was resuspended in glial medium and grown in a T75 flask for at least 14 days *in vitro* (DIV) before sub-culturing.

2.2.5.3 Sub-culturing rat glial cells

Glial cultures were harvested for replating once cells reach approximately 80-90% confluence. Microglia contaminating these cultures were removed by a quick smack of the flask on a tabletop. The media was then removed, and the cells were washed with 10 mL HBSS per flask before incubating the cells for 5-10 min at 37 °C in 10 ml of 0.05% Trypsin with EDTA. After the addition of glial media (10 ml) to stop the reaction, glia cells were detached from the flask by pipetting the media up and down several times. Cells were collected in a 15 ml conical tube, centrifuged at 1000 g for 5 min at room temperature and

resuspended in glial media. The cells from one flask were split and transferred into thirty 60 mm plates five days before hippocampal neuron preparation.

2.2.5.4 Hippocampal neuronal culture preparation

Hippocampal cultures were prepared using a modified Banker culture protocol (Banker and Goslin 1988; Tanaka 2002; Meberg and Miller 2003). Primary cultures of hippocampal neurons were prepared from embryonic E18-19 Sprague Dawley rats (Charles River). Pregnant rats were euthanized with CO₂ as approved by the Stanford Administrative Panel on Laboratory Animal Care (APLAC), the IACUC at Stanford University, and the uterus was removed and placed in a sterile 100 mm Petri dish. The remaining steps were performed in a laminar flow hood. Ideally, hippocampal neurons were prepared on embryonic day 18 when the fetus was approximately 25 mm from crown to rump. From the heads of decapitated fetuses, the brain was removed and placed in calcium- and magnesium-free HBSS. Each hippocampus was removed under a dissection microscope. Meninges were stripped away, and the isolated hippocampi were placed in a 60 mm Petri dish in HBSS. Hippocampi (16 to 20 hippocampi) were then transferred to a 15 ml centrifuge tube (Falcon) with 5 ml of TrypLE and incubated at 37 °C for 30 min. The trypsin was then removed, and the hippocampi were washed three times with 14 ml of HBSS plus 10 mM HEPES pH 7.4 for 5 min per wash. The final volume was brought to 3 ml. Cells were then dissociated by pipetting up and down, first with a normal Pasteur pipette and then with a fire polished pipette with a tip of nearly half the normal diameter (~1mm). Continuous pipetting was done until there was a homogenous single cell suspension. Cells were counted using a hemocytometer. Approximately 800,000 cells are then added to a 100 mm dish containing 6 poly-L-lysine-treated coverslips in 10 ml of plating media. After 1 hr, coverslips with neurons attached were flipped over and transferred to 60 mm dishes containing glial cells in 4 ml of Neurobasal media. Our standard plating density was ~130,000 cells per coverslip. Note: the coverslips were turned over so that the neurons were facing down, towards the glial cells. After three days, 3 ml of medium was removed and replaced with 3 ml of fresh Neurobasal media and weekly thereafter.

2.2.6 Gene transfer into cells

2.2.6.1 Cell transfections with Lipofectamine 2000

HEK293T, COS-7 and neuronal cells were transfected with Lipofectamine 2000 (Invitrogen) as described by the manufacturer. Briefly, 15 µl of Lipofectamine 2000 was combined with 0.5 ml OptiMEM (Invitrogen) (solution A), and 10 µg of plasmid DNA with 0.5 ml OptiMEM media (solution B). Solutions were incubated for at least 5 min at room

temperature before combining the solutions together. For complete complex formation, this mixture was incubated for at least 20 min at room temperature. Finally, the 1.0 ml transfection mixture was added to cells in 10 cm Petri dish in a “spiral” pattern, starting from the periphery of the plate towards the center of it. Experiments were performed 24 to 60 hrs after transfection.

2.2.6.2 Cell transfections by electroporation

Plasmids were also introduced into neurons using electroporation. Here, electroporation of a cell/plasmid suspension was conducted in Gene Pulser Cuvettes (Bio Rad Laboratories; 0.4 cm gap width) with approximately 4×10^6 cells in 500 μ l of glia-conditioned media and 40 μ g of plasmid using a Gene Pulser (Bio-Rad Laboratories) with the following settings: 0.250 kV with Set High Capacitance 0.975 (μ F*1000).

2.2.6.3 Lentivirus production

Lentivirus was produced by transfecting a three-plasmid vector system, comprised of a shuttle plasmid (e.g. FUGW or FUSyn::EGFPW) and two packaging plasmids pCMV Δ R8.9 and pHCMV VSVg into HEK293T cells as described previously (Lois, Hong et al. 2002). In brief, HEK293T transfections were conducted on confluent (60 to 80%) cell cultures with Lipofectamine 2000 (Invitrogen), using 10 μ g of 10 kb of shuttle vector, 7.5 μ g of pCMV Δ R8.9 and 5 μ g of pHCMV VSVg and 50 μ l of Lipofectamine 2000 per 10 cm Petri dish. The media was changed 16 to 24 hr after transfection with Neurobasal media supplemented with B-27 and Glutamax and maintained at 32°C and 5% CO₂ in an incubator. The virus-containing medium was collected 48 to 56 hr post-transfection, passed through a 0.45 μ m filter to remove cell debris, and frozen at -80 °C in a cryogenic container. The viral titer was determined by fluorescence analysis of infected HEK293T cells, the total number of cells infected correspond to infectivity unit (I.U).

2.2.6.4 Lentivirus infection of neurons

Lentiviral infection of culture hippocampal neurons was conducted after transferring neuron/coverslips into 60 mm dishes. Under these conditions, we routinely use 10 μ l of undiluted high titer virus/dish to infect 20-30% of cells (for imaging experiments) and 100 μ l/dish to super-infect approximately 100% of cells (for all biochemical experiments).

2.2.7 Immunocytochemistry and electron microscopy

2.2.7.1 Lorene's fixative solution

Paraformaldehyde was dissolved in H₂O to create a 4% solution. To adjust the pH for improved solubility, a few drops of 10N NaOH was added while stirring and heating in the fume hood. Once dissolved, the solution was allowed to cool at room temperature. PIPES, HEPES, EGTA, MgCl₂ and sucrose were all added, and the final solution was adjusted to a pH of 7.3-7.4. The solution was adjusted to the appropriate final volume with H₂O and was frozen in aliquots at -20°C. For use, the solution was thawed at 37°C and used (do not refreeze).

2.2.7.2 Immunohistochemistry

Hippocampal neuronal cultures, grown for 5-21 DIV, were fixed with either Lorene's fixative solution for 10 min or 100% ice-cold methanol for 20 min. Cells were then permeabilized with 0.5% Triton X-100 in 1X PBS solution for 5 min, washed in 1X PBS, incubated in blocking solution for 15 min at room temperature, and incubated overnight at 4°C with primary antibodies diluted in blocking solution or for 2 hr at RT. Afterwards, cells are rinsed 3-4 times in 1X PBS, incubated for 1 hr at RT or at 4°C overnight with secondary antibodies in blocking solution, rinsed again 3-4 times in 1X PBS followed by a final rinse in deionized water, dried, and mounted in mounting solution (Vectashield).

2.2.7.3 Image acquisition for immunocytochemistry

Fluorescent images were acquired using a Zeiss Axiovert 200M microscope equipped with oil immersion 100× Plan-Neofluar (NA 1.3) or 40× Plan-Neofluar (NA 1.3) objectives (Zeiss) and the following filter sets BFP, FITC and Texas Red (Chroma, VT). Fluorescence images were acquired using OpenLab software (Molecular Devices) and a CCD-camera (Hamamatsu ORCA-ER; 1344 x 1022 resolution, 12 bits/pixel). Some images were acquired using a spinning disk confocal microscope (Perkin Elmer) built on a Axiovert 200M microscope (Zeiss) equipped with an argon/krypton laser (Melles Griot 43 series), using a 63x Plan-Apochromat objective (NA 1.4), Photometrics Cascade 512B digital camera (Roper Scientific) and MetaMorph software (Molecular Devices).

2.2.7.4 Electron microscopy of VAMP2-HRP expressing neurons

Ultrastructural analysis of glutamatergic asymmetric synapses was performed on dissociated cultures of hippocampal neurons transfected by electroporation at the time of plating (e.g. with pZOff-VAMP2-HRP). Samples were fixed with 2.5% glutaraldehyde or 4%

formaldehyde/0.5% glutaraldehyde in 0.15 M cacodylate buffer for 1 hr and processed as described previously (Micheva and Smith 2005) with a few modifications. Following fixation, neurons were incubated with 1 mg/mL diaminobenzidine (DAB) in 50 mM Tris, pH 7.5 for 10 min. 0.01% H₂O₂ (Sigma) was added to the solution for 30 min at room temperature to stimulate HRP-mediated DAB precipitation. After extensive washing, neurons were prepared for electron microscopy by a microwave irradiation protocol described previously in detail (Micheva, Buchanan et al. 2003). Following infiltration in Embed 812 (EMS), glass coverslips were removed by dissolution in hydrofluoric acid. Ultrathin 60 nm sections were cut with an ultramicrotome (Ultracut UCT; Leica) and placed on copper grids. Samples were post-stained with 5% uranyl acetate dissolved in ultrapure water for 15 min followed by 4 min of staining in 0.2% lead citrate. Grids were extensively rinsed in water during and after post-staining. Samples were imaged with a JEM-1230 transmission electron microscope (JEOL, Peabody, MA) at 80 kV accelerated voltage using a Gatan (Pleasanton, CA) 791 CCD camera. All sample processing and electron microscopy were done in the Cell Sciences Imaging Facility at Stanford University.

2.2.8 Live cell microscopy and analysis

2.2.8.1 Live imaging of XFP-tagged synaptic proteins

All live cell imaging experiments were performed on a custom-built (S. Smith and N. Ziv) laser scanning confocal microscope built on an Axiovert 100TV microscope (Zeiss) equipped with a 40x Plan Neofluar oil immersion objective (1.3 NA; Zeiss), 488 nm and 514 nm lasers (Coherent; Sapphire 488-20CDRH and Compass 215M-20) or a custom-built (C. Garner) laser scanning confocal microscope built on an Axiovert 200M (Zeiss) equipped with a 40x objective (1.3 NA; Zeiss Plan Neofluar), 488-514 nm laser (Spectra-Physics). Both systems were driven by a custom-written acquisition software, OpenView (N. Ziv, Technion Institute, Haifa, Israel). Neuronal coverslips were mounted in a custom-built chamber designed for perfusion and electrical stimulation, heated to 37 °C by a forced air blower and perfused with Tyrode's saline solution.

2.2.8.2 FM loading/destaining of neuronal synapses

Functional presynaptic boutons were labeled with FM4-64 or FM5-95 dye (Molecular Probes) by incubation in high K⁺ Tyrode's solution containing 1 µg/ml FM dye (1.64 M of FM4-64 or 1.76 M of FM5-95) for 60 sec followed by normal Tyrode's + FM dye for 30 sec. Neurons were then washed for 5 min before imaging. Destaining was performed by electrical stimulation at the following frequencies (10 Hz, 5 Hz, 2 Hz) and time intervals (180 sec, 90

sec, 30 sec) specified for each experiment or by perfusion of high K^+ Tyrode's solution for 60 sec.

To measure % FM colocalization with EGFP::SynIa clusters, the number of FM-containing clusters were divided by the total number of EGFP::SynIa clusters and multiplied by 100. To calculate relative FM intensities at boutons containing or lacking Piccolo, FM intensity values for infected neurons were normalized against those from neighboring uninfected neurons in the same field of view, enabling cross-coverslip comparisons.

For FM destaining experiments at 5 and 10 Hz, the total number of action potentials elicited and images acquired were kept constant. Thus, at 10 Hz stimulation, images were acquired every 5 sec for a total of 90 sec, while at 5 Hz they were acquired every 10 sec for a total of 180 sec. In all cases, intensity values for a given FM punctum at each time point were expressed as a % of its initial fluorescence intensity prior to destaining using the following equation: (FM intensity at a given time point t /initial FM intensity) x 100. For each condition (e.g. EGFP::Syn), intensity curves that did not exhibit FM destaining (i.e. values >90% for all time points) were eliminated from the analysis. Remaining curves were pooled, averaged, and plotted using Excel (Microsoft).

2.2.8.3 Calculating the size of the readily releasable pool (RRP) of SV as well as neurotransmitter release probability (P_r)

Boutons were loaded using high K^+ Tyrode's solution to label the total recycling pool (TRP) of SV/bouton. RRP release was induced with either by adding 500 mM sucrose (60 sec) or low frequency electrical stimulation (2 Hz for 30 sec; RRP release). Total FM destaining was induced with high K^+ stimulation for 60 sec (background). To calculate the RRP size, puncta intensity values were put into the following equation to express the RRP as a % of the TRP: $[(TRP \text{ label} - \text{background}) - (RRP \text{ release} - \text{background})] / (TRP \text{ label} - \text{background}) \times 100$. To calculate P_r , the TRP was loaded with FM5-95 using high K^+ Tyrode's solution, and release of the RRP was induced using 2 Hz for 30 sec electrical stimulation. During stimulation, images were acquired every 5 sec. Intensity values were expressed as % initial fluorescence intensity; those exhibiting minimal destaining (values >95% for all time points) were eliminated from the analysis, and remaining curves averaged and plotted as described above.

2.2.8.4 Fluorescent recovery after photobleaching (FRAP) acquisition and analysis

EGFP::SynIa or EGFP::SV2 puncta were bleached to approximately 20% of their initial fluorescence by a high intensity laser beam (488 nm wavelength). Images were taken 15 x 1

minute to monitor fluorescence recovery for EGFP::Syn1a, and 4 x 1 minute followed by 6 x 5 min for EGFP::SV2. For each time point, intensity values were expressed as % starting fluorescence prior to bleaching. To control for non-specific photobleaching during image acquisition, intensity of bleached puncta were normalized against those of unbleached puncta for each time point, as described (Tsuruel, Geva et al. 2006), with the following equation: $[(\text{intensity of bleached Synapsin punctum at time } t)/(\text{average intensity of all unbleached puncta in field of view at time } t)] \times 100$. To control for variability in the extent of bleaching for each puncta, values were further normalized, making zero the default value for bleached puncta and enabling us to pool and average all recovery curves for a given condition. Tau values were calculated using a custom macro written in Excel (N. Ziv; see (Tsuruel, Geva et al. 2006)).

2.2.8.5 Defining EGFP::Syn1a dispersion kinetics

Dispersion of EGFP::Syn1a was induced by electrical stimulation (10 Hz, 90 sec), as previously described (Chi, Greengard et al. 2001). Puncta intensity values were expressed as % initial fluorescence intensity prior to stimulation. Curves for all EGFP::Syn1a puncta were combined for a given condition, averaged, and plotted. For this analysis, puncta that did not exhibit dispersion (% initial fluorescence values > 90 for all time points) were excluded.

To compare extent of Synapsin dispersion to that of FM destaining, EGFP::Syn1a intensity was monitored during the 5 Hz destaining experiment (see FM destaining protocol above).

To assess the role of CaMKII α in Synapsin dispersion, coverslips were perfused with normal Tyrode's solution containing 10 μM KN-62 ($\text{IC}_{50} = 0.9 \mu\text{M}$) (Tocris) and incubated in the drug for 20 min prior to eliciting dispersion. EGFP::Syn1a intensity was monitored either prior to stimulation and every 5 sec during stimulation (for dispersion curves) or prior to stimulation and at the last time point ($t=90$ sec) (for bar graphs).

FM5-95 destaining was also monitored after incubation with 10 μM KN-62. For this experiment, boutons were first loaded with FM5-95 using high K^+ stimulation as described above. After waiting 15 min to allow for some recovery of EGFP::Syn1a after stimulation, cells were incubated for an additional 20 min in 10 μM KN-62. SV exocytosis was then elicited by 5 Hz stimulation for 180 sec, and both FM intensity and EGFP::Syn1a intensity were monitored over this time period (images taken every 10 sec). Destaining curves were then plotted as described above and compared with destaining curves from untreated coverslips of cultures infected with LV/EGFP::Syn1a or LV/EGFP::Syn1a/Pclo28.

2.2.8.6 Quantification of EGFP::Syn1a dispersion and FM destaining kinetics

As described previously (Chi et al., 2001), dispersion or destaining curves for EGFP::Syn1a or FM4-64 puncta were obtained using the equation: $(F_0 - F_t)/F_0$ where F_0 = initial fluorescence intensity prior to stimulation (obtained by averaging puncta intensities from 2 images taken 5 sec apart) and F_t = fluorescence intensity at each of the 18 time points t during stimulation, from $t=5$ to $t=90$ sec. Curves for each puncta in a field of view were pooled and averaged to give a single destaining curve per coverslip. Curves for individual puncta containing values > 0 for time points > 20 sec were eliminated from the analysis (to correct for imperfections in the puncta-tracking software).

To calculate the average extent of EGFP::Syn1a dispersion or FM4-64 destaining for each coverslip, the $\Delta F/F_0$ intensity values for the last five time points ($t = 70-90$ sec) were averaged to give $avg Ft=70-90$ (see Fig. S2). To express % increase in EGFP::Syn1a dispersion or FM destaining for condition B (i.e. Pclo28 knockdown) vs. condition A (i.e. wild-type), both imaged on a given day, the following equation was used: $[(avg Ft=70-90 (B) / avg Ft=70-90 (A)) - 1] \times 100$. Resulting data points were then plotted on a column graph, enabling comparisons between experiments performed in different batches of neurons. This measurement was used to compare phenotypes induced by pharmacological or genetic manipulation to the typical conditions observed in wild-type neurons.

To express % decrease in dispersion or destaining for a coverslip of condition A (i.e. wild-type neurons) vs. condition B (i.e. Pclo28-expressing neurons), the same general strategy was used with the following equation: $[1 - (avg Ft=70-90 (A) / avg Ft=70-90 (B))] \times 100$.

2.2.8.7 Image analysis of live cell experiments

Image analysis and quantification were performed with custom-written OpenView software (Noam Ziv) and Excel (Microsoft). GraphPad Prism (GraphPad software, Inc.) was used for curve fitting, graph plotting, and statistical analyses.

3. Results

3.1 Optimization and characterization of cryopreserved astrocyte cultures and hippocampal neuronal cultures

Dissociated hippocampal neuronal cultures remain the workhorse of many molecular and cellular neuroscience laboratories due to the fact that they are well characterized and currently serve as the best system for experimentation in living neurons. Low-density embryonic hippocampal neurons in the “Banker” style (Banker and Goslin 1988; Tanaka 2002; Meberg and Miller 2003; Kaech and Banker 2006) offer a culture system that is amenable to cells manipulation, gene transfer, electrophysiology and biochemistry, for example. However, these types of cultures can be labor intensive and time consuming. Strategies that would allow both the expansion and preservation of astrocytes would reduced the need for extra animals and the weekly time commitment to dissect, dissociate, and culture these cells. However, there are concerns that repeated passaging of astroglia led to alterations in cellular phenotypes, the overgrowth of macrophages and microglia and the inability of astroglia to support the growth and differentiation of hippocampal neurons. In an attempt to streamline this process, detailed optimization and characterization of both cryopreserved astrocytes and hippocampal neuronal cultures were done.

3.1.1 Cryopreservation of glial cells

For an initial characterization, astroglial cultures were frozen and thawed three times and then examined for their basic morphological features, including a large flat cell appearance, immunoreactivity for Glial Fibrillary Acidic Protein (GFAP) and robust β -actin staining. No differences were seen in morphology, GFAP or β -actin staining between any of these cells even after the third freeze/thaw (Figure 3.1A).

Contamination of astrocyte cultures with macrophages and microglia is a major concern that can adversely affect the growth of cultured hippocampal neurons. As previously reported (Banker and Goslin 1988), macrophage and microglia were found to increased in number in our cultures, as determined by morphology and appearance. Microglia were seen as round phase bright, loosely attached cells resting on top of the astroglial monolayer, while macrophages were identified by morphology. Intriguingly, these cells were readily removed or reduced by a quick smack of the flask on a flat surface prior to washing and replating. Only very few microglia were found in astroglial cultures after the second passage.

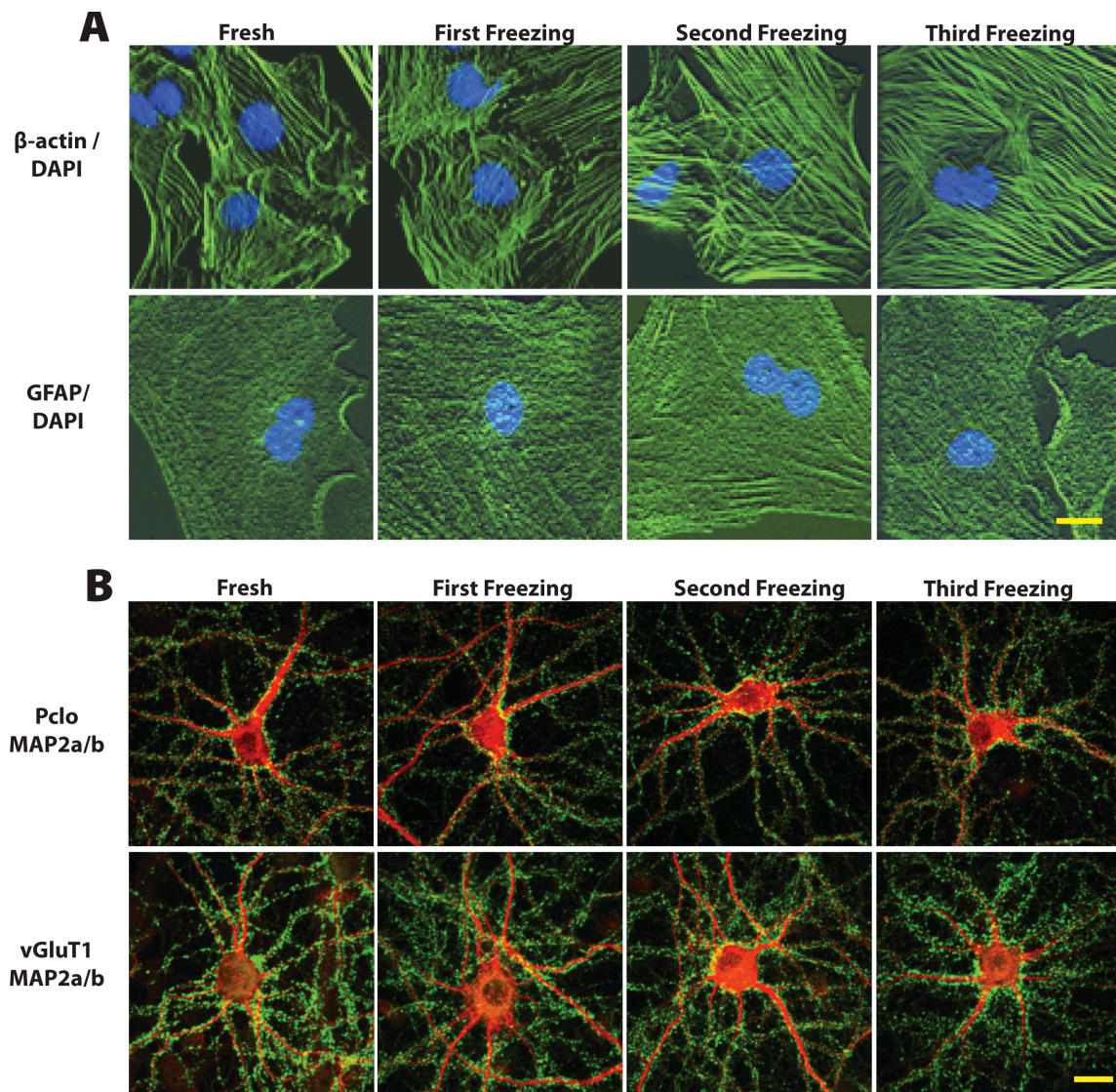


Fig. 3.1 Cryopreserved glia support the growth and differentiation of rat hippocampal neurons

(A) Glia prepared from P1 rat cerebral cortex were frozen and then thawed 1-3 times before replating. Glial cells were grown on coverslips for 1 week prior to fixation in 4% PFA and immunostained with antibodies against β -actin (upper images; green; Alexa 488) or GFAP (lower images; green; Alexa 488) and DAPI (blue). (B) Freshly prepared hippocampal neurons from E18 rats were plated on coverslips and grown in the presence of glia that had been frozen and thawed 1-3 times. Neurons were then fixed after 21 DIV and immunostained with antibodies against Piccolo (upper images; green; Alexa 488) or vGluT1 (lower images; green; Alexa 488) and MAP2a/b (red; Alexa 568). Scale bars = 10 μ m.

Next, cryopreserved astrocytes that had undergone three cycles of growth and cryopreservation were evaluated if they could support the growth and maturation of hippocampal neurons. Hippocampal neurons from E18 rats cultured in the presence of freshly prepared astrocytes grew and differentiated into mature cells with elaborate axon and dendritic arbors and extensive synaptic contacts (Figure 3.1B). Moreover, astroglia, grown and refrozen three times, also supported the survival of the neurons for 3-4 weeks with no visible differences in morphology and number of synapse per dendrite from freshly prepared glia (Figure 3.1B).

These results indicate that repeated freezing and passaging of astroglia prepared from the rat cortex does not adversely affect their ability to support the long-term survival (three week) and differentiation of co-cultures of dissociated rat hippocampal neurons. This suggests that cryopreservation can provide a significant savings in time and costs with respect to resources, animals, and glial cell production when taking these simple measures.

3.1.2 Viability of cryopreserved dissociated hippocampal neurons

A further improvement to streamline Banker style cultures would be the ability to cryopreserve dissociated hippocampal neurons. Although cryopreservation of hippocampal tissue has been achieved previously (Jensen, Sorensen et al. 1984; Sorensen, Jensen et al. 1986), cryopreservation of dissociated hippocampal neurons has not yet been described. To this end, focus was placed on the type of cryomedia to improve neuronal viability.

Traditional cryopreservation of cells and brain tissue typically uses a cryomedia of growth media and 10% dimethyl sulfoxide (DMSO) (Paynter 2008). Slow freezing of freshly prepared and dissociated neuron in Neurobasal media supplemented with B-27 and GlutaMAX failed to yield a significant number of viable cells that differentiated into neurons when cultured with fresh astroglia (Figure 3.2A). To improve hippocampal neuron viability, a cryopreservation media typically used for sensitive cell lines [recommended by AMB at UMBC (Applied Molecular Biology at University of Maryland, Baltimore County) and Atlanta Biologicals] consisting of 90% Fetal Bovine Serum (FBS) and 10% DMSO was tested. Greater than 60% of the neurons survived after being previously frozen in 90% FBS/10% DMSO and stored in liquid N₂ for 9 months (Figure 3.2A).

As neurons are generally vulnerable to glutamate toxicity, blockers of NMDA and AMPA receptors (10 μ M APV and 50 μ M CNQX, respectively) were added to the freezing media in an attempt to enhance the viability of frozen neurons. This manipulation failed to further improve viability of neurons frozen in 90% FBS/10% DMSO. Furthermore, hippocampal neurons frozen in a defined optimized serum substitute used in the culture neuronal culture media (B-27) with 10% DMSO with and without 10 μ M APV and 50 μ M CNQX both failed to significantly support the survival of frozen neuron (< 10% survival; Figure 3.2A).

3.1.3 Morphological characterization of cryopreserved neurons

In addition to cell viability, morphology and synapse formation are other important characteristics for experimental use of these cultures. In an initial set of experiments, hippocampal neurons frozen in 90% FBS/10% DMSO were studied for the number of

dendrites. Neurons were fixed after 5 to 6 DIV with 4% paraformaldehyde (PFA) and stained with antibodies against the dendritic microtubule protein MAP2a/b. Images revealed that freshly prepared and frozen neurons exhibited nearly identical neuronal morphologies (Figure 3.2B). To confirm this conclusion, the total number of MAP2a/b positive primary dendritic process were quantified (Figure 3.2C) as well as the number of dendritic branches per cell (Figure 3.2D). No significant difference between neurons prepared freshly or frozen could be found for any of these parameters.

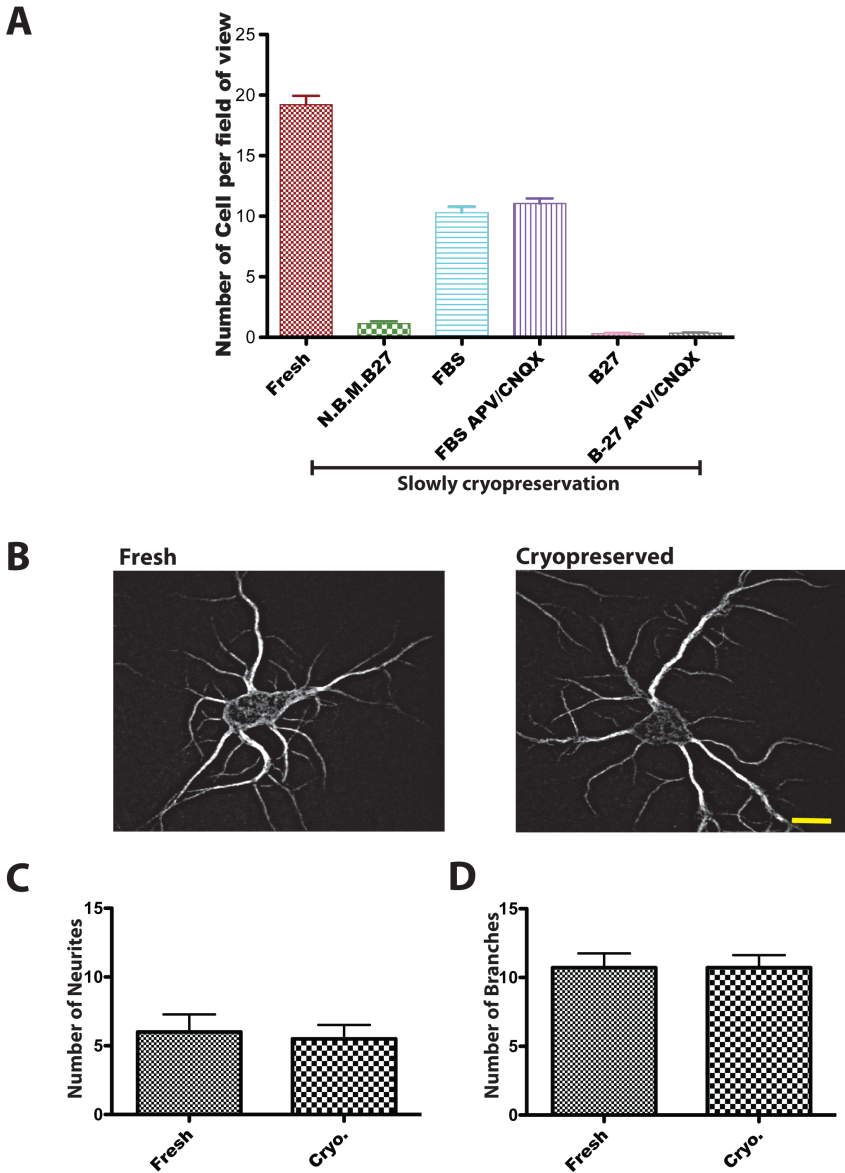


Fig. 3.2 Viability of cryopreserved neurons and normal differentiation

(A) The viability of fresh or cryopreserved neurons was analyzed by determining the number of cells/field of view with a 10x objective. Equal numbers of freshly prepared hippocampal neurons were either plated 1) directly or first frozen in 2) Neurobasal media supplemented with B27, 1X GlutaMAX and 10% DMSO, 3) 90% FBS and 10% DMSO; 4) 90% FBS and 10% DMSO plus CNQX/APV; 5) B27 media or 6) B27 media with CNQX/APV before plating. After 14 DIV, the cells were fixed and the number of neurons/field of view was determined. ($p < 0.0001$, ANOVA; $n =$ total number from 3 separate experiments, each experiment with 8 different coverslips and ~30 different fields of view per coverslip. (B) Freshly prepared neurons and cryopreserved neurons plated

in the presence of glia, after 6 DIV cells were fixed and immunostained with antibodies against MAP2a/b. **(C)** Quantification of the number primary neurites of freshly plated and cryopreserved neurons. $p < 0.0001$, t-test; $n=?$. **(D)** Analysis of the number of branch points per neuron of freshly prepared and cryopreserved neurons. $p < 0.0001$, t-test, $n = 5$ separate experiments, each consisting of 4 different coverslips with approximately 20 different cells per coverslip. Scale bars = 10 μ m. Error bars are SEM.

In a second set of experiments, cryopreserved neurons were examined for their ability to form synapses. Here neurons were grown for 14 DIV before fixing and staining with antibodies against MAP2a/b, the synaptic vesicle protein Synaptophysin and postsynaptic density protein Homer 1 (Figure 3.3A). Once again, neurons were observed to exhibit complex MAP2a/b positive dendritic arbors that resembled those from freshly plated neurons. Moreover, numerous Synaptophysin and Homer 1 positive puncta were found to colocalize and decorate these dendritic profiles (Figure 3.3A). Image analysis revealed that pre and postsynaptic markers colocalize to similar extents between freshly plated and cryopreserved neurons. These data indicate that neuronal cells that survive freezing in 90% FBS/10% DMSO are able to differentiate normally.

3.1.4 Characterization of lentiviral use in cryopreserved neurons

Since delivering recombinant molecules and/or short hairpin RNAs (shRNAs) into neurons with lentivirus is a critical method for studying the function of specific neuronal proteins at or near endogenous levels (Leal-Ortiz, Waites et al. 2008; Waites, Specht et al. 2009; Torres, Barra et al. 2010; Hua, Leal-Ortiz et al. 2011; Waites, Leal-Ortiz et al. 2011) (see also section 3.2 below), particularly for this work, cryopreserved neurons frozen in 90% FBS/10% DMSO were infected with lentivirus pre and post thawing to determine whether this altered their viability and/or ability to differentiate. For comparison, neurons were infected with a lentivirus for EGFP expression in the following conditions: 1) freshly prepared neurons infected one day after plating; 2) frozen and thawed neurons infected one day after plating; and 3) neurons infected prior to freezing that were frozen and thawed. Neurons were fixed and analyzed after 6 DIV (Figure 3.3C). EGFP-positive neurons were detected in both axons and dendrites irrespective of the conditions (Figure 3.3C).

In a second set of experiments, synapses formed between neurons that were infected either before or after being cryopreserved were analyzed. For these experiments, neurons were infected with an EGFP-tagged Synapsin1a (EGFP::Syn1a) to mark the presynaptic boutons of infected neurons. Neurons were maintained in culture for 16 DIV before fixation and were stained with antibodies against MAP2a/b to identify dendritic arbors and Synaptophysin to visualize synaptic vesicle clusters (Figure 3.3D). EGFP::Syn1a positive

puncta were detected situated on the spines of MAP2a/b-positive dendrites that also colocalized with Synaptophysin positive puncta. This pattern was observed irrespective of whether neurons were freshly prepared and infected one day after plating, frozen and infected one day after plating or infected before freezing (Figure 3.3D).

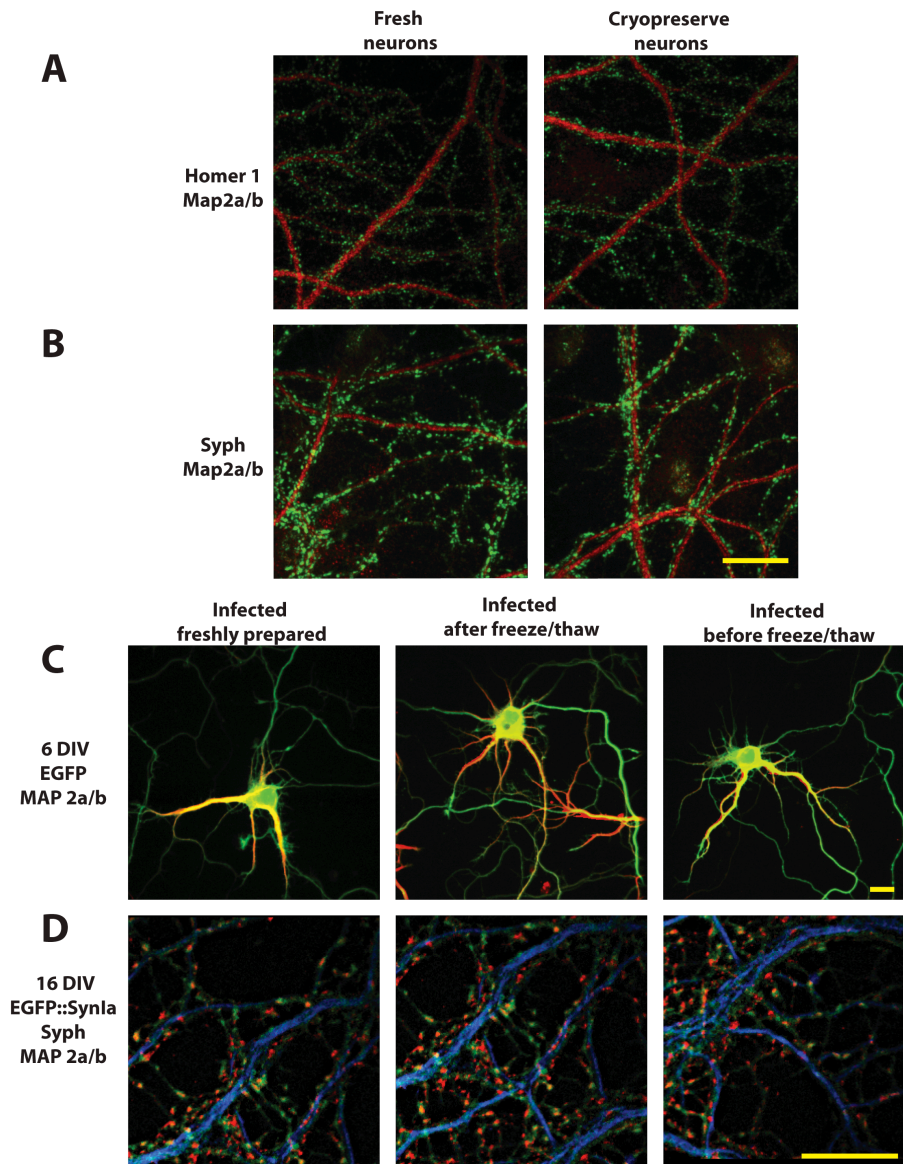


Fig. 3.3 Synaptic contacts and lentiviral infections of cryopreserved hippocampal neurons

Images of freshly prepared or cryopreserved neurons grown for 14 DIV before fixing in 4% PFA and immunostaining with antibodies against MAP2a/b (red; Alexa 568) and (A) Homer 1 (green; Alexa 488) or (B) Synaptophysin (green; Alexa 488). Images reveal the presence of synapses along MAP2a/b-positive dendrites. (C) Freshly prepared or cryopreserved neurons infected with FUGW either on the day of plating or before freezing. After 6 DIV cells were fixed and immunostained with antibodies against MAP2a/b (red; Alexa 568). Soluble expressed EGFP (green) fills both axonal and dendritic processes. (D) Fluorescent images of freshly prepared or cryopreserved neurons infected with FU-EGFP::Syn1a-W either on the day of plating or before freezing. After 16 DIV, neurons were fixed and immunostained with antibodies against MAP2a/b (blue; Alexa 350) and Synaptophysin (red; Alexa 568). EGFP/Syn1a positive puncta (green) are seen to colocalize with Synaptophysin puncta (red) along MAP2a/b positive dendrites (blue). Scale bars = 10 μ m.

The identification of these EGFP-Syn1a puncta as synaptic was confirmed by immunostaining each of these cultures with antibodies against MAP2a/b and the postsynaptic dendritic spine protein Homer1 or the presynaptic active zone protein Piccolo (Figure 3.4A and 3.4C). Together, these data demonstrate that freezing freshly dissociated hippocampal neurons in 90% FBS/10% DMSO does not adversely affect their ability to be infected with lentivirus either before or after freezing, nor their ability to survive for more than 2 weeks in culture and differentiate into mature neurons (Figure 3.4B & D).

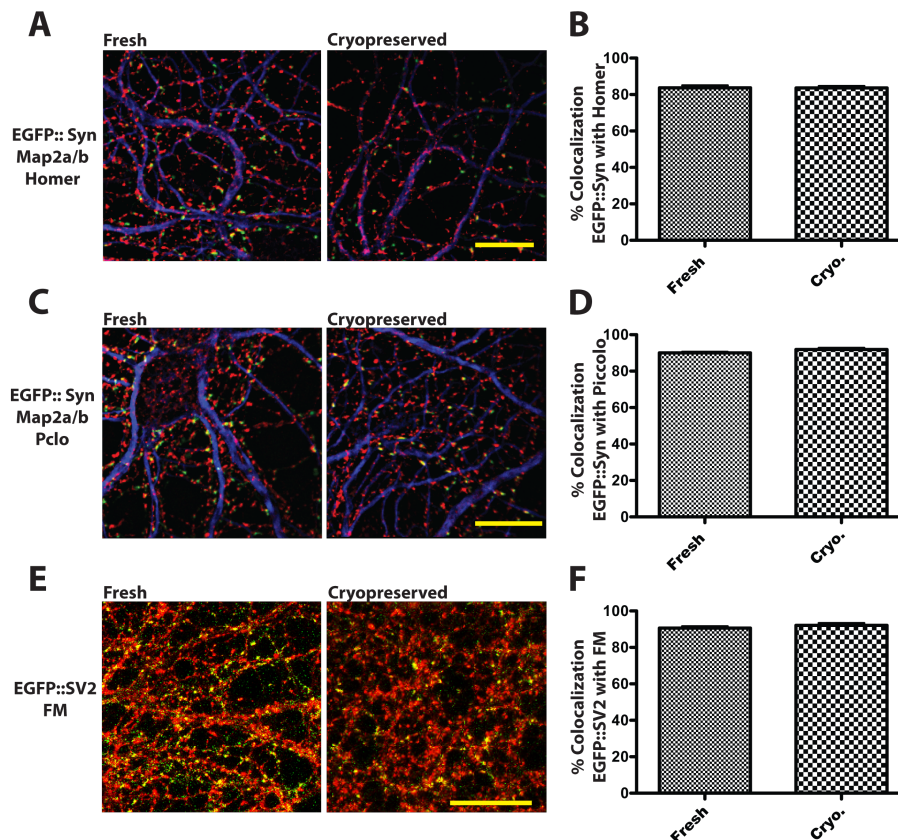


Fig. 3.4 Infected cryopreserved neurons form normal numbers and functional synapses Fluorescent images of freshly prepared or cryopreserved neurons infected with FU-EGFP::Syn1a-W (green) on the day of plating. After 16 DIV, neurons were fixed and immunostained with antibodies against MAP2a/b (blue; Alexa 647) and (A) Homer 1 (red; Alexa 568) or (C) Piccolo (red; Alexa 568). Quantification reveals that over 80% of the EGFP::Syn1a puncta colocalize with (B) Homer1 or (D) Piccolo (Pclo) puncta. (E) Fluorescent images of freshly prepared or cryopreserved hippocampal neurons infected with FU-EGFP::SV2-W (green) on the day of plating. After 14 DIV, infected neurons were mounted in an imaging chamber and stimulated with 90 mM KCl in the presence of FM4-64 (red). (F) Quantification of colocalization of EGFP::SV2 puncta (green) with FM4-64 (red) puncta. ($p < 0.0001$, t-test) $n = 3$ different experiments, each experiment 4 different coverslip and each coverslip ~10 different cells. Scale bars = 10 μm. Error bars are SEM.

In a third set of experiments, cryogenic neurons infected with lentivirus were assessed for their functional properties by examining whether frozen neurons retained their capacity to recycle their SVs in an activity-dependent manner. Here, a 10 Hz 1 min stimulation protocol was used to load functional presynaptic boutons with the styryl dye FM4-64 (Leal-Ortiz,

Waites et al. 2008) of fresh or frozen neurons infected with EGFP::SV2 grown for 14 DIV. A high percentage of EGFP::SV2 puncta (>90) was found to colocalize with FM4-64 recycling sites (Figure 3.4E). Quantification of these data revealed that the fraction of EGFP::SV2 sites capable of recycling FM4-64 was nearly identical whether fresh neurons were infected one day after plating, frozen and infected one day after plating or infected before freezing (Figure 3.4F). No statistical difference was found between the different two conditions.

3.1.5 Electrophysiological characterization of cryopreserved neurons

Finally, intrinsic and synaptic electrophysiological properties, including excitatory postsynaptic current (EPSC) amplitude and frequency, were assessed for both fresh and cryopreserved neurons in collaboration with Julia Brill at Stanford University. Fresh and cryopreserved neurons showed no difference in input resistance (fresh: $242 \pm 40 \text{ M}\Omega$, $n=8$; frozen: $215 \pm 27 \text{ M}\Omega$, $n=17$) and resting membrane potential (fresh: $-56.0 \pm 1.6 \text{ mV}$, $n=8$; frozen: $-54.8 \pm 1.1 \text{ mV}$, $n=16$). However, cryopreserved neurons showed a significantly smaller capacitance (fresh: $40.6 \pm 4.1 \text{ pF}$, $n=8$; frozen: $29.5 \pm 2.3 \text{ pF}$, $n=17$; $p < 0.05$) than control freshly prepared neurons. Fresh and cryopreserved neurons had similar responses to hyperpolarizing and depolarizing current injections (-100 to $+250 \text{ pA}$ in 25 pA increments), as seen in representative traces from a control (black trace) and a cryopreserved (red trace) neuron (Figure 3.5A). No significant differences in input/output curves, i.e the number of action potentials generated in response to depolarizing current steps, were found between 5 control and 15 cryopreserved neurons (Figure 3.5B). This shows that cryopreserved neurons do not differ from control neurons in terms of expression of ion channels (mainly sodium and potassium).

To confirm whether cryopreserved neurons formed functional synapses onto each other, we recorded spontaneous excitatory postsynaptic potentials (EPSCs) in voltage clamp mode. Representative recordings of spontaneous activity in a control and a previously frozen neuron held at a membrane potential of -60 mV it is shown in Figure 3.5C. Spontaneous EPSC parameters amplitude, rise time, half width and frequency were analyzed in 4 control and 7 cryopreserve neurons, no significant differences in amplitude, kinetics and frequency of events were found (Figure 3.5D). This indicates that cryopreserved and control neurons form similar numbers of functional excitatory synapses and that those synapses have indistinguishable properties. In summary, we found no different between fresh and cryopreserve cells, which demonstrated that our cryopreservation methodology do not affect the electrical properties of neurons.

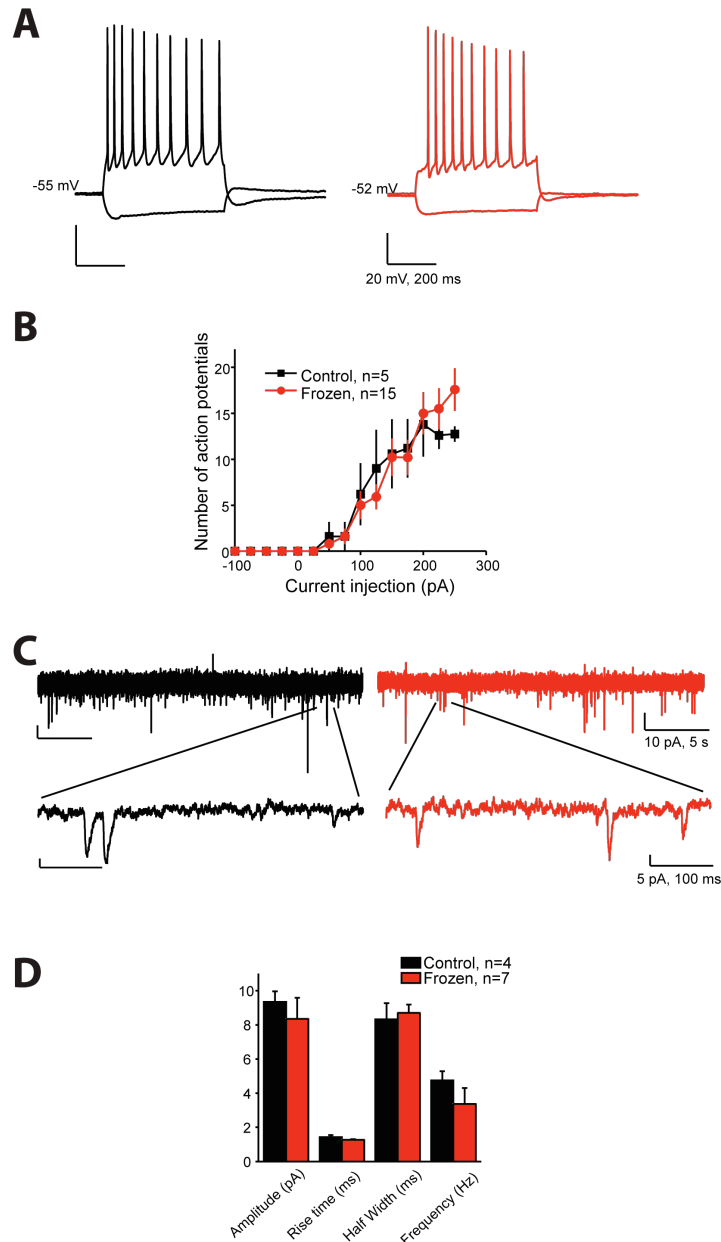


Fig. 3.5 Cryopreserved hippocampal neurons exhibit normal electrophysiological properties

Intrinsic and synaptic properties of fresh and frozen neurons grown for 14DIV. Data is shown as average \pm standard error (number of cells). **(A)** Current clamp recordings show similar responses of fresh (black trace) and cryopreserved neurons (red trace) to hyperpolarizing and depolarizing current injections (-100 pA, +200 pA). **(B)** Input/output curves. Number of action potentials generated in response to hyperpolarizing and depolarizing current injections. No significant differences between control (n=5) and previously frozen neurons (n=15) were detected. **(C)** Representative voltage clamp recordings of spontaneous activity in a control and a previously frozen neuron held at -60 mV. Downward deflections are spontaneous EPSCs, demonstrating the presence of functional synapses between the cultured neurons. Expanded traces at bottom show individual EPSCs. **(D)** Summary of spontaneous EPSC parameters in 4 control and 7 previously frozen neurons. There were no significant differences in amplitude, kinetics and frequency of events. **(Data collected by Julia Brill)** All the data is shown as average \pm standard error (number of cells).

3.2 Development of vectors for the effective expression of recombinant protein and shRNA in cultured hippocampal neurons

The true strength of cellular science is the ability to monitor changes in the dynamics and function of individual molecules in real time. Challenges associated with the delivery of recombinant molecules, near endogenous levels, to neuronal cells have greatly hampered our understanding of the cellular mechanisms underlying synapse formation and synaptic transmission. To overcome these limitations, I have developed both plasmid and viral system that allow for the efficient delivery and expression of recombinant XFP-tagged proteins and/or shRNAs into neurons. The results presented below describe the evolution of these vectors and their utility as tools to study the cellular dynamics of proteins as well as the contribution of individual molecules to neuronal function.

3.2.1 Custom design of a short hairpin RNA expression vector for the efficient knockdown of multiple synaptic proteins

The study of presynaptic boutons is an exceptionally challenging problem for cell-biologist as they can form 100um away from the cell soma. To overcome this limitation and allow investigators to the assessment the impact of shRNA mediated knockdown on presynaptic function, a set of vectors were developed to assess the effectiveness of both plasmids and lentiviral vectors to deliver both presynaptic reporter molecules and multiple shRNA expression cassettes in one vector. To this end, a plasmid-based vector was initially created that contains an shRNA expression system, an shRNA target mRNA/protein reporter, as well as a reporter that is insensitive to shRNA-mediated knockdown. Elements from different plasmids were combined to form a new plasmid named “pZoff” (Figure 3.6A-C). This new vector contains an EGFP expression cassette including the CMV promoter, EGFP and multicloning site (MCS) (CMV-EGFP-MCS) from the “Clontech” vector pEGFP-C1. The neomycin/kanamycin-resistant gene was also included to allow for antibiotic selection in both prokaryotic and eukaryotic cells. Antibodies against the neomycin resistance gene product in eukaryotic cells provide a constitutively active reporter that can be used to normalize transfection efficiency in cellular lysates. Moreover, by creating a fusion protein between a target gene sequence (X) and EGFP (EGFP-X), one can use antibodies to EGFP to monitor changes of target protein expression levels. Finally, the polymerase III H1 or U6 cassettes from pSuper plasmid with multicloning sequence were introduced into this plasmid allowing any target shRNA to be cloned via a pair of oligonucleotides into the BglII and HindIII sites (Figure 3.6D, E).

3.2.2 Design of shRNAs for selective and efficient knockdown of Piccolo and Bassoon

The utility of the PZoff vector was initially explored in experiments to assess the effectiveness of shRNAs to efficiently knockdown the expression of Bassoon and Piccolo isoforms in cultured hippocampal neurons. This was accomplished by generating several shRNAs against sequences situated in the N-terminus of Bassoon and Piccolo (Figure 3.7A) (tom Dieck, Sanmarti-Vila et al. 1998; Fenster and Garner 2002). This region has been shown to encode segments of both high (Figure 3.7A) and low molecular weight isoforms of Bassoon and Piccolo (Cases-Langhoff, Voss et al. 1996; Fenster, Chung et al. 2000; Zhai, Olias et al. 2000; Fenster and Garner 2002)(see also Figure 3.28D).

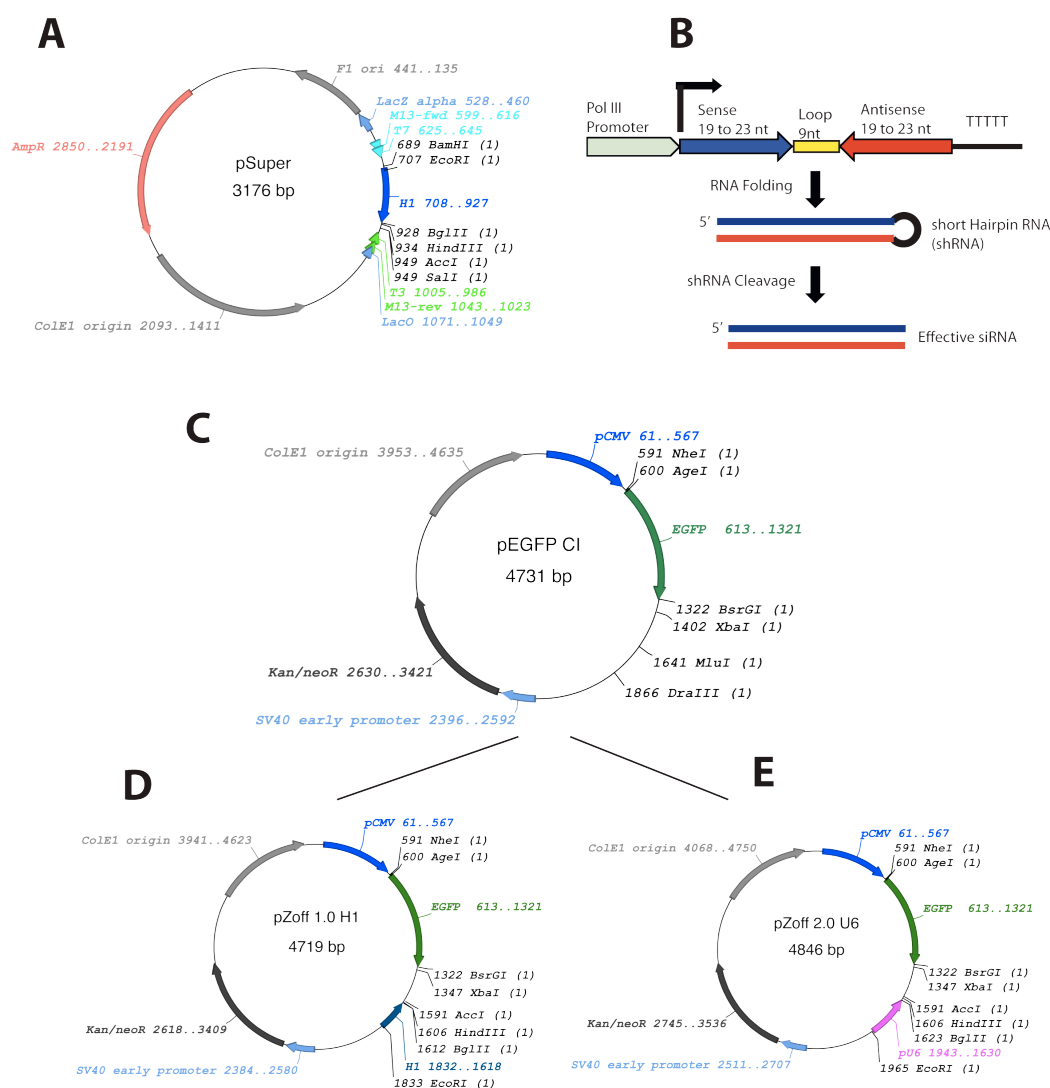


Fig. 3.6 Schematic flow diagram used to create the pZoff shRNA expression vector

(A) Plasmid map of pSuper (Addgene) revealing relative position of the Polymerase III promoter H1, the multicloning site (MCS) for shRNA as well as Ampicillin resistant gene. (B) Graphical representation of how short hairpin RNAs (shRNAs) were synthesized and processed following transcription. (C) Schematic diagram of the pEGFP-C1 vector (Clontech), which expresses EGFP and a Kanamycin resistant gene. (D) Schematic diagram of the pZoff-1.0 H1 plasmid, which contains the H1-shRNA expression cassette and the CMV-EGFP minigene. (E) Schematic diagram of pZoff-2.0, which is identical to pZoff-1.0 except the H1-shRNA expression cassette was replaced with an alternative polymerase III promoter U6.

Each target sequence was selected using a program called “super RNAi” (Mekentosj.com). This program determines shRNAs that contain approximately 50% GC content and a low ΔG at the 3' and/or 5' end of each oligo. It also allows the inclusion of BglIII and HindIII linker sequences at the 5' and 3' of these oligos, respectively, and a loop linking the two complementary 21 nucleotide segments as well as a 3' polymerase III termination signal comprised of five thymidines (T5) (Figure 3.7B). For these N-terminal sequences, the program selected two shRNA for Piccolo (called Pclo6 & Pclo28) and one for Bassoon (Bsn16). Each was subcloned into the pZoff 1.0 H1 vector with BglIII and HindIII thereby generating three new plasmids called pZoff-Pclo6, pZoff-Pclo28 and pZoff-Bsn16 (Figure 3.7A).

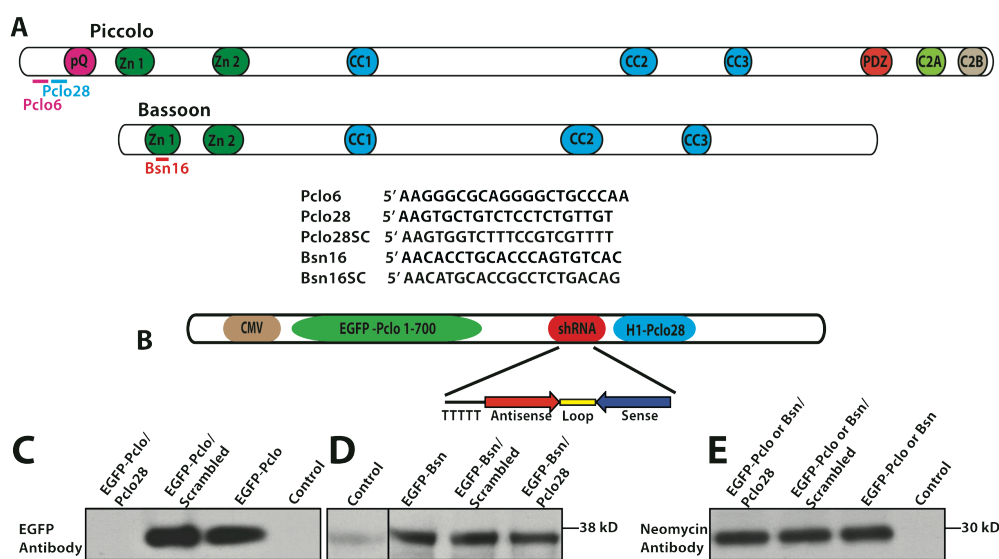


Fig. 3.7 shRNA mediated knock down of EGFP-Piccolo

(A) Schematic diagram of Piccolo and Bassoon, illustrating their multidomain structure. Highlighted are the polyglutamate (pQ) region, two double zinc finger domains (Zn1/2), three coiled-coil domains (CC1-3), PDZ domain, and two C-terminal C2 domains (C2A/B) in these proteins. Also shown are the locations and sequences of shRNAs generated against Piccolo and Bassoon. These include Pclo6, Pclo28, Bsn16 and a scrambled control Pclo28SC and Bsn16SC. (B) Schematic diagram of the pZoff-plasmid expressing an N-terminal segment of Piccolo (nucleotides 1-700) fused to EGFP (EGFP::Pclo) and the shRNA against Piccolo (Pclo28) (pZoff/EGFP::Pclo/H1-Pclo28). (C) Western blots of cellular extracts from COS7 cells transfected with pZoff plasmids expressing a 700 bp N-terminal fragment of Piccolo (pZoff/EGFP::Pclo) and shRNAs against either Piccolo (Pclo28 or Pclo28SC) checking the efficiency of Pclo28 using EGFP antibody. (D) Western blots of cellular extracts from COS7 cells transfected with pZoff plasmids expressing a 900 bp N-terminal fragment of Bassoon (pZoff/EGFP::Bsn) and shRNAs against either Piccolo (Pclo28 or Pclo28SC) checking the specificity of Pclo28 using EGFP antibody. (E) Western blots of cellular extracts from COS7 cells transfected with pZoff/EGFP::Bsn or pZoff/EGFP::Pclo and shRNAs against either Piccolo (Pclo28 or Pclo28SC) checking the normalization of protein using Neomycin antibody.

3.2.3 Assessment of shRNAs for selective and efficient knockdown of Piccolo and Bassoon

To assess the effectiveness of these shRNAs, a reporter system was designed in which the N-terminal segment of Piccolo, containing the Pclo28 target sequence, was fused in-frame

with the C-terminal end of EGFP in the pZoff-Pclo28 vector, creating pZoff/EGFP-N-Pclo/H1-Pclo28. As a control, the Pclo28 shRNA sequence was scrambled, such that it would no longer hybridize with the Piccolo mRNA (Pclo28SC), yet would still form a stable hairpin, creating pZoff/EGFP-N-Pclo/H1-Pclo28SC. As an initial evaluation of specificity, two additional pZoff vectors were created that expressed an N-terminal segment of Bassoon fused to EGFP and either Pclo28 (pZoff/EGFP-N-Bsn/H1-Pclo28) or Pclo28SC (pZoff/EGFP-N-Bsn/H1-Pclo28SC). Each of these vectors were then used to transfect HEK293 cells and the cellular lysates were run out on an SDS-PAGE gel, transferred to nitrocellulose and probed with antibodies against EGFP and neomycin (Figure 3.7C-E). [Note: the pZoff vector also expresses the neomycin resistance gene. These levels were used to normalize expression levels between experiments (Figure 3.7E)]. As shown in Figure 7C, Pclo28 caused the selective down-regulation of EGFP-N-Pclo but not EGFP-N-Bsn (Figure 3.7D). Pclo28SC had no effect on the expression of either EGFP-fusion protein (Figure 3.7C). These data suggest that Pclo28 could be an effective reagent to selectively down-regulate the expression of Piccolo. They also nicely illustrate the utility of the pZoff vector system for exploring the potential utility of different shRNAs.

Next, we evaluated whether shRNAs generated against Piccolo and Bassoon could also knockdown the expression of endogenous Piccolo and Bassoon. As discussed in the introduction, Piccolo and Bassoon are large structural proteins of presynaptic active zones accumulating at nascent synapses as they form. In cultured hippocampal neurons, both are expressed at the earliest stages of neuronal differentiation and begin to accumulate at nascent presynaptic boutons around 7 days *in vitro* (DIV). Both are also present at mature synapses *in vivo* and *in vitro* (Cases-Langhoff, Voss et al. 1996; tom Dieck, Sanmarti-Vila et al. 1998; Fenster, Chung et al. 2000; Garner, Kindler et al. 2000; Gundelfinger and tom Dieck 2000; Dresbach, Qualmann et al. 2001; Zhai, Vardinon-Friedman et al. 2001; Fenster and Garner 2002).

A major challenge with studying the expression and function of these presynaptic proteins is that axons extend hundreds of microns from the cell soma forming synapses on hundreds of target neurons. Thus, identifying the boutons of a small subset of transfected neurons even in dissociated cultures is a daunting task. To address this problem, pZoff vector was modified to express a recombinant EGFP-tagged presynaptic protein. In initial experiments, utility of Synapsin1a, a presynaptic vesicle-associated protein, as such a reporter was examined. Here, EGFP in the pZoff vector was replaced with EGFP-tagged Synapsin1a (EGFP-Syn1a). As reported previously (Chi, Greengard et al. 2001; Chi, Greengard et al. 2003), presynaptic boutons of neurons transfected with pZoff-EGFP-Syn1a

were easily identifiable, exhibiting a punctate pattern along the dendrites of fixed and immunostained untransfected cells that colocalized with other pre- and postsynaptic markers (Figure 3.8A).

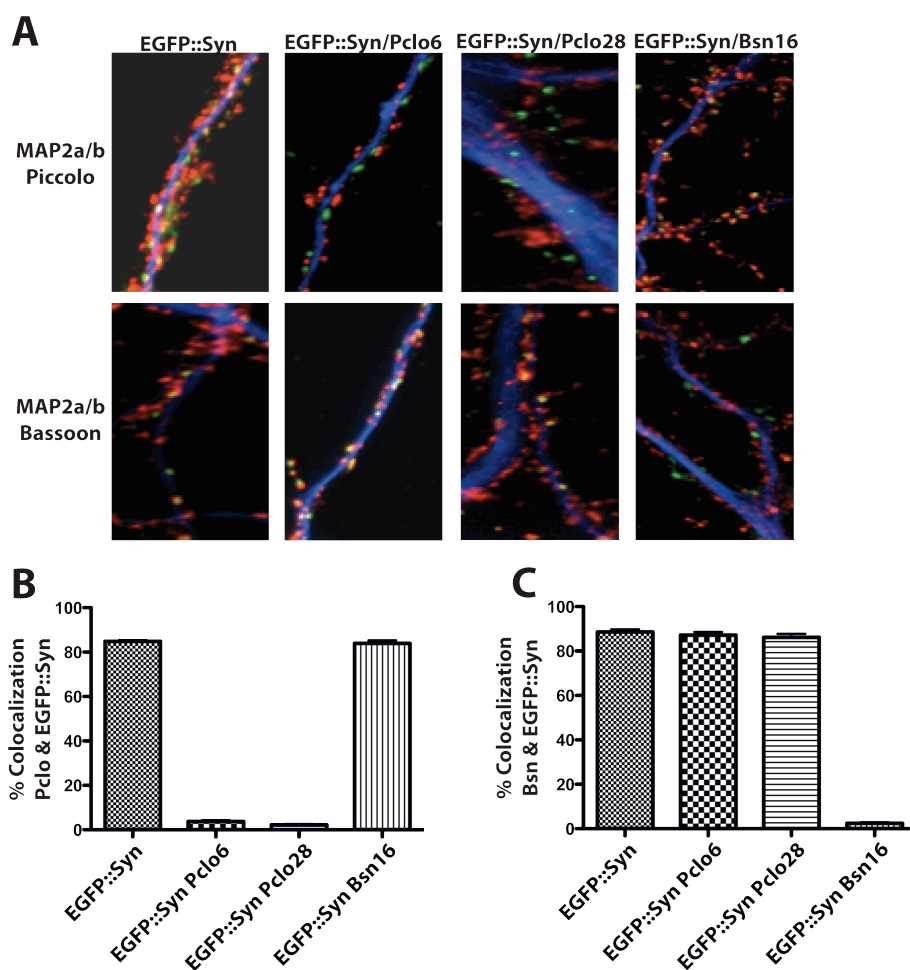


Fig. 3.8 shRNA-mediated knockdown of Piccolo and Bassoon with the pZoff vector in cultured hippocampal neurons

(A) Fluorescent images of hippocampal neurons transfected with either pZoff/EGFP::Syn1a, pZoff/EGFP::Syn1a/Pclo6, pZoff/EGFP::Syn1a/Pclo28 or pZoff/EGFP::Syn1a/Bsn16 plasmids. After 14DIV, neurons were fixed and immunostained with antibodies against MAP2a/b (blue) and Piccolo (top panels; red) or Bassoon (bottom panels; red). Note Piccolo immunofluorescence is absent at EGFP::Syn1a (green) puncta in neurons expressing Pclo6 and Pclo28 but not Bsn16. Conversely, Bassoon immunoreactivity is only lacking from Bsn16-expressing presynaptic boutons. (B) Quantification of % colocalization of Piccolo immunoreactive puncta and EGFP::Syn1a puncta along dendritic profiles. (C) Quantification of % colocalization of Bassoon immunoreactive puncta and EGFP::Syn1a puncta along dendritic profiles.

To explore whether shRNAs against Piccolo and Bassoon efficiently knockdown the expression of these AZ proteins, cultured hippocampal neurons were transfected by electroporation at the day of plating with vectors expressing EGFP::Syn1a and each of the Piccolo/Bassoon shRNAs (pZoff-EGFP::Syn1a/Pclo6, pZoff-EGFP::Syn1a/Pclo28 or pZoff-EGFP::Syn1a/Bsn16). Neuronal cultures were then fixed in 4% PFA at 14 to 18 DIV, and immunostained with antibodies against MAP2a/b and Piccolo or Bassoon. As seen in Figure

3.8A, selective loss of Piccolo immunoreactivity was observed in EGFP::SynIa positive boutons from cells expressing Pclo6 or Pclo28 and Bassoon immunoreactivity in neurons expressing Bsn16. Quantifying these data revealed that nearly 95% of all EGFP::SynIa positive puncta lacked either Piccolo or Bassoon immunoreactivity, respectively (Figure 3.8B, C). No change in the expression of these AZ proteins was seen in neurons only expressing EGFP::SynIa.

In summary, these pZoff vectors not only allow for the efficient knockdown of neuronal proteins, e.g. the presynaptic AZ proteins Piccolo and Bassoon, but also permits the quantification of knockdown efficiency in heterologous cells or within neuronal microdomains, such as presynaptic boutons. Utilizing these vectors, specific shRNA were developed that efficiently knockdown the expression of two structurally related presynaptic active zone proteins, Piccolo and Bassoon.

3.2.4 Harnessing viruses for the efficient expression of shRNAs and recombinant proteins in cultured neuronal cells

Although the pZoff vector system readily supports the cell-autonomous elimination of proteins, in general the poor efficiency of plasmid-based transfection systems limits the utility of this strategy to explore more global changes in protein or mRNA expression. Moreover, plasmid-based systems are prone to overexpression artifacts and often create pools of soluble recombinant proteins that mask the normal distribution and/or drives these molecules into inappropriate membrane compartments protein complexes. To overcome these problems, alternatives like lentivirus were explored that allowed for lower expression and higher efficiency of gene transfer into neurons.

3.2.5 Expressing recombinant proteins at endogenous levels with lentivirus

In general for the expression of a single recombinant protein, a lentiviral backbone was used that was based on a self-inactivating vector FUGW (Figure 3.9A, D & F). This lentivirus vector was engineered to contain a human ubiquitin-C promoter driving the GFP reporter gene (Schmidt, Christoph et al. 1990; Niwa, Yamamura et al. 1991; Schorpp, Jager et al. 1996). To increase transcription levels, the woodchuck hepatitis virus posttranscriptional regulatory element (WRE) was inserted downstream of GFP (Zufferey, Donello et al. 1999). To increase viral titers, the human immunodeficiency virus-1 (HIV-1) flap element (Zennou, Petit et al. 2000) was inserted between the 5' long terminal repeat (LTR) to generate the viral vector called FUGW (Lois, Hong et al. 2002) (Figure 3.9A, D & F). To test this, one of the first vectors created was for the expression of EGFP-SynIa (FU

EGFP::Syn1a-W)(Figure 3.9A). High-titer lentiviruses were made and found to infect over 50% of the 80,000 cells with only 25 to 50 μ l of virus harvested from the supernatant. Cells were infected the same day after plating, grown for 14 DIV, fixed and stained with the Synapsin antibodies (Figure 3.9B). No significant overexpression of Synapsin1a per bouton was found, indicating that the FU-EGFP::Syn1a-W vector resulted in EGFP-Syn1a expression at levels that allowed neurons to maintain expression near the endogenous level of Synapsin within a presynaptic bouton (Figure 3.9C).

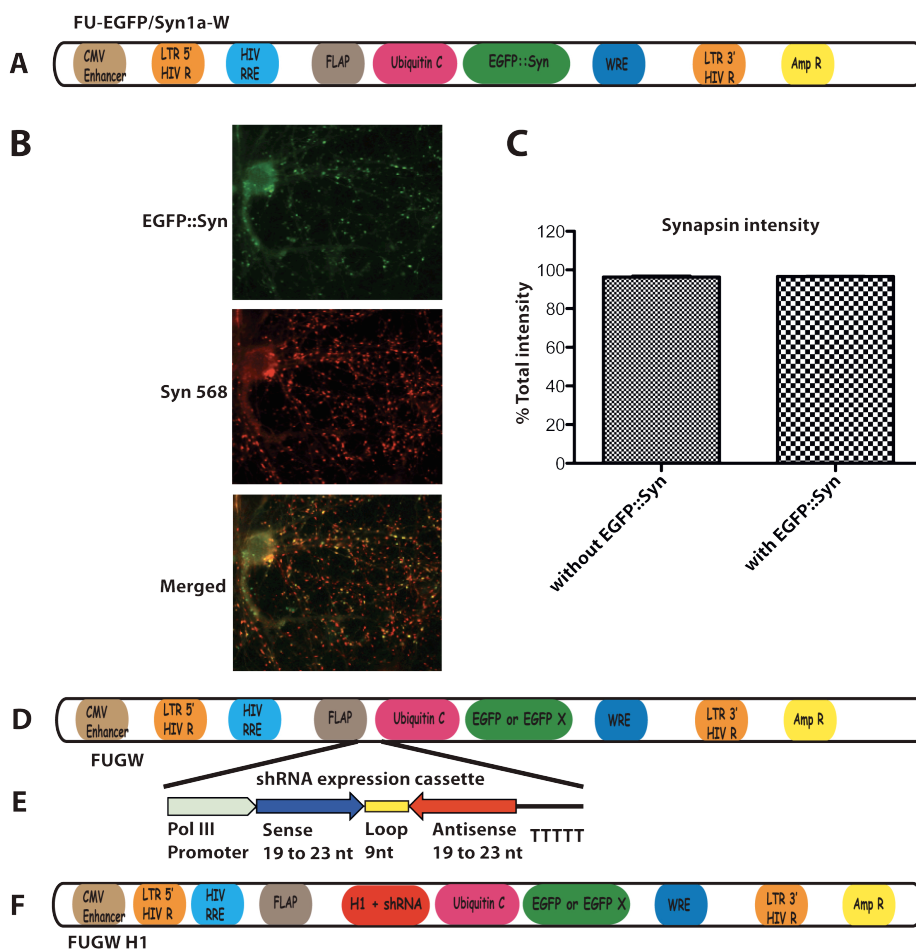


Fig. 3.9 Lentiviral expression of EGFP::Syn1a at endogenous levels and schematic diagram of the lentiviral vector (FUGW) used to express XFP-tagged proteins and shRNA

(A) Schematic diagram of EGFP-Synapsin1a in a lentiviral expression vector. (B) Fluorescent images of hippocampal neurons infected with FU-EGFP::Syn1a-W (green) on the day of plating. After 14 DIV, neurons were fixed and immunostained with an antibody to Synapsin1a (red). (C) Quantitation of the intensity of Synapsin1a immunoreactivity at boutons with or without EGFP::Syn1a. Total Synapsin1a levels were similar for infected and uninfected neurons, indicating that lentiviruses express recombinant proteins does not drive Synapsin1 expression above endogenous levels. SEM bars plotted ($n > 100$ puncta/condition). (D) Schematic diagram of the FUGW vector which contains a CMV enhancer, 5' and 3' LTR's, HIV RRE, Flap, UbiquitinC promoter, EGFP coding sequence, WRE element and the ampicillin resistant gene. (E) Schematic diagram of the shRNA expression cassette and insertion of this element between the Flap and Ubiquitin promoter in FUGW. (F) The resulting FUGW-H1 expression vector, which can be used to express both shRNAs and different XFP tagged proteins such as EGFP::Syn1a or EGFP-SV2 under the Ubiquitin-C promoter.

3.2.6 Development of bicistronic lentiviral vectors for the down-regulation of presynaptic proteins

For expression of interference RNAs in a lentiviral vector, the H1 promoter cassette was introduced upstream of the Ubiquitin C promoter in the FUGW vector. This new vector, called FUGW H1 (Figure 3.9F), was further modified to allow for the insertion of different shRNAs by subcloning the shRNA fragments from the pZoff plasmids, such as Pclo28, Pclo6 and Bsn16. These new plasmids (called FUGW Pclo28, FUGW Pclo6 and FUGW Bsn16, respectively) contained a specific shRNA of interest and EGFP to identify infected cells. To monitor the effects of Piccolo and Bassoon down-regulation on presynaptic bouton function, EGFP was replaced with different XFP-tagged presynaptic proteins. For example, in one set of vectors, EGFP::SynIa (Figure 3.9A)(Chi, Greengard et al. 2001; Chi, Greengard et al. 2003) was inserted into each of these vectors, creating LV/EGFP::SynIa, LV/EGFP::SynIa/Pclo6 LV/EGFP::SynIa/Pclo28 LV/EGFP::SynIa/Bsn16 (Figure 3.10A) (LV for lentivirus vector FU(tag)W).

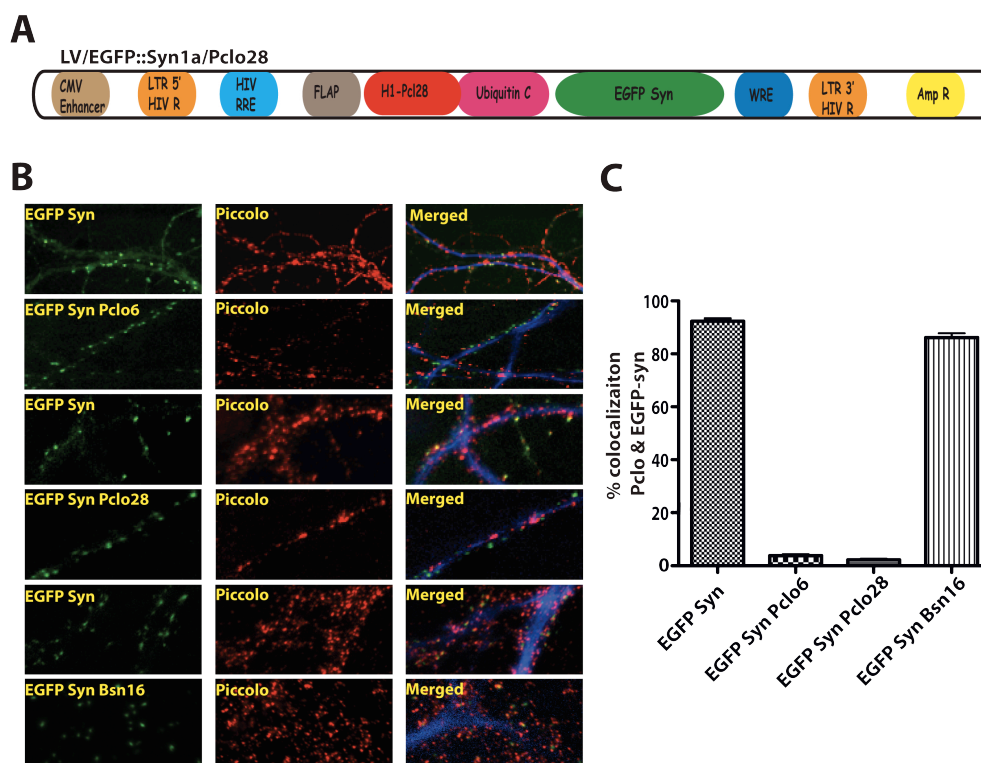


Fig. 3.10 Lentivirus-mediated knockdown of Piccolo with interference RNAs

Schematic diagram of LV/EGFP::SynIa/Pclo28 lentiviral expression vector. (B) Fluorescent images of hippocampal neurons infected with LV/EGFP::SynIa, LV/EGFP-SynIa/Pclo6, LV/EGFP::SynIa/Pclo28 LV/EGFP::SynIa/Bsn16 on the day of plating. After 14 DIV, neurons were fixed and immunostained with antibodies against MAP2 (blue, merged) and Piccolo (red). Only a fraction of presynaptic boutons express EGFP::SynIa; the remaining Piccolo immunoreactivity seen is from the boutons of uninfected neurons (merged). Scale bars = 10 μ m. (C) Quantification of the percent colocalization of EGFP-SynIa puncta with Piccolo immunoreactive puncta situated along MAP2 positive dendritic profiles ($n > 2000$ puncta/condition, 5 expts). Error bars show SEM.

Virus prepared from these plasmids were used to infect neurons on the day of plating (0 DIV). After 14 DIV, neurons were fixed with 4% PFA and immunostained with antibodies against MAP2a/b and Piccolo or Bassoon. In neurons expressing shRNAs for Pclo28, Pclo6 or Bsn16, over 95% of EGFP::SynIa positive puncta lacked Piccolo or Bassoon, respectively (Figure 3.10B, C). As Pclo28 produced a slightly better down-regulation of Piccolo compared of Pclo6, the majority of the subsequent experiments used the Pclo28 shRNA (Figure 3.11A, B). To assess the specificity of these shRNA, we evaluated whether Piccolo or Bassoon levels were altered in neurons expressing Bsn16 or Pclo28, respectively. Synaptic levels of Piccolo and Bassoon were identical to control (e.g. the boutons of uninfected neurons), suggesting that our shRNA are highly specific for their corresponding proteins (Figure 3.10B,C & 3.11A,B)

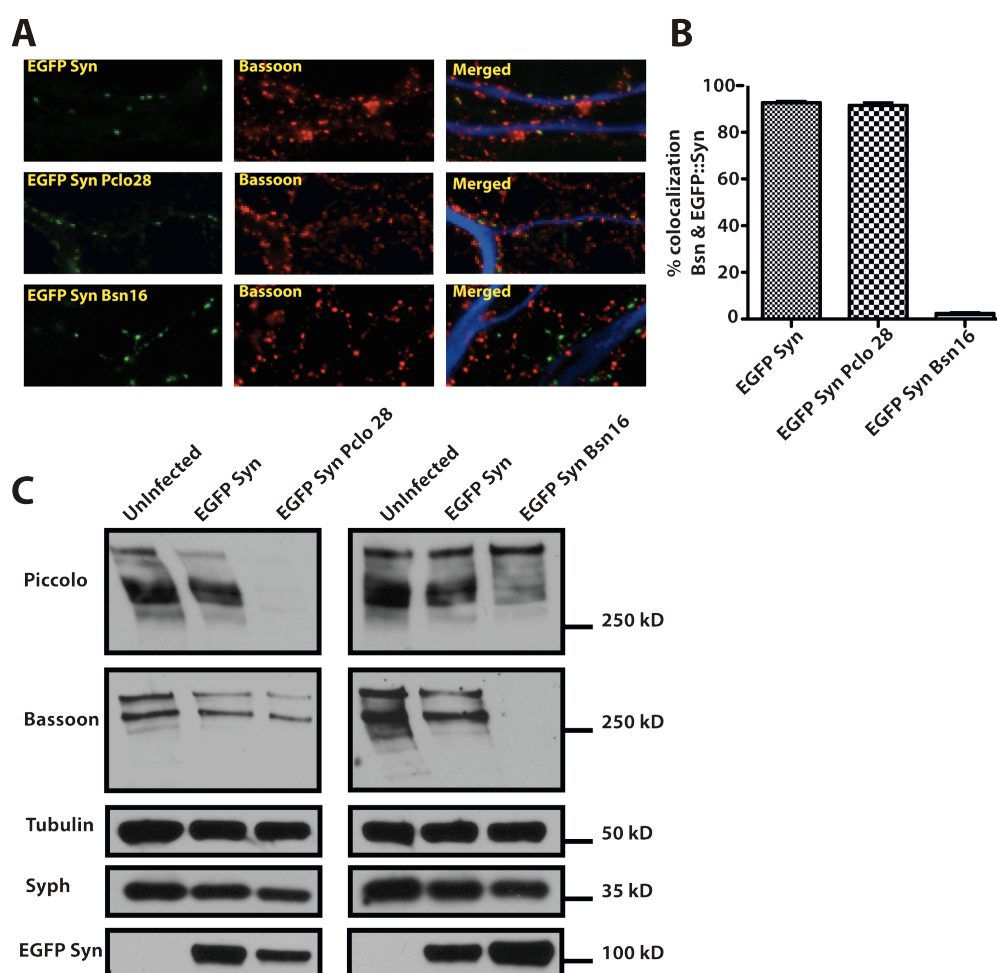


Fig. 3.11 Lentivirus-mediated knockdown of Piccolo and Bassoon

(A) Fluorescent images of hippocampal neurons infected with LV/EGFP::SynIa, LV/EGFP::SynIa/Pclo28, LV/EGFP::SynIa/Bsn16 on the day of plating. After 14 DIV, neurons were fixed and immunostained with antibodies against MAP2a/b (blue, merged) and Bassoon (red). Only a fraction of presynaptic boutons expressed EGFP::Syn. The remaining Bassoon immunoreactivity seen in LV/EGFP::SynIa/Bsn16 (lower panel) was from the boutons of uninfected neurons. Scale bars = 10 μ m. (B) Quantification of colocalization of EGFP::SynIa puncta with Bassoon puncta along MAP2 positive dendritic profiles ($n > 2000$ puncta/condition, 5 expts). Error bars show SEM. (C) Western blots of cellular lysates from hippocampal neurons uninfected or infected with LV/EGFP::SynIa

LV/EGFP::SynIa/Pclo28 or LV/EGFP::SynIa/Bsn16 on the day of plating. Lysates were harvested at 14 DIV, and blots were probed with antibodies against Piccolo, Bassoon, Tubulin, Synaptophysin (Syph), and EGFP for EGFP::Syn. Protein molecular weights are indicated (right).

To directly monitor changes in proteins levels over time, neurons were grown in flasks (T-25) and infected to near 100% with one of three viruses (LV/EGFP::SynIa, LV/EGFP::SynIa/Pclo28 and LV/EGFP::SynIa/Bsn16) on the day of plating (0 DIV). After 14 DIV cellular lysates were collected, Western blotted and probed with antibodies against Piccolo, Bassoon and Tubulin. The latter was used as a loading control. These data revealed that Pclo28 or Bsn16 caused a greater than 90% down-regulation Piccolo and Bassoon levels, respectively. Importantly, neither shRNA affected the expression of synaptic vesicle proteins, Synaptophysin or Tubulin, (Figure 3.11C).

3.2.7 Design of a tricistronic lentiviral vector for the down-regulation of multiple synaptic proteins

Due to potential redundancies in Piccolo and Bassoon function, the elimination of both proteins in the same cell would be particularly advantageous. While this can be achieved by infecting two different bicistronic lentiviral vectors expressing different XFP-reporters and shRNAs, technical challenges associated with co-infection, the used of multiple fluorophores and/or identifying co-expressing cells limits the utility of this strategy. Therefore, a new tricistronic lentiviral vector was developed to place multiple shRNAs within the same reporter vector. Starting with the bicistronic vector expressing FUGW/Pclo28, a new cassette expressing the shRNA for Bassoon (Bsn16) driven by the H1 polymerase III promoter was inserted in different positions and orientations (Figure 3.12A).

These custom-designed lentiviral expression vectors allow for high rates of gene transfer to a population of neurons for expression of recombinant protein encoded by cDNAs up to 4000 base pairs. Moreover, by introducing the H1 polymerase III cassette, shRNAs can be co-expressed in these vectors leading to the efficient and specific down-regulation of neuronal proteins, such as Piccolo or Bassoon. Down-regulation of both Piccolo and Bassoon expression was seen when plasmid versions were electroporated into hippocampal neurons on the day of plating. However, it was not possible to generate lentiviruses from these vectors (Figure 3.12A, B).

One likely explanation was that virus production is adversely affected by the presence of repetitive sequence elements (e.g. two H1 promoter sequences) between the LTRs. To explore this possibility, we created a second-generation FUGW/DKD vector (LV/EGFP/DKD) in which the Bsn16 shRNA was driven by the U6 polymerase III promoter

(Figure 3.12C). In parallel, a control vector FUGW/SC (LV/EGFP/SC) was created with the same structural organization as FUGW/DKD 2.0 yet expressed scrambled versions of the Pclo28 (Pclo28SC) and Bsn16 (Bsn16SC) that retain their ability to form shRNAs (Figure 3.12D). High-titer lentivirus production was successful from these new constructs (e.g., 50 to 75 μ l of virus infected more than 90% of the 80,000 neurons plated on one coverslip).

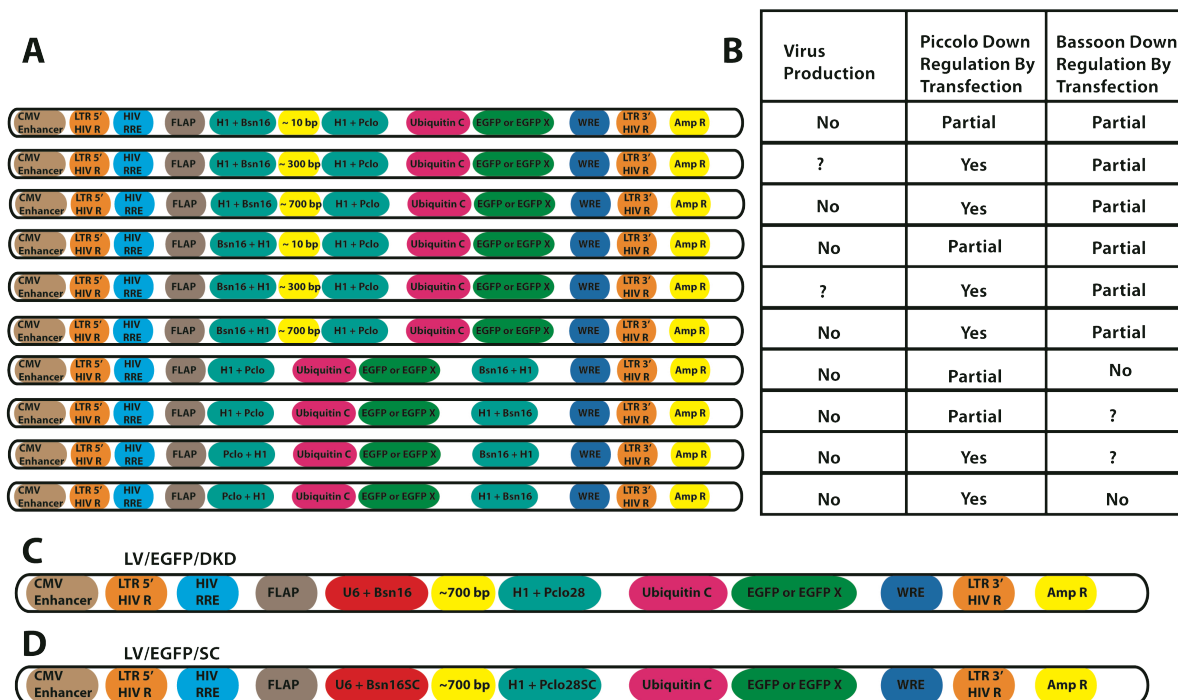


Fig. 3.12 Schematic diagrams of double knockdown vectors

A) Schematic diagram of a vector contain two different shRNA expression cassette which includes the polymerase III promoter H1 and U6 and different spacer size in between of two pol. III promoter **(B)** Table showing which vector can produce down-regulation of Piccolo and Bassoon. **(C)** LV/EGFP/DKD vector. **(D)** LV/EGFP/SC.

To study the potential for these lentiviruses for biochemical experiments, high titer LV/EGFP/DKD or LV/EGFP/SC lentivirus was used to infect a population of (~500,000 neurons) near 100%. Protein lysates from neurons 14 DIV were then probed for Piccolo, Bassoon or Tubulin (Figure 3.13A). Quantification and normalization to Tubulin revealed that the levels of Piccolo and Bassoon in LV/EGFP/SC versus uninfected cells lysates were not different. In contrast, there was a greater than 90% knockdown of Piccolo and Bassoon expression in neurons infected with LV/EGFP/DKD (Figure 3.13B). This level of down-regulation was similar to neurons infected with single knockdown vectors (FUGW/Bsn16 or FUGW/Pclo28).

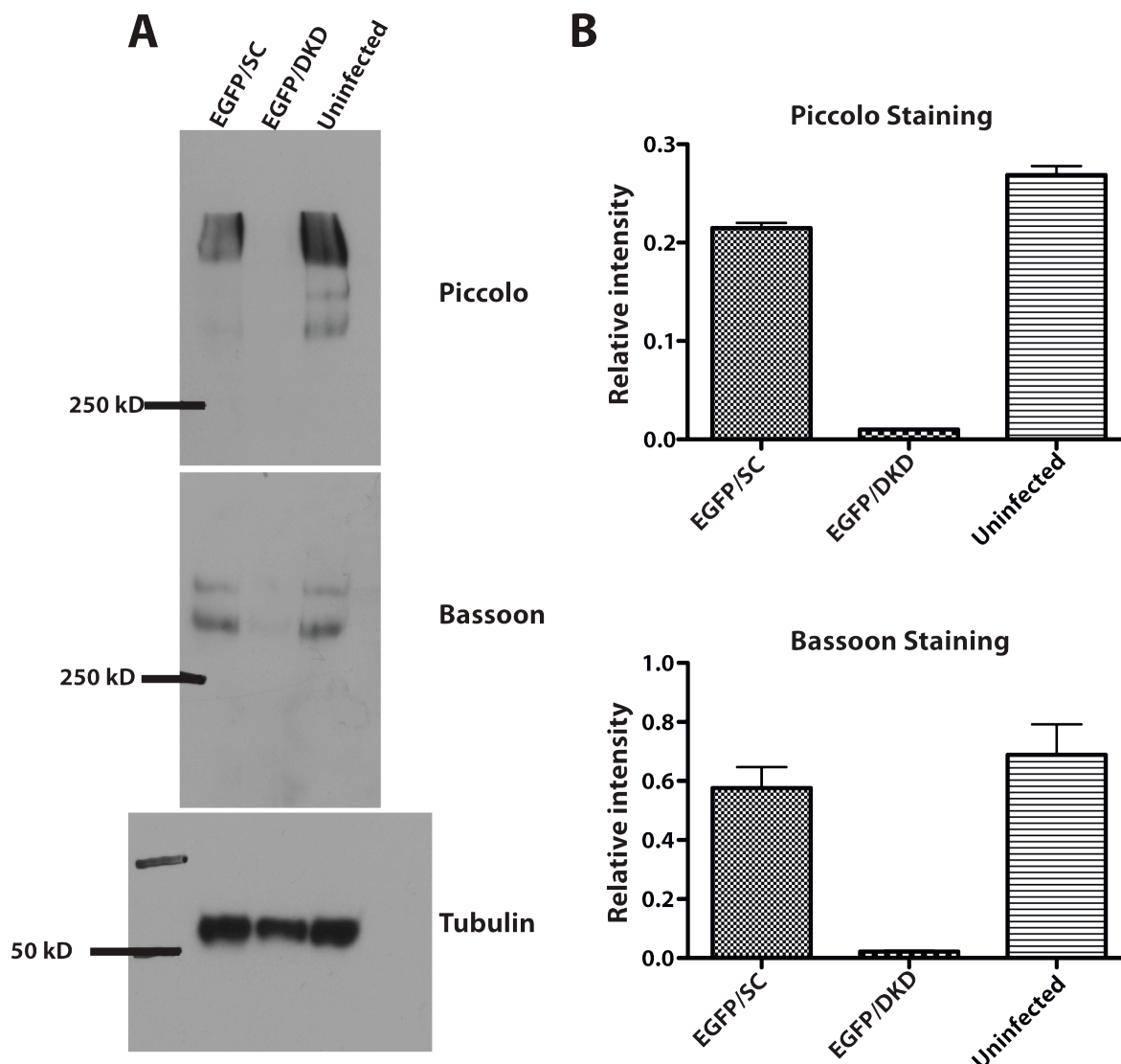


Fig. 3.13 Western analysis of Piccolo and Bassoon double knockdown (DKD).

(A) Western blots of cellular lysates prepared from rat hippocampal neurons infected on the day of plating with lentiviruses expressing soluble EGFP together with shRNAs against Piccolo and Bassoon (LV/EGFP/DKD) (H1 Pclo28 and U6 Bsn16 or scrambled controls for each shRNA (LV/EGFP/SC) (H1 Pclo28SC and U6 Bsn16SC). After 14 DIV, lysates from uninfected cells or those infected with LV/EGFP/SC or LV/EGFP/DKD were harvested and probed with antibodies against Piccolo, Bassoon, or Tubulin as indicated. Note that immunoreactivity for Piccolo and Bassoon is nearly absent from EGFP/DKD-infected lysates. (B) Quantification of Piccolo or Bassoon normalized to tubulin ($n=3$ expts.). Error bars show SEM.

Taken together, these data reveal that lentiviruses hold a great deal of utility not only to express various recombinant proteins but also shRNAs. They should allow molecules to be expressed near endogenous levels and support the expression of multiple shRNA, as long as repeat sequence elements, which can cause recombination events, are not included between the two LTRs. Furthermore, a tricistronic vector was developed that not only supported the double knockdown (DKD) of Piccolo and Bassoon but also included reporter proteins that

permitted the identification of boutons from neurons lacking these proteins in a cell autonomous and synapse-specific manner.

3.2.8 Expressing full-length Bassoon for rescue experiments using a helper-dependent adenoviral vector (HDAd)

Due to the packaging limit of lentiviruses, gene transfer of large molecules, such as Bassoon (~12,000 bp), is not viable using this type of approach. Therefore, for rescue experiments with full-length Bassoon, helper-dependent adenoviral vectors (HDAd) were utilized that permit a cloning capacity of up to 37 kb (Palmer and Ng, 2008; Palmer and Ng, 2011). Thus with the goal of rescuing of the Piccolo/Bassoon double knockdown (DKD) phenotypes, we designed and built an HDAd vector that expressed full-length mRFP-tagged Bassoon (HDAd mRFP-Bsn SM16) (Figure 3.14A). To allow this recombinant Bassoon to be resistant to our shRNA Bsn16, silent point mutations were placed in the sequence of Bassoon to prevent Bsn16 targeted destruction. A helper-dependent, non-replicating adenovirus was produced by the Ng Lab (Department of Molecular and Human Genetics, Baylor College of Medicine, Houston, Texas), which enabled the efficient (>40%) infection of hippocampal neurons with this ~14 kb cDNA.

The HDAd mRFP-Bsn SM16 adenovirus was initially characterized in HEK293T cells to assess whether full-length Bassoon was expressed. Western blotting performed with cellular lysates prepared 48 hrs post-infection revealed the presence of a prominent band of ~450 kD that is similar in size to endogenous Bassoon (Figure 3.14B). To functionally characterize the recombinant Bassoon expressed from HDAd mRFP-Bsn SM16 virus was then used to infect neurons grown for 5 to 7 DIV and imaged 48 to 72 hr later. In live imaging experiments, highly mobile mRFP-Bsn puncta were observed along axonal processes consistent with previous studies showing that Bassoon was transported in association with vesicular transport intermediates along axons (Dresbach, Torres et al. 2006; Cai, Pan et al. 2007; Fejtova, Davydova et al. 2009)(Figure 3.14C). To examine if this Bassoon reached the synapse, HDAd mRFP-Bsn/SM16 infected neurons at 7 DIV were fix at 14 DIV with 4% PFA and immunostained with antibodies against Synaptophysin and MAP2a/b. Here, mRFP-Bsn SM16 positive puncta were observed that colocalize with Synaptophysin along MAP2a/b positive dendrites consistent with its appropriate presynaptic localization (Figure 14D). Based on this characterization, adenovirus technology allows us to express a full-length fluorescently tagged Bassoon for rescue experiments that shows proper expression and localization of our fusion protein of interest.

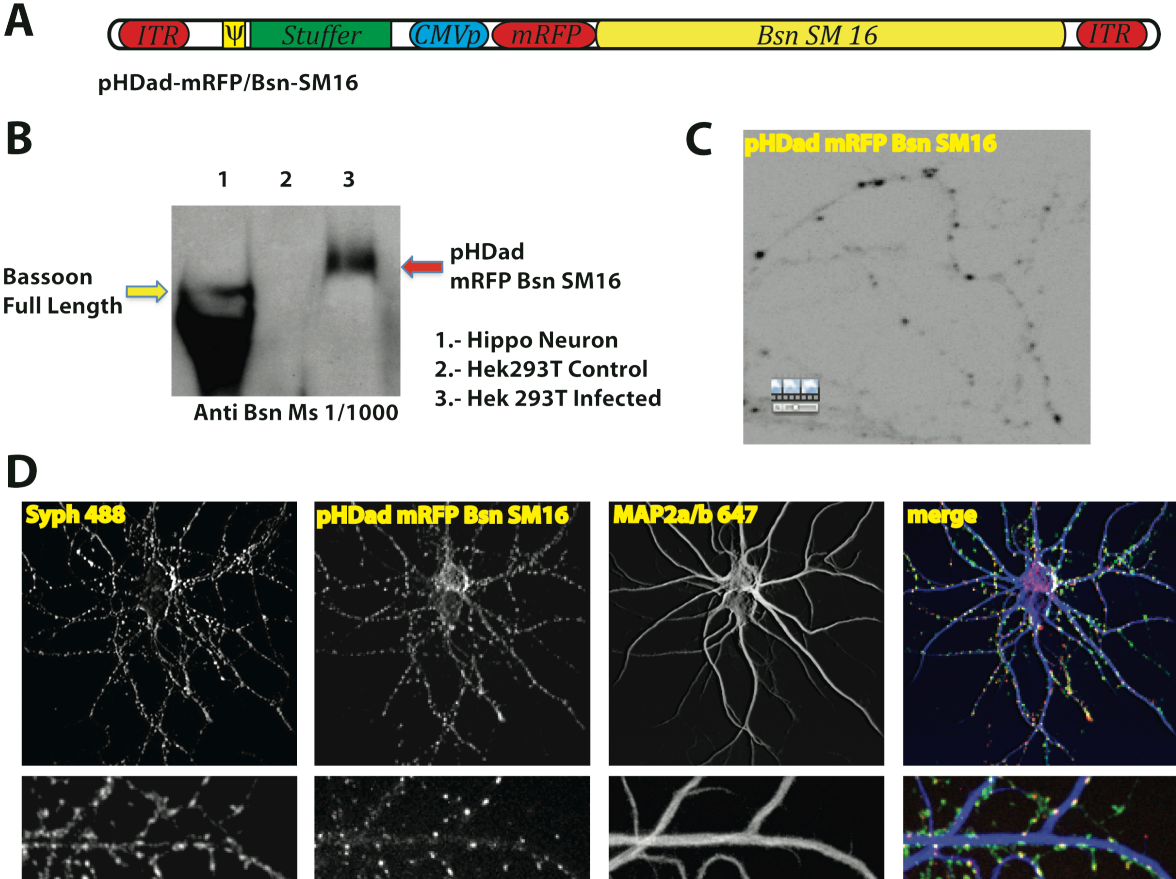


Fig. 3.14 Expression of full-length mRFP-tagged Bassoon using Adenovirus
(A) Schematic diagram of high capacity adenovirus (HDad) developed for the expression of full-length Bassoon. The N-terminus of Bassoon was tagged with mRFP, and nucleotides involved in shRNA-mediated knockdown by Bsn16 were mutated (SM16). (B) Western blots of lysates from uninfected neurons or HEK293T with and without infection with HDad-mRFP/Bsn-SM16 and then immunostained with Bassoon antibodies. (C) Live imaging of mRFP;;Bsn-SM16 positive puncta in the axons of hippocampal neurons 5DIV. These puncta represent transport vesicles for active zone proteins. (D) Spatial distribution of mRFP/Bsn-SM16 expressed in cultured hippocampal neurons. Neurons were infected on the day of plating and immunostained at 14 DIV with antibodies against MAP2a/b (Alexa 647; blue) or synaptophysin (Alexa 488; green).

3.3 Assessing the role of Piccolo in presynaptic assembly and function

Piccolo is structurally related to a second active zone protein, Bassoon. As both proteins are co-expressed at a variety of synaptic types (glutamatergic, GABAergic, glycinergic, dopaminergic, and cholinergic, among others), it appears that many functions performed by Piccolo may be shared or redundant to those of Bassoon. However, each has their own distinct sequence and are hypothesized to also have unique functions in the presynaptic bouton. In a set of studies described below, shRNA-mediated knockdown of Piccolo was used to assess its contribution to synapse assembly and function. Studies presented in the next section are designed to identify functions shared with Bassoon.

3.3.1 Loss of Piccolo does not affect synapse formation or morphology

As discussed in section 3.2, bicistronic lentiviral vectors were generated that express not only shRNAs against Piccolo (Pclo6 and Pclo28) but also have a presynaptic marker, EGFP-tagged SV protein Synapsin1a (e.g LV/EGFP::Syn1a/Pclo28). In neurons infected with LV/EGFP::Syn1a or LV/EGFP::Syn1a/Pclo28, clusters of EGFP::Syn1a along the dendritic arbors of uninfected cells were seen. Immunostaining of these cultures revealed that Bassoon clusters were found to colocalize with the EGFP-Syn1a clusters along dendritic that contained or lacked Piccolo, respectively (Figure 3.11). These data suggest that Piccolo may not be required for synapse formation.

To further test this hypothesis, cultured hippocampal neurons infected with either LV/EGFP::Syn1a or LV/EGFP::Syn1a/Pclo28 were also immunostained with antibodies against several key presynaptic (Synaptophysin, RIM1 α , Munc13-1) and postsynaptic (PSD-95, NR1) proteins (Figure 3.15A & B). As shown, each exhibited a punctate pattern that reliably colocalized with EGFP-Syn1a clusters along dendritic profiles, regardless of whether Piccolo was present (Figure 3.15A) or absent (Figure 3.15B). These data indicate that the loss of Piccolo does not disrupt the synaptic targeting of multiple key pre and postsynaptic proteins.

To assess whether the loss of Piccolo affected synapse ultrastructure, a strategy was developed for visualizing the boutons of neurons expressing Pclo28 by electron microscopy (EM). This was achieved by replacing EGFP::Syn1a in the pZOff vector with a second SV protein VAMP2 tagged at its C terminus with horseradish peroxidase (HRP) (VAMP2::HRP) (Figure 3.16A). VAMP2 is an essential transmembrane component of SVs (Elferink, Trimble et al. 1989; Sudhof, Baumert et al. 1989), and in VAMP2::HRP, the C-terminal HRP is situated within the vesicle lumen. Upon reaction with hydrogen peroxide and diaminobenzidine (DAB), HRP forms an electron-dense precipitate, enabling visualization of

vesicles within boutons of neurons expressing pZOff/VAMP2::HRP (Figure 3.16B). To verify that VAMP2::HRP did not affect Piccolo down regulation, cultures expressing pZOff/VAMP2::HRP or pZOff/VAMP2::HRP/Pclo28 were immunostained with antibodies against Piccolo and HRP at 6 DIV (Figure 3.17A). Under these conditions, Piccolo immunoreactivity was detected in the axons of untransfected neurons or those expressing VAMP2::HRP alone but not in axons of neurons expressing Pclo28. These data indicate that the down regulation of Piccolo by Pclo28 shRNA was not hampered by coexpression of VAMP2::HRP.

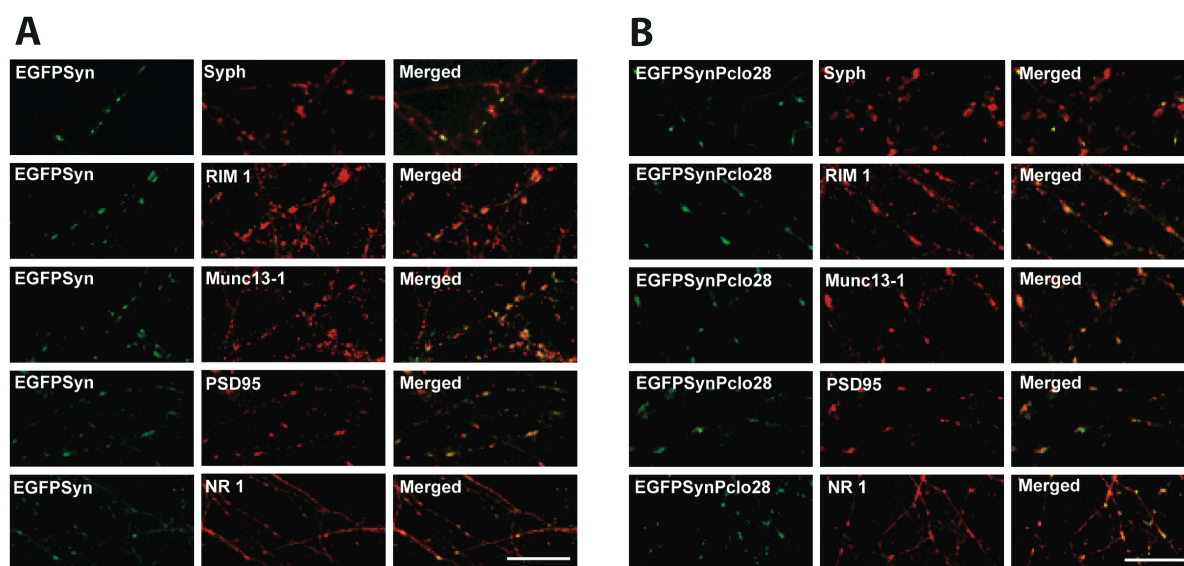


Fig. 3.15 Piccolo is not essential for the clustering of key pre and postsynaptic proteins
(A) Hippocampal neurons infected with LV/EGFP::Syn1a or **(B)** LV/EGFP::Syn1a/Pclo28 and immunostained with antibodies against Synaptophysin (Syph), RIM1 α , Munc13-1, PSD-95, or NR1 subunits of the NMDA receptor after 14 DIV. Shown are EGFP::Syn1a (green) puncta along MAP2 positive dendrites (not depicted) that colocalize (Merged) with each pre- or postsynaptic protein (red). Scale bars = 10 μ m.

To visualize synapses, hippocampal neurons electroporated at the time of plating with pZOff/VAMP2::HRP or pZOff/VAMP2::HRP/Pclo28 were fixed and processed for EM at 14 DIV. In both cases, presynaptic boutons expressing VAMP2::HRP were readily identified based on the presence of electron-dense SVs (Figure 3.16B and 3.17B).

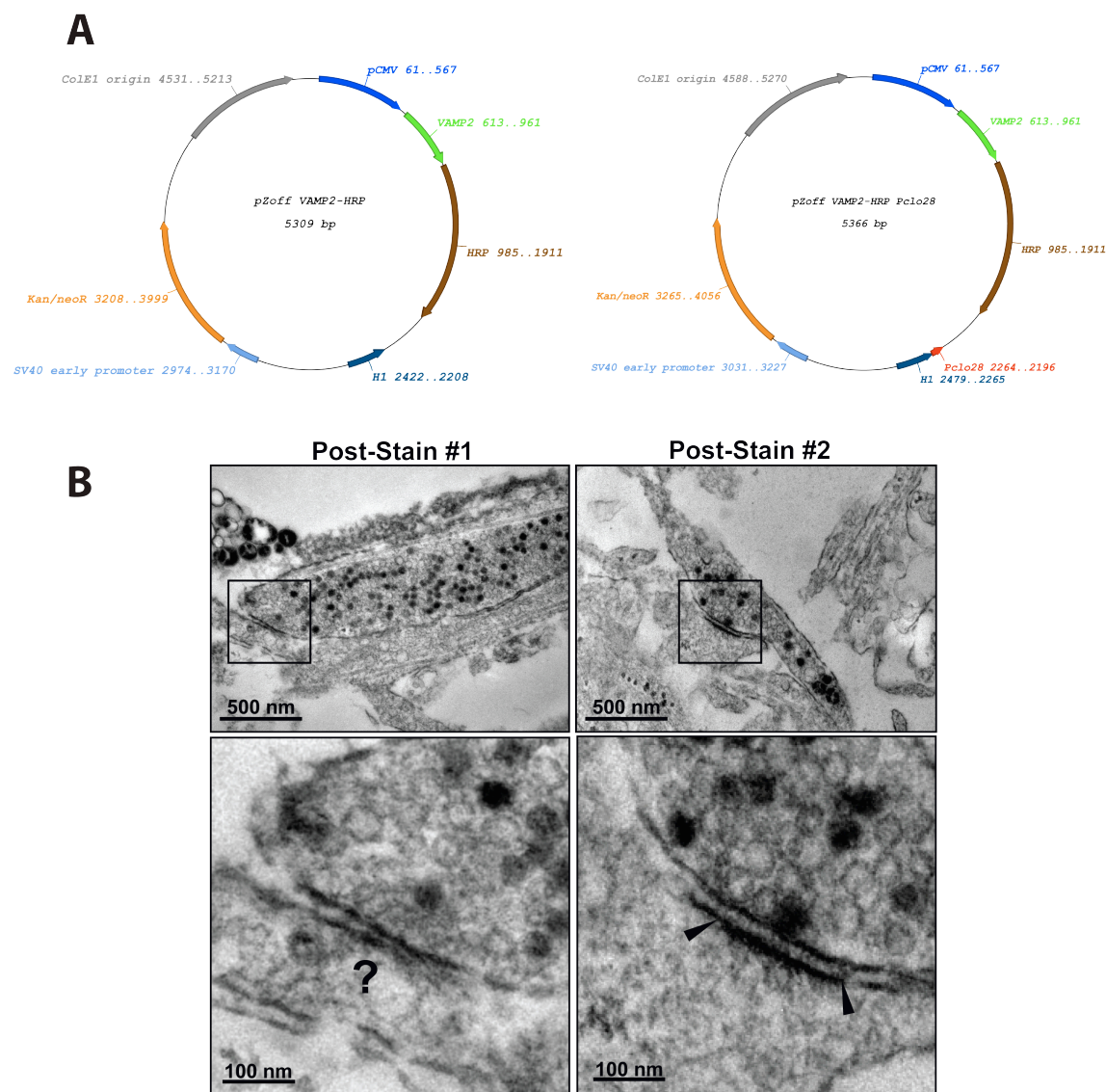


Fig. 3.16 Ultrastructural characterization of excitatory synapses with Horseradish peroxidase (HRP) tagged VAMP2

(A) Schematic diagram of the pZoff/VAMP2::HRP and pZoff/VAMP2::HRP/Pclo28 vectors used to express the shRNA against Piccolo (Pclo28). With HRP placed within the lumen of synaptic vesicles, VAMP2::HRP can be used to unambiguously label subsets of synaptic vesicles within presynaptic boutons of transfected neurons, without obscuring the synaptic junction or other synaptic structures when observed by electron microscopy. (B) Low (upper panels) and higher (lower panels) magnification electron micrographs of VAMP2::HRP positive axonal varicosities post-stained with either 3.5% uranyl acetate in 50% acetone (Post Stain #1) or 15 minutes of 5% uranyl acetate in aqueous solution (Post Stain #2). The latter stain, used for a majority of the studies, allows for a clearer visualization of the PSD in these preparations. In both conditions, the general bouton structure and other cellular organelles were appropriately stained and labeled SVs were clearly visible (top panels). In all samples with VAMP2::HRP, some darkening of the plasma membrane occurs, likely due to the presence of some protein on the plasma membrane. In the post-stain #1 condition, despite bouton proximity to adjacent neuronal plasma membranes, electron dense synaptic junctions were virtually absent (bottom left panel, for example). However, post-stain #2 adequately labeled synaptic junctions and post-synaptic densities (arrowheads in bottom right panel). These experiments demonstrate that the presence of labeled VAMP2-HRP on the synaptic plasma membrane was distinct from the electron-dense synaptic junction, which could be discerned and further analyzed.

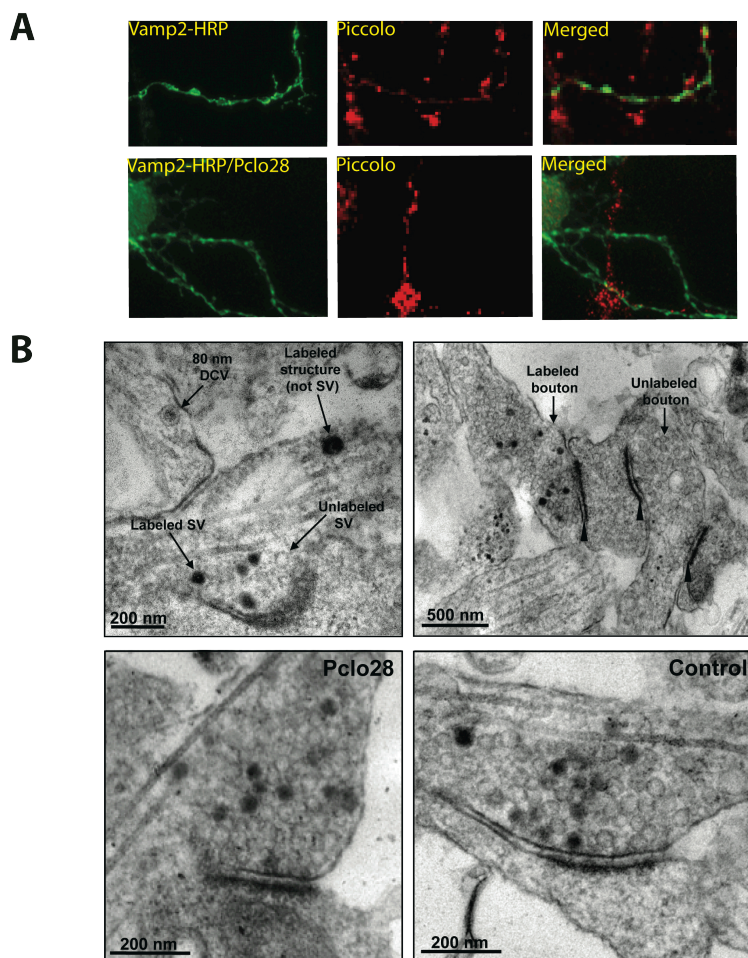


Fig. 3.17 Ultrastructural characterization of excitatory synapses lacking Piccolo

(A) Hippocampal neurons electroporated at the time of plating with pZOff/VAMP2-HRP or pZOff/VAMP2::HRP/Pclo28 and immunostained at 6 DIV with HRP (488/Alexa; green) and Piccolo (568/Alexa; red) antibodies. Note the lack of Piccolo immunoreactivity in Pclo28-expressing axons. (B) Transmission EM micrograph of a VAMP2::HRP positive bouton containing both clear-centered (unlabeled SV) and dark-centered SVs (labeled SV). HRP-labeled vesicles are easily distinguished from 80-nm DCVs and other labeled structures. Synaptic boutons from VAMP2::HRP expressing (labeled bouton) and untransfected (unlabeled bouton) neurons. Arrowheads denote synaptic junctions, identified based on electron-dense PSDs. An excitatory synapse formed between a pZOff/VAMP2::HRP/Pclo28 transfected presynaptic bouton and a postsynaptic spine. An excitatory synapse formed between a pZOff/VAMP2-HRP (control) transfected presynaptic bouton and a postsynaptic spine.

These labeled SVs were easily distinguishable from both unlabeled SVs and the 80 nm dense core vesicles hypothesized to carry Piccolo and Bassoon to nascent synapses (Figure 3.17B)(Zhai, Vardinon-Friedman et al. 2001). Qualitatively, no gross morphological differences were detected between unlabeled synapses, those expressing only VAMP2::HRP, and those expressing VAMP2::HRP/Pclo28 (Figure 3.17B). Furthermore, when synapses were carefully quantified for bouton area, AZ/PSD length, docked SVs/AZ length, and SV density (# vesicles/bouton area), no morphological differences were found (Table 3.1). These data strongly suggest that Piccolo is not essential for the structural assembly of excitatory asymmetric synapses.

Parameter	VAMP2 HRP	VAMP2 HRP Pclo28
AZ Length (nm)	0.258 ± 0.142	0.229 ± 0.102
Docked SVs/AV Length (n/um)	13.87 ± 6.26	14.29 ± 5.30
SV Density (n/um)	163.8 ± 58.36	169.0 ± 49.02
Percentage of SVs Labeled	20.4 ± 12.5%	24.5 ± 14.8%

Table 3.1 Quantitative ultrastructural analysis of synapses with or without Pclo28

All data are from boutons with at least two clearly labeled synaptic vesicles opposed to a distinct synaptic junction. All parameters were measured by an observer blind to phenotype. $n= 64$ boutons with 66 active zones for control and 53 boutons with 55 active zones for +Pclo28. Data are shown \pm standard deviation. t tests revealed no significant differences, with no $P < 0.05$.

3.3.2 Synapses lacking Piccolo exhibit faster rates of SV exocytosis

Although synapses still form in the absence of Piccolo, its large size and multiple binding partners suggest that it may be functionally important for SV recycling. To test this hypothesis, styryl FM dyes (Cochilla, Angleson et al. 1999) were used to analyze presynaptic function. To examine whether boutons lacking Piccolo were presynaptically active, the total recycling pool (TRP) of vesicles was labeled with FM4-64 (90 mM KCl, 60 sec) (Pyle, Kavalali et al. 2000) in neuronal cultures infected with either LV/EGFP::SynIa, LV/EGFP::SynIa/Pclo28, LV/EGFP::SV2, or LV/EGFP::SV2/Pclo28. At boutons with (EGFP::SynIa or EGFP::SV2) or without (EGFP::SynIa/Pclo28 or EGFP::SV2/Pclo28) Piccolo, more than 80% of EGFP::SynIa or EGFP::SV2 clusters co-localized with FM4-64 puncta (Figure 3.18A, B, C & D). These data indicated that synapses lacking Piccolo are presynaptically functional and no more likely to be silent than control boutons.

To determine the relative sizes of the total recycling pool (TRP) of SVs, the total FM fluorescence intensity at boutons containing or lacking Piccolo was examined. No difference was observed in the average intensity of FM4-64 fluorescence (Figure 3.19A), indicating that TRP size was unaffected by the absence of Piccolo. To evaluate whether the loss of Piccolo led to changes in SV exocytosis, the destaining kinetics of the TRP using both 10 and 5Hz electrical stimulation was compared (Figure 3.19B, C). Intriguingly, boutons lacking Piccolo destained more quickly than those expressing only EGFP-SynIa (two-way ANOVA; $p < 0.0001$ for both conditions)(Figure 3.19B, C), indicating that Piccolo is a negative regulator of SV exocytosis.

Piccolo could regulate SV exocytosis by influencing vesicle docking and/or fusion with the AZ plasma membrane, or by controlling SV translocation from the reserve to readily releasable pools. To explore possible changes in SV docking and/or fusion, the size of the

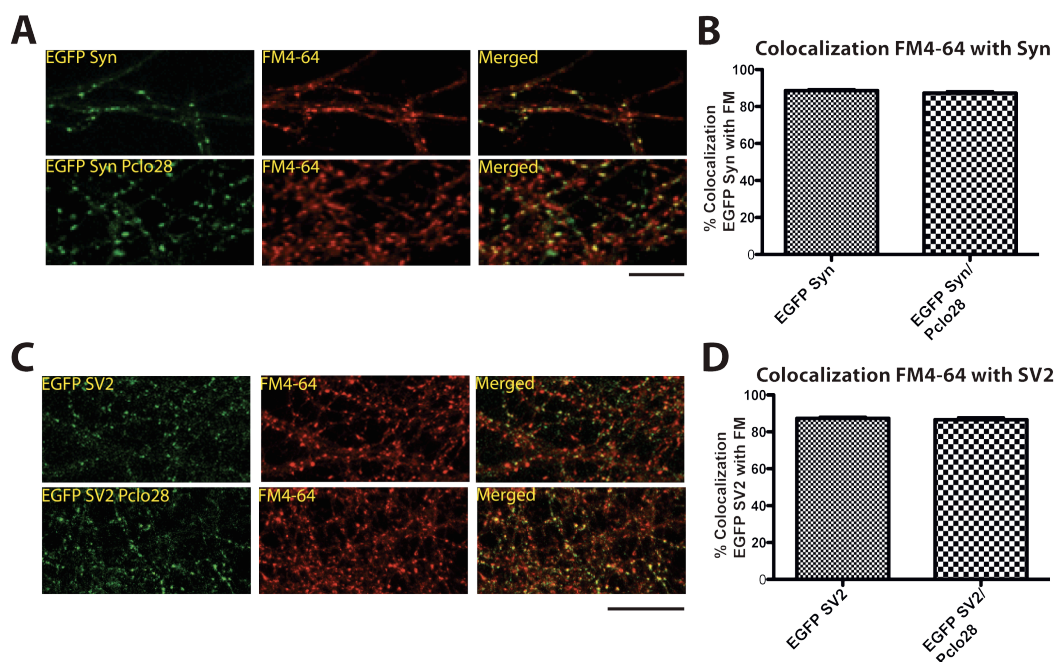


Fig. 3.18 Synapses lacking Piccolo have functional boutons

(A) Fluorescent images of 14 DIV hippocampal neurons infected with LV/EGFP::Syn1a or LV/EGFP::Syn1a/Pclo28 and loaded with FM4-64 (red) with 90mM K⁺. Note the high degree of match between EGFP-Syn1a and FM4-64 in both merged images. (B) Bar graphs quantifying the % colocalization between EGFP::Syn1a and FM4-64 puncta in control cultures (EGFP::Syn) or those lacking Piccolo (EGFP::Syn1a/Pclo28) ($n > 800$ puncta/condition, 2 expts) are over 80%. (C) Images of 14 DIV hippocampal neurons infected with LV/EGFP::SV2-W or LV/EGFP::SV2-W/Pclo28 were loaded with FM4-64 (red) using high K⁺ Tyrodes solution. (D) Bar graph quantifying the % colocalization of EGFP::SV2 puncta with FM4-64 in the presence or absence (Pclo28) of Piccolo. FM4-64 has over 80% of colocalization with EGFP-SV2 puncta. Like EGFP::Syn1a, EGFP::SV2 is a reliable marker of presynaptic boutons. Scale bars = 10 μm. Error bars are SEM.

readily releasable pool (RRP) of SVs or release probability (Pr) was monitored in the absence of Piccolo (Figure 3.19D & E). RRP represents the subpopulation of SVs that are docked at the active zone plasma membrane and poised to undergo fusion with the arrival of an action potential, while Pr is a measure of the probability that SVs in the RRP will undergo fusion. Two methods were used to estimate RRP size, one utilizing hypertonic sucrose (500 mM; ~800 mOsm) and the other a weak electrical stimulus (2Hz, 30 sec)(Pyle, Kavalali et al. 2000). Under both conditions, no significant difference in RRP size between wild type synapses and those lacking Piccolo was found (t test; $p > 0.5$)(Figure 3.19D).

To determine Pr, the destaining kinetics of boutons under conditions that stimulate RRP release was measured, as previously reported (Ryan, Reuter et al. 1993; Pyle, Kavalali et al. 2000; Mozhayeva, Sara et al. 2002; Sankaranarayanan, Atluri et al. 2003). Again, no significant difference in release probability between wild-type boutons and those lacking Piccolo was found (t test; $p > 0.5$)(Figure 3.19E). Taken together, these data indicated that the increased SV exocytosis rates observed at 5 and 10 Hz are not due to increased RRP size or Pr.

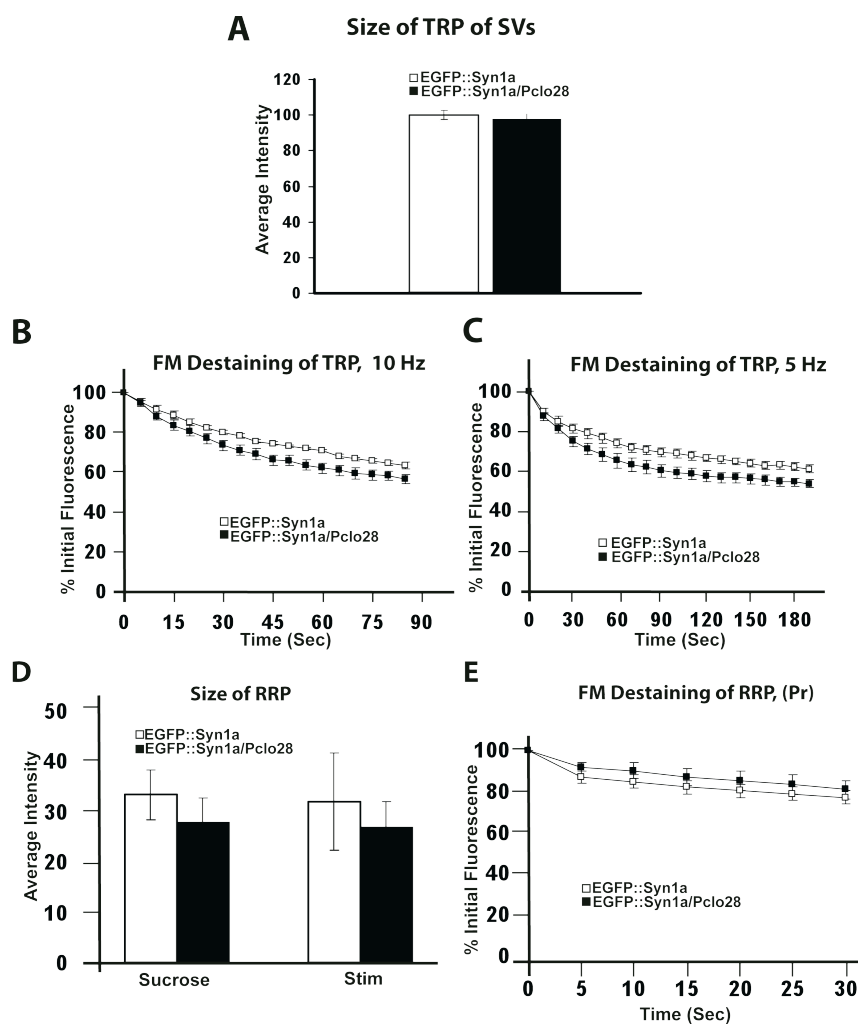


Fig. 3.19 Loss of Piccolo enhances the rate and does not affect the size of the readily releasable pool of synaptic vesicles

(A) Graphs bar of FM4-64 fluorescence intensity at EGFP::Syn1a puncta, comparing the relative sizes of the Total Recycling Pool (TRP) of SVs at control synapses (EGFP::Syn1a) and those lacking Piccolo (EGFP::Syn/Pclo28). FM4-64 intensity values at EGFP::Syn1a-expressing boutons were normalized against those from neighboring uninfected cells to enable cross-coverslip comparison. Average normalized FM4-64 intensity from control boutons was set to 100; that from Pclo28 boutons was ratio against this value ($n > 800$ puncta, 2 expts). (B & C) Destaining kinetics of the TRP at 10Hz B and 5Hz C, comparing synapses with EGFP::Syn1a and EGFP::Syn1a/Pclo28. (D) Graphs Bar comparing the size of the readily releasable pool (RRP) of synaptic vesicles in boutons expressing EGFP::Syn1a or EGFP::Syn1a/Pclo28, as determined by either the application of 500mM sucrose (left) or 2 Hz, 30sec stimulation (right). No significant differences were found (t test; $p > 0.5$). Sucrose experiments were performed twice for each condition, stimulation experiments 3 times, shown no difference on control versus shRNA of Piccolo. (E) Destaining kinetics of the RRP during 2 Hz, 30sec stimulation for control (EGFP::Syn1a) boutons and those lacking Piccolo (EGFP::Syn1a/Pclo28) ($n = 5$ expts/condition). SEM bars plotted.

3.3.3 Piccolo modulates the dispersion kinetics of Synapsin1a

From the above results, it would appear that Piccolo's negative regulation of SV exocytosis was unlikely to occur at the level of SV priming or fusion, as described for RIM1 α and Munc13 (Augustin, Rosenmund et al. 1999; Schoch, Castillo et al. 2002; Weimer and Richmond 2005; Gracheva, Burdina et al. 2006; Weimer, Gracheva et al. 2006), but rather at an earlier step, such as translocation of SVs from the reserve pool to the RRP.

To date, the only protein that has been implicated in regulating SV translocation is the SV-associated phosphoprotein Synapsin (De Camilli, Benfenati et al. 1990; Greengard, Valtorta et al. 1993; Ryan, Li et al. 1996; Chi, Greengard et al. 2003). Synapsin is hypothesized to mediate the clustering and retention of SVs within boutons (Greengard, Valtorta et al. 1993; Ceccaldi, Grohovaz et al. 1995). Activity-dependent phosphorylation/dephosphorylation of Synapsin by CaMKII, protein kinase A (PKA), MAPK, and protein phosphatases 2A and 2B (PP2A and PP2B) appears to regulate the exocytosis kinetics of SVs, presumably by regulating Synapsin binding to SVs and/or the actin cytoskeleton (Greengard, Valtorta et al. 1993; Ryan, Reuter et al. 1993; Jovanovic, Czernik et al. 2000; Pyle, Kavalali et al. 2000; Jovanovic, Sihra et al. 2001; Mozhayeva, Sara et al. 2002; Chi, Greengard et al. 2003; Sankaranarayanan, Atluri et al. 2003). Importantly, Synapsin has also been shown to undergo an activity-dependent dispersion away from presynaptic boutons (Chi, Greengard et al. 2001), and the rate of dispersion is linked to its phosphorylation state (Chi, Greengard et al. 2001; Chi, Greengard et al. 2003).

To explore whether the loss of Piccolo impacts SV translocation via alterations in the properties of Synapsin, the association and/or dispersion kinetics of Synapsin1a within presynaptic boutons were examined. For these experiments, the shRNA expression vector containing EGFP::Syn1a was used. Similar to experiments using LV/EGFP::Syn1a, no increase in Synapsin immunostaining at boutons expressing EGFP::Syn1a was found (Figure 3.9B,C), indicating that endogenous Synapsin expression is down-regulated in the presence of EGFP-Syn1a to maintain similar total levels/bouton. These levels were quantified and compared to the synaptic levels of EGFP::Syn1a in boutons of control neurons and those expressing Pclo28. No discernable differences in fluorescence intensity were observed when cultures were fixed with 4% paraformaldehyde (Figure 3.20A). However, when cultures were fixed with methanol, which extracts soluble proteins, a significant decrease (t-test; $p < 0.0001$) in the intensity of EGFP::Syn1a at boutons lacking Piccolo was detected (Figure 3.20A). This suggested that EGFP::Syn1a was not as tightly associated with SVs and/or actin-related structures in the absence of Piccolo but rather was shifted into a more soluble fraction.

To test this concept, Fluorescence Recovery After Photobleaching (FRAP) was used to monitor the steady-state exchange kinetics of EGFP::Syn1a fluorescence at individual boutons (Figure 3.20B, C). EGFP::Syn1a fluorescence recovered more quickly at boutons lacking Piccolo (Figure 3.28D) ($t_{\text{fast}} = 1.2$ min, $t_{\text{slow}} = 11.9$ min vs. $t_{\text{fast}} = 2.2$ min, $t_{\text{slow}} = 33.7$ min for control boutons; two-way ANOVA, $p < 0.0001$), indicating that mechanisms regulating the association of Synapsin1a with SVs and/or the actin/spectrin cytoskeleton were altered in the absence of Piccolo.

To assess whether the faster exchange kinetics of EGFP::Syn1a in the absence of Piccolo were due to decreased presynaptic stability and/or decreased association of SVs with synapses, the turnover rates of SV2, a SV integral membrane protein, in the presence and absence of Piccolo was examined. Here, an N-terminally EGFP-tagged SV2 was subcloned into our lentiviral vectors in place of EGFP::Syn1a. Similar to EGFP::Syn1a, EGFP::SV2 reliably labeled presynaptic boutons, exhibiting a high degree of colocalization with FM4-64 (Figure 3.18C, D). However, in contrast to EGFP::Syn1a, the exchange kinetics of EGFP::SV2 was not altered in the absence of Piccolo (Figure 3.20D, E), indicating that general presynaptic stability and SV retention were not significantly altered in the absence of Piccolo.

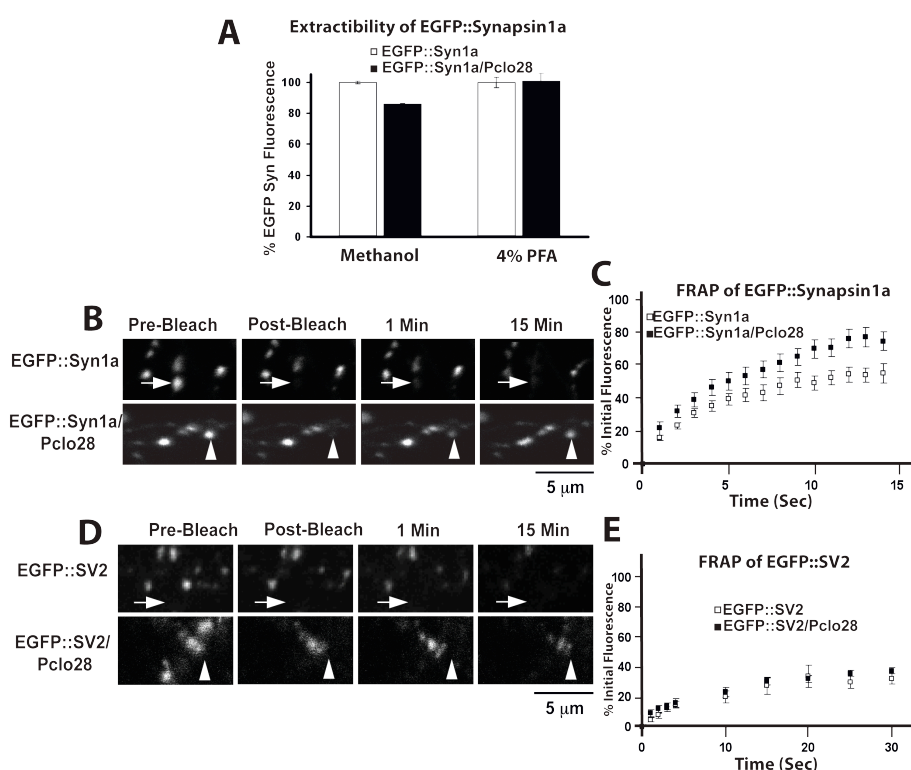


Fig. 3.20 Loss of Piccolo increases the solubility and exchange kinetics of Synapsin1a within presynaptic boutons

(A) Bar graphs of EGFP::Syn1a fluorescence intensity at presynaptic boutons from neurons expressing EGFP::Syn1a or EGFP::Syn1a/Pclo28. Data compare the effect of methanol versus 4% paraformaldehyde fixation ($n > 800$ puncta, 7 fields of view/condition). (B) Time-lapse images of EGFP::Syn1a puncta. Single fluorescent puncta (indicated by arrows) were photobleached and their recovery monitored over time. (C) Fluorescence recovery curves for puncta at boutons with EGFP::Syn1a, $n = 20$ or without Piccolo EGFP::Syn1a/Pclo28, $n = 17$. (D) Images of puncta at boutons with EGFP::SV2 or without Piccolo EGFP::SV2/Pclo28. (E) Fluorescence recovery curves for EGFP::SV2 puncta at synapses with EGFP::SV2, $n = 8$ or without Piccolo EGFP::SV2/Pclo28, $n = 12$ SEM bars plotted.

Differences in steady-state exchange kinetics could translate into activity-dependent differences in the dispersion kinetics of EGFP::Syn1a. Therefore, an electrical stimulation protocol (10 Hz, 90 sec) shown to promote the dispersion of EGFP::Syn1a was employed

(Chi, Greengard et al. 2001; Chi, Greengard et al. 2003). Changes in the fluorescence intensity of EGFP::SynIa at individual boutons were monitored both during stimulation and for the subsequent 10 min recovery period. In contrast to wild-type boutons, a more complete dispersion of EGFP::SynIa and a slower rate of recovery in boutons lacking Piccolo were observed (two-way ANOVA; $p < 0.0001$) (Figure 3.21A, B). A previously unreported heterogeneity in the extent of EGFP::SynIa dispersion at individual boutons under both conditions was observed.

To evaluate whether the extent of EGFP::SynIa dispersion was coupled to the rate of SV exocytosis, the loss of EGFP::SynIa and FM5-95 fluorescence from boutons during 5 Hz stimulation was simultaneously monitored for 3 min. The analysis revealed a tight correlation between the two events. At boutons with minimal EGFP::SynIa dispersion ($< 10\%$ for all time points), very little FM5-95 destaining occurred (Figure 3.21 C, D). In contrast, synapses with more complete EGFP::SynIa dispersion ($> 40\%$ after 30 sec stimulation) exhibited dramatic FM5-95 destaining (Figure 3.21C, D). This feature was present both at control synapses (Figure 3.21C) and those lacking Piccolo (Figure 3.21D). A statistical analysis of the final fluorescence intensity values for EGFP::SynIa and FM5-95 after the 3 min stimulation revealed a strong correlation between the extent of EGFP::SynIa dispersion and that of FM5-95 destaining at both control boutons and those lacking Piccolo ($r = 0.58$, $p < 0.0001$ for control; $r = 0.59$, $p < 0.0001$ for Pclo28) (Figure 3.21E, F). Although this tight correlation was observed for all synapses, the average degree of EGFP::SynIa dispersion and FM5-95 destaining was greater at boutons lacking Piccolo, significantly shifting these correlation values to the lower right (Figure 3.21E, F). These data strongly indicate that the accelerated SV exocytosis rates observed at synapses lacking Piccolo are coupled to concomitant increases in the dispersion kinetics of SynIa.

3.3.4 Changes in SV exocytosis and Synapsin dynamics are not observed at synapses lacking Bassoon

Boutons lacking Bassoon were tested to determine if phenotypes seen at boutons lacking Piccolo were similarly observed. To this end, sets of shRNAs against Bassoon were generated and subcloned into the LV/EGFP::SynIa vector under the control of the H1 promoter (Figure 3.9 & 3.11). This Bsn16-shRNA was found to efficiently and specifically reduce the expression of Bassoon in lysates of cultures infected with LV/EGFP::SynIa/Bsn16 on the day of plating and then harvested after 14 DIV (Figure 3.11).

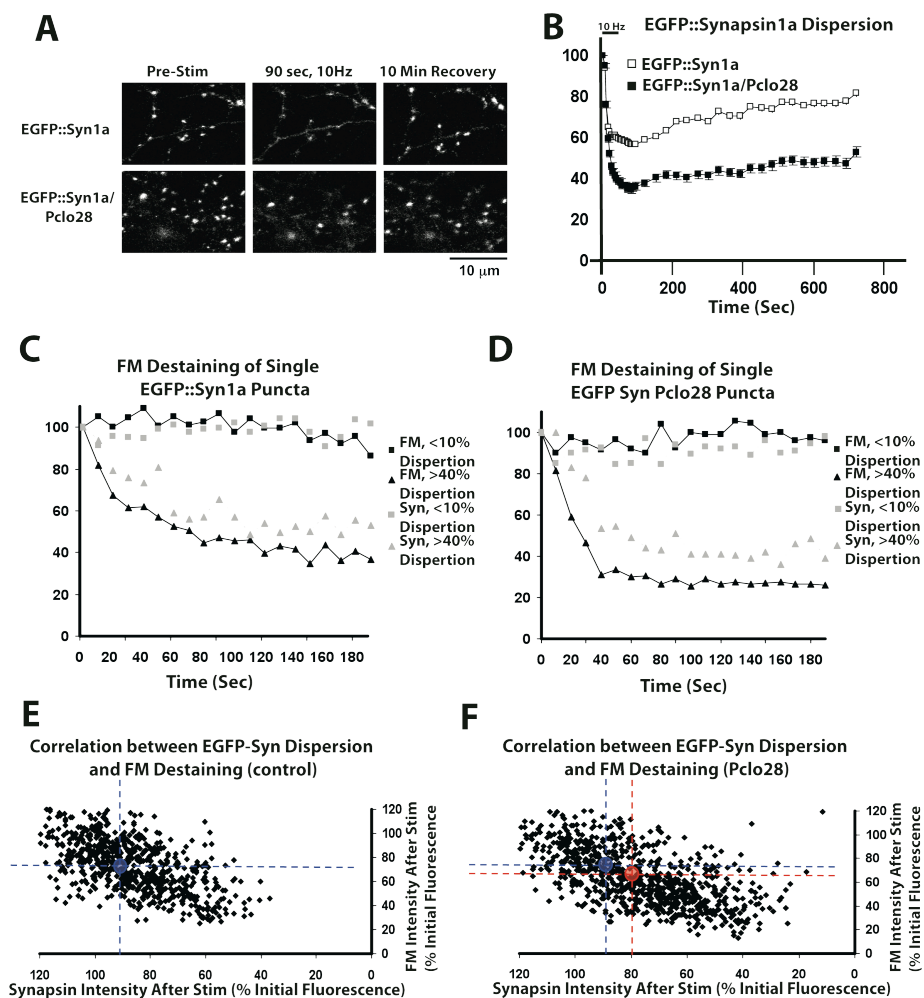


Fig. 3.21 Loss of Piccolo increases Synapsin1a dispersion and FM5-95 destaining kinetics

(A) Time lapse images of EGFP::Syn1a puncta. Images were acquired before, during, and after EGFP::Syn1a dispersion was elicited with 10Hz, 90 sec stimulation. Shown here are sample images taken before (pre) and immediately following stimulation (90 sec, 10Hz), as well as after 10 min of recovery. (B) Graphical representation of data from A, plotting the average change in fluorescence intensity over time at boutons with or without Piccolo ($n > 100$ puncta/condition). Bar in upper left indicates time during which stimulation (10Hz) was applied. Synapsin1a dispersion and FM destaining are tightly correlated. (C & D) FM5-95 destaining curves for individual EGFP::Syn1a puncta at boutons with C or without Piccolo D. Shown in black are examples of FM5-95 destaining curves for which there was either dramatic ($>40\%$; triangles) or minimal ($<10\%$; squares) dispersion of EGFP::Syn1a. Shown in light gray are EGFP::Syn1a intensities for these boutons. Correlation analysis of EGFP::Syn1a dispersion and FM5-95 destaining at synapses with E or without Piccolo F. Plotted are EGFP::Syn1a and FM5-95 intensity values (expressed as % initial fluorescence) at the final timepoint ($t=180$ seconds) of 5 Hz stimulation (control = 709 puncta, Pclo28 = 855 puncta). Dashed lines and circles indicate average intensity values for EGFP::Syn1a and FM5-95 at control boutons (blue; $90.8 \pm 1.0\%$ and $75.6 \pm 0.9\%$, respectively) and those lacking Piccolo (red; $79.2 \pm 0.9\%$ and $65.5 \pm 0.8\%$, respectively). Note that values for boutons lacking Piccolo are significantly shifted toward the lower right. SEM bars plotted

Similarly, at the synaptic level, a dramatic decrease ($>95\%$) in the percent co-localization of Bassoon and EGFP::Syn1a in axons along dendritic profiles was observed (Figure 3.11). This decrease was not observed for Piccolo (Figure 3.10), indicating that the Bsn16 shRNA is specific for Bassoon.

Using dynamic imaging, the dispersion and reclustering rates of EGFP::Syn1a was examined in boutons lacking Bassoon. As shown in Figure 3.11, synapses lacking Bassoon exhibited no detectable defects in EGFP::Syn1a dispersal or reclustering (Figure 3.22A), and no change in the destaining kinetics of FM5-95 (Figure 3.22B). Together, these observations strongly argue that the phenotypes observed for Piccolo are real and not artifacts of long-term shRNA expression. Moreover, they indicate that sequence elements unique to Piccolo play a fundamental role in negatively regulating SV exocytosis, apparently by influencing the activity-dependent dispersion of Synapsin1a.

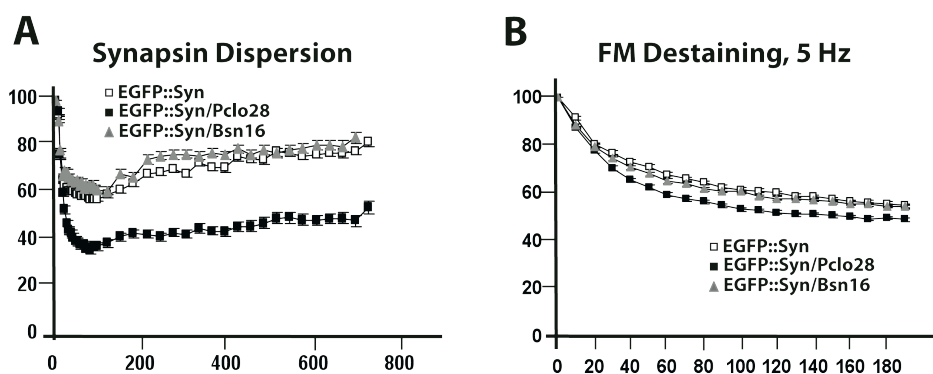


Fig. 3.22 Loss of Piccolo but not Bassoon from presynaptic boutons alters the dispersion kinetics of Synapsin1a and the destaining kinetics of FM5-95

(A) Dispersion and reclustering kinetics of EGFP::Syn1a in control boutons (EGFP::Syn1a) and those lacking Piccolo (EGFP::Syn1a/Pclo28) or Bassoon (EGFP::Syn1a/Bsn16). (B) EGFP::Syn1a and EGFP::Syn1a/Pclo28 curves are from **Fig. 3.21** ($n \sim 100$ puncta/condition). Destaining kinetics of FM5-95 during 5Hz stim for control boutons (EGFP::Syn1a) and those lacking Piccolo (EGFP::Syn1a/Pclo28) or Bassoon (EGFP::Syn1a/Bsn16). ($n > 200$ puncta, 2 expts/condition). SEM bars plotted.

3.3.5 Loss of Piccolo enhances the CaMKII sensitivity of Synapsin 1a

The association of Synapsin1a with SVs and the Actin cytoskeleton in nerve terminals is thought to be regulated by CaMKII phosphorylation (Schiebler, Jahn et al. 1986; Benfenati, Valtorta et al. 1992; Greengard, Valtorta et al. 1993; Stefani, Onofri et al. 1997; Chi, Greengard et al. 2001; Chi, Greengard et al. 2003). Thus, the altered dynamics of EGFP::Syn1a dispersion in the absence of Piccolo was hypothesized to be due to changes in its CaMKII-dependent phosphorylation. This was examined by blocking CaMKII activity with 10 μ M KN62 prior to and during a 10 Hz stimulation for 90 sec. KN62 had no significant effect on the dispersion kinetics or total amount of dispersion observed for EGFP::Syn1a in wild-type boutons (two-way ANOVA; $p = 0.15$) (Figure 3.23A, B). However, this treatment caused a dramatic reduction in EGFP::Syn1a dispersion at Pclo28 boutons, “rescuing” dispersion to levels seen at wild-type boutons (two-way ANOVA; $p < .0001$) (Figure 3.23B, C). To determine whether this decrease in dispersion was accompanied

by a decrease in SV exocytosis rate, the impact of KN62 on the destaining kinetics of FM5-95 at Pclo28 boutons was examined. Again, KN62 attenuated the Pclo28 phenotype, slowing the accelerated exocytosis of SVs seen in the absence of Piccolo (two-way ANOVA; $p < 0.0001$) (Figure 3.23D). These results indicate that the effects of Piccolo loss of function (LOF) are mediated in part by CaMKII. Moreover, they provide further evidence that the Synapsin dispersion and SV exocytosis phenotypes are mechanistically linked.

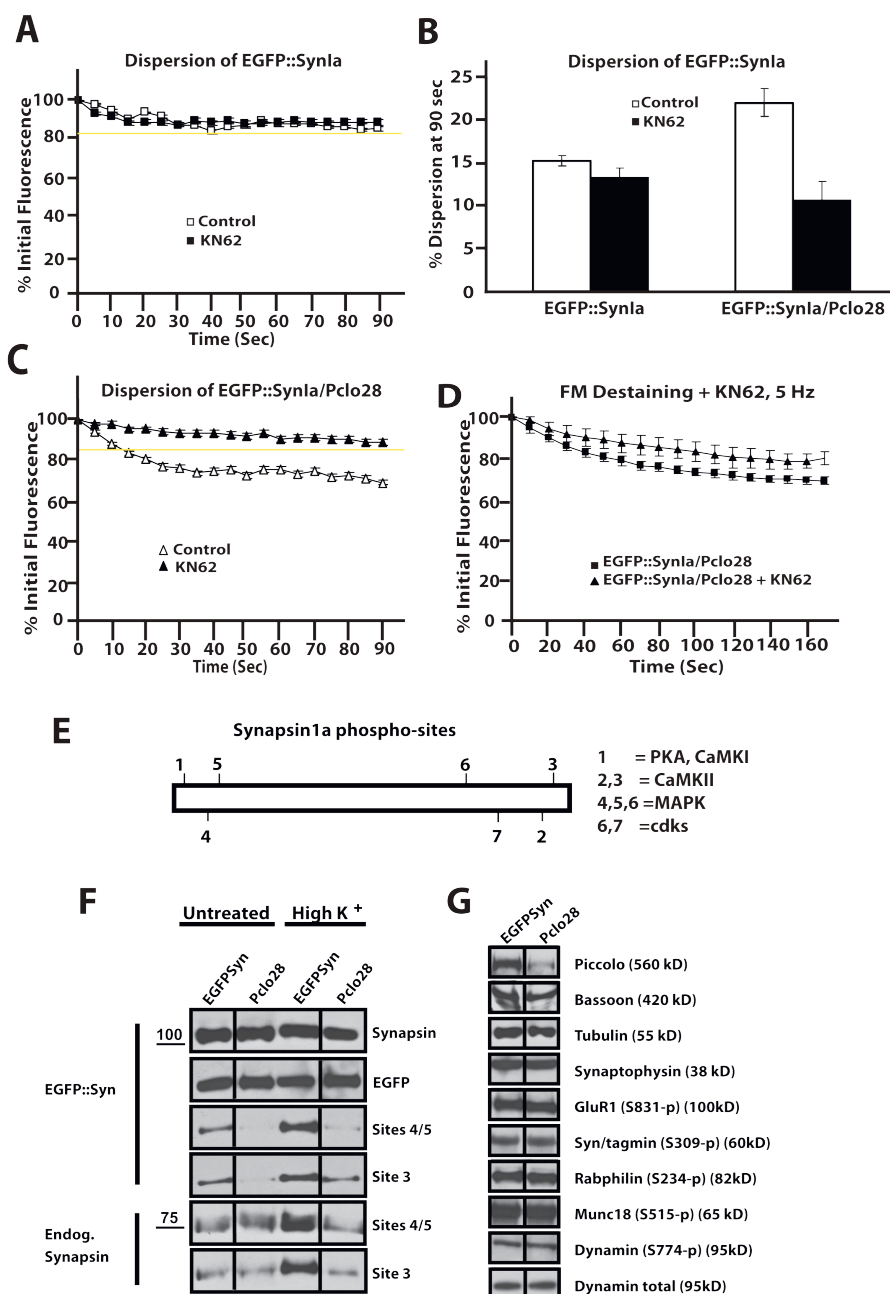


Fig. 3.23 CaMKII inhibition rescues Pclo28 phenotypes and synapsin1a is hypo-phosphorylated in the absence of Piccolo

(A) Dispersion kinetics of EGFP::Syn1a in wild-type neurons incubated with (KN62) or without (control) 10 μ M KN62 during a 90 sec, 10 Hz stim. Yellow line indicates maximal amount of dispersion (expressed as % of initial fluorescence intensity prior to stimulation) seen in these neurons without KN62 ($n > 100$ puncta/condition). (B) Bar graphs summarizing the % dispersion of EGFP::Syn1a puncta at synapses with EGFP::Syn1a or without Piccolo EGFP::Syn1a/Pclo28 in the presence (black) or absence (white) of KN62. % dispersion = $(100 - \% \text{ initial fluorescence})$ was

measured at 90 sec following a 10Hz, 90sec stim (n=2 expts, 905 puncta for control w/o KN62; 3 expts, 1070 puncta for control +KN62; 7 expts, 2195 puncta for Pclo28 w/o KN62; 8 expts, 2341 puncta for Pclo28 +KN62). SEM bars plotted. (C) Dispersion kinetics of Synapsin1a in neurons lacking Piccolo and incubated with (KN62) or without (control) KN62 during a 90 sec, 10 Hz stimulation. For comparison, yellow line indicating maximal amount of dispersion observed in wild-type neurons is included (n>100 puncta/condition). (D) Destaining kinetics of FM5-95 at boutons lacking Piccolo in the presence (triangles) or absence (squares) of KN62, during a 5Hz, 180sec (900 pulse) stimulation (n=5 expts, 1134 puncta for Pclo28 w/o KN62; 2 expts, 437 puncta for Pclo28 +KN62). SEM bars plotted. (E) Schematic diagram of Synapsin1a, illustrating the names and positions of each of its seven characterized phospho-sites. (F) Western blot of hippocampal lysates from 14 DIV control cells EGFP::Syn1a and those lacking Piccolo EGFP::Syn1a/Pclo28, untreated or treated with high K⁺ (2min, 90mM KCl) and probed with phospho-Synapsin1a antibodies recognizing Site 3 or Sites 4/5, as well as antibodies against total Synapsin1a and EGFP. Upper panels are EGFP::Syn1a, lower panels are endogenous Synapsin. This experiment was repeated 3 times to verify the results. (G) Western blot of lysates from unstimulated control cells EGFP::Syn1a and those lacking Piccolo EGFP::Syn1a/Pclo28, probed with antibodies against Piccolo, Tubulin, Synaptophysin, and Dynamin, as well as phospho-antibodies against GluR1, Synaptotagmin, Rabphilin, Munc18, and Dynamin. This experiment was performed twice to verify the results.

3.3.6 Synapsin1a is hypophosphorylated in the absence of Piccolo

The ability of KN62 to rescue the Pclo28 phenotypes suggested that Synapsin might be hyperphosphorylated by CaMKII in the absence of Piccolo. To test this idea, Western blots of hippocampal lysates containing (EGFP::Syn1a) or lacking (EGFP::Syn1a/Pclo28) Piccolo were probed with two phospho-Synapsin1a antibodies that recognize sites phosphorylated by CaMKII or MAPK (Figure 3.23E) (Chi, Greengard et al. 2003). In these experiments, lysates from 14 DIV cultures were analyzed either directly (untreated) or after high K⁺ treatment (90 mM KCl, 2 min) to stimulate Synapsin phosphorylation. As expected, the levels of both endogenous and EGFP::Syn1a phosphorylation at sites 3, 4 and 5 increased in all lysates after high K⁺ stimulation (Figure 3.23F). However, in lysates from Pclo28 neurons, the levels of phosphorylation at these sites under both basal and high K⁺ conditions were dramatically reduced (Figure 3.23F). This unexpected finding suggested that the kinase/phosphatase balance at boutons lacking Piccolo was altered and that perhaps these boutons exhibited enhanced phosphatase activity. To test this hypothesis, a panel of phospho-specific antibodies against a number of pre and postsynaptic proteins, including GluR1, Synaptotagmin, Rabphilin, Munc18, and Dynamin were screened. The phosphorylation levels of these proteins as assessed by Western blot were not altered in the absence of Piccolo (Figure 3.23G), indicating that the effect could be specific to Synapsin.

3.3.7 Altered Synapsin phosphorylation does not mediate the Piccolo LOF phenotypes

Activity-dependent phosphorylation of Synapsin1a by multiple kinases (Figure 3.23E) has been shown to regulate its association with SVs and the actin cytoskeleton (Schiebler, Jahn et al. 1986; Benfenati, Valtorta et al. 1992; Ceccaldi, Grohovaz et al. 1995; Hosaka,

Hammer et al. 1999; Chi, Greengard et al. 2001; Jovanovic, Sihra et al. 2001; Chi, Greengard et al. 2003). For instance, serine to alanine (S/A) phospho-mutants that prevent PKA and/or CaMKII phosphorylation of EGFP-Syn exhibit decreased t values of activity-dependent dispersion and FM destaining, suggesting that they dissociated more slowly from SVs and/or the actin cytoskeleton within presynaptic boutons (Chi, Greengard et al. 2001; Chi, Greengard et al. 2003). This raised the question of whether Pclo28 phenotypes are mediated via the altered phosphorylation of Synapsin.

This was examined by exploring whether the Synapsin S23A phospho-mutant, which prevents CaMKII phosphorylation and slows both dispersion and FM destaining kinetics in wild-type neurons (Chi, Greengard et al. 2001; Chi, Greengard et al. 2003), could suppress synapsin dispersion kinetics in synapses lacking Piccolo. Surprisingly, this mutation did not decrease the extent of Synapsin dispersion (Figure 3.24A, B). Moreover, treating neurons with KN62 to inhibit CaMKII activity only partially rescued the extent of wild-type Synapsin dispersion or that of the S23A mutant in boutons lacking Piccolo, (Figure 3.24A, B). These data indicate that CaMKII phosphorylation of Synapsin does not mediate its enhanced dispersion in the absence of Piccolo. To further investigate whether other Synapsin phosphorylation sites could contribute to the Pclo28 phenotypes, additional phospho-mutants were examined. Specifically, mutations that disrupted the PKA phosphorylation site (S1A) or nearly all Synapsin phosphorylation sites (S12346A) were generated and their dispersion kinetics measured in neurons lacking Piccolo. As with S23A, neither of these mutants rescued the Pclo28 phenotypes (Figure 3.24C, D). For example, S12346A partially rescued Synapsin dispersion but had no effect on FM destaining (Figure 3.24D, E, F), while S1A, like S23A, had no effect on Synapsin dispersion but completely rescued the extent of FM destaining (Figure 3.24D, E, F). Similarly, the addition of PKA and/or MAPK inhibitors (KT5720 & PD98, respectively) had no effect on EGFP::SynIa dispersion (Figure 3.24G, H), suggesting that of the kinases examined, only CaMKII is linked to the Pclo28 phenotypes. Taken together, these data indicate that while Synapsin phosphorylation and exchange kinetics are altered in the absence of Piccolo, the alteration in the properties of Synapsin cannot account for the Pclo28 phenotypes.

3.3.8 Activity-dependent F-actin assembly is disrupted in the absence of Piccolo

An alternative explanation for the observed phenotypes in neurons lacking Piccolo is that they are due to altered presynaptic actin dynamics. Supporting this concept, actin depolymerization has been shown to enhance EGFP-SynIa dispersion and FM4-64

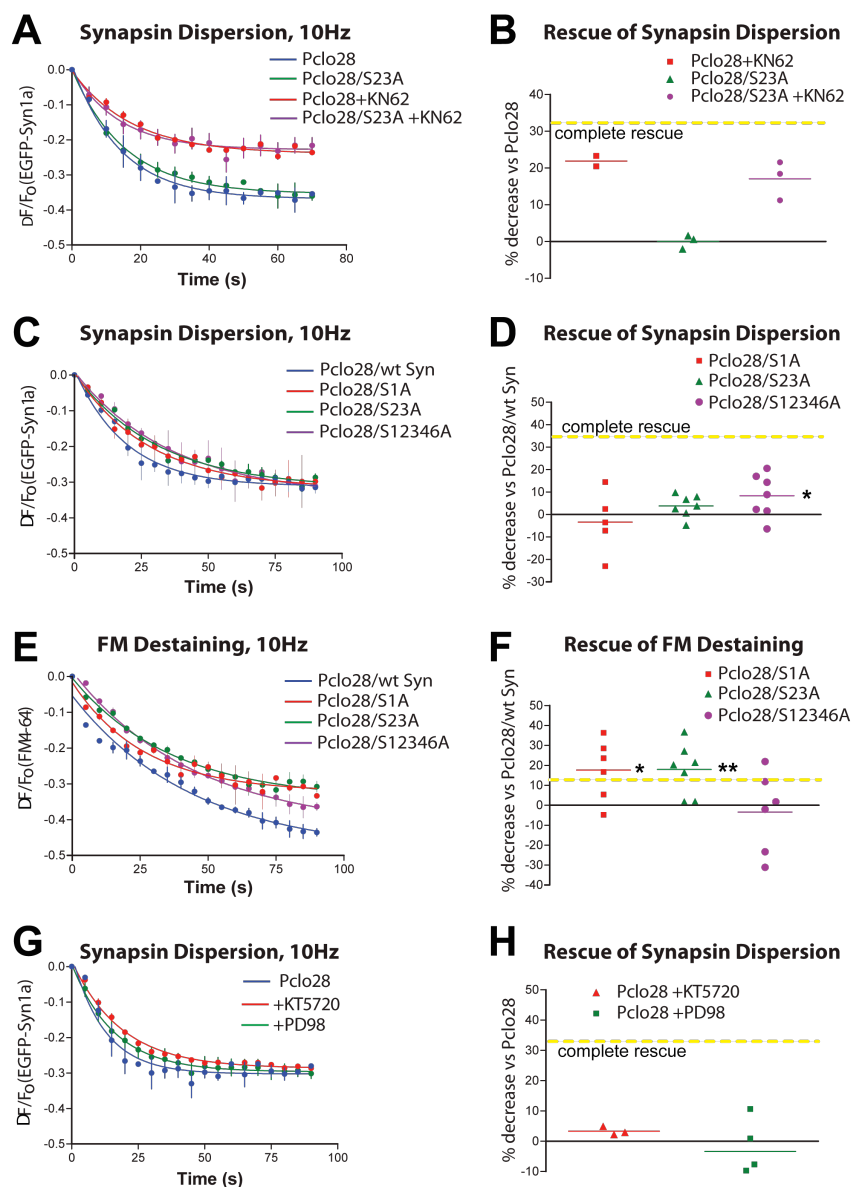


Fig. 3.24 Aberrant Synapsin1a phosphorylation does not cause the Pclo28 phenotypes

(A) Timecourse of dispersion for wild-type and S23A mutant Synapsin1a in neurons lacking Piccolo, in the presence or absence of KN62. KN62 attenuates the dispersion of both wild-type and S23A Synapsin1a. (B) Average extent of EGFP::Syn1a dispersion +/- KN62, expressed as % decrease in EGFP::Syn1a dispersion for S23A vs. wild-type EGFP::Syn1a in the Pclo28 background (n=2 coverslips for EGFP::Syn1a + KN62, 3 for S23A, 3 for S23A + KN62; 2 batches of neurons). Yellow line denotes “complete rescue” of Pclo28 phenotype, defined as the % decrease in EGFP::Syn1a dispersion observed in wild-type neurons vs. Pclo28 neurons (=33%). (C) Timecourse of dispersion for wild-type (wt), S1A, S23A, and S12346A EGFP::Syn1a mutant constructs in neurons expressing Pclo28. S12346A partially rescues the EGFP::Syn1a dispersion phenotype, with 8.4% less dispersion than wt EGFP::Syn1a in Pclo28 boutons (*= p<0.05, t-test). (D) Average extent of EGFP::Syn1a dispersion, expressed as % decrease in EGFP::Syn1a dispersion for phospho-mutants vs. wt EGFP::Syn1a in neurons expressing Pclo28. Yellow line denotes complete rescue of the Pclo28 phenotype. (E) Timecourse of FM4-64 destaining at boutons expressing wild-type (wt), S1A, S23A, and S12346A EGFP::Syn1a mutant constructs in neurons expressing Pclo28. (F) Average extent of FM destaining, expressed as % decrease in FM destaining for phospho-mutants vs. wild-type EGFP::Syn1a in neurons expressing Pclo28 (n=5 coverslips for S1A, 7 for S23A and S12346A; 3 batches of neurons). Yellow line denotes complete rescue of Pclo28 phenotype, defined as the % decrease in FM4-64 destaining observed in wt neurons vs. Pclo28 neurons (=11.6%). S1A and S23A both rescue the enhanced FM4.64 destaining (by 17.6% and 17.9%, respectively), but S12346A does not (*= p<0.05; ** = p<0.005, t-test). (G) Timecourse of EGFP::Syn1a dispersion in neurons

expressing Pclo28, in the presence of PKA (KT5720) and MAP kinase (PD98) blockers. SEM values shown ($n > 3$ experiments/condition). SEM bars plotted. **(H)** Average extent of Synapsin dispersion in the presence of PKA and MAPK inhibitors. Neither has a significant effect on EGFP::Syn1a dispersion.

destaining in cultured hippocampal neurons (Sankaranarayanan, Atluri et al. 2003), similar to Piccolo knockdown. As an initial test of this hypothesis, Pclo28-expressing neurons were treated with the F-actin stabilizing drug jasplakinolide, which largely normalized the enhanced EGFP::Syn1a dispersion and FM4-64 destaining (Figure 3.25A, B C, D, & E).

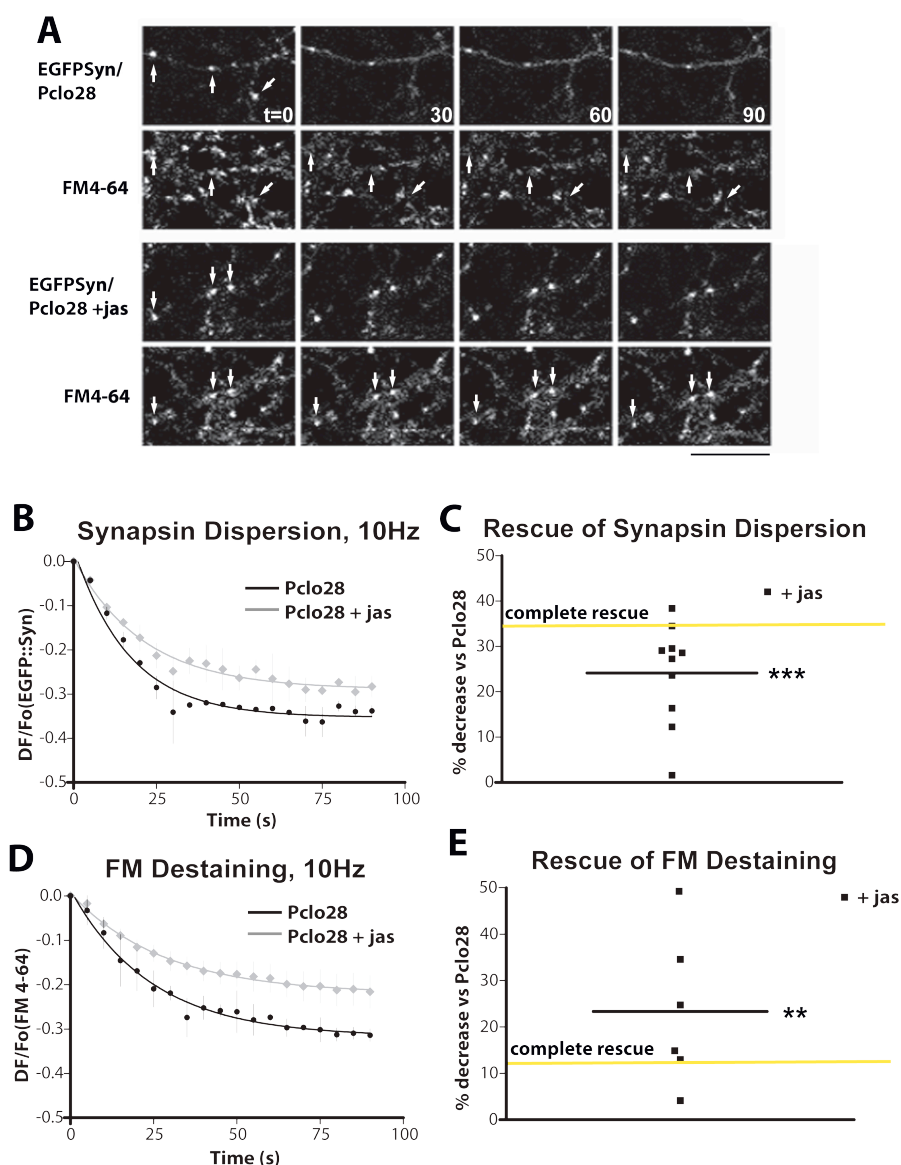


Fig. 3.25 Inhibiting F-actin assembly with Jasplakinolide rescues the Pclo28 phenotypes **(A)** EGFP-Syn1a dispersion and FM4-64 destaining in boutons of neurons infected with LV/EGFP::Syn1a/Pclo28 and treated with +/- 5 mM jasplakinolide. Arrows denote colocalized EGFP::Syn1a and FM4-64 puncta. 15 μ m size bars. **(B)** Timecourse of EGFP::Syn1a dispersion at boutons lacking Piccolo, in the absence (black) or presence (gray) of jasplakinolide. SEM bars shown ($n=2$ experiments/condition). **(C)** Average extent of EGFP::Syn1a dispersion in the boutons of neurons expressing Pclo28 and treated with jasplakinolide ($n=10$ coverslips). Complete rescue (Yellow line). Jasplakinolide decreases the extent of dispersion by 24.1% (**= $p < 0.0001$, t-test). **(D)** Timecourse of FM4-64 destaining at boutons lacking Piccolo, in the absence (black) or presence

(gray) of jasplakinolide. SEM values shown (n=2 expts/condition). (E) Average extent of FM destaining at Pclo28 boutons treated with jasplakinolide (n=6). Complete rescue (dashed line). Jasplakinolide decreases the extent of FM4-64 destaining by 23.3% (**= p<0.005, t-test).

To directly assess F-actin polymerization in neurons lacking Piccolo, the dynamic behavior of EGFP:: β -actin was monitored in these neurons. Previous studies showed that EGFP:: β -actin clusters at presynaptic boutons in response to synaptic depolarization, and that this phenomenon represented F-actin polymerization (Colicos, Collins et al. 2001; Sankaranarayanan, Atluri et al. 2003). In our experiments, EGFP:: β -actin clustering was induced by stimulating neurons for 30-45 sec with high K^+ (90 mM KCl) Tyrodes solution containing FM4-64 to allow for simultaneous label of functional presynaptic boutons. Here, the high K^+ treatment caused a robust recruitment of EGFP:: β -actin to presynaptic sites in wild-type neurons, as indicated by approximately 60% colocalization of EGFP:: β -actin clusters with FM4-64 as well as with Piccolo and synaptophysin immunostaining (Figure 3.26A, B). Together these data indicate that changes in presynaptic function observed in the absence of Piccolo are largely accountable through a role of Piccolo in regulating the dynamic assembly presynaptic F-actin.

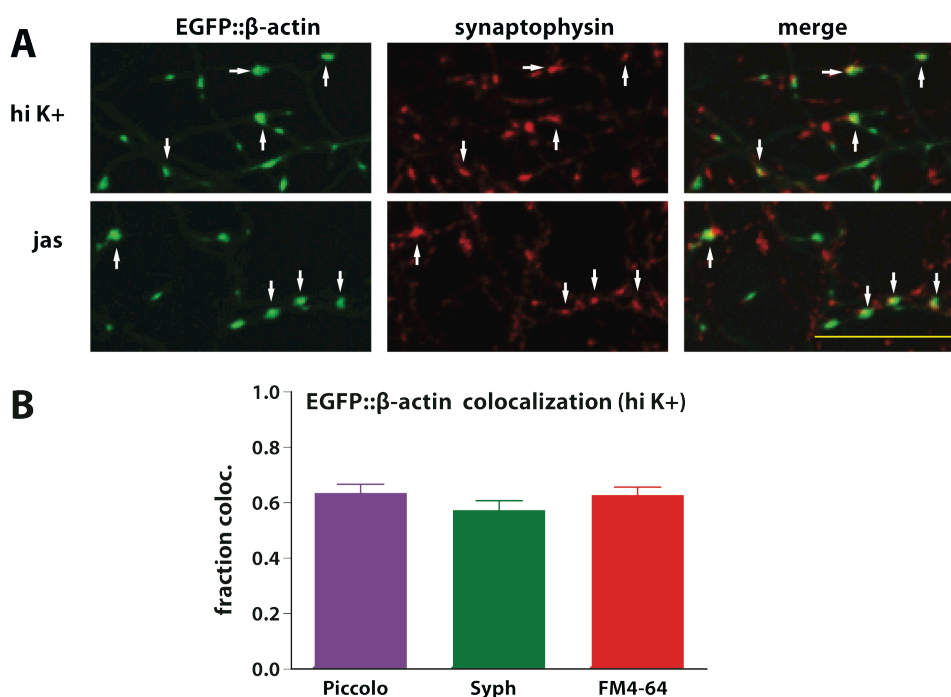


Fig. 3.26 Presynaptic localization of EGFP::Actin markers

(A) Fluorescent images of hippocampal neurons 14DIV expressing EGFP:: β -actin. Following either a high K^+ stimulation (90mM KCl) or the addition of 5 mM jasplakinolide, axonal EGFP:: β -actin is found to coalesce into puncta that, colocalize with synaptophysin immunoreactive puncta (indicated by arrows), indicating that synaptic activity directs the presynaptic recruitment/assembly of F::Actin. Size bar is 10 μ m. (B) Quantification of the fraction of EGFP:: β -actin puncta that colocalize with Piccolo or synaptophysin immunoreactive puncta. Also quantified is the % colocalization of EGFP:: β -actin puncta with sites of synaptic vesicle recycling as measured by FM4-64 uptake following a High K^+ stimulation. Note, approximately 60% of EGFP:: β -actin puncta (induced by high

K⁺ stimulation for these experiments) are presynaptic based on colocalization with all three markers (n=6 fields of view for Piccolo, 5 for synaptophysin, 9 for FM4-64).

3.3.9 CaMKII dynamics are altered in axons lacking Piccolo

Like Actin, the signaling molecule CaMKII, implicated in pre and postsynaptic plasticity mechanisms, has been shown to undergo activity-dependent clustering at presynaptic boutons (Tao-Cheng, Dosemeci et al. 2006). These findings suggest that presynaptic CaMKII dynamics could depend upon F-actin assembly and might be altered in the absence of Piccolo. To test this idea, the activity-dependent clustering of YFP::CaMKII α in control boutons was compared to neurons treated with latrunculin A. As in the EGFP:: β -actin experiments, high K⁺ induced strong clustering of YFP::CaMKII α at presynaptic boutons. However, pre-treatment with latrunculin A blocked this effect (Figure 3.27A-C). Moreover, in neurons lacking Piccolo, YFP::CaMKII α clustering was significantly reduced (Figure 3.27A-C), indicating that Piccolo indeed facilitates the activity-dependent recruitment of CaMKII into presynaptic boutons via its regulation of F-actin assembly. This defect in presynaptic CaMKII clustering could explain the lower levels of activity-dependent, CaMKII-mediated Synapsin phosphorylation observed in neurons lacking Piccolo described previously (see 3.3.8).

3.3.10 Pclo Δ Ex14 $-/-$ mice exhibit normal F-actin assembly

A recent study described mice with a targeted deletion of exon 14 in the PCLO gene (Pclo Δ Ex14), encoding 125 nucleotides of the C2A domain (Mukherjee, Yang et al. 2010) (Figure 3.41). The authors reported a >95% reduction in Piccolo protein levels based on Western blots using a C-terminal antibody, yet no defects in neurotransmission or synaptic plasticity (Mukherjee, Yang et al. 2010). These data suggest clear difference with our experiments using Pclo28 shRNA. To reconcile these differences, the protein expression patterns and primary synaptic phenotype of Pclo28-expressing neurons with those prepared from Pclo Δ Ex14 mice were compared.

To reassess the impact of deleting this C-terminal exon on the expression of the 560 kDa Piccolo, the expression pattern of Piccolo isoforms in total brain homogenates from wild-type, heterozygous, and Pclo Δ Ex14 littermates were examined by Western blot using our well-characterized 44aII antibody (Cases-Langhoff, Voss et al. 1996; Fenster, Chung et al. 2000; Fenster and Garner 2002); (Figure 3.28A).

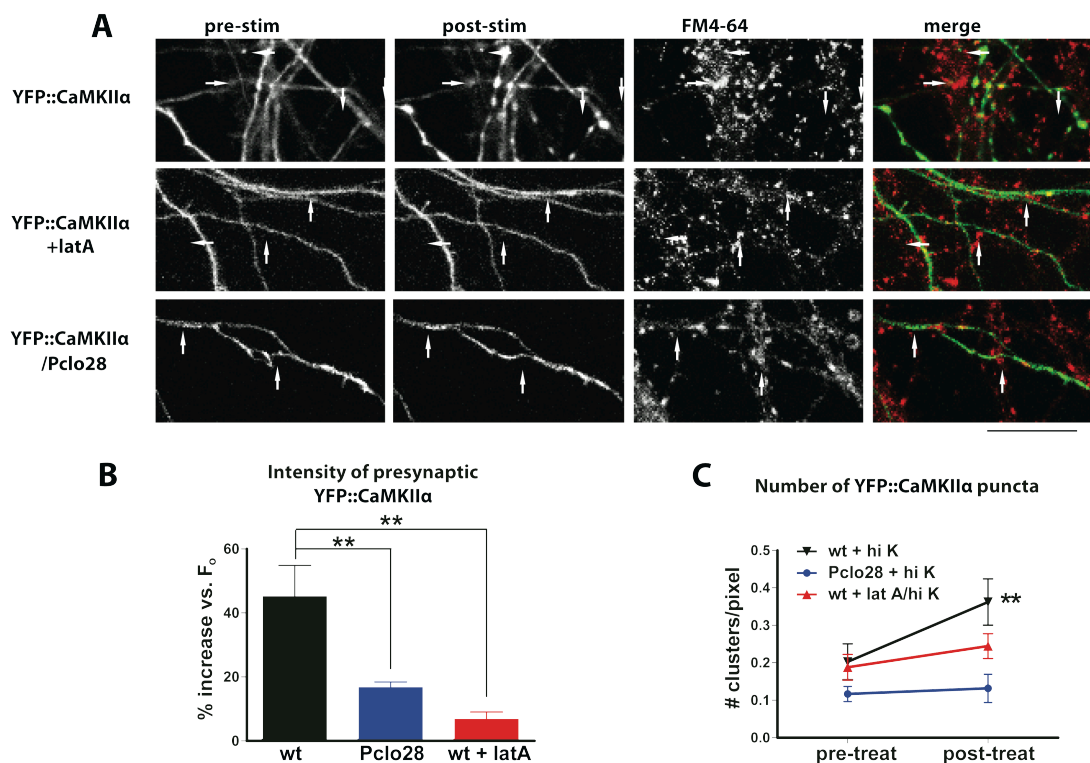


Fig. 3.27 CaMKII α recruitment to presynaptic boutons is impaired in Piccolo knockdown neurons

(A) Fluorescent images of YFP::CaMKII α expressing rat hippocampal neurons grown for 14DIV. Initial YFP::CaMKII α fluorescent is evenly distributed within axons and then becomes concentrated within presynaptic boutons following a High K⁺ stimulation. Boutons in these live experiments are identified by labeling recycling pools of synaptic vesicles with FM4-64 during the High K⁺ stimulation. Shown is the redistribution of YFP::CaMKII α in control, latrunculin A-treated, and Pclo28-expressing axons, before (pre) and after (post) stimulation with 90 mM KCl Tyrodes buffer + FM4-64. Arrows indicate presynaptic sites based on FM4-64 labeling. In wild-type axons, YFP::CaMKII α becomes more punctuate after stimulation; latrunculin A and Pclo28 shRNA block this effect. 15 μ m size bar. (B) Bar graphs quantifying the percent increase in YFP-CaMKII α fluorescence intensity at presynaptic boutons following high K⁺ stimulation. Fluorescence increases 45% in wild-type neurons, but only 17% in the Piccolo knockdown and 7% in the presence of latrunculin (n=8 for wt, 6 for Pclo28, 3 for latA; **= p<0.005, t-test) SEM bars plotted. (C) Number of YFP-CaMKII α puncta/unit axon length before (pre-treat) and after (post-treat) high K⁺ stimulation or latrunculin treatment (same n values as B). Pclo28-expressing axons have fewer YFP-CaMKII α puncta prior to stimulation than wild-type axons (0.12 vs. 0.20 puncta/pixel, respectively). High K⁺ induces new puncta in wild-type neurons (from 0.20 to 0.36 puncta/pixel; **= p<0.005, paired t-test), but not those treated with latrunculin A or lacking Piccolo.

This antibody was raised against a ~1,686 amino acid region of Piccolo that contains binding sites for two Actin regulators, GIT1 and Profilin (Figure 3.28A) (Wang, Kibschull et al. 1999; Kim, Ko et al. 2003). In wild-type lysates, we observed a typical pattern of Piccolo immunoreactive bands at ~560, 500, 400, 350, 300 and 200 kD (Figure 3.28B), thought to arise by alternative splicing of the 350 kb, 26 exon PCLO gene (Fenster and Garner, 2002) and BioGPS.org web page (Figure 3.28D). In Pclo Δ Ex14 lysates, a selective reduction of the 560, 500, and 400 kDa bands was observed (Figure 3.28 B), supporting the concept that alternative splicing and not protein degradation of the 560 kD protein gave rise to this

pattern. In contrast, neurons expressing Pclo28, targeting a sequence in exon 1 (Figure 3.28A), lost all immunoreactive bands (Figure 3.28C). These data demonstrate that Pclo Δ Ex14 mice were not complete Piccolo nulls and suggest that the absence of synaptic phenotypes in Pclo Δ Ex14 mice is not due to an inconsequential role for Piccolo in neurotransmitter release but rather to the continued expression of multiple isoforms containing the central region of Piccolo.

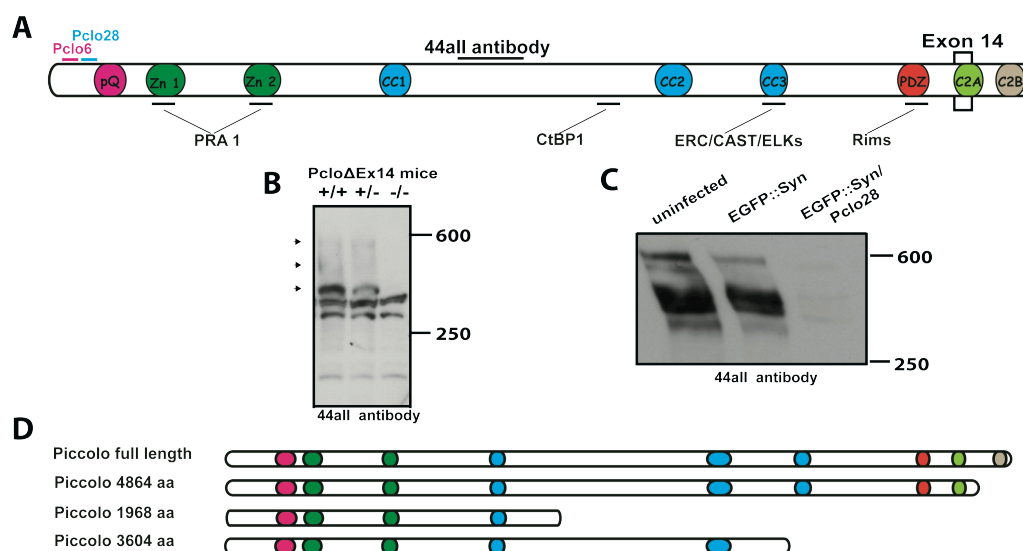


Fig. 3.28 Piccolo isoform expression in Pclo Δ Ex14 mice and rat hippocampal neurons expressing Pclo28 shRNA

(A) Schematic diagram of Piccolo depicting its multiple domains (Q, two Zinc finger (Zn), three coiled-coil (CC), PDZ, C2A and C2B), regions targeted by Pclo28 shRNA, exon 14 deletion, 44aII antibody and binding partner PRAI, CtBP1, ERC/CAST/ELKs and Rims. (B) Western blot of brain homogenates from wild-type (+/+), heterozygous (+/-), and Pclo Δ Ex14 (-/-) mice, probed with the 44aII antibody. Black arrowheads indicate major immunoreactive bands (~560, 500, and 400 kD) that are absent in -/- mice. (C) Western blot of lysates from rat hippocampal neurons infected with EGFP-Synapsin1a +/- Pclo28, probed with 44aII antibodies. Note the disappearance of all immunoreactive bands in lysates expressing Pclo28. Data indicate that eliminating exon 14 from the mouse Piccolo gene only affects the expression of a subset of Piccolo isoforms. (D) Schematic diagram of Piccolo isoforms predicted from BioGPS.org web page.

To directly test this hypothesis, the most prominent Pclo28 phenotype, impaired F-Actin assembly, was examined in hippocampal neurons cultured from PcloDEx14 mice. As in the rat experiments, neurons were infected with EGFP:: β -actin or EGFP:: β -actin Pclo28 constructs at the time of plating, grown for 10 days, and then depolarized with high K⁺ for 1 minute prior to fixation and immunostaining with 44aII antibody. Intriguingly, high K⁺-induced EGFP:: β -actin clustering was robust in both wildtype and PcloDEx14 axons (Figure 3.29A). No significant differences in presynaptic cluster intensity or number of clusters per unit length of axon were detected between the two genotypes (Figure 3.29B, C). Moreover, while Piccolo levels were ~75% lower in PcloDEx14 neurons, remaining immunoreactivity was presynaptic and >70% colocalized with EGFP:: β -actin clusters, similar to wild-type

neurons (Figure 3.29A-D). In contrast, Pclo28 expression eliminated both high K^+ -induced EGFP:: β -actin clustering and Piccolo immunoreactivity from axons of both genotypes (Figure 3.29A-D). These results clearly demonstrate that Piccolo isoforms containing the central domain are synaptically localized in PcloDEx14 neurons and can support activity-dependent F-actin assembly. Since Piccolo regulates neurotransmitter release via F-actin assembly, these data further illustrate the need for transgenic animals with a more complete genetic knockout of Piccolo with which to study the synaptic and behavioral consequences of its loss-of-function.

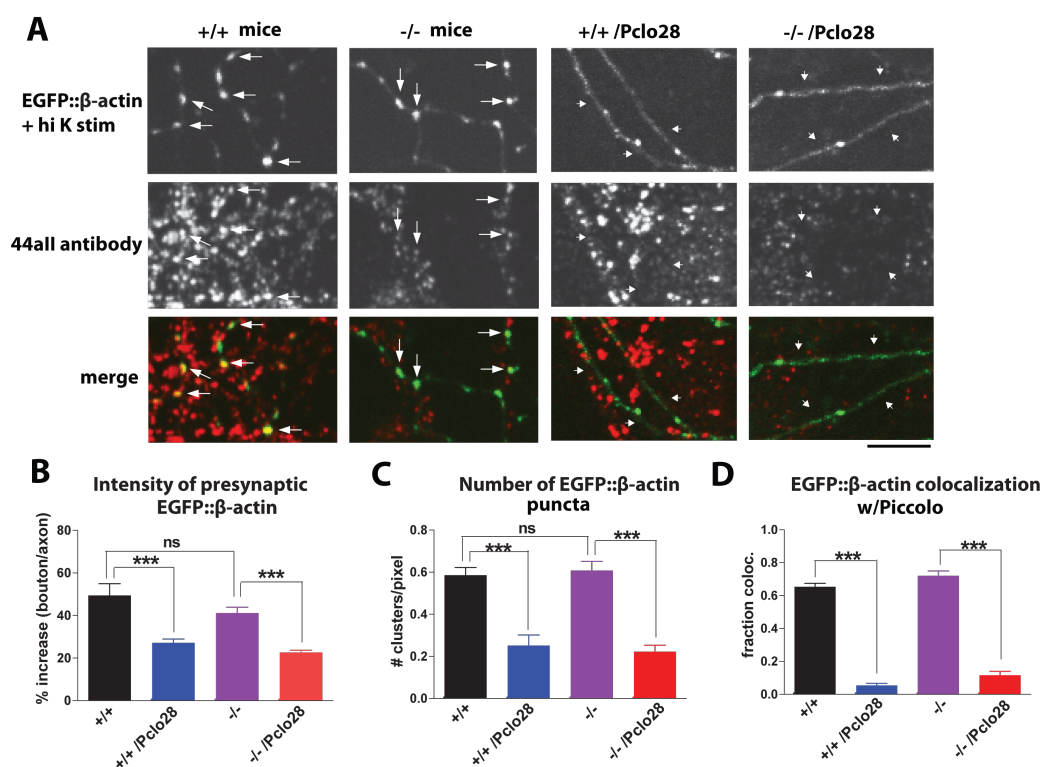


Fig. 3.29 Pclo Δ Ex14 mice exhibit normal presynaptic F-Actin assembly

(A) Fluorescent images of EGFP:: β -actin in axons of 10 DIV +/+ and -/- hippocampal neurons, + or - Pclo28 shRNA, treated with high K^+ (1 min) and immunostained with 44aII antibodies. For both genotypes, extensive axonal EGFP:: β -actin clustering is induced by high K^+ , and clusters colocalize with presynaptic Piccolo immunoreactivity (arrows). Pclo28 eliminates EGFP:: β -actin clustering and Piccolo immunoreactivity for both genotypes (arrowheads). Image gain is set $\sim 5X$ higher for EGFP:: β -actin (but not Piccolo) in Pclo28-infected axons to enable its visualization, as it is largely diffuse. 10 μ m size bar. (B) Bar graphs quantifying the intensity of high K^+ -induced EGFP:: β -actin puncta at presynaptic boutons, expressed as % increase in bouton/axon fluorescence (+/+ n=5 images from 2 animals; -/- n=14 images, 2 animals; +/+ /Pclo28 n=8, 2 animals; -/- /Pclo28 n=14, 2 animals). For both genotypes, presynaptic EGFP:: β -actin fluorescence is $>40\%$ increased vs. axon fluorescence, but only $\sim 20\%$ increased in the presence of Pclo28 (***) = $p < 0.0001$, t-test). (C) Number of EGFP:: β -actin puncta/unit axon length (n values same as B). For both genotypes, high K^+ stimulation induces EGFP:: β -actin puncta densities of ~ 0.6 /pixel axon length, and Pclo28 reduces this value three-fold (***) = $p < 0.0001$, t-test). (D) Fraction colocalization of EGFP:: β -actin puncta with Piccolo immunostaining (n values same as B). For both genotypes, EGFP:: β -actin puncta exhibit a similar degree of colocalization with Piccolo (~ 0.65). Although Piccolo immunoreactivity is substantially weaker in -/- neurons, it is still readily detectable with 44aII antibodies. Pclo28 significantly reduces Piccolo immunoreactivity, and hence colocalization with axonal EGFP:: β -actin clusters, in both genotypes (to < 0.11 ; ***) = $p < 0.0001$, t-test).

3.4 Assessing the role of Bassoon and Piccolo on the maintenance Synaptic Vesicle Pools.

Studies of synapses lacking either Piccolo or Bassoon reveal that neither protein alone is essential for nascent synapse formation (Altrock, tom Dieck et al. 2003; Hallermann, Fejtova et al. 2010), though each contributes to the regulated release of neurotransmitters (Leal-Ortiz, Waites et al. 2008; Ibi, Nitta et al. 2010; Waites, Leal-Ortiz et al. 2011). One potential explanation for these relatively mild phenotypes is that these molecules are functionally redundant. Given that the shRNAs are capable of eliminating over 90% of all Piccolo and Bassoon isoforms (Figure 3.11), it was of interest to explore whether an RNA-interference based strategy could provide clues to the redundant functions of these active zone proteins.

3.4.1 Characterization of synapses lacking Bassoon and Piccolo

For these studies, a tricistronic lentiviral vector was created containing the Bassoon (Bsn16) and Piccolo (Pclo28) shRNAs or a scrambled version of Bassoon (Bsn16SC) and Piccolo (Pclo28SC) driven by separate polymerase III promoters (U6 and H1, respectively), as well as a reporter protein (i.e. EGFP) driven by the Ubiquitin C promoter (Figure 3.12C, D). To test the efficacy of this DKD vector (LV/EGFP/DKD), hippocampal cultures were infected at high titers with lentivirus at the time of plating (ensuring approximately 90% infection) and harvested at 14 days *in vitro* (DIV), a time at which the neurons were mature and still appeared healthy. Western blot analysis revealed that LV/EGFP/DKD (Figure 3.12C) eliminated expression of all Bassoon and Piccolo isoforms from neurons, while the control vector containing scrambled versions of both shRNAs (LV/EGFP/SC) (Figure 3.12D), did not have this effect (Figure 3.13). The levels of other presynaptic proteins, including the SV-associated proteins SV2, Synaptophysin, Rab3a, Syntaxin, and SNAP25, were also significantly reduced in lysates from DKD neurons (Figure 3.30A).

Although DKD-infected cultures appeared healthy, it seemed reasonable that the dramatic reduction of SV-associated proteins could be due to abnormal neuronal development and/or poor cell health in the absence of Bassoon and Piccolo. An examination of dendritic morphology, using antibodies against MAP2a/b, revealed that LV/EGFP/DKD infected neurons at 14DIV had similar dendritic morphologies as those infected with LV/EGFP/SC (Figure 3.30B, C). Furthermore, no beading of MAP2a/b was observed (Park, Bateman et al. 1996; Hoskison, Yanagawa et al. 2007), suggesting that overall cell health and development were unaffected by Bassoon/Piccolo DKD. LV/EGFP/SC and LV/EGFP/DKD-infected neurons were also morphologically similar to uninfected neurons and to those infected with

EGFP alone (data not shown), indicating that there were no significant off-target effects resulting from expression of two shRNAs from a single vector.

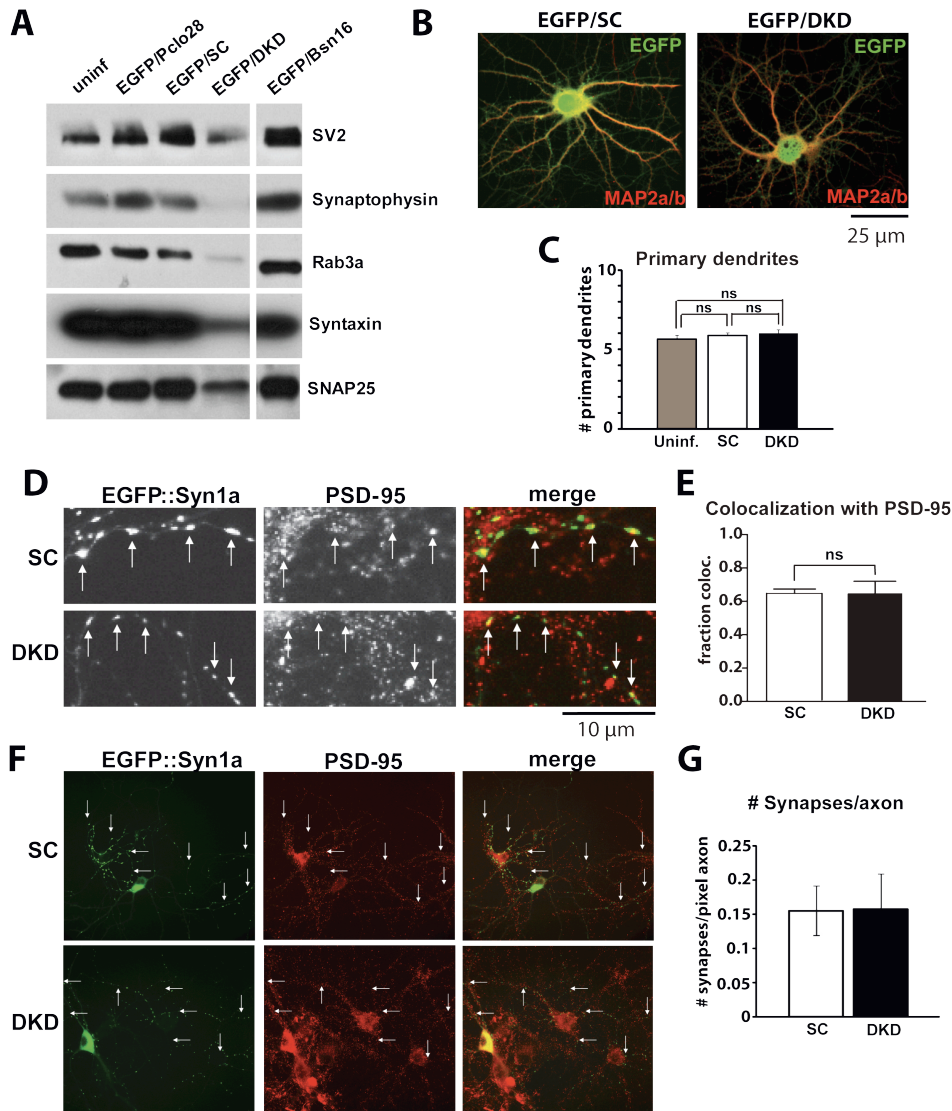


Fig. 3.30 Double knockdown of Bassoon and Piccolo reduces the expression of synaptic vesicle proteins but not hippocampal neuronal differentiation, made smaller synapses but does not affect synapse density.

(A) Western blots of cellular lysates from hippocampal neurons infected with the following lentivirus LV/EGFP/Pclo28; LV/EGFP/Bsn16; LV/EGFP/SC; or LV/EGFP/DKD at the time of plating. Samples collected after 14DIV were probed with antibodies against a series of SV-associated proteins (SV2, Synaptophysin, Rab3a, Syntaxin, and SNAP25). All of these proteins are dramatically reduced in the DKD condition. Similar results were obtained in 3 independent experiments. (B) Images of cell bodies and dendrites from 14 DIV neurons infected with LV/EGFP/SC or LV/EGFP/DKD (green) at 0 DIV and immunostained with antibodies against MAP2a/b (red). Size bar is 25 mm. (C) Quantification of primary dendrite number in uninfected cells and those infected with LV/EGFP/SC or /DKD. No difference was observed between the 3 conditions (n=22 cells/condition). (D) Fluorescent images of 14 DIV neurons expressing EGFP::Syn1a together with scrambled shRNAs (SC) or Bsn16/Pclo28 (DKD), immunostained with PSD-95 antibodies. Note that a majority of EGFP::Syn1a puncta colocalize with PSD-95 in both SC and DKD conditions, yet are visually smaller. Size bar is 10 mm. (E) Quantification of the fraction of EGFP::Syn1a puncta that colocalize with PSD-95 puncta under SC and DKD conditions. No significant difference in the fraction of colocalization was observed (n>6 fields of view/condition, >100 puncta/field, unpaired t-test). (F) Fluorescent images of 14 DIV neurons infected on 0 DIV with LV/EGFP::Syn1a/SC or /DKD, and immunostained with antibodies against PSD-95 to label postsynaptic densities. Arrows indicate a

subset of the LV/EGFP::SynIa puncta that colocalize with PSD-95. (G) Quantification of synapse density in LV/EGFP::SynIa/SC and DKD-expressing axons. Synapses are defined as sites with colocalized EGFP::SynIa and PSD-95 puncta (white arrows). Values are depicted as # of synapses/unit length axon. There is no significant difference between the SC and DKD conditions, indicating that synapse formation is not altered in axons lacking Bassoon/Piccolo.

One potential consequence of decreased levels of SV-associated proteins in DKD lysates might be an inability of DKD-infected neurons to form presynaptic boutons. This outcome seemed possible, especially given the early appearance of Bassoon and Piccolo at nascent presynaptic sites (Zhai, Olias et al. 2000) and their hypothesized roles in scaffolding a series of proteins to define the CAZ (Ziv and Garner, 2004). Therefore, to visualize presynaptic boutons in DKD-infected neurons, soluble EGFP in the SC and DKD vectors was replaced with EGFP::SynIa (pEGFP::SynIa/SC or /DKD), a SV-associated protein whose localization is almost exclusively presynaptic (Chi, Greengard et al. 2001). Neurons were electroporated with vectors at the time of plating and examined at 14 DIV. EGFP::SynIa was found to be still clustered in the axons of DKD-expressing neurons with these clusters colocalizing with the postsynaptic protein PSD-95, indicating that they were synaptic (Figure 3.30D, E). Furthermore, EGFP::SynIa colocalized with PSD-95 to a similar extent in SC and DKD-expressing neurons, and the density of EGFP::SynIa with PSD-95 clusters along axons was similar for both conditions (Figure 3.30F, G). These data indicated that synapse formation was not directly affected by Bassoon/Piccolo DKD (Figure 3.30D, E, F, G). However, the size and intensity of EGFP::SynIa puncta were significantly reduced in the DKD background, suggesting that SV pool size maybe reduced (Figure 3.30D).

3.4.2 Decreased SV pool size in the absence of Bassoon and Piccolo

Immunostaining on EGFP::Syn/SC and EGFP::Syn/DKD-expressing neurons was performed using antibodies to a series of SV-associated proteins to examine SV pool size in presynaptic boutons lacking Bassoon and Piccolo. The intensities of all proteins examined by immunofluorescence confocal microscopy (Synaptophysin, SV2, VGLUT1 (not shown), VAMP2 (not shown)) were reduced by ~50% in the bouton of EGFP::SynIa/DKD expressing neurons compared to SC controls (Figure 3.31A-G). Moreover, their degrees of colocalization with EGFP::SynIa were reduced by ~40% compared to control boutons (shown for Synaptophysin; Figure 3.31A, B), reflecting the fact that SV proteins at many DKD expressing boutons were below the threshold of detection for our puncta analysis software. In contrast, the intensities of postsynaptic proteins (Homer1b and PSD-95) juxtaposed to EGFP::SynIa/DKD boutons were not significantly decreased (Figure 3.31E, I,

J). These findings indicated that loss of Bassoon and Piccolo from presynaptic boutons leads primarily to a dramatic reduction in SV pool size.

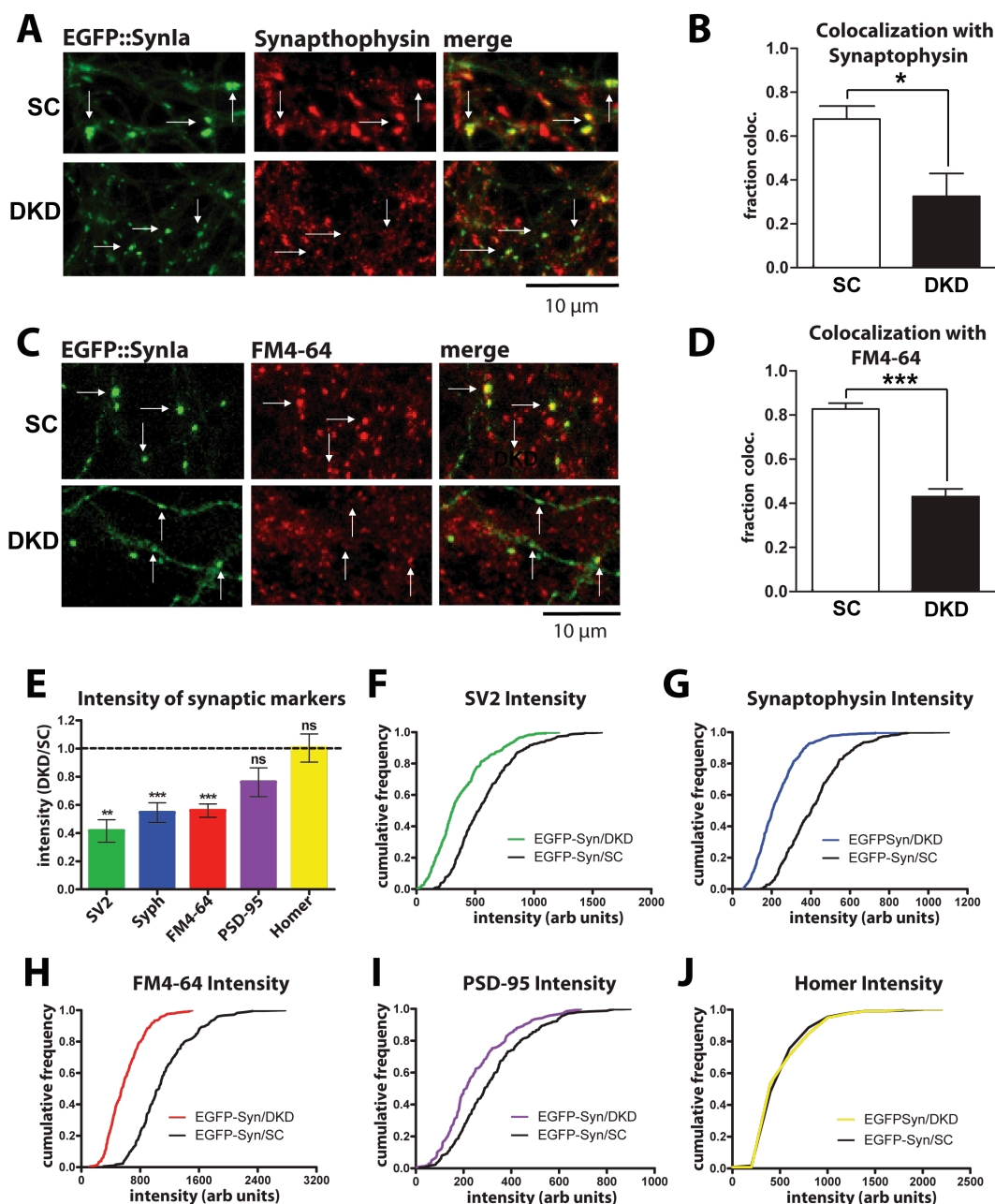


Fig. 3.31 Loss of Piccolo and Bassoon reduces SV pool size in presynaptic boutons

(A) Fluorescent image of 14 DIV neurons expressing EGFP::SynIa/SC or EGFP::SynIa/DKD, immunostained with synaptophysin antibodies. Size bar is 10 μ m. (B) Quantification of EGFP::SynIa colocalization with Synaptophysin for SC and DKD conditions. Significantly fewer EGFP::SynIa puncta colocalize with Synaptophysin in the DKD (~30% vs. 70%; $n > 3$ fields of view/condition, with > 50 puncta/field; * = $p < 0.05$, unpaired t-test). (C) Images of 14 DIV neurons expressing EGFP::SynIa/SC and /DKD, loaded with FM4-64 using 10Hz stimulation for 60 sec. Size bar is 10 μ m. (D) Quantification of EGFP::SynIa colocalization with FM4-64 for SC and DKD conditions. Significantly fewer EGFP::SynIa puncta colocalize with FM4-64 in DKD boutons (~80% vs. ~40%; $n > 5$ fields of view/condition, > 50 puncta/field; *** = $p < 0.0001$, unpaired t-test). (E) Quantification of fluorescence intensities for a series of synaptic markers at EGFP::SynIa/DKD boutons, expressed as fractions of fluorescence intensity for the same marker at EGFP::SynIa/SC boutons. Dotted line at 1.0 indicates the average fractional intensity for all markers at SC control boutons (ie. SC/SC). Note that presynaptic markers (SV2, Synaptophysin, FM4-64) are reduced by ~50% at DKD boutons, while postsynaptic markers (PSD-95, Homer1b) remain unchanged ($n > 4$ fields of view/condition, > 30

boutons/field; ** = $p < 0.005$, *** = $p < 0.0001$, unpaired t-test). (F) Cumulative frequency distribution of SV2 immunofluorescence intensity at EGFP::SynIa/SC (black line) or /DKD (green line) expressing boutons. Note that the distribution is shifted to the left for DKD boutons, indicating smaller SV pool size. SV2 intensity values are from (n=332 DKD and 360 SC boutons from 5 fields of view). (G) Similar to F, but for Synaptophysin (n=635 DKD and 369 SC boutons, 7 fields of view). (H) Similar to F, but for FM4-64 (n=254 DKD and 177 SC boutons, 8 fields of view). (I) Cumulative frequency distribution of PSD-95 immunofluorescence intensity at postsynaptic sites juxtaposed to EGFP-Syn-expressing boutons. The distribution of PSD-95 intensity is slightly left-shifted for DKD boutons, but not to the extent of the presynaptic markers (n=144 DKD and 251 SC boutons, 4 fields of view). (J) Similar to E, but for Homer1b. The Homer1b puncta intensity distribution is nearly identical for SC and DKD-expressing boutons (n=119 DKD and 221 SC boutons, 4 fields of view).

FM4-64 dye uptake at EGFP::SynIa/DKD boutons during a train of 600 action potentials was examined (10 Hz, 60 sec) to determine whether this reduction translated into a defect in SV recycling. As observed for other SV markers, both the intensity and colocalization of FM4-64 with EGFP::SynIa were significantly reduced in DKD versus SC boutons (Figure 3.31C, D, E, H), suggesting that SV cycling was also likely perturbed in the absence of Bassoon and Piccolo.

3.4.3 SV pool size is rescued by the expression of full-length, shRNA-resistant, Bassoon

To rule out off-target effects of the shRNA DKD-induced SV loss, we examined whether this phenotype could be rescued by expressing full-length Bassoon in the DKD background. For this experiment, we created SC and DKD vectors that express the EGFP-tagged SV integral membrane protein SV2 as a reporter (pEGFP::SV2/SC; pEGFP::SV2/DKD). Endogenous SV2 was dramatically reduced in the DKD background (Figure 3.30A), and EGFP::SV2 (Figure 3.32A) was less prone to overexpression than EGFP-tagged Synapsin1a, making it a more reliable readout of SV pool size. Neurons were electroporated with pEGFP::SV2/SC or pEGFP::SV2/DKD vectors prior to plating, then infected with an adenoviral vector (HDAd) expressing an shRNA-resistant, mRFP-tagged Bassoon (HDAd-mRFP::Bsn/SM16) (see section 3.2.8) at 5 DIV (Figure 3.32A). The ability of mRFP::Bsn/SM16 to rescue DKD-induced SV loss was assessed at 14 DIV. Reassuringly, mRFP::Bsn/SM16 expression prevented the dramatic loss of EGFP::SV2 fluorescence normally seen in DKD expressing boutons (Figure 3.32A, B, D). The intensity of Synaptophysin immunostaining within these boutons was also similar to wildtype levels, indicating that the effect was not specific for SV2 (Figure 3.32A, C, E). These findings indicated that off-target effects of my shRNAs are not responsible for the loss of SVs, as Bassoon expression alone rescued this phenotype.

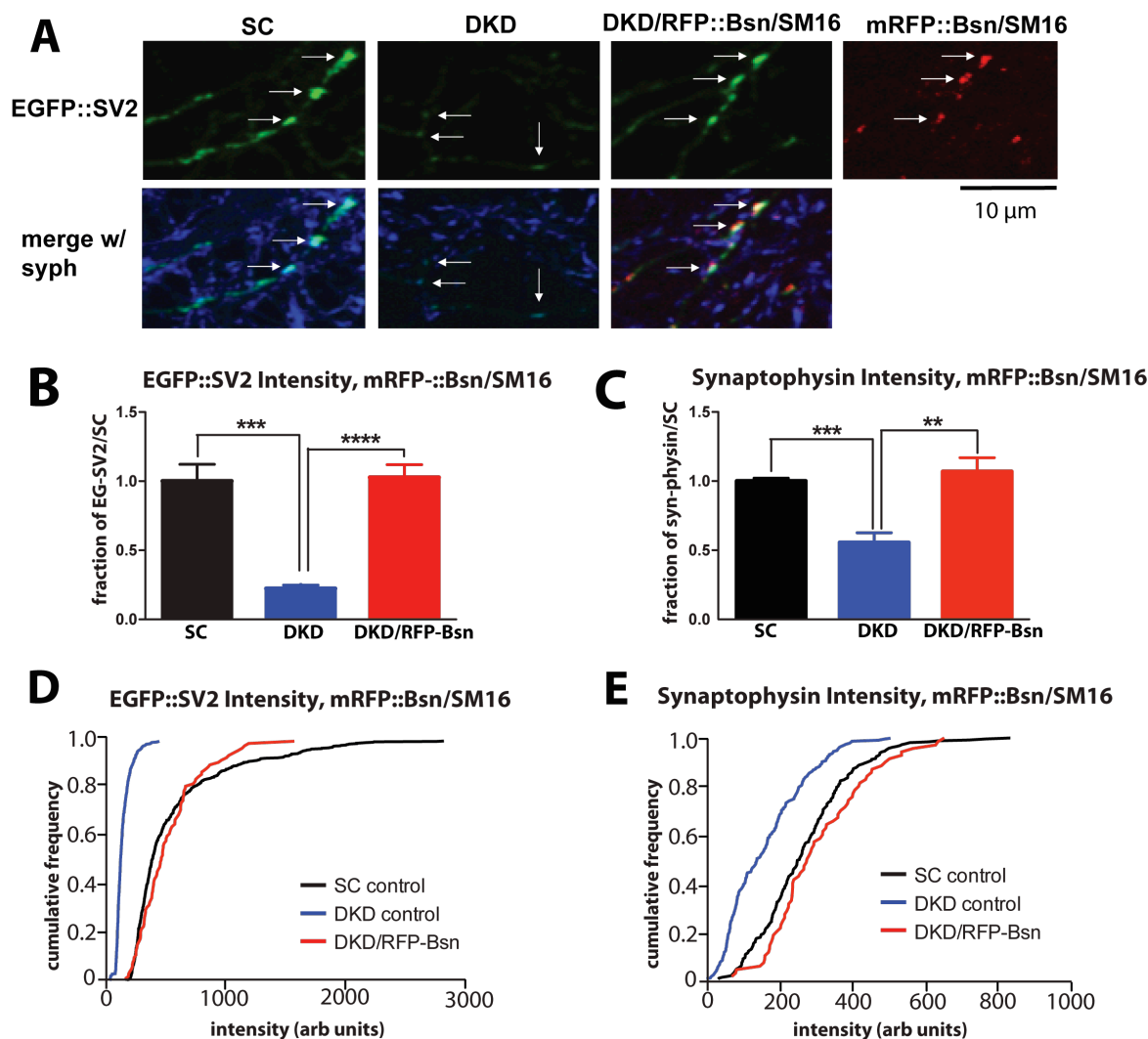


Fig. 3.32 Expression of mRFP::Bsn-SM16 rescues SV pool size at DKD boutons

(A) Fluorescent image of 14 DIV neurons expressing pEGFP::SV2/SC alone, pEGFP::SV2/DKD alone, or pEGFP::SV2/DKD together with shRNA-resistant mRFP::Bsn/SM16, and immunostaining with Synaptophysin antibodies. mRFP::Bsn/SM16 (mRFP::Bsn*) expression rescues the dramatic loss of EGFP-SV2 and Synaptophysin immunofluorescence from DKD boutons. Size bar is 10 μ m. (B) Quantification of EGFP::SV2 fluorescence intensity at boutons expressing SC, DKD, and DKD/mRFP::Bsn/SM16 vectors. Values are expressed as fraction of EGFP-SV2 intensity at SC boutons. EGFP-SV2 intensity is reduced by \sim 80% in the DKD background, but rescued to control levels in the presence of mRFP::Bsn-SM16 ($n > 4$ fields of view/condition, > 100 boutons/field; ***= $p < 0.0005$, ****= $p < 0.0001$, unpaired t-test). (C) Quantification of Synaptophysin immunofluorescence intensity at SC, DKD, and DKD/mRFP::Bsn-SM16 boutons. Synaptophysin intensity is reduced by \sim 50% in the DKD background, but like EGFP::SV2 is rescued to control levels by mRFP::Bsn-SM16 ($n > 3$ fields of view/condition, > 50 boutons/field; **= $p = 0.005$, ***= $p = 0.0001$, unpaired t-test). (D) Cumulative frequency distribution of EGFP::SV2 fluorescence intensity at SC, DKD, or DKD/mRFP::Bsn/SM16 (mRFP::Bsn*) expressing boutons. This curve is left-shifted in the DKD condition, indicating dramatically smaller SV pool size, but is similar to the SC control in the presence of mRFP::Bsn/SM16 ($n = 673$ SC, 541 DKD, and 101 DKD/mRFP::Bsn/SM16 boutons, ≥ 4 fields of view/condition). (E) Cumulative frequency distribution of Synaptophysin immunofluorescence intensity at SC, DKD, and DKD/mRFP::Bsn/SM16 boutons. Again, the curve is left-shifted in the DKD condition, but similar to SC control in the presence of mRFP::Bsn/SM16 ($n = 261$ SC, 236 DKD, and 70 DKD/mRFP-Bsn/SM16 boutons, ≥ 3 fields of view/condition).

3.4.4 Ultrastructure of boutons lacking Bassoon and Piccolo

Our fluorescence imaging studies described thus far indicated that Bassoon and Piccolo are important for maintaining SV pool size but not necessarily for synapse formation. To confirm this conclusion, the ultrastructural properties of boutons lacking both proteins were examined. Similar to ultrastructural studies on synapses lacking Piccolo (Figure 3.16 & 3.17), SC and DKD vectors expressing the SV integral membrane protein VAMP2 conjugated to horseradish peroxidase (VAMP2::HRP) was used to identify the boutons and axon of transfected neurons by electron microscopy (EM). Again, neurons were electroporated with pVAMP2::HRP/SC and pVAMP2::HRP/DKD constructs prior to plating, then fixed and processed for EM analysis on 14 DIV.

As anticipated, presynaptic boutons expressing the pVAMP2::HRP/SC control vector were morphologically normal, containing many ~40 nm diameter SVs of uniform density juxtaposed to prominent postsynaptic densities (PSDs) (Figure 3.33A). In contrast, boutons from pVAMP2::HRP/DKD expressing neurons had highly variable and abnormal morphologies (Figure 3.33B) with few 40 nm SVs but instead a variety of pleiomorphic vesicles greater than 80 nm in diameter. Some of these were tubulovesicular structures resembling early endosomes (Parton, Simons et al. 1992), while others were spherical and reminiscent of late endosomes/multi-vesicular bodies (MVBs) that transport organelles and proteins to lysosomes (Almeida, Takahashi et al. 2006; Altick, Baryshnikova et al. 2009; Lee, Sato et al. 2011) (Figure 3.33B). Moreover, juxtaposed PSDs were noticeably less electron-dense, suggesting that postsynaptic structures were also affected by the presynaptic loss of Bassoon and Piccolo. This implies that more general facets of synapse structural integrity are being impaired in the absence of Piccolo and Bassoon.

As it was often difficult to readily visualize synapses (e.g. with both pre and postsynaptic specialization) in these samples, pVAMP2::HRP/DKD neurons from an earlier timepoint (9 DIV) were examined to obtain more quantitative measurements of their features. Indeed, boutons pVAMP2::HRP/DKD transfected neurons at 9 DIV typically had multiple 40 nm SVs juxtaposed to an identifiable postsynaptic structure (Figure 3.33B). However, these boutons also displayed significantly more pleiomorphic vesicles than their pVAMP2::HRP/SC counterparts (Figure 3.33A-D), and juxtaposed PSDs were often less electron-dense. In addition, SV morphology was altered at many of these boutons, with abnormally elongated or enlarged vesicles (Figure 3.33B, E). These data illustrate that Bassoon/Piccolo loss dramatically alters synaptic integrity and that many of these changes can be detected at a relatively early timepoint (9 DIV).

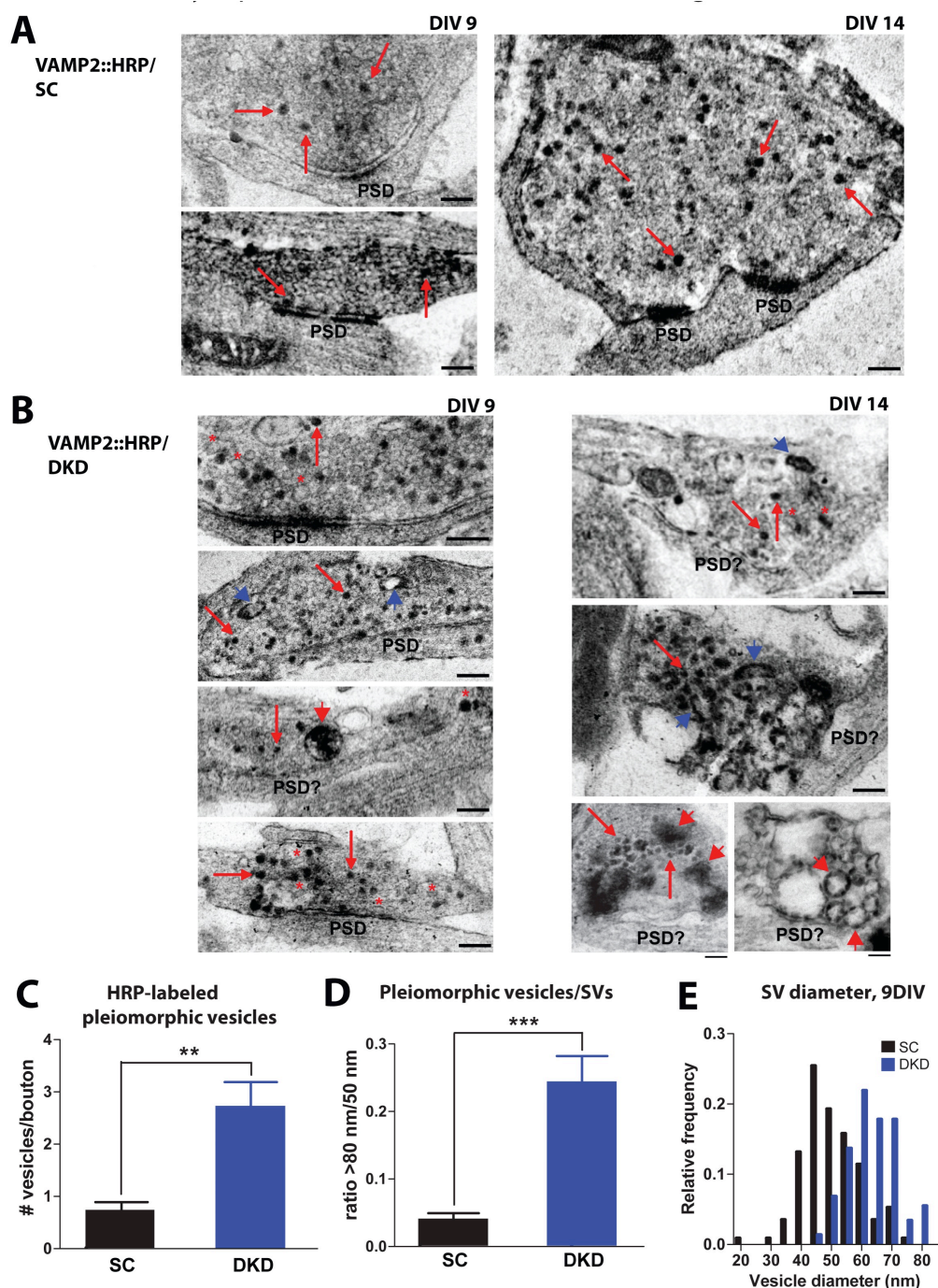


Fig. 3.33 Quantification of synaptic ultrastructure in boutons lacking Bassoon and Piccolo

(A) Electron micrographs of boutons from neurons electroporated with pVAMP2::HRP/SC at 9 (left) or 14 (right) DIV. Red arrows indicate SVs labeled with VAMP2::HRP, which forms an electron-dense precipitate within the vesicle lumen. PSD = postsynaptic density. (B) Micrographs of boutons from neurons electroporated with pVAMP2::HRP/DKD at 9 (left) or 14 (right) DIV. Red arrows indicate labeled SVs, red asterisks (placed immediately above vesicles) indicate abnormally-shaped SVs, blue arrowheads indicate tubulovesicular structures, and red arrowheads indicate multi-vesicular bodies. Note the increase in tubulovesicular structures and MVBs, and concomitant decrease in SVs, at 14 vs. 9 DIV. Size bars are 200 nm. (C) Quantification of HRP-labeled pleiomorphic vesicles (>80 nm diameter)/bouton for boutons from neurons electroporated with pVAMP2-HRP/SC or /DKD. DKD boutons have significantly more pleiomorphic vesicles than SC control boutons ($n=22$ boutons for SC, 45 boutons for DKD; $**=p<0.005$, unpaired t-test). (D) Quantification of the ratio of pleiomorphic vesicles (>80 nm diameter) to SVs (50 nm diameter) per bouton for SC and DKD-expressing boutons. DKD boutons have a significantly greater average ratio, reflecting their increased

number of pleiomorphic vesicles and decreased number of SVs ($n= 22$ SC and 45 DKD boutons; $***=p<0.0005$, unpaired t-test). (E) Relative frequency histogram of SV diameters in boutons from neurons expressing pVAMP2::HRP/SC vs. /DKD at 9 DIV. Values are shifted to the right for DKD boutons, indicating larger SV diameters ($n=114$ SVs from 5 boutons for SC, 146 SVs from 10 boutons for DKD).

3.4.5 SV degradation is enhanced in the absence of Bassoon and Piccolo

A fundamental question raised by the analysis of DKD neurons is what causes the decrease in the number of SV per bouton. One likely possibility is that DKD-induced SV loss involves the activation of lysosomes and/or proteasomes, the two major cellular organelles responsible for protein degradation (Waites and Garner 2011). EGFP::SV2/SC and EGFP::SV2/DKD expressing neurons cultured for 12 DIV were incubated for 16 hr with 200 mM chloroquine/100 mM leupeptin (chloro/leu) or 0.1 mM epoxomicin (epoxo) to inhibit lysosomal or proteasomal activity, respectively (Ehlers 2000; Lee, Tee et al. 2004; Willeumier, Pulst et al. 2006). EGFP::SV2 fluorescence intensity was then compared in treated vs. untreated neurons. Chloro/leu treatment was found to completely prevent the loss of EGFP::SV2 fluorescence in DKD boutons but had no effect on the fluorescence intensities of these molecules in SC control boutons (Figure 3.34A, B, C). Similarly, epoxo treatment significantly increased EGFP::SV2 fluorescence in the DKD but not the SC background (Figure 3.34A, C, F). These data demonstrate that protein degradation is responsible for the loss of SVs in boutons lacking Bassoon and Piccolo.

Proteins are targeted for lysosomal or proteasomal degradation through ubiquitination, a posttranslational modification wherein ubiquitin molecules are attached to specific lysine residues of the target protein (Varshavsky 2005; Yi and Ehlers 2005; Waites and Garner 2011). Ubiquitination requires the coordinated activity of a series of enzymes, including an E1 ubiquitin activating enzyme, E2 ubiquitin conjugating enzymes, and E3 ubiquitin ligases (Ding and Shen 2008; Lehman 2009). To test whether DKD-mediated SV degradation required protein ubiquitination, neurons expressing the pEGFP::SV2/SC or pEGFP::SV2/DKD constructs were treated for 16 hr (from 12-13 DIV) with 1 mM ziram, a drug that blocks the E1 ubiquitin activating enzyme (Chou, Maidment et al. 2008; Rinetti and Schweizer 2010). As with chloro/leu and epoxo, ziram treatment significantly increased EGFP::SV2 fluorescence intensity at DKD boutons without affecting SC control boutons (Figure 3.34A, D, G), suggesting that SV protein ubiquitination was enhanced at boutons lacking Bassoon and Piccolo.

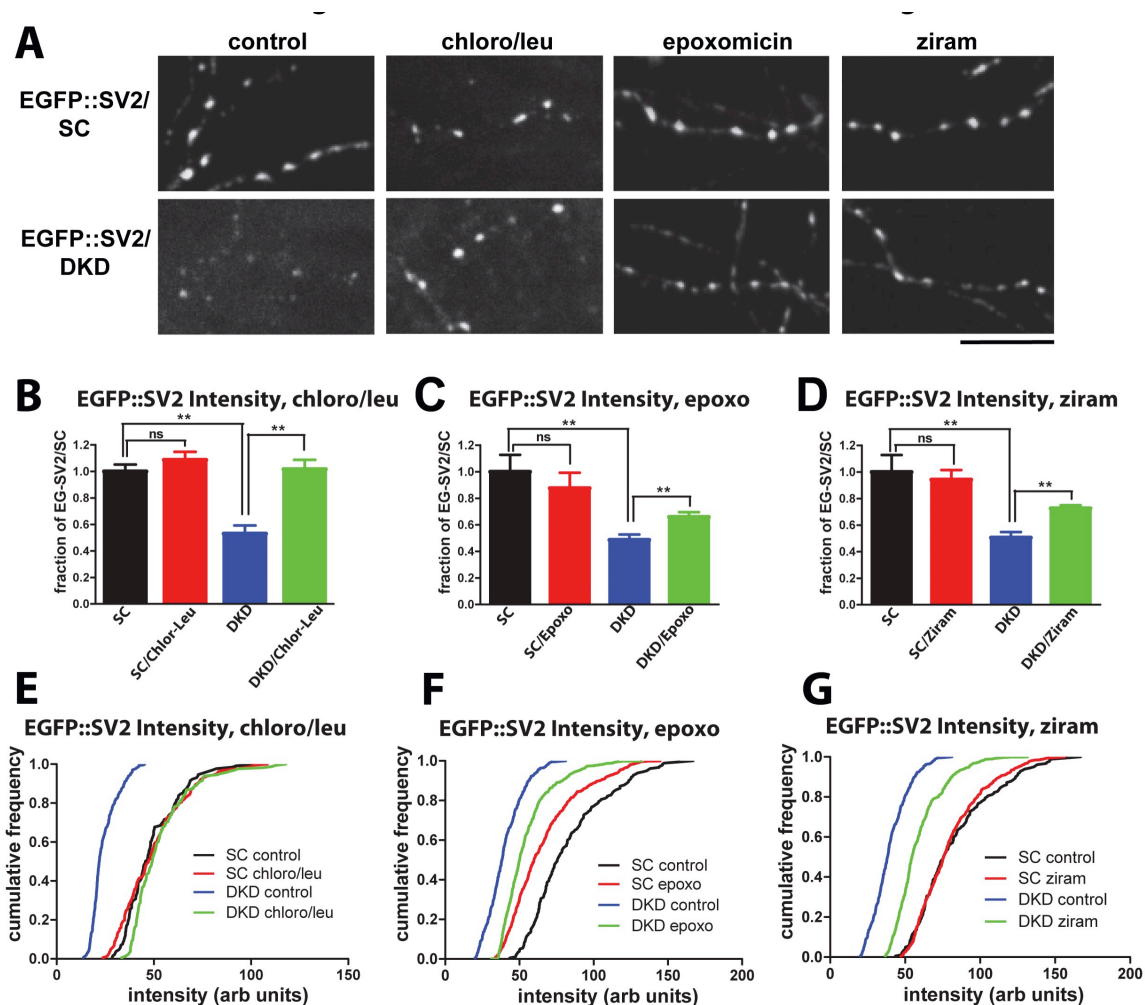


Fig. 3.34 Protein degradation drives SV loss in the DKD background

(A) Fluorescent image of 13 DIV neurons expressing pEGFP::SV2/SC or /DKD constructs, at baseline (control) or treated for 16 hrs with 200 mM chloroquine/100 mM leupeptin to block lysosomal degradation, 0.1 mM epoxomicin to block the proteasome, or 1 mM ziram to block protein ubiquitination. Note that all treatments increase EGFP::SV2 fluorescence in the DKD background. Size bar is 10 μ m. (B) Quantification of EGFP::SV2 fluorescence intensity in the boutons of pEGFP::SV2/SC or /DKD expressing neurons treated with chloro/leu. Values are expressed as fraction of EGFP::SV2 intensity at untreated SC boutons. EGFP::SV2 fluorescence is reduced by ~50% at DKD boutons. Chloro/leu treatment completely rescues this phenotype, but has no significant effect on SC boutons ($n=3$ fields of view/condition, >50 boutons/field; $**=p<0.005$, unpaired t-test). Results were confirmed in 3 independent experiments. (C) Similar to B, but for epoxomicin treatment. Epoxomicin boosts EGFP::SV2 fluorescence by ~20% in the DKD background, but has no significant effect on SC boutons ($n>3$ fields of view/condition, >60 boutons/field; $**=p<0.005$, unpaired t-test). Results were confirmed in 3 independent experiments. (D) Similar to B, but with ziram. Like epoxomicin, ziram boosts EGFP::SV2 fluorescence in the DKD background by ~22% but does not alter EGFP::SV2 intensity in SC boutons ($n>3$ fields of view/condition, >60 boutons/field; $**=p<0.009$, unpaired t-test). Results were confirmed in 3 experiments. (E) Cumulative frequency distribution of EGFP::SV2 intensity at SC and DKD boutons treated with chloro/leu. Note that the DKD control curve is significantly left-shifted, but that chloro/leu treatment “rescues” the DKD intensity distribution to match those of the SC and SC chloro/leu conditions ($n=130$ SC control, 181 SC chloro/leu, 269 DKD control, and 166 DKD chloro/leu boutons). (F) Similar to E, but for epoxomicin treatment. Like chloro/leu, epoxomicin shifts the DKD curve to the right, indicating some rescue of the phenotype ($n=180$ SC control, 350 DKD control, 469 SC epoxomicin, and 611 DKD epoxomicin boutons). (G) Similar to E and F, but for ziram treatment. Ziram also shifts the DKD curve to the right, but has no effect on the SC curve ($n=180$ SC control, 350 DKD control, 551 SC/ziram, and 495 DKD/ziram boutons).

3.4.6 Bassoon and Piccolo zinc finger domains mediate synaptic vesicle elimination in DKD neurons

How could the loss of two active zone-associated proteins lead to enhanced protein ubiquitination? One possibility is that Bassoon and Piccolo regulate one or more of the enzymes that catalyze ubiquitination. Of these, the most plausible candidates are E3 ligases, which provide substrate specificity and exhibit restricted spatial and temporal expression patterns. Our collaborator Drs Gundelfinger, Altmann and Fejtova identified the E3 ligase Siah1 in a yeast two-hybrid screen for Bassoon interacting partners. Siah1 was particularly interesting to us in the context of SV degradation because it is expressed in neurons (Moriyoshi, Iijima et al. 2004) and a number of its targets (Synaptophysin, β -catenin, α -Synuclein, Synphilin-1) are SV-associated proteins (Wheeler, Chin et al. 2002; Matsuzawa, Li et al. 2003; Liani, Eyal et al. 2004; Santelli, Leone et al. 2005; Szargel, Rott et al. 2009; Dimitrova, Li et al. 2010). In addition, the region of Bassoon shown to interact with Siah1 by yeast two-hybrid, the N terminal domain containing amino acids 1-609, has two zinc fingers (ZFD) that are also present in Piccolo (Figure 3.35 A).

As an initial test of a potential Siah link to the DKD phenotype, we examined whether the Zinc-finger region of Bassoon was capable of regulating presynaptic SV pool size. This was accomplished by expressing an EGFP-tagged N-terminal segment of Bassoon (residues 1-609)(EGFP-BsnZFD) in neurons. This region of Bassoon contains both of its zinc fingers (ZF) and was previously shown to associate with SVs and become localized at presynaptic boutons, yet was not incorporated into AZs (Dresbach, Hempelmann et al. 2003). Monitoring the expression levels of endogenous Synaptophysin in neurons overexpressing EGFP-BsnZFD, we observed a dramatic increase in the synaptic levels of Synaptophysin. The over-expression of BsnZFD did not affect the levels of other AZ proteins, such as Piccolo (Figure 3.35B). These results are consistent with a role for the Bassoon ZFDs in regulating SV pool size/bouton.

In the next phase of this work, we sought to confirm that the Bassoon ZFs bound Siah. Siah is comprised of a RING domain that binds different E2 ligases and a Sina domain for docking proteins are targeted for ubiquitination (Wheeler, Chin et al. 2002). This was accomplished using a cellular binding/colocalization assay in which different segments of Bassoon were co-expressed with subdomains of Siah in COS7 cells. Here, full-length Bassoon and N-terminal segments that contained the ZFs of Bassoon colocalized with full-length Siah and Siah's RING domain, but not its Sina domain (Figure 3.35C, D). Next, we examined whether Siah1 interacted selectively one or both of the Bassoon ZFs as well as the two homologous ZFs in Piccolo using immunoprecipitation. Here, we co-expressed each of

the four ZFs tagged with mCherry in HEK cells together with myc-tagged Siah1. Immunoprecipitation with anti-myc antibodies followed by Western blotting revealed that each of the four ZFs could be co-immunoprecipitated with myc-Siah, (Figure 3.35E), confirming the YTH binding data.

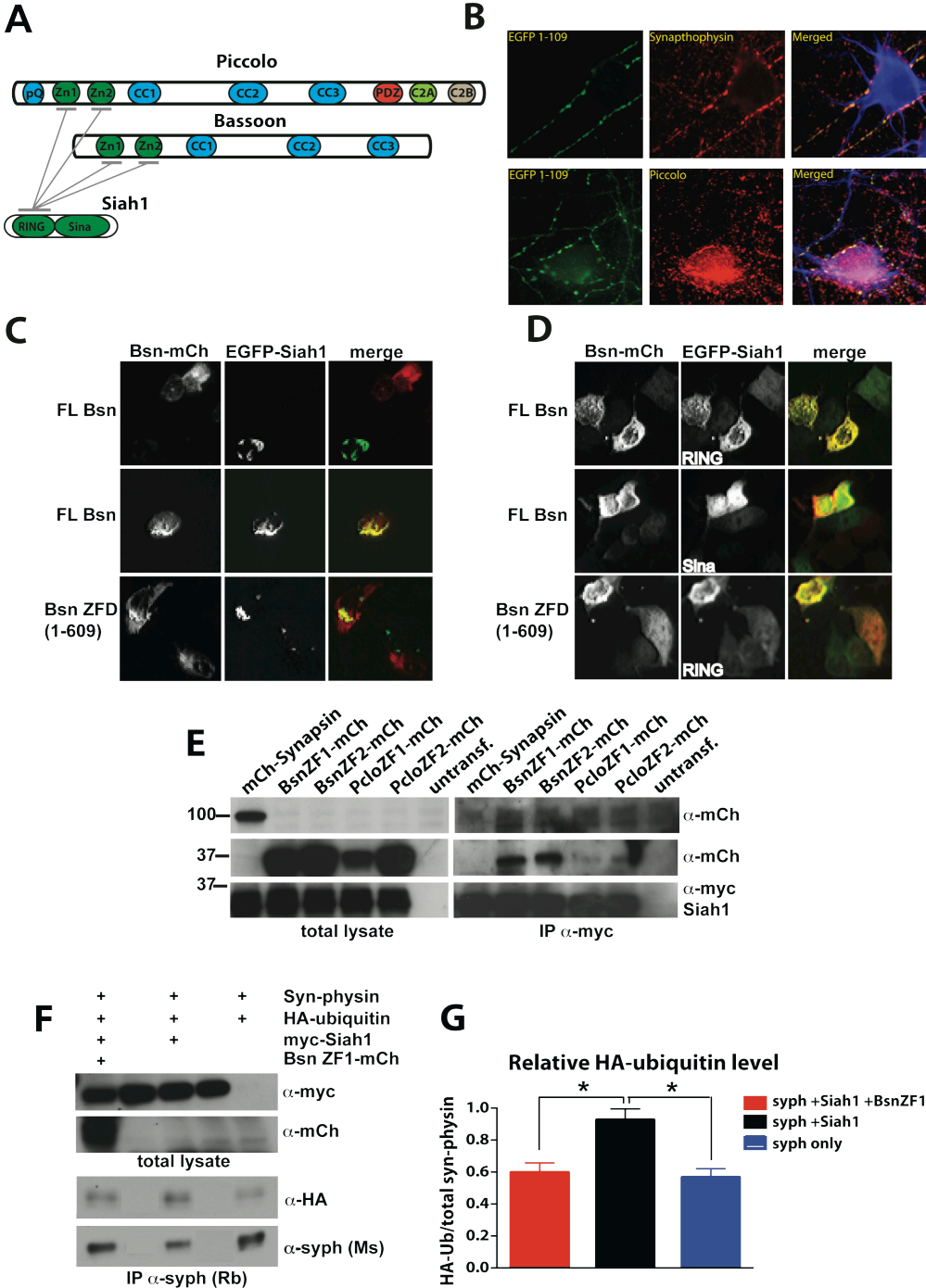


Fig. 3.35 Bassoon and Piccolo interact with Siah1 and modulate its activity
 (A) Schematic diagram showing the interacting domains of Piccolo, Bassoon, and Siah1. Piccolo and Bassoon each have two zinc finger domains (ZF1, ZF2), and all four of these interact with the RING domain of Siah1. (B) Fluorescent image of 14 DIV neurons expressing EGFP-Bsn1-609 and immunostaining with MAP2 (blue) and Synaptophysin (red) or Piccolo (red). (C) Images of HEK cells cotransfected with mCh-tagged Bassoon constructs and EGFP-Siah1. Note that full-length (FL) Bassoon has a relatively diffuse distribution when singly transfected, but is recruited to EGFP-Siah1 positive structures when cotransfected. The zinc finger domain (ZFD) of Bassoon (amino acids 1-

609)(Bsn-ZFD), which contains two zinc fingers (ZFs) and interacts with Siah1 by yeast two-hybrid screen, exhibits a similar behavior. **(D)** Images of HEK cells cotransfected with mCh-tagged Bassoon constructs and EGFP-tagged RING or Sina domains of Siah1. Both FL-Bassoon and Bsn-ZFD interacted with the RING but not the Sina domain based on colocalization. **(E)** Western blots depicting coimmunoprecipitation (co-IP) of mCherry-tagged Bassoon and Piccolo ZF domains with myc tagged Siah1. Left panels show immunoreactivity from total HEK cell lysates prior to co-IP, and right panels from material immunoprecipitated with myc antibody. Top row depicts mCherry immunoreactivity at 100kD, size of the mCh-Synapsin1a control; middle row depicts mCh-tagged Bassoon and Piccolo ZFs at ~37kD; bottom row depicts myc-Siah1 at ~30kD. Similar results were obtained in 3 independent experiments. **(F)** Western blots showing Synaptophysin (Synp) ubiquitination in the presence or absence of Siah1 and Bassoon ZF1 (BsnZF1). Upper two panels show total lysates probed with either myc antibody to detect Siah1, or mCh antibody to detect BsnZF1. Unrelated lanes are blocked out with gray background. Lower two panels show immunoprecipitated Synaptophysin, probed with HA antibody to detect ubiquitination and mouse Synaptophysin antibody to detect total Synaptophysin levels. Unrelated lanes are blocked out with gray background. **(G)** Quantification of C. HA-ubiquitin intensity is divided by total Synaptophysin intensity for each condition, giving relative HA-ubiquitin levels for Synaptophysin. Note that Siah1 increases Synaptophysin ubiquitination above baseline, and that BsnZF1 blocks this effect (n=3 experiments, * = $p < 0.05$, unpaired t-test).

The ability of the Piccolo and Bassoon ZFs to bind the RING domain in Siah suggest that an association of Siah with these two AZ proteins could inhibit its activity, perhaps explaining why enhanced ubiquitination in the absence of Piccolo and Bassoon leads to a reduction of SV pools. To test this hypothesis, we performed Siah dependent ubiquitination assays in HEK cells, as developed by Wheeler and colleagues (Wheeler, Chin et al. 2002). As a substrate, we used the SV protein Synaptophysin, a documented substrate of Siah1 (Wheeler, Chin et al. 2002). In brief, HEK cells were co-transfected with Synaptophysin and HA-ubiquitin in the presence or absence of myc-Siah1 and mCherry-tagged ZF1 of Bassoon. Twenty-four hours after transfection and four hours after treatment with 0.1mM epoxomicin to inhibit the proteasome, Synaptophysin was immunoprecipitated from each sample, and the amount of ubiquitinated Synaptophysin measured by Western blotting with HA antibodies. As previously reported, the over expression of Siah1 significantly increased the baseline ubiquitination of Synaptophysin (Figure 3.35F, G)(Wheeler, Chin et al. 2002). Interestingly, the simultaneous expression of the first ZF of Bassoon (Bsn-ZF1) almost completely blocked this increase (Figure 3.35F, G). Similar results were obtained with each of the Piccolo/Bassoon ZFs (data not shown) indicating that Bassoon and Piccolo can negatively regulate Siah1 activity through their ZFs.

One prediction of this model is that the overexpression of the Bassoon or Piccolo ZFs in neurons should suppress DKD-induced SV loss. To test this prediction, neurons were electroporated with pEGFP::SV2/SC or pEGFP::SV2/DKD were subsequently infected (on 1 DIV) with either mCherry alone or one of the four Bassoon/Piccolo mCherry-tagged ZFs (Figure 3.36A). All of these constructs exhibited relatively diffuse expression patterns in cell bodies and dendrites but accumulated in axonal varicosities and exhibited a high degree of

colocalization with EGFP-SV2 (Figure 3.36A). While mCherry alone had no effect on presynaptic EGFP-SV2 fluorescence in SC and DKD neurons, each of the four ZFs largely rescued the loss of EGFP-SV2 fluorescence at DKD boutons (Figure 3.36A-C). Intriguingly, mChr-BsnZF2 expression significantly increased EGFP::SV2 fluorescence intensity at SC boutons (Figure 3.36B), suggesting that these domains play as specific role in the regulation of SV pool size perhaps through their binding to Siah1. Taken together, these findings suggest a model wherein Bassoon/Piccolo knockdown leads to the overactivation of Siah1 within presynaptic boutons, followed by excessive ubiquitination of its SV-associated protein substrates and subsequent SV degradation.

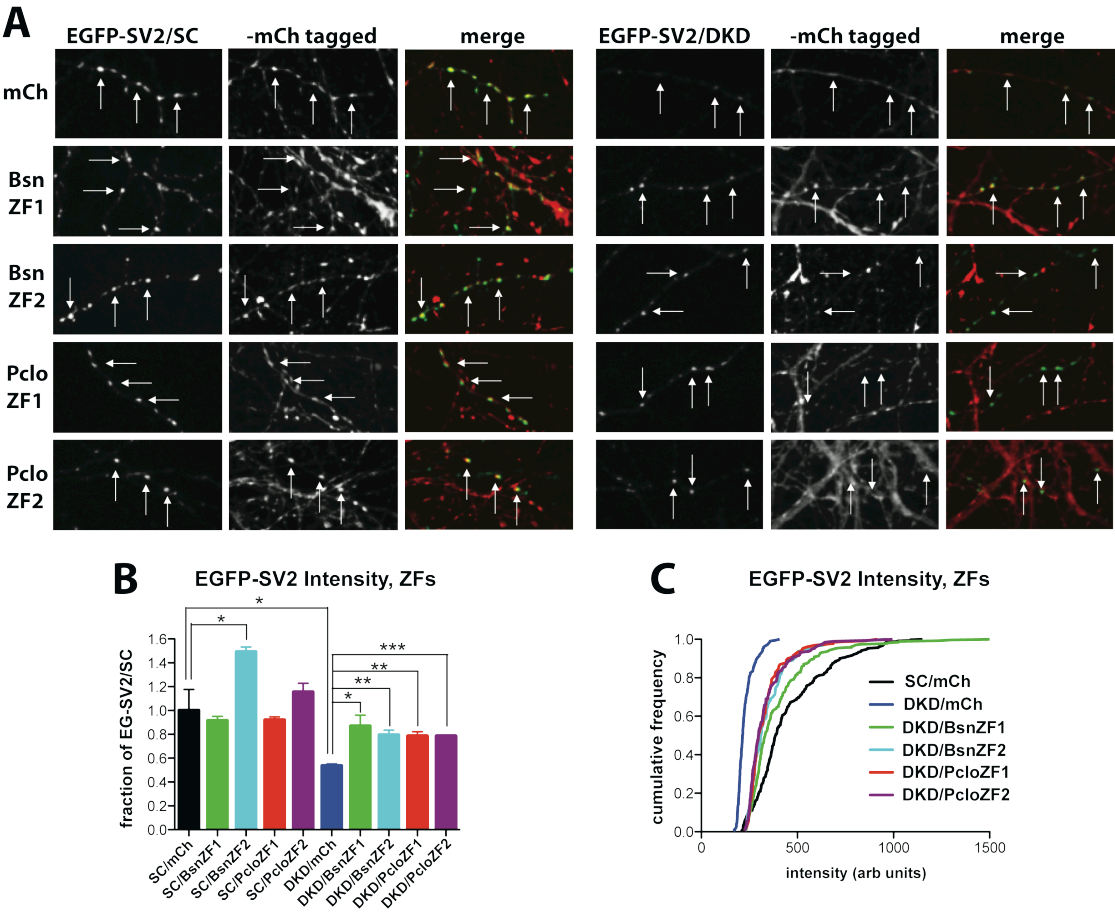


Fig. 3.36 Zinc finger domains in Piccolo and Bassoon regulate SV loss in DKD neurons

(A) Fluorescent images of 14 DIV neurons expressing EGFP::SV2/SC or /DKD together with either soluble mCherry or one of the four mCh-tagged Zinc fingers from Piccolo (PcloZF1; PcloZF2) and Bassoon (BsnZF1; BsnZF2). Size bar is 10 μ m. (B) Quantification of EGFP::SV2 fluorescence intensity in SC or DKD boutons co-expressing soluble mCh or one of the four mCh-tagged ZFs. Note that each ZF partially rescues EGFP-SV2 fluorescence (by ~30%) in the DKD background, and that BsnZF2 significantly increases EGFP-SV2 fluorescence (by ~50%) in SC control boutons (n=3 fields of view/condition, >60 boutons/field; ***=p<0.0005, **=p<0.005, *=p<0.05, unpaired t-test). (C) Cumulative frequency distribution of EGFP::SV2 fluorescence intensity in DKD boutons expressing the ZFs. Each ZF partially rescues the DKD phenotype, shifting the intensity distribution toward the right. The distribution of EGFP::SV2 in SC control boutons expressing mCherry is shown for comparison (black curve)(n=350 SC/mCh, 215 DKD/mCh, 260 DKD/BsnZF1, 130 DKD/BsnZF2, 130 DKD/PcloZF1, 190 DKD/PcloZF2 boutons).

4. Discussion

The goal of this thesis is to define unique and shared functions of Piccolo and Bassoon within presynaptic AZs. A significant portion of this work has been devoted to the development of new technologies that allow the cell autonomous and synapse specific analysis of presynaptic boutons. Innovations included the creation of a library of bi and tricistronic plasmid and lentiviral vectors that support not only the expression of synaptic proteins at or near endogenous levels, but also the expression of shRNAs to dramatically reduce the expression of multiple neuronal proteins. In addition, this work explored strategies for the cryopreservation of genetically modified glia and neuronal cells, a technology that facilitates the sharing of reagents with defined characteristics, at reduced cost. These advances have allowed the detailed analysis of presynaptic boutons lacking Piccolo and Bassoon, uncovering functions that were hereto unattainable by other technologies. For example, utilizing bicistronic vectors expressing different XFP-tagged presynaptic proteins and shRNAs against Piccolo, it was possible to show that together the various Piccolo isoforms play a fundamental role in the regulated recycling of SVs by controlling the dynamic assembly of presynaptic F-Actin. Studies of boutons lacking both Piccolo and Bassoon demonstrate that these two AZ proteins contribute to the proteostasis of presynaptic bouton, as in their absence, SV pools and synapse integrity are compromised. Mechanistically, Piccolo and Bassoon were found to use their zinc finger domains to suppress the activity of Siah, an E3 ubiquitin ligase known to ubiquitinate SV-proteins. Together these results suggest that Piccolo and Bassoon are important regulators of core functions within presynaptic bouton, such as the activity dependent assembly of F-actin and SV exocytosis as well as the local activity of components of the ubiquitin/lysosome/proteasome system.

4.1 Cryopreserving hippocampal neurons

Neuronal networks established by cultured neurons have become invaluable for studying the molecular, cellular and physiological mechanisms underlying neuronal morphogenesis, nascent synapse formation and synaptic function. Although dissociated cultures can be prepared from most brain regions, cultures prepared from the hippocampus, in particular those by the method of Goslin and Banker (Banker and Goslin 1988; Banker and Goslin 1998; Tanaka 2002), are some of the most reliable for the long term study of mature neuronal circuits as well as early stages of neuronal differentiation, acquiring features nearly indistinguishable from cells *in vivo*. Neurons in these cultures are also readily amenable to genetic manipulation via plasmids and viruses, yet the challenges and cost associated with the

preparation of separate glia and neurons are not trivial requiring dedicated personnel, hours of weakly preparation and large numbers of animal. In this project, we explored whether cryopreservation methods could be used to store stocks of glia and neurons for months and whether upon thawing they would readily differentiate, exhibit normal electrophysiological properties and survive pre-infection with lentivirus. Our studies demonstrate that cryopreservation of neurons and glia can not only be achieved but can reduce costs and provide collaborators with genetically defined and well-characterized neurons.

Over the last three decade, multiples groups have made significant advances in cryopreserving cells from different brain regions, embryonic neuronal tissue and even blocks of brain tissue (Houle and Das 1980; Kawamoto and Barrett 1986; Ruwe and Trumble 1990; Otto, Gortz et al. 2003; Paynter 2008). Cyropreservation has also been achieved for specific human neuronal cell types including: mesencephalic dopamine neuron or adherent neuronal network (Silani, Pizzuti et al. 1988; Petite and Calvet 1997; Ma, O'Shaughnessy et al. 2006), as well as for transfected primary dorsal root ganglia (Negishi, Ishii et al. 2002; Seggio, Ellison et al. 2008) or Glia (Banker and Goslin 1988; Banker and Goslin 1998; Tanaka 2002). A survey of this literature reveals that most of these protocol are very well develop for cryopreserving tissues but not dissociated cells (neurons and glia). For example, Banker and Goslin state that glia exhibit morphological and differentiation problem following cryopreservation. Based on these technologies, companies such as Invitrogen/Gibco now offer cryopreserved dissociated cells from cortex and hippocampus. Not surprising, the composition of the media used for cryopreservation is not stated and only very small amounts of cells are provided (e.g. 1 ml containing 1×10^6 neurons) making this avenue extremely expensive.

Currently, investigators study non-neural cells use 90% FBS and 10% DMSO for cryoprotection, which provides more protection than simply using Cell Freezing Medium-I that contains DMEM 4.5 gm/l D-glucose, 20% Fetal Bovine Serum and 10% DMSO, as recommended by Applied Molecular Biology at University of Maryland, Baltimore County and Atlanta Biologicals. In my studies, it was found that large numbers of glia and >60% neurons survive using 90% FBS and 10% DMSO. Further improvement in cell survival by adding CNQX and APV, to block glutamate receptor mediated cytotoxicity, was not observed. For comparison, we examined whether freezing media sold by Invitrogen that contains serum supplemented with B27 was effective in cyropreserving neurons. Surprisingly, neurons did not survive well in this media even when CNQX and APV were included.

Beyond cell survival, we also examine whether the differentiation state and functionality of glia and neurons were maintained after cryopreservation in 90% FBS and 10% DMSO. For example, using this protocol it was possible to freeze/thaw primary cultures of glia at least three times without loss of their capacity to differentiate into GFAP positive astrocytes and support the growth and differentiation of primary hippocampal neurons. Notably, we found that using a simple “slap” technique, it was possible to dislodge and thus remove unwanted microglia from these cultures, a problem known to limit the propagation and maintenance of astrocytes in a form that support neuronal cell differentiation (Banker and Goslin 1988; Banker and Goslin 1998).

With regard to neuronal functionality following cryopreservation, we found that our 90% FBS and 10% DMSO freezing media supported >60% nerve cell survival. Moreover, we find that these neurons differentiate at a normal rate, forming elaborate dendritic arbors with synapses studded along their length. Electrophysiological recording reveals that these neurons are electrically active, and support synaptic transmission. Intriguingly, we found that post-thawing neurons were readily infected with lentiviral vectors expressing and delivering reporter molecules such as GFP-tagged Synapsin1a to presynaptic boutons. Moreover, we found that infecting neurons with lentiviruses prior to freezing did not affect neuronal cell viability or their capacity to differentiate forming extensive neuronal networks. This is a significant advance in this technology and will facilitate long-distant collaboration where genetically manipulated neuronal cells can be shipped and studied in greater detail.

In summary, we have found that both glia and neurons can easily be cryoprotected with 90% FBS and 10% DMSO, stored for months and used at later times or other laboratories. This simple technology should also dramatically reduce the cost of producing primary neural cells and glia.

4.2 Assessing the role of Piccolo and Bassoon in the assembly, function and integrity of excitatory hippocampal synapses

A major focus of this thesis was to uncover the function of two large presynaptic AZ proteins, Piccolo and Bassoon. They are rapidly recruited to nascent synapses and are stably maintained at presynaptic AZs at mature synapses in the adult brain suggesting a core role in synapse assembly, function and tenacity (Gundelfinger and tom Dieck 2000; Fejtova and Gundelfinger 2006). Given their large size, complex gene structure and extensive alternative splicing traditional knockout strategies have only succeeded in eliminating Bassoon, but not Piccolo from synapse throughout the brain (Altrock, tom Dieck et al. 2003; Hallermann, Fejtova et al. 2010; Mukherjee, Yang et al. 2010). These studies have clearly shown that

Bassoon is essential for tethering ribbons to the archiform density of ribbon synapses in the retina and inner ear. It has also been shown to regulate synaptic transmission at conventional synapses but is dispensable for synapse formation and stability. A likely explanation for these limited phenotypes is the broad and overlapping expression of Piccolo, a structurally related AZ protein. The experiments performed in this doctoral thesis were design to fill some of these gaps in our understanding primarily by first examining how the loss of Piccolo affects synapse assembly and function and second to assess the overlapping functions of Piccolo and Bassoon.

4.3 Roles of CAZ proteins at presynaptic boutons

Loss of function studies on CAZ proteins over the last two decades have primarily demonstrated defects in SV docking, priming and fusion, as seen for Munc18, Munc13 and Rim1 α (Augustin, Rosenmund et al. 1999; Verhage, Maia et al. 2000; Schoch, Castillo et al. 2002; Weimer and Richmond 2005; Schoch and Gundelfinger 2006; Bykhovskaia 2011; Deng, Kaeser et al. 2011; Han, Kaeser et al. 2011; Kaeser, Deng et al. 2011). Until recently, it was unclear whether Piccolo and Bassoon were involved in these processes. Their high structural similarity, near-complete overlap of binding partners (Wang, Kibschull et al. 1999; Fenster, Chung et al. 2000; Fenster, Kessels et al. 2003; Kim, Ko et al. 2003; tom Dieck, Altmann et al. 2005; Fejtova and Gundelfinger 2006; Fejtova, Davydova et al. 2009), and thus likely functional redundancy will make this issue difficult to resolve until the analysis of synapses lacking both proteins is possible.

However, studies of synapses lacking Piccolo and/or Bassoon are beginning to reveal unique roles for each. For example, studies of photoreceptor ribbon synapses demonstrate a crucial functional role for Bassoon in the attachment of ribbons to the archiform density, and in neurotransmission at these synapses (Altmann, tom Dieck et al. 2003; Dick, tom Dieck et al. 2003; tom Dieck, Altmann et al. 2005). Furthermore, the increase in number of presynaptically silent synapses in Bassoon-deficient hippocampal neurons (Altmann, tom Dieck et al. 2003) argues for a potential role of Bassoon in key aspects of vesicle release, perhaps similar to Munc13, Munc18 and Rim1 α (Weimer and Richmond 2005; Schoch and Gundelfinger 2006) and speed vesicle reloading at a central excitatory synapse (Hallermann, Fejtova et al. 2010). In contrast, we found no evidence that loss of Piccolo had any affect on the fraction of presynaptically silent synapses or on the size or release probability of the RRP of SVs. These data indicate that Piccolo does not directly participate in SV docking, priming or fusion. Instead, our data reveal that Piccolo, but not Bassoon, influences the translocation of SVs from the reserve pool to the RRP by regulating the dynamic properties of Synapsin1a

and F-actin. These findings suggest that Piccolo may perform an integrative function within presynaptic boutons, coupling SV docking and fusion to the mobilization/recruitment of SVs from the reserve pool to the AZ.

4.4 Changes in the rates of SV exocytosis in neurons lacking Piccolo can be linked to altered Synapsin dynamics

Synapsins are a well-characterized family of presynaptic phospho-proteins thought to regulate the translocation of SVs from the reserve to the readily-releasable pools (De Camilli, Benfenati et al. 1990; Greengard, Valtorta et al. 1993; Hilfiker, Pieribone et al. 1999). This concept is supported by knockout studies showing that Synapsins are essential for maintaining the size of the reserve pool of SVs (Li, Chin et al. 1995; Ryan, Li et al. 1996), and by dynamic imaging studies, including this one, demonstrating that they regulate SV exocytosis rates at a range of stimulus frequencies (Chi, Greengard et al. 2001; Chi, Greengard et al. 2003). Importantly, the dynamic properties of Synapsin, particularly its activity-dependent dissociation from SVs and the actin cytoskeleton, are regulated by phosphorylation (Torri Tarelli, Bossi et al. 1992; Hilfiker, Pieribone et al. 1999).

Although Synapsin is phosphorylated by multiple kinases, several studies have implicated CaMKII as its most prominent regulator (Schiebler, Jahn et al. 1986; Benfenati, Valtorta et al. 1992; Ceccaldi, Grohovaz et al. 1995; Stefani, Onofri et al. 1997). However, these studies utilized *in vitro* binding assays, and none assessed the direct contribution of CaMKII to either the dispersion kinetics of Synapsin or to SV exocytosis in intact neurons. Two studies that did examine these functions used serine to alanine phospho-mutants to demonstrate that the two identified CaMKII sites were important for regulating the rates of Synapsin dispersion and SV exocytosis (Chi, Greengard et al. 2001; Chi, Greengard et al. 2003). However, neither was performed at physiological temperatures, and neither used pharmacological tools to assess the role of CaMKII in these processes.

In our analysis of boutons lacking Piccolo, we have carefully examined the relationship between Piccolo, Synapsin dispersion, SV exocytosis, and the regulation of these events by CaMKII in intact neurons at physiological temperature. Our analysis of thousands of boutons revealed a remarkable and previously unreported heterogeneity in the degree of EGFP-Synapsin dispersion and FM5-95 destaining per bouton (from >50% to 0%) in wild-type neurons. We also observed a tight correlation between Synapsin dispersion and SV exocytosis. Though other studies have suggested such a relationship, ours is the first to conclusively demonstrate it. We have also closely examined the role of CaMKII in regulating Synapsin dispersion. Surprisingly, blocking CaMKII activity with KN62 did not alter

Synapsin dispersion in wild-type neurons, suggesting that other kinases may mediate this activity. This concept is supported by several previous studies indicating that PKA and MAPK are important regulators of Synapsin, modulating its association with SVs or F-actin, respectively, and, in the case of MAPK, mediating SV exocytosis via Synapsin phosphorylation (Jovanovic, Benfenati et al. 1996; Hosaka, Hammer et al. 1999; Jovanovic, Czernik et al. 2000; Jovanovic, Sihra et al. 2001). Intriguingly, removing Piccolo from synapses caused Synapsin dispersion to be regulated by CaMKII. Furthermore, under these conditions, the enhanced rate of SV exocytosis was also CaMKII-dependent, as both phenotypes could be rescued by inhibiting CaMKII with KN62. These data support our general conclusion that Piccolo negatively regulates SV exocytosis, apparently via a CaMKII-mediated mechanism.

We have also examined the phosphorylation state of Synapsin in the absence of Piccolo. We found that under basal conditions, Synapsin was hypophosphorylated at both CaMKII and MAPK sites. While the levels of phosphorylation at both sites increased during stimulation, absolute levels of phosphorylation were always below those found in wild-type neurons. This finding was unexpected, as we had predicted based on multiple previous studies and our own experiments with KN62 that hyperphosphorylation of Synapsin would mediate its enhanced dispersion. However, total phosphorylation levels of Synapsin may not be predictive of its dispersion kinetics, as two other imaging studies have demonstrated that Synapsin dynamics are regulated through a complex combinatorial code of phosphorylation and dephosphorylation at its seven phospho-sites (Chi, Greengard et al. 2001; Chi, Greengard et al. 2003). Furthermore, given Piccolo's putative role as a molecular organizer of the AZ, multiple signaling pathways may be subtly altered in its absence, affecting the balance of presynaptic phosphorylation/dephosphorylation in ways that are difficult to detect or interpret. In such a scenario, Synapsin would likely be one of many phospho-proteins indirectly affected by the loss of Piccolo. On the other hand, if Synapsin dynamics/phosphorylation alone are altered (still a possibility given the lack of other detectable phenotypes), this would provide evidence for a more direct Piccolo-Synapsin interaction, perhaps through one of the F-actin regulating proteins (ie. GIT1, Abp1, Profilin, Daam1 and Trio) known to bind Piccolo.

4.5 Altered phosphorylation of Synapsin in boutons lacking Piccolo cannot account for Piccolo dependent changes in SV exocytosis and Synapsin dispersion

Initially, we considered the possibility that altered CaMKII phosphorylation of Synapsin1a caused the Piccolo knockdown phenotypes. Consistent with this hypothesis, the

CaMKII inhibitor KN62 rescued these phenotypes, and CaMKII-mediated phosphorylation of Synapsin1a was impaired in neurons lacking Piccolo. In addition, the Synapsin1a S23A phospho-mutant (lacking CaMKII phosphorylation) slowed SV exocytosis in wild-type hippocampal neurons (Chi, Greengard et al. 2001; Chi, Greengard et al. 2003) and rescued the enhanced SV exocytosis seen at boutons without Piccolo. However, this mutant did not rescue the enhanced Synapsin1a dispersion phenotype. Moreover, KN62 treatment attenuated the enhanced dispersion of the S23A mutant, suggesting that CaMKII substrates other than Synapsin1a were responsible for this phenotype. Since our data demonstrate that Synapsin1a dispersion and FM destaining are tightly linked, we hypothesized that an upstream molecule was responsible for coordinately regulating both events. One likely candidate is F-actin, previously shown to modulate both activity-dependent SV exocytosis and Synapsin1a dispersion (Morales, Colicos et al. 2000; Sankaranarayanan, Atluri et al. 2003; Cingolani and Goda 2008).

4.6 Piccolo is an essential regulator of activity dependent presynaptic F-actin assembly

Three functions have been ascribed to presynaptic F-actin. These include a barrier function at the AZ plasma membrane that limits SV fusion (Morales, Colicos et al. 2000), a translocation function that regulates RP maintenance and RRP refilling during periods of sustained synaptic activity, often in association with Synapsin1a (Greengard, Benfenati et al. 1994; Hilfiker, Pieribone et al. 1999; Jensen, Walaas et al. 2007; Cingolani and Goda 2008), and an endocytic function that facilitates SV retrieval (Kuromi and Kidokoro 1998; Shupliakov, Bloom et al. 2002; Bloom, Evergren et al. 2003; Richards, Rizzoli et al. 2004). Whether these functions correspond to spatially and/or morphologically distinct pools of F-actin within presynaptic boutons remains unclear. Also unclear is the precise regulatory nature of each function, which appears to differ depending on synapse type. At central glutamatergic synapses, F-actin negatively regulates several aspects of SV exocytosis. For example, acute F-actin depolymerization in dissociated hippocampal neurons has been shown to enhance Pr (Morales, Colicos et al. 2000), presumably by dismantling an F-actin “barrier” that limits SV fusion at the AZ. In addition, a recent study performed in hippocampal slices suggests that F-actin functions to separate the RP from the RRP, thus limiting SV mobilization into the RRP and preserving synaptic efficacy during sustained activity (Jensen, Walaas et al. 2007). Interestingly, this study also showed that mobilization of the RP was dependent on Synapsins 1 and 2, supporting the concept that both F-actin and Synapsins are important mediators of RRP refilling during sustained activity (Jensen, Walaas et al. 2007).

These studies indicate that F-actin negatively regulates both SV translocation and fusion at glutamatergic synapses.

Which of these functions are regulated by Piccolo? Our experiments so far indicate that Piccolo regulates SV translocation. Activity-dependent Synapsin1a dispersion is dramatically enhanced in the absence of Piccolo, suggesting that Synapsin1a-associated functions of F-actin are compromised. In addition, SV exocytosis rates during 10 Hz, 90 s stimulation, shown to mobilize the RP (Jensen, Walaas et al. 2007), are significantly enhanced at boutons lacking Piccolo, while F-actin levels are reduced, suggesting the absence of a regulatory barrier (i.e., F-actin) during SV translocation/RRP refilling. Whether Piccolo also regulates the AZ-associated barrier function or putative endocytic function of F-actin is unknown, although its binding partners Abp1 and Profilin2 both have demonstrated roles in endocytosis (Kessels, Engqvist-Goldstein et al. 2001; Mise-Omata, Montagne et al. 2003; Gareus, Di Nardo et al. 2006), suggesting that Piccolo may also function in this process. Future studies should address these issues.

We have also uncovered a novel role for Piccolo-mediated F-actin assembly in facilitating the activity-dependent recruitment of CaMKII α to presynaptic boutons. Specifically, we found that like F-actin, EGFP-CaMKII α failed to undergo activity dependent recruitment in the absence of Piccolo. This lack of translocation could account for the hypophosphorylation of Synapsin1a in neurons lacking Piccolo, although the functional relevance of this defect is unclear. Since CaMKII α is an important signaling molecule with multiple presynaptic substrates, including Synapsin1a and BK channels (Wang 2008), it is possible that other aspects of presynaptic function and plasticity are affected by Piccolo loss (Ninan and Arancio 2004; Wang 2008).

4.7 Piccolo dependent presynaptic phenotypes are not exhibited by neurons cultured from *Pclo* Δ Ex14 mice

Recently, Mukherjee and colleagues described a mouse with a targeted deletion of exon 14 of the *Pclo* gene (*Pclo* Δ Ex14) (Mukherjee, Yang et al. 2010). This exon encodes a small part of the C-terminal C2A domain. Before excising exon14 with CRE, the authors reported a >95% loss of Piccolo protein, but no defects in neurotransmission or synaptic plasticity, while post excision the levels of Piccolo were not affected. This suggests that the neomycin (neo) selectable marker for the knockin was adversely affecting the expression of Piccolo. The lack of overt synaptic phenotypes in cultured neurons from these mice lead to the suggestion that Piccolo is dispensable for these processes (Mukherjee, Yang et al. 2010). These data are at odds with our studies using shRNAs to knockdown Piccolo. However,

using well-characterized antibodies that recognize a central region of Piccolo present in most of the >8 Piccolo isoforms, revealed that neo cassette near exon 14 only affects a subset of isoforms (>400 kDa) (Figure 3.28). This latter finding is consistent with known and predicted alternatively splicing of 3' exons in the Pclo gene (Fenster and Garner 2002). Importantly, immuno-reactivity associated with the remaining (~200–400 kDa) isoforms was detected within presynaptic boutons of neurons cultured from (Pclo Δ Ex14/neo) mice. Moreover, no deficits in activity dependent F-actin assembly could be detected in the presynaptic boutons of these neurons. Taken together these data suggest that the remaining isoforms support many of the activity dependent function of Piccolo. To test this hypothesis, we infected Pclo Δ Ex14/neo neurons with the Piccolo shRNA Pclo28. Under these conditions, the remaining Piccolo immuno-reactivity in these boutons was loss and activity-dependent F-actin assembly was disrupted. These observations suggest that the Pclo Δ Ex14/neo mice will not be very useful for assessing core contribution of Piccolo to synaptic function. This said, a number of recent studies have shown that the C2A domain in Piccolo can be mutated in a subpopulation of patients with major depressive disorder (Bochdanovits, Verhage et al. 2009; Sullivan, de Geus et al. 2009; Furukawa-Hibi, Nitta et al. 2010). This suggest that Pclo Δ Ex14/- mice may prove useful for studying the underlying molecular mechanisms associated with of major depressive disorders (Bochdanovits, Verhage et al. 2009; Sullivan, de Geus et al. 2009; Furukawa-Hibi, Nitta et al. 2010).

4.8 Bassoon and Piccolo regulate of SV proteostasis

Although the loss of either Bassoon or Piccolo from central glutamatergic synapses produces relatively mild phenotypes, their striking shared structural homology along most of their length indicates that they likely have significant functional redundancy within presynaptic boutons. As an initial attempt to unmask these shared roles, we designed a tricistronic lentiviral vector that can simultaneous knockdown of both proteins with greater than 90% efficiency. As discussed below double-knockdown (DKD) of Bassoon and Piccolo induced a dramatic reduction of SV proteins in lysates from DKD neurons as well as a progressive loss of SVs from presynaptic boutons. Intriguingly, drugs that blocked the proteasome and lysosomal systems restored SV pool size. These findings indicate that Piccolo/Bassoon may function together to regulate aspects of pre-synaptic proteostasis.

Several lines of evidence support a shared role for Bassoon and Piccolo in the proteostasis of SVs, also referred to as SV-stasis. First, knockdown of both proteins causes a dramatic reduction in the expression of multiple SV-associated proteins, including Synaptophysin, VAMP2, Rab3a, SV2, VGLUT1, and Synapsin1a, as assessed by Western

blotting, immunostaining, and expression of recombinant EGFP-tagged proteins. This reduction does not occur in neurons expressing scrambled control shRNAs or single shRNAs against either Piccolo or Bassoon. Importantly, this phenotype can be rescued by the expression of full-length, shRNA-resistant mRFP-Bassoon, arguing that it is not due to off-target effects of the shRNAs. Second, ultrastructural examination of boutons lacking Bassoon and Piccolo reveals significant abnormalities in SV morphology and pool size, including decreased numbers of SVs/bouton, increased numbers of elongated/enlarged SVs, and the appearance of numerous pleiomorphic vesicles reminiscent of early and late endosomes. Between 9 and 14 DIV, pleiomorphic/endosomal structures increase dramatically in prevalence while SVs decreased, suggesting that these structures represent intermediates in a pathway for SV degradation. Finally, pharmacological manipulations that inhibit protein ubiquitination (Ziram), proteasomes (epoxomicin), or lysosomes (chloroquinone/leupeptin) mitigate the DKD-induced loss of SV-associated proteins. Taken together, these findings indicate that Bassoon and Piccolo are critically important for maintaining SV pools within presynaptic boutons.

Although less robust, a similar phenotype of SV loss was observed by Mukherjee and colleagues in their recent study of neurons with reduced levels of Bassoon and Piccolo (Mukherjee, Yang et al. 2010). These authors performed an ultrastructural analysis of neurons cultured from *Pclo Δ Ex14/neo* mice that were also infected with an shRNA against Bassoon. Under these conditions, they found a ~50% reduction in the numbers of both total and docked SVs/bouton. No other morphological defects were detected, leading the authors to conclude that Bassoon and Piccolo have a relatively minor role in SV clustering. However, we believe that their findings reflect a weak version of the DKD phenotype caused by incomplete knockdown of both proteins. This conclusion is supported by the authors' own experiments demonstrating that only ~60% of Bassoon was eliminated by shRNA knockdown (Mukherjee, Yang et al. 2010). Moreover, our re-analysis of the *Pclo Δ Ex14/neo* mice revealed that only three of the seven identified Piccolo isoforms are eliminated. Importantly, these remaining isoforms all contain the two Piccolo double Zinc Finger domains and localize to presynaptic boutons. Importantly, we also find that Piccolo loss-of-function phenotypes are not present in neurons cultured from *Pclo Δ Ex14/neo* mice, unless the remaining Piccolo isoforms are eliminated from these neurons by shRNA knockdown (Figure 3.29). Thus, we believe that the ultrastructural data from the study by Mukherjee and colleagues are consistent with ours, demonstrating a role for Piccolo and Bassoon in regulating SV pool size and not just SV clustering.

4.9 ZF domains in Bassoon and Piccolo modulate SV pool size

We have also explored the molecular mechanisms underlying Piccolo/Bassoon dependent regulation of SV-stasis. Maintenance of SV pools requires a delicate balance between *de-novo* synthesis, recycling, and degradation of SV-associated peripheral and integral membrane proteins. Ubiquitination is hypothesized to regulate two of these steps. The recycling of SV proteins during exo/endocytosis is potentially mediated by monoubiquitination, while their degradation by lysosomes or proteasomes is mediated by polyubiquitination (DiAntonio and Hicke 2004; Varshavsky 2005; Yi and Ehlers 2005; Waites and Garner 2011). To test whether enhanced ubiquitination contributes to the DKD phenotype, we treated neurons with ziram, a drug that blocks the initial step of protein ubiquitination. We find that ziram substantially attenuates DKD-induced loss of EGFP-SV2 fluorescence, suggesting that Bassoon and Piccolo regulate the activity of one or more ubiquitinating enzymes.

Consistent with this concept, studies by Altrock, Fetjova and Gundelfinger (Personal communication) have found in a yeast-two hybrid screen that several subdomains in Bassoon can interact with a number of E3 ligases. For our studies the most intriguing is Siah1a which was found to directly interact with the Zinc finger (ZF) domains in Bassoon. This E3 has been previously found to ubiquitinate a number of SV associated proteins including alpha-synuclein, synaptophysin and beta-catenin (Wheeler, Chin et al. 2002; Liani, Eyal et al. 2004; Lee, Wheeler et al. 2008; Rott, Szargel et al. 2008; Dimitrova, Li et al. 2010). To explore whether the zinc finger domains in Bassoon, which are highly conserved in Piccolo (Fenster, Chung et al. 2000), we performed two types of experiments. First, we used immunoprecipitation to confirm that the ZF domains in both Bassoon and Piccolo could associate with recombinant myc-tagged Siah1a. Next, we over-expressed the N-terminal segment of Bassoon (residues 1-609), which includes its two ZF domains, as a fusion protein with EGFP (EGFP-Bsn1-609). As reported previously, this region of Bassoon was found to localize within presynaptic boutons of wild-type neurons (Dresbach, Hempelmann et al. 2003)(Figure 3.35). Intriguingly, double label immuno-fluorescent microscopy revealed that EGFP-Bsn1-609 over-expression triggered a dramatic increase in the intensity of SV marker like synaptophysin compared to untransfected control neurons. Moreover, when EGFP-Bsn1-609 was expressed in DKD neurons, the levels of SV proteins were restored. A similar result was obtained when the Bassoon and Piccolo ZnF domain were individually expressed in DKD neurons. Taken together, these data explain why the loss of SV phenotype is not observed in neurons lacking only Piccolo or Bassoon and/or in neurons from *Pclo* Δ Ex14/*neo* mice infected with an shRNA that only modestly knocks down Bassoon. Mechanistically, our data

also indicate that the ZF domains in Piccolo and Bassoon function to regulate SV-stasis in part by negatively regulating the poly-ubiquitination of SV proteins within presynaptic boutons.

4.10 Ubiquitination in presynaptic structure and function

Ubiquitination has recently emerged as an important regulator of presynaptic function, with roles in SV exocytosis and presynaptic plasticity. For example, acute inhibition of protein ubiquitination by ziram has been shown to dramatically increase neurotransmitter release in cultured hippocampal neurons (Rinetti and Schweizer 2010), suggesting that the dynamic ubiquitination of presynaptic proteins regulates SV fusion. Moreover, the activity-dependent ubiquitination and degradation of two CAZ proteins that regulate SV priming and fusion, RIM1 and Munc13, appears to underlie a form of presynaptic silencing induced by strong depolarization (Jiang, Litkowski et al. 2010). Specific E3 ligases are likely to mediate these effects, and several with presynaptic substrates have been identified. For instance, the synaptically-localized E3 ligases Scrapper and Fbxo45 have been shown to bind and ubiquitinate RIM1 and Munc13-1, respectively (Yao, Takagi et al. 2007; Tada, Okano et al. 2010). Scrapper and Fbxo45 knockout mice both exhibit enhanced neurotransmitter release, consistent with the increased levels and decreased turnover of RIM1 and Munc13-1, respectively, observed in the brains of these mice. Interestingly, Scrapper may also regulate SV pool size, as its levels are inversely related to those of several SV-associated proteins, including Synaptophysin, SynapsinIIa, and Synaptotagmin (Yao, Takagi et al. 2007). Furthermore, ultrastructural analysis of presynaptic boutons from Scrapper KO mice shows that they have higher SV density than wild-type mice, indicating larger SV pools (Yao, Takagi et al. 2007).

In addition to Scrapper, another group of E3 ligases that appear to regulate SV pool size is the PHR family, composed of human PAM, *Drosophila* highwire, *C. elegans* RPM-1, and mouse Phr (Jin and Garner 2008). Although these ligases have diverse functions depending on organism and synapse type, all seem to regulate the formation and/or stability of presynaptic boutons. For example, RPM-1 loss of function reduces total synapse density and the number of SVs/bouton in *C. elegans*, and also causes disorganized presynaptic architecture (Schaefer, Hadwiger et al. 2000; Zhen, Huang et al. 2000), suggesting a critical role for RPM-1 in bouton formation and/or stability. Studies of Phr knockout mice further support a role for this E3 ligase in presynaptic maintenance, as the neuromuscular junctions of Phr *-/-* mice undergo atrophy due to retraction of their presynaptic terminals (Lewcock, Genoud et al. 2007; Saiga, Fukuda et al. 2009). Interestingly, a similar phenotype is seen in

mice lacking Fbxo45, the murine homolog of *C. elegans* FSN-1, which functions in the same pathway as RPM-1/Phr (Liao, Hung et al. 2004; Saiga, Fukuda et al. 2009).

4.11 Ubiquitination and neurodegeneration

A common theme emerging from these and other E3 ligase loss-of-function studies is that subtle imbalances in protein ubiquitination within specific synaptic compartments can trigger neurodegeneration (Almeida, Takahashi et al. 2006; Chou, Maidment et al. 2008; Ding and Shen 2008; Engelender 2008; Lehman 2009). In addition to Phr and Fbxo45, knockout of several other presynaptically-localized murine E3 ligases, including Scrapper and the deubiquitinating enzyme UCH-L1, causes alterations in bouton morphology, including increased or decreased SV density, and eventual central or peripheral nervous system neurodegeneration (Yao, Sugiura et al. 2008; Chen, Sugiura et al. 2010). In our studies, we find that Bassoon/Piccolo knockdown also leads to the progressive loss of SVs and disorganization of synaptic architecture. Since these phenotypes emerge concomitantly with Bassoon/Piccolo loss, it seems reasonable to speculate that DKD induced changes in protein ubiquitination originate at or near the presynaptic AZ. Moreover, the phenotypic parallels between Bassoon/Piccolo DKD and other genetic manipulations that induce neurodegeneration, including UCH-L1 knockout or overexpression of α -Synuclein (Chen, Sugiura et al. 2010; Scott, Tabarean et al. 2010), suggest that the DKD will also adversely impact neuronal health over time. Future studies will explore this issue.

5. General conclusions

In summary, we have found that Piccolo is not essential for excitatory synapse formation, but is a negative regulator of SV exocytosis. These results indicate that one of Piccolo's functions at the AZ is to regulate the translocation of SVs from the reserve to the readily releasable pool through modulation of Synapsin dynamics. Further, our results demonstrate that this role is not shared by Bassoon, providing one of the first indications that these proteins have non-overlapping functions. Rather puzzling is the absence of other presynaptic phenotypes, especially given the large size of Piccolo and its numerous binding partners. One likely explanation is that redundant features in Bassoon mask many of these.

We have also demonstrated that Piccolo is an important regulator of presynaptic F-actin, functioning to coordinate its activity-dependent assembly from within the AZ and thereby modulating neurotransmitter release. Future studies should seek to resolve the molecular pathway through which Piccolo regulates F-actin polymerization, and which functions of F-actin [i.e., initial synapse formation (Lucido, Suarez Sanchez et al. 2009), maturation (Zhang

and Benson 2001; Shen, Wu et al. 2006), or presynaptic plasticity (Jensen, Walaas et al. 2007; Antonova, Lu et al. 2009)] are regulated by Piccolo.

Through the creation of tricistronic lentiviral vectors that express multiple shRNAs, it has also been possible to efficiently knockdown the expression of both Piccolo and Bassoon and thus begin the exploration of their shared/redundant function. In our initial analysis, we observed that the DKD of Piccolo/Bassoon triggered the dramatic loss of SV pools, a phenotype that requires functional lysosomal, proteasome and ubiquitin systems. These data point to a fundamental role for these AZ proteins in SV-stasis. Although SV loss is the dominant phenotype observed in DKD boutons, it is currently unclear whether SV-stasis is the primary function of Piccolo/Bassoon or whether their loss triggers aberrant local protein hyper poly-ubiquitination, similar to what may occur in neurodegenerative disorders such as Parkinson's, Huntington's and Alzheimer's diseases. Since Bassoon and Piccolo are core components of the CAZ, it is tempting to speculate that they normally regulate the local ubiquitination of presynaptic proteins and receptors as they dynamically transit into and out of the AZ plasma membrane. A number of emerging studies suggest that such a role would be instrumental for proper synaptic function, given the importance of ubiquitination in neurotransmitter release, presynaptic plasticity, and neurotrophin retrograde signaling (Hicke 2001; Hicke and Dunn 2003; DiAntonio and Hicke 2004; Varshavsky 2005; Geetha and Wooten 2008; Rinetti and Schweizer 2010). Future studies will need to investigate the role of the Bassoon/Piccolo interaction in these processes.

6. Bibliography

- Almeida, C. G., R. H. Takahashi, et al. (2006). "Beta-amyloid accumulation impairs multivesicular body sorting by inhibiting the ubiquitin-proteasome system." *The Journal of neuroscience : the official journal of the Society for Neuroscience* **26**(16): 4277-4288.
- Altick, A. L., L. M. Baryshnikova, et al. (2009). "Quantitative analysis of multivesicular bodies (MVBs) in the hypoglossal nerve: evidence that neurotrophic factors do not use MVBs for retrograde axonal transport." *The Journal of comparative neurology* **514**(6): 641-657.
- Altrock, W. D., S. tom Dieck, et al. (2003). "Functional inactivation of a fraction of excitatory synapses in mice deficient for the active zone protein bassoon." *Neuron* **37**(5): 787-800.
- Andrews-Zwilling, Y. S., H. Kawabe, et al. (2006). "Binding to Rab3A-interacting molecule RIM regulates the presynaptic recruitment of Munc13-1 and ubMunc13-2." *The Journal of biological chemistry* **281**(28): 19720-19731.
- Antonova, I., F. M. Lu, et al. (2009). "Rapid and long-lasting increase in sites for synapse assembly during late-phase potentiation in rat hippocampal neurons." *PLoS one* **4**(11): e7690.
- Aravamudan, B., T. Fergestad, et al. (1999). "Drosophila UNC-13 is essential for synaptic transmission." *Nature neuroscience* **2**(11): 965-971.
- Augustin, I., A. Betz, et al. (1999). "Differential expression of two novel Munc13 proteins in rat brain." *The Biochemical journal* **337** (Pt 3): 363-371.
- Augustin, I., C. Rosenmund, et al. (1999). "Munc13-1 is essential for fusion competence of glutamatergic synaptic vesicles." *Nature* **400**(6743): 457-461.
- Awatramani, G. B. and M. M. Slaughter (2001). "Intensity-dependent, rapid activation of presynaptic metabotropic glutamate receptors at a central synapse." *The Journal of neuroscience : the official journal of the Society for Neuroscience* **21**(2): 741-749.
- Banker, G. and K. Goslin (1988). "Developments in neuronal cell culture." *Nature* **336**(6195): 185-186.
- Banker, G. and K. Goslin (1998). *Culturing Nerve Cells (Second Edition)*. Cambridge, MA, MIT Press.
- Baron, M. K., T. M. Boeckers, et al. (2006). "An architectural framework that may lie at the core of the postsynaptic density." *Science* **311**(5760): 531-535.
- Benfenati, F., F. Valtorta, et al. (1992). "Synaptic vesicle-associated Ca²⁺/calmodulin-dependent protein kinase II is a binding protein for synapsin I." *Nature* **359**(6394): 417-420.
- Beresewicz, M. (2007). "[Scaffold proteins (MAGUK, Shank and Homer) in postsynaptic density in the central nervous system]." *Postepy biochemii* **53**(2): 188-197.
- Betz, A., U. Ashery, et al. (1998). "Munc13-1 is a presynaptic phorbol ester receptor that enhances neurotransmitter release." *Neuron* **21**(1): 123-136.
- Betz, A., P. Thakur, et al. (2001). "Functional interaction of the active zone proteins Munc13-1 and RIM1 in synaptic vesicle priming." *Neuron* **30**(1): 183-196.
- Bloom, O., E. Evergren, et al. (2003). "Colocalization of synapsin and actin during synaptic vesicle recycling." *The Journal of cell biology* **161**(4): 737-747.
- Bochdanovits, Z., M. Verhage, et al. (2009). "Joint reanalysis of 29 correlated SNPs supports the role of PCLO/Piccolo as a causal risk factor for major depressive disorder." *Molecular psychiatry* **14**(7): 650-652.
- Boeckers, T. M. (2006). "The postsynaptic density." *Cell and tissue research* **326**(2): 409-422.
- Brenner, S. (1974). "The genetics of *Caenorhabditis elegans*." *Genetics* **77**(1): 71-94.
- Brose, N., K. Hofmann, et al. (1995). "Mammalian homologues of *Caenorhabditis elegans* unc-13 gene define novel family of C2-domain proteins." *The Journal of biological chemistry* **270**(42): 25273-25280.
- Brunetti-Pierri, N., T. Ng, et al. (2006). "Improved hepatic transduction, reduced systemic vector dissemination, and long-term transgene expression by delivering helper-dependent adenoviral vectors into the surgically isolated liver of nonhuman primates." *Human gene therapy* **17**(4): 391-404.
- Brunetti-Pierri, N., T. C. Nichols, et al. (2005). "Sustained phenotypic correction of canine hemophilia B after systemic administration of helper-dependent adenoviral vector." *Human gene therapy* **16**(7): 811-820.
- Burns, M. E. and G. J. Augustine (1995). "Synaptic structure and function: dynamic organization yields architectural precision." *Cell* **83**(2): 187-194.
- Bykhovskaia, M. (2011). "Synapsin regulation of vesicle organization and functional pools." *Seminars in cell & developmental biology* **22**(4): 387-392.
- Cai, Q., P. Y. Pan, et al. (2007). "Syntabulin-kinesin-1 family member 5B-mediated axonal transport contributes to activity-dependent presynaptic assembly." *The Journal of neuroscience : the official journal of the Society for Neuroscience* **27**(27): 7284-7296.
- Cases-Langhoff, C., B. Voss, et al. (1996). "Piccolo, a novel 420 kDa protein associated with the presynaptic cytomatrix." *European journal of cell biology* **69**(3): 214-223.
- Castillo, P. E., S. Schoch, et al. (2002). "RIM1alpha is required for presynaptic long-term potentiation." *Nature* **415**(6869): 327-330.

- Ceccaldi, P. E., F. Grohovaz, et al. (1995). "Dephosphorylated synapsin I anchors synaptic vesicles to actin cytoskeleton: an analysis by videomicroscopy." *The Journal of cell biology* **128**(5): 905-912.
- Cen, X., A. Nitta, et al. (2008). "Identification of Piccolo as a regulator of behavioral plasticity and dopamine transporter internalization." *Molecular psychiatry* **13**(4): 349, 451-363.
- Chen, F., Y. Sugiura, et al. (2010). "Ubiquitin carboxyl-terminal hydrolase L1 is required for maintaining the structure and function of the neuromuscular junction." *Proceedings of the National Academy of Sciences of the United States of America* **107**(4): 1636-1641.
- Chen, J., S. E. Billings, et al. (2011). "Calcium channels link the muscle-derived synapse organizer laminin beta2 to Bassoon and CAST/Erc2 to organize presynaptic active zones." *The Journal of neuroscience : the official journal of the Society for Neuroscience* **31**(2): 512-525.
- Cheung, G. and M. A. Cousin (2011). "Quantitative analysis of synaptic vesicle pool replenishment in cultured cerebellar granule neurons using FM dyes." *Journal of visualized experiments : JoVE*(57).
- Chi, P., P. Greengard, et al. (2001). "Synapsin dispersion and recluster during synaptic activity." *Nature neuroscience* **4**(12): 1187-1193.
- Chi, P., P. Greengard, et al. (2003). "Synaptic vesicle mobilization is regulated by distinct synapsin I phosphorylation pathways at different frequencies." *Neuron* **38**(1): 69-78.
- Cho, K. O., C. A. Hunt, et al. (1992). "The rat brain postsynaptic density fraction contains a homolog of the Drosophila discs-large tumor suppressor protein." *Neuron* **9**(5): 929-942.
- Choi, K. H., B. W. Higgs, et al. (2011). "Gene expression and genetic variation data implicate PCLO in bipolar disorder." *Biological psychiatry* **69**(4): 353-359.
- Chou, A. P., N. Maidment, et al. (2008). "Ziram causes dopaminergic cell damage by inhibiting E1 ligase of the proteasome." *The Journal of biological chemistry* **283**(50): 34696-34703.
- Cingolani, L. A. and Y. Goda (2008). "Actin in action: the interplay between the actin cytoskeleton and synaptic efficacy." *Nature reviews. Neuroscience* **9**(5): 344-356.
- Citri, A. and R. C. Malenka (2008). "Synaptic plasticity: multiple forms, functions, and mechanisms." *Neuropsychopharmacology : official publication of the American College of Neuropsychopharmacology* **33**(1): 18-41.
- Cline, H. T. (1998). "Topographic maps: developing roles of synaptic plasticity." *Current biology : CB* **8**(23): R836-839.
- Cochilla, A. J., J. K. Angleson, et al. (1999). "Monitoring secretory membrane with FM1-43 fluorescence." *Annual review of neuroscience* **22**: 1-10.
- Cole, J. C., B. R. Villa, et al. (2000). "Disruption of actin impedes transmitter release in snake motor terminals." *The Journal of physiology* **525 Pt 3**: 579-586.
- Colicos, M. A., B. E. Collins, et al. (2001). "Remodeling of synaptic actin induced by photoconductive stimulation." *Cell* **107**(5): 605-616.
- Coppola, T., S. Magnin-Luthi, et al. (2001). "Direct interaction of the Rab3 effector RIM with Ca²⁺ channels, SNAP-25, and synaptotagmin." *The Journal of biological chemistry* **276**(35): 32756-32762.
- Dai, Y., H. Taru, et al. (2006). "SYD-2 Liprin-alpha organizes presynaptic active zone formation through ELKS." *Nature neuroscience* **9**(12): 1479-1487.
- De Camilli, P., F. Benfenati, et al. (1990). "The synapsins." *Annual review of cell biology* **6**: 433-460.
- Deguchi-Tawarada, M., E. Inoue, et al. (2006). "Active zone protein CAST is a component of conventional and ribbon synapses in mouse retina." *The Journal of comparative neurology* **495**(4): 480-496.
- Deguchi-Tawarada, M., E. Inoue, et al. (2004). "CAST2: identification and characterization of a protein structurally related to the presynaptic cytomatrix protein CAST." *Genes to cells : devoted to molecular & cellular mechanisms* **9**(1): 15-23.
- Deken, S. L., R. Vincent, et al. (2005). "Redundant localization mechanisms of RIM and ELKS in *Caenorhabditis elegans*." *The Journal of neuroscience : the official journal of the Society for Neuroscience* **25**(25): 5975-5983.
- Deng, L., P. S. Kaeser, et al. (2011). "RIM proteins activate vesicle priming by reversing autoinhibitory homodimerization of Munc13." *Neuron* **69**(2): 317-331.
- Depienne, C., P. Roques, et al. (2000). "Cellular distribution and karyophilic properties of matrix, integrase, and Vpr proteins from the human and simian immunodeficiency viruses." *Experimental cell research* **260**(2): 387-395.
- DiAntonio, A. and L. Hicke (2004). "Ubiquitin-dependent regulation of the synapse." *Annual review of neuroscience* **27**: 223-246.
- Dick, O., S. tom Dieck, et al. (2003). "The presynaptic active zone protein bassoon is essential for photoreceptor ribbon synapse formation in the retina." *Neuron* **37**(5): 775-786.
- Dillon, C. and Y. Goda (2005). "The actin cytoskeleton: integrating form and function at the synapse." *Annual review of neuroscience* **28**: 25-55.
- Dimitrova, Y. N., J. Li, et al. (2010). "Direct ubiquitination of beta-catenin by Siah-1 and regulation by the exchange factor TBL1." *The Journal of biological chemistry* **285**(18): 13507-13516.

- Ding, M. and K. Shen (2008). "The role of the ubiquitin proteasome system in synapse remodeling and neurodegenerative diseases." BioEssays : news and reviews in molecular, cellular and developmental biology **30**(11-12): 1075-1083.
- Dresbach, T., A. Hempelmann, et al. (2003). "Functional regions of the presynaptic cytomatrix protein bassoon: significance for synaptic targeting and cytomatrix anchoring." Molecular and cellular neurosciences **23**(2): 279-291.
- Dresbach, T., B. Qualmann, et al. (2001). "The presynaptic cytomatrix of brain synapses." Cellular and molecular life sciences : CMLS **58**(1): 94-116.
- Dresbach, T., V. Torres, et al. (2006). "Assembly of active zone precursor vesicles: obligatory trafficking of presynaptic cytomatrix proteins Bassoon and Piccolo via a trans-Golgi compartment." The Journal of biological chemistry **281**(9): 6038-6047.
- Dulubova, I., X. Lou, et al. (2005). "A Munc13/RIM/Rab3 tripartite complex: from priming to plasticity?" The EMBO journal **24**(16): 2839-2850.
- Ehlers, M. D. (2000). "Reinsertion or degradation of AMPA receptors determined by activity-dependent endocytic sorting." Neuron **28**(2): 511-525.
- Elferink, L. A., W. S. Trimble, et al. (1989). "Two vesicle-associated membrane protein genes are differentially expressed in the rat central nervous system." The Journal of biological chemistry **264**(19): 11061-11064.
- Engelender, S. (2008). "Ubiquitination of alpha-synuclein and autophagy in Parkinson's disease." Autophagy **4**(3): 372-374.
- Engqvist-Goldstein, A. E. and D. G. Drubin (2003). "Actin assembly and endocytosis: from yeast to mammals." Annual review of cell and developmental biology **19**: 287-332.
- Evergren, E., F. Benfenati, et al. (2007). "The synapsin cycle: a view from the synaptic endocytic zone." Journal of neuroscience research **85**(12): 2648-2656.
- Fejtova, A., D. Davydova, et al. (2009). "Dynein light chain regulates axonal trafficking and synaptic levels of Bassoon." The Journal of cell biology **185**(2): 341-355.
- Fejtova, A. and E. D. Gundelfinger (2006). "Molecular organization and assembly of the presynaptic active zone of neurotransmitter release." Results and problems in cell differentiation **43**: 49-68.
- Fenster, S. D., W. J. Chung, et al. (2000). "Piccolo, a presynaptic zinc finger protein structurally related to bassoon." Neuron **25**(1): 203-214.
- Fenster, S. D. and C. C. Garner (2002). "Gene structure and genetic localization of the PCLO gene encoding the presynaptic active zone protein Piccolo." International journal of developmental neuroscience : the official journal of the International Society for Developmental Neuroscience **20**(3-5): 161-171.
- Fenster, S. D., M. M. Kessels, et al. (2003). "Interactions between Piccolo and the actin/dynamin-binding protein Abp1 link vesicle endocytosis to presynaptic active zones." The Journal of biological chemistry **278**(22): 20268-20277.
- Fire, A., S. Xu, et al. (1998). "Potent and specific genetic interference by double-stranded RNA in *Caenorhabditis elegans*." Nature **391**(6669): 806-811.
- Fischer, A., S. Hacein-Bey-Abina, et al. (2011). "Gene therapy for primary adaptive immune deficiencies." The Journal of allergy and clinical immunology **127**(6): 1356-1359.
- Fouquet, W., D. Oswald, et al. (2009). "Maturation of active zone assembly by *Drosophila* Bruchpilot." The Journal of cell biology **186**(1): 129-145.
- Frank, T., M. A. Rutherford, et al. (2010). "Bassoon and the synaptic ribbon organize Ca²⁺ channels and vesicles to add release sites and promote refilling." Neuron **68**(4): 724-738.
- Fujimoto, K., T. Shibasaki, et al. (2002). "Piccolo, a Ca²⁺ sensor in pancreatic beta-cells. Involvement of cAMP-GEFII.Rim2. Piccolo complex in cAMP-dependent exocytosis." The Journal of biological chemistry **277**(52): 50497-50502.
- Furukawa-Hibi, Y., A. Nitta, et al. (2010). "Overexpression of piccolo C2A domain induces depression-like behavior in mice." Neuroreport **21**(18): 1177-1181.
- Galli, T. and V. Haucke (2004). "Cycling of synaptic vesicles: how far? How fast!" Science's STKE : signal transduction knowledge environment **2004**(264): re19.
- Garcia, E. P., P. S. McPherson, et al. (1995). "rbSec1A and B colocalize with syntaxin 1 and SNAP-25 throughout the axon, but are not in a stable complex with syntaxin." The Journal of cell biology **129**(1): 105-120.
- Garcia, J., S. H. Gerber, et al. (2004). "A conformational switch in the Piccolo C2A domain regulated by alternative splicing." Nature structural & molecular biology **11**(1): 45-53.
- Gareus, R., A. Di Nardo, et al. (2006). "Mouse profilin 2 regulates endocytosis and competes with SH3 ligand binding to dynamin 1." The Journal of biological chemistry **281**(5): 2803-2811.
- Garner, C. C. and S. Kindler (1996). "Synaptic proteins and the assembly of synaptic junctions." Trends in cell biology **6**(11): 429-433.
- Garner, C. C., S. Kindler, et al. (2000). "Molecular determinants of presynaptic active zones." Current opinion in neurobiology **10**(3): 321-327.

- Garner, C. C., R. G. Zhai, et al. (2002). "Molecular mechanisms of CNS synaptogenesis." Trends in neurosciences **25**(5): 243-251.
- Geetha, T. and M. W. Wooten (2008). "TrkA receptor endolysosomal degradation is both ubiquitin and proteasome dependent." Traffic **9**(7): 1146-1156.
- Gitler, D., Y. Xu, et al. (2004). "Molecular determinants of synapsin targeting to presynaptic terminals." The Journal of neuroscience : the official journal of the Society for Neuroscience **24**(14): 3711-3720.
- Gracheva, E. O., A. O. Burdina, et al. (2006). "Tomosyn inhibits synaptic vesicle priming in *Caenorhabditis elegans*." PLoS biology **4**(8): e261.
- Graham, F. L., J. Smiley, et al. (1977). "Characteristics of a human cell line transformed by DNA from human adenovirus type 5." The Journal of general virology **36**(1): 59-74.
- Gray, E. G. (1959). "Axo-somatic and axo-dendritic synapses of the cerebral cortex: an electron microscope study." Journal of anatomy **93**: 420-433.
- Gray, E. G. (1959). "Electron microscopy of synaptic contacts on dendrite spines of the cerebral cortex." Nature **183**(4675): 1592-1593.
- Greengard, P., F. Benfenati, et al. (1994). "Synapsin I, an actin-binding protein regulating synaptic vesicle traffic in the nerve terminal." Advances in second messenger and phosphoprotein research **29**: 31-45.
- Greengard, P., F. Valtorta, et al. (1993). "Synaptic vesicle phosphoproteins and regulation of synaptic function." Science **259**(5096): 780-785.
- Gundelfinger, E. D., T. M. Boeckers, et al. (2006). "A role for zinc in postsynaptic density assembly and plasticity?" Trends in biochemical sciences **31**(7): 366-373.
- Gundelfinger, E. D. and S. tom Dieck (2000). "Molecular organization of excitatory chemical synapses in the mammalian brain." Die Naturwissenschaften **87**(12): 513-523.
- Hallermann, S., A. Fejtova, et al. (2010). "Bassoon speeds vesicle reloading at a central excitatory synapse." Neuron **68**(4): 710-723.
- Hammond, S. M., E. Bernstein, et al. (2000). "An RNA-directed nuclease mediates post-transcriptional gene silencing in *Drosophila* cells." Nature **404**(6775): 293-296.
- Han, Y., P. S. Kaeser, et al. (2011). "RIM determines Ca(2)+ channel density and vesicle docking at the presynaptic active zone." Neuron **69**(2): 304-316.
- Haucke, V., E. Neher, et al. (2011). "Protein scaffolds in the coupling of synaptic exocytosis and endocytosis." Nature reviews. Neuroscience **12**(3): 127-138.
- Heyden, A., M. C. Ionescu, et al. (2011). "Hippocampal enlargement in Bassoon-mutant mice is associated with enhanced neurogenesis, reduced apoptosis, and abnormal BDNF levels." Cell and tissue research **346**(1): 11-26.
- Hibino, H., R. Pironkova, et al. (2002). "RIM binding proteins (RBPs) couple Rab3-interacting molecules (RIMs) to voltage-gated Ca(2+) channels." Neuron **34**(3): 411-423.
- Hicke, L. (2001). "Protein regulation by monoubiquitin." Nature reviews. Molecular cell biology **2**(3): 195-201.
- Hicke, L. and R. Dunn (2003). "Regulation of membrane protein transport by ubiquitin and ubiquitin-binding proteins." Annual review of cell and developmental biology **19**: 141-172.
- Hida, Y. and T. Ohtsuka (2010). "CAST and ELKS proteins: structural and functional determinants of the presynaptic active zone." Journal of biochemistry **148**(2): 131-137.
- Hilfiker, S., V. A. Pieribone, et al. (1999). "Synapsins as regulators of neurotransmitter release." Philosophical transactions of the Royal Society of London. Series B, Biological sciences **354**(1381): 269-279.
- Hill-Eubanks, D. C., M. E. Werner, et al. (2011). "Calcium signaling in smooth muscle." Cold Spring Harbor perspectives in biology **3**(9): a004549.
- Hoopmann, P., S. O. Rizzoli, et al. (2012). "FM Dye Photoconversion for Visualizing Synaptic Vesicles by Electron Microscopy." Cold Spring Harbor protocols **2012**(1).
- Hosaka, M., R. E. Hammer, et al. (1999). "A phospho-switch controls the dynamic association of synapsins with synaptic vesicles." Neuron **24**(2): 377-387.
- Hoskison, M. M., Y. Yanagawa, et al. (2007). "Calcium-dependent NMDA-induced dendritic injury and MAP2 loss in acute hippocampal slices." Neuroscience **145**(1): 66-79.
- Houle, J. D. and G. D. Das (1980). "Freezing of embryonic neural tissue and its transplantation in the rat brain." Brain research **192**(2): 570-574.
- Hua, Z., S. Leal-Ortiz, et al. (2011). "v-SNARE composition distinguishes synaptic vesicle pools." Neuron **71**(3): 474-487.
- Ibi, D., A. Nitta, et al. (2010). "Piccolo knockdown-induced impairments of spatial learning and long-term potentiation in the hippocampal CA1 region." Neurochemistry international **56**(1): 77-83.
- Inoue, E., M. Deguchi-Tawarada, et al. (2006). "ELKS, a protein structurally related to the active zone protein CAST, is involved in Ca2+-dependent exocytosis from PC12 cells." Genes to cells : devoted to molecular & cellular mechanisms **11**(6): 659-672.
- Jahn, R. and T. C. Sudhof (1999). "Membrane fusion and exocytosis." Annual review of biochemistry **68**: 863-911.

- Jensen, S., T. Sorensen, et al. (1984). "Intraocular grafts of fresh and freeze-stored rat hippocampal tissue: a comparison of survivability and histological and connective organization." The Journal of comparative neurology **227**(4): 559-568.
- Jensen, V., S. I. Walaas, et al. (2007). "A delayed response enhancement during hippocampal presynaptic plasticity in mice." The Journal of physiology **583**(Pt 1): 129-143.
- Jessell, T. M. and E. R. Kandel (1993). "Synaptic transmission: a bidirectional and self-modifiable form of cell-cell communication." Cell **72 Suppl**: 1-30.
- Jeyifous, O., C. L. Waites, et al. (2009). "SAP97 and CASK mediate sorting of NMDA receptors through a previously unknown secretory pathway." Nature neuroscience **12**(8): 1011-1019.
- Jiang, X., P. E. Litkowski, et al. (2010). "A role for the ubiquitin-proteasome system in activity-dependent presynaptic silencing." The Journal of neuroscience : the official journal of the Society for Neuroscience **30**(5): 1798-1809.
- Jin, Y. and C. C. Garner (2008). "Molecular mechanisms of presynaptic differentiation." Annual review of cell and developmental biology **24**: 237-262.
- Jose, M., D. K. Nair, et al. (2008). "Investigating interactions mediated by the presynaptic protein bassoon in living cells by Foerster's resonance energy transfer and fluorescence lifetime imaging microscopy." Biophysical journal **94**(4): 1483-1496.
- Jovanovic, J. N., F. Benfenati, et al. (1996). "Neurotrophins stimulate phosphorylation of synapsin I by MAP kinase and regulate synapsin I-actin interactions." Proceedings of the National Academy of Sciences of the United States of America **93**(8): 3679-3683.
- Jovanovic, J. N., A. J. Czernik, et al. (2000). "Synapsins as mediators of BDNF-enhanced neurotransmitter release." Nature neuroscience **3**(4): 323-329.
- Jovanovic, J. N., T. S. Sihra, et al. (2001). "Opposing changes in phosphorylation of specific sites in synapsin I during Ca²⁺-dependent glutamate release in isolated nerve terminals." The Journal of neuroscience : the official journal of the Society for Neuroscience **21**(20): 7944-7953.
- Kaech, S. and G. Banker (2006). "Culturing hippocampal neurons." Nature protocols **1**(5): 2406-2415.
- Kaesler, P. S., L. Deng, et al. (2009). "ELKS2alpha/CAST deletion selectively increases neurotransmitter release at inhibitory synapses." Neuron **64**(2): 227-239.
- Kaesler, P. S., L. Deng, et al. (2011). "RIM proteins tether Ca²⁺ channels to presynaptic active zones via a direct PDZ-domain interaction." Cell **144**(2): 282-295.
- Kaesler, P. S., H. B. Kwon, et al. (2008). "RIM1alpha and RIM1beta are synthesized from distinct promoters of the RIM1 gene to mediate differential but overlapping synaptic functions." The Journal of neuroscience : the official journal of the Society for Neuroscience **28**(50): 13435-13447.
- Kandel, E. R., M. Klein, et al. (1986). "Some principles emerging from the study of short- and long-term memory." Neuroscience research **3**(6): 498-520.
- Kaufmann, N., J. DeProto, et al. (2002). "Drosophila liprin-alpha and the receptor phosphatase Dlar control synapse morphogenesis." Neuron **34**(1): 27-38.
- Kawamoto, J. C. and J. N. Barrett (1986). "Cryopreservation of primary neurons for tissue culture." Brain research **384**(1): 84-93.
- Kazanietz, M. G., N. E. Lewin, et al. (1995). "Characterization of the cysteine-rich region of the Caenorhabditis elegans protein Unc-13 as a high affinity phorbol ester receptor. Analysis of ligand-binding interactions, lipid cofactor requirements, and inhibitor sensitivity." The Journal of biological chemistry **270**(18): 10777-10783.
- Kessels, M. M., A. E. Engqvist-Goldstein, et al. (2001). "Mammalian Abp1, a signal-responsive F-actin-binding protein, links the actin cytoskeleton to endocytosis via the GTPase dynamin." The Journal of cell biology **153**(2): 351-366.
- Kim, E., K. O. Cho, et al. (1996). "Heteromultimerization and NMDA receptor-clustering activity of Chapsyn-110, a member of the PSD-95 family of proteins." Neuron **17**(1): 103-113.
- Kim, E. and J. Ko (2006). "Molecular organization and assembly of the postsynaptic density of excitatory brain synapses." Results and problems in cell differentiation **43**: 1-23.
- Kim, I. H., A. Jozkowicz, et al. (2001). "Lifetime correction of genetic deficiency in mice with a single injection of helper-dependent adenoviral vector." Proceedings of the National Academy of Sciences of the United States of America **98**(23): 13282-13287.
- Kim, S., J. Ko, et al. (2003). "The GIT family of proteins forms multimers and associates with the presynaptic cytomatrix protein Piccolo." The Journal of biological chemistry **278**(8): 6291-6300.
- Kistner, U., B. M. Wenzel, et al. (1993). "SAP90, a rat presynaptic protein related to the product of the Drosophila tumor suppressor gene dlg-A." The Journal of biological chemistry **268**(7): 4580-4583.
- Kittel, R. J., C. Wichmann, et al. (2006). "Bruchpilot promotes active zone assembly, Ca²⁺ channel clustering, and vesicle release." Science **312**(5776): 1051-1054.
- Ko, J., S. Kim, et al. (2003). "Interaction between liprin-alpha and GIT1 is required for AMPA receptor targeting." The Journal of neuroscience : the official journal of the Society for Neuroscience **23**(5): 1667-1677.

- Ko, J., M. Na, et al. (2003). "Interaction of the ERC family of RIM-binding proteins with the liprin-alpha family of multidomain proteins." *The Journal of biological chemistry* **278**(43): 42377-42385.
- Kornau, H. C., L. T. Schenker, et al. (1995). "Domain interaction between NMDA receptor subunits and the postsynaptic density protein PSD-95." *Science* **269**(5231): 1737-1740.
- Kuromi, H. and Y. Kidokoro (1998). "Two distinct pools of synaptic vesicles in single presynaptic boutons in a temperature-sensitive *Drosophila* mutant, *shibire*." *Neuron* **20**(5): 917-925.
- Kuromi, H. and Y. Kidokoro (2005). "Exocytosis and endocytosis of synaptic vesicles and functional roles of vesicle pools: lessons from the *Drosophila* neuromuscular junction." *The Neuroscientist : a review journal bringing neurobiology, neurology and psychiatry* **11**(2): 138-147.
- Landis, D. M. (1988). "Membrane and cytoplasmic structure at synaptic junctions in the mammalian central nervous system." *Journal of electron microscopy technique* **10**(2): 129-151.
- Landis, D. M., A. K. Hall, et al. (1988). "The organization of cytoplasm at the presynaptic active zone of a central nervous system synapse." *Neuron* **1**(3): 201-209.
- Langnaese, K., C. Seidenbecher, et al. (1996). "Protein components of a rat brain synaptic junctional protein preparation." *Brain Res Mol Brain Res* **42**(1): 118-122.
- Lanpher, B., N. Brunetti-Pierri, et al. (2006). "Inborn errors of metabolism: the flux from Mendelian to complex diseases." *Nature reviews. Genetics* **7**(6): 449-460.
- Leal-Ortiz, S., C. L. Waites, et al. (2008). "Piccolo modulation of Synapsin I dynamics regulates synaptic vesicle exocytosis." *The Journal of cell biology* **181**(5): 831-846.
- Lee, C. S., L. Y. Tee, et al. (2004). "A proteasomal stress response: pre-treatment with proteasome inhibitors increases proteasome activity and reduces neuronal vulnerability to oxidative injury." *Journal of neurochemistry* **91**(4): 996-1006.
- Lee, J. T., T. C. Wheeler, et al. (2008). "Ubiquitination of alpha-synuclein by Siah-1 promotes alpha-synuclein aggregation and apoptotic cell death." *Human molecular genetics* **17**(6): 906-917.
- Lee, S., Y. Sato, et al. (2011). "Lysosomal proteolysis inhibition selectively disrupts axonal transport of degradative organelles and causes an Alzheimer's-like axonal dystrophy." *The Journal of neuroscience : the official journal of the Society for Neuroscience* **31**(21): 7817-7830.
- Lehman, N. L. (2009). "The ubiquitin proteasome system in neuropathology." *Acta neuropathologica* **118**(3): 329-347.
- Lewcock, J. W., N. Genoud, et al. (2007). "The ubiquitin ligase Phr1 regulates axon outgrowth through modulation of microtubule dynamics." *Neuron* **56**(4): 604-620.
- Li, L., L. S. Chin, et al. (1995). "Impairment of synaptic vesicle clustering and of synaptic transmission, and increased seizure propensity, in synapsin I-deficient mice." *Proceedings of the National Academy of Sciences of the United States of America* **92**(20): 9235-9239.
- Liani, E., A. Eyal, et al. (2004). "Ubiquitylation of synphilin-1 and alpha-synuclein by SIAH and its presence in cellular inclusions and Lewy bodies imply a role in Parkinson's disease." *Proceedings of the National Academy of Sciences of the United States of America* **101**(15): 5500-5505.
- Liao, E. H., W. Hung, et al. (2004). "An SCF-like ubiquitin ligase complex that controls presynaptic differentiation." *Nature* **430**(6997): 345-350.
- Limbach, C., M. M. Laue, et al. (2011). "Molecular in situ topology of Aczonin/Piccolo and associated proteins at the mammalian neurotransmitter release site." *Proceedings of the National Academy of Sciences of the United States of America* **108**(31): E392-401.
- Lois, C., E. J. Hong, et al. (2002). "Germline transmission and tissue-specific expression of transgenes delivered by lentiviral vectors." *Science* **295**(5556): 868-872.
- Lonart, G., S. Schoch, et al. (2003). "Phosphorylation of RIM1alpha by PKA triggers presynaptic long-term potentiation at cerebellar parallel fiber synapses." *Cell* **115**(1): 49-60.
- Lu, J., H. Li, et al. (2005). "Solution structure of the RIM1alpha PDZ domain in complex with an ELKS1b C-terminal peptide." *Journal of molecular biology* **352**(2): 455-466.
- Lu, J., M. Machius, et al. (2006). "Structural basis for a Munc13-1 homodimer to Munc13-1/RIM heterodimer switch." *PLoS biology* **4**(7): e192.
- Lucido, A. L., F. Suarez Sanchez, et al. (2009). "Rapid assembly of functional presynaptic boutons triggered by adhesive contacts." *The Journal of neuroscience : the official journal of the Society for Neuroscience* **29**(40): 12449-12466.
- Lujan, R., J. D. Roberts, et al. (1997). "Differential plasma membrane distribution of metabotropic glutamate receptors mGluR1 alpha, mGluR2 and mGluR5, relative to neurotransmitter release sites." *Journal of chemical neuroanatomy* **13**(4): 219-241.
- Ma, W., T. O'Shaughnessy, et al. (2006). "Cryopreservation of adherent neuronal networks." *Neurosci Lett* **403**(1-2): 84-89.
- Maas, C., V. I. Torres, W. Altrock, S. A. Leal-Ortiz, D. Wagh, R. T. Terry-Lorenzo, A. Fejtova, E. D. Gundelfinger, N. Ziv, and C. C. Garner "Formation of Golgi-derived active zone precursor vesicles." *Journal of Neuroscience, in press*

- Malenka, R. C. and R. A. Nicoll (1999). "Long-term potentiation--a decade of progress?" Science **285**(5435): 1870-1874.
- Malinow, R. and R. C. Malenka (2002). "AMPA receptor trafficking and synaptic plasticity." Annual review of neuroscience **25**: 103-126.
- Mammano, F., V. Trouplin, et al. (2000). "Retracing the evolutionary pathways of human immunodeficiency virus type 1 resistance to protease inhibitors: virus fitness in the absence and in the presence of drug." Journal of virology **74**(18): 8524-8531.
- Martinez, J., A. Patkaniowska, et al. (2002). "Single-stranded antisense siRNAs guide target RNA cleavage in RNAi." Cell **110**(5): 563-574.
- Matsuzawa, S., C. Li, et al. (2003). "Structural analysis of Siah1 and its interactions with Siah-interacting protein (SIP)." The Journal of biological chemistry **278**(3): 1837-1840.
- Meberg, P. J. and M. W. Miller (2003). "Culturing hippocampal and cortical neurons." Methods in cell biology **71**: 111-127.
- Miller, K. E., J. DeProto, et al. (2005). "Direct observation demonstrates that Liprin-alpha is required for trafficking of synaptic vesicles." Current biology : CB **15**(7): 684-689.
- Miller, M. D., C. M. Farnet, et al. (1997). "Human immunodeficiency virus type 1 preintegration complexes: studies of organization and composition." Journal of virology **71**(7): 5382-5390.
- Mise-Omata, S., B. Montagne, et al. (2003). "Mammalian actin binding protein 1 is essential for endocytosis but not lamellipodia formation: functional analysis by RNA interference." Biochemical and biophysical research communications **301**(3): 704-710.
- Monier, S., F. Jollivet, et al. (2002). "Characterization of novel Rab6-interacting proteins involved in endosome-to-TGN transport." Traffic **3**(4): 289-297.
- Montgomery, J. M., P. L. Zamorano, et al. (2004). "MAGUKs in synapse assembly and function: an emerging view." Cellular and molecular life sciences : CMLS **61**(7-8): 911-929.
- Morales, M., M. A. Colicos, et al. (2000). "Actin-dependent regulation of neurotransmitter release at central synapses." Neuron **27**(3): 539-550.
- Moriyoshi, K., K. Iijima, et al. (2004). "Seven in absentia homolog 1A mediates ubiquitination and degradation of group 1 metabotropic glutamate receptors." Proceedings of the National Academy of Sciences of the United States of America **101**(23): 8614-8619.
- Mozhayeva, M. G., Y. Sara, et al. (2002). "Development of vesicle pools during maturation of hippocampal synapses." The Journal of neuroscience : the official journal of the Society for Neuroscience **22**(3): 654-665.
- Mukherjee, K., X. Yang, et al. (2010). "Piccolo and bassoon maintain synaptic vesicle clustering without directly participating in vesicle exocytosis." Proceedings of the National Academy of Sciences of the United States of America **107**(14): 6504-6509.
- Muller, B. M., U. Kistner, et al. (1996). "SAP102, a novel postsynaptic protein that interacts with NMDA receptor complexes in vivo." Neuron **17**(2): 255-265.
- Muller, B. M., U. Kistner, et al. (1995). "Molecular characterization and spatial distribution of SAP97, a novel presynaptic protein homologous to SAP90 and the Drosophila discs-large tumor suppressor protein." J Neurosci **15**(3 Pt 2): 2354-2366.
- Nakata, T., Y. Kitamura, et al. (1999). "Fusion of a novel gene, ELKS, to RET due to translocation t(10;12)(q11;p13) in a papillary thyroid carcinoma." Genes, chromosomes & cancer **25**(2): 97-103.
- Negishi, T., Y. Ishii, et al. (2002). "Cryopreservation of brain tissue for primary culture." Exp Anim **51**(4): 383-390.
- Negri, D. R., Z. Michelini, et al. (2011). "Integrase-defective lentiviral-vector-based vaccine: a new vector for induction of T cell immunity." Expert opinion on biological therapy **11**(6): 739-750.
- Ninan, I. and O. Arancio (2004). "Presynaptic CaMKII is necessary for synaptic plasticity in cultured hippocampal neurons." Neuron **42**(1): 129-141.
- Niwa, H., K. Yamamura, et al. (1991). "Efficient selection for high-expression transfectants with a novel eukaryotic vector." Gene **108**(2): 193-199.
- Nusser, Z., R. Lujan, et al. (1998). "Cell type and pathway dependence of synaptic AMPA receptor number and variability in the hippocampus." Neuron **21**(3): 545-559.
- Nykanen, A., B. Haley, et al. (2001). "ATP requirements and small interfering RNA structure in the RNA interference pathway." Cell **107**(3): 309-321.
- Ohtsuka, T., E. Takao-Rikitsu, et al. (2002). "Cast: a novel protein of the cytomatrix at the active zone of synapses that forms a ternary complex with RIM1 and munc13-1." The Journal of cell biology **158**(3): 577-590.
- Okabe, S. (2007). "Molecular anatomy of the postsynaptic density." Molecular and cellular neurosciences **34**(4): 503-518.
- Olsen, O., K. A. Moore, et al. (2005). "Neurotransmitter release regulated by a MALS-liprin-alpha presynaptic complex." The Journal of cell biology **170**(7): 1127-1134.
- Olsen, O., K. A. Moore, et al. (2006). "Synaptic transmission regulated by a presynaptic MALS/Liprin-alpha protein complex." Current opinion in cell biology **18**(2): 223-227.

- Otto, F., P. Gortz, et al. (2003). "Cryopreserved rat cortical cells develop functional neuronal networks on microelectrode arrays." *J Neurosci Methods* **128**(1-2): 173-181.
- Owald, D. and S. J. Sigrist (2009). "Assembling the presynaptic active zone." *Current opinion in neurobiology* **19**(3): 311-318.
- Palmer, D. J. and P. Ng (2005). "Helper-dependent adenoviral vectors for gene therapy." *Human gene therapy* **16**(1): 1-16.
- Palmer, D. J. and P. Ng (2008). "Methods for the production of first generation adenoviral vectors." *Methods in molecular biology* **433**: 55-78.
- Palmer, D. J. and P. Ng (2011). "Rescue, amplification, and large-scale production of helper-dependent adenoviral vectors." *Cold Spring Harbor protocols* **2011**(7): 857-866.
- Park, J. S., M. C. Bateman, et al. (1996). "Rapid alterations in dendrite morphology during sublethal hypoxia or glutamate receptor activation." *Neurobiol Dis* **3**(3): 215-227.
- Parton, R. G., K. Simons, et al. (1992). "Axonal and dendritic endocytic pathways in cultured neurons." *The Journal of cell biology* **119**(1): 123-137.
- Paynter, S. J. (2008). "Principles and practical issues for cryopreservation of nerve cells." *Brain Res Bull* **75**(1): 1-14.
- Peters, A. (2007). "Golgi, Cajal, and the fine structure of the nervous system." *Brain research reviews* **55**(2): 256-263.
- Petite, D. and M. C. Calvet (1997). "Morphometric characteristics of cryopreserved mesencephalic dopamine neurons in culture." *Brain Res* **769**(1): 1-12.
- Petralia, R. S., N. Sans, et al. (2005). "Ontogeny of postsynaptic density proteins at glutamatergic synapses." *Mol Cell Neurosci* **29**(3): 436-452.
- Pobbati, A. V., A. Stein, et al. (2006). "N- to C-terminal SNARE complex assembly promotes rapid membrane fusion." *Science* **313**(5787): 673-676.
- Pyle, J. L., E. T. Kavalali, et al. (2000). "Rapid reuse of readily releasable pool vesicles at hippocampal synapses." *Neuron* **28**(1): 221-231.
- Reynolds, A., D. Leake, et al. (2004). "Rational siRNA design for RNA interference." *Nature biotechnology* **22**(3): 326-330.
- Richards, D. A., S. O. Rizzoli, et al. (2004). "Effects of wortmannin and latrunculin A on slow endocytosis at the frog neuromuscular junction." *The Journal of physiology* **557**(Pt 1): 77-91.
- Richmond, J. E., W. S. Davis, et al. (1999). "UNC-13 is required for synaptic vesicle fusion in *C. elegans*." *Nature neuroscience* **2**(11): 959-964.
- Richter, K., K. Langnaese, et al. (1999). "Presynaptic cytomatrix protein bassoon is localized at both excitatory and inhibitory synapses of rat brain." *The Journal of comparative neurology* **408**(3): 437-448.
- Rinetti, G. V. and F. E. Schweizer (2010). "Ubiquitination acutely regulates presynaptic neurotransmitter release in mammalian neurons." *The Journal of neuroscience : the official journal of the Society for Neuroscience* **30**(9): 3157-3166.
- Robert, F., J. F. Cloix, et al. (2012). "Ultrastructural characterization of rat neurons in primary culture." *Neuroscience* **200**: 248-260.
- Rosahl, T. W., M. Geppert, et al. (1993). "Short-term synaptic plasticity is altered in mice lacking synapsin I." *Cell* **75**(4): 661-670.
- Rosenmund, C., J. Rettig, et al. (2003). "Molecular mechanisms of active zone function." *Curr Opin Neurobiol* **13**(5): 509-519.
- Rosenmund, C., A. Sigler, et al. (2002). "Differential control of vesicle priming and short-term plasticity by Munc13 isoforms." *Neuron* **33**(3): 411-424.
- Rott, R., R. Szargel, et al. (2008). "Monoubiquitylation of alpha-synuclein by seven in absentia homolog (SIAH) promotes its aggregation in dopaminergic cells." *The Journal of biological chemistry* **283**(6): 3316-3328.
- Ruwe, P. A. and T. E. Trumble (1990). "A functional evaluation of cryopreserved peripheral nerve autografts." *J Reconstr Microsurg* **6**(3): 239-244.
- Ryan, T. A., L. Li, et al. (1996). "Synaptic vesicle recycling in synapsin I knock-out mice." *The Journal of cell biology* **134**(5): 1219-1227.
- Ryan, T. A., H. Reuter, et al. (1993). "The kinetics of synaptic vesicle recycling measured at single presynaptic boutons." *Neuron* **11**(4): 713-724.
- Sachdeva, G., J. D'Costa, et al. (2007). "Chimeric HIV-1 and HIV-2 lentiviral vectors with added safety insurance." *Journal of medical virology* **79**(2): 118-126.
- Saiga, T., T. Fukuda, et al. (2009). "Fbxo45 forms a novel ubiquitin ligase complex and is required for neuronal development." *Molecular and cellular biology* **29**(13): 3529-3543.
- Sankaranarayanan, S., P. P. Atluri, et al. (2003). "Actin has a molecular scaffolding, not propulsive, role in presynaptic function." *Nature neuroscience* **6**(2): 127-135.
- Santelli, E., M. Leone, et al. (2005). "Structural analysis of Siah1-Siah-interacting protein interactions and insights into the assembly of an E3 ligase multiprotein complex." *The Journal of biological chemistry* **280**(40): 34278-34287.

- Schaefer, A. M., G. D. Hadwiger, et al. (2000). "rpm-1, a conserved neuronal gene that regulates targeting and synaptogenesis in *C. elegans*." Neuron **26**(2): 345-356.
- Schiebler, W., R. Jahn, et al. (1986). "Characterization of synapsin I binding to small synaptic vesicles." The Journal of biological chemistry **261**(18): 8383-8390.
- Schmidt, E. V., G. Christoph, et al. (1990). "The cytomegalovirus enhancer: a pan-active control element in transgenic mice." Molecular and cellular biology **10**(8): 4406-4411.
- Schoch, S., P. E. Castillo, et al. (2002). "RIM1 alpha forms a protein scaffold for regulating neurotransmitter release at the active zone." Nature **415**(6869): 321-326.
- Schoch, S. and E. D. Gundelfinger (2006). "Molecular organization of the presynaptic active zone." Cell and tissue research **326**(2): 379-391.
- Schorpp, M., R. Jager, et al. (1996). "The human ubiquitin C promoter directs high ubiquitous expression of transgenes in mice." Nucleic acids research **24**(9): 1787-1788.
- Scott, D. A., I. Tabarean, et al. (2010). "A pathologic cascade leading to synaptic dysfunction in alpha-synuclein-induced neurodegeneration." The Journal of neuroscience : the official journal of the Society for Neuroscience **30**(24): 8083-8095.
- Seggio, A. M., K. S. Ellison, et al. (2008). "Cryopreservation of transfected primary dorsal root ganglia neurons." J Neurosci Methods **173**(1): 67-73.
- Serra-Pages, C., N. L. Kedersha, et al. (1995). "The LAR transmembrane protein tyrosine phosphatase and a coiled-coil LAR-interacting protein co-localize at focal adhesions." The EMBO journal **14**(12): 2827-2838.
- Shen, W., B. Wu, et al. (2006). "Activity-induced rapid synaptic maturation mediated by presynaptic cdc42 signaling." Neuron **50**(3): 401-414.
- Sheng, M. and C. C. Hoogenraad (2007). "The postsynaptic architecture of excitatory synapses: a more quantitative view." Annual review of biochemistry **76**: 823-847.
- Shibasaki, T., Y. Sunaga, et al. (2004). "Interaction of ATP sensor, cAMP sensor, Ca²⁺ sensor, and voltage-dependent Ca²⁺ channel in insulin granule exocytosis." The Journal of biological chemistry **279**(9): 7956-7961.
- Shupliakov, O., O. Bloom, et al. (2002). "Impaired recycling of synaptic vesicles after acute perturbation of the presynaptic actin cytoskeleton." Proceedings of the National Academy of Sciences of the United States of America **99**(22): 14476-14481.
- Siegelbaum, S. A. and E. R. Kandel (1991). "Learning-related synaptic plasticity: LTP and LTD." Current opinion in neurobiology **1**(1): 113-120.
- Sigrist, S. J. and D. Schmitz (2011). "Structural and functional plasticity of the cytoplasmic active zone." Current opinion in neurobiology **21**(1): 144-150.
- Silani, V., A. Pizzuti, et al. (1988). "Human neuronal cell viability demonstrated in culture after cryopreservation." Brain Res **473**(1): 169-174.
- Skorobogatko, Y. V., J. Deuso, et al. (2011). "Human Alzheimer's disease synaptic O-GlcNAc site mapping and iTRAQ expression proteomics with ion trap mass spectrometry." Amino acids **40**(3): 765-779.
- Sorensen, T., S. Jensen, et al. (1986). "Intracerebral transplants of freeze-stored rat hippocampal tissue." The Journal of comparative neurology **252**(4): 468-482.
- Spencer, H. T., G. Denning, et al. (2011). "Lentiviral vector platform for production of bioengineered recombinant coagulation factor VIII." Molecular therapy : the journal of the American Society of Gene Therapy **19**(2): 302-309.
- Srinivasakumar, N. (2001). "HIV-1 vector systems." Somatic cell and molecular genetics **26**(1-6): 51-81.
- Stefani, G., F. Onofri, et al. (1997). "Kinetic analysis of the phosphorylation-dependent interactions of synapsin I with rat brain synaptic vesicles." The Journal of physiology **504** (Pt 3): 501-515.
- Stigloher, C., H. Zhan, et al. (2011). "The presynaptic dense projection of the *Caenorhabditis elegans* cholinergic neuromuscular junction localizes synaptic vesicles at the active zone through SYD-2/liprin and UNC-10/RIM-dependent interactions." The Journal of neuroscience : the official journal of the Society for Neuroscience **31**(12): 4388-4396.
- Stryker, E. and K. G. Johnson (2007). "LAR, liprin alpha and the regulation of active zone morphogenesis." Journal of cell science **120**(Pt 21): 3723-3728.
- Sudhof, T. C., M. Baumert, et al. (1989). "A synaptic vesicle membrane protein is conserved from mammals to *Drosophila*." Neuron **2**(5): 1475-1481.
- Sudhof, T. C. and J. Rizo (1996). "Synaptotagmins: C2-domain proteins that regulate membrane traffic." Neuron **17**(3): 379-388.
- Sullivan, P. F., E. J. de Geus, et al. (2009). "Genome-wide association for major depressive disorder: a possible role for the presynaptic protein piccolo." Molecular psychiatry **14**(4): 359-375.
- Suzuki, Y. and R. Craigie (2007). "The road to chromatin - nuclear entry of retroviruses." Nature reviews. Microbiology **5**(3): 187-196.
- Szargel, R., R. Rott, et al. (2009). "Synphilin-1A inhibits seven in absentia homolog (SIAH) and modulates alpha-synuclein monoubiquitylation and inclusion formation." The Journal of biological chemistry **284**(17): 11706-11716.

- Tada, H., H. J. Okano, et al. (2010). "Fbxo45, a novel ubiquitin ligase, regulates synaptic activity." The Journal of biological chemistry **285**(6): 3840-3849.
- Takao-Rikitsu, E., S. Mochida, et al. (2004). "Physical and functional interaction of the active zone proteins, CAST, RIM1, and Bassoon, in neurotransmitter release." The Journal of cell biology **164**(2): 301-311.
- Takumi, Y., V. Ramirez-Leon, et al. (1999). "Different modes of expression of AMPA and NMDA receptors in hippocampal synapses." Nat Neurosci **2**(7): 618-624.
- Tanaka, H. (2002). "[Culturing hippocampal neurons]." Nihon yakurigaku zasshi. Folia pharmacologica Japonica **119**(3): 163-166.
- Toietta, G., V. P. Mane, et al. (2005). "Lifelong elimination of hyperbilirubinemia in the Gunn rat with a single injection of helper-dependent adenoviral vector." Proceedings of the National Academy of Sciences of the United States of America **102**(11): 3930-3935.
- Tokoro, T., S. Higa, et al. (2007). "Localization of the active zone proteins CAST, ELKS, and Piccolo at neuromuscular junctions." Neuroreport **18**(4): 313-316.
- tom Dieck, S., W. D. Altmann, et al. (2005). "Molecular dissection of the photoreceptor ribbon synapse: physical interaction of Bassoon and RIBEYE is essential for the assembly of the ribbon complex." The Journal of cell biology **168**(5): 825-836.
- tom Dieck, S., L. Sanmarti-Vila, et al. (1998). "Bassoon, a novel zinc-finger CAG/glutamine-repeat protein selectively localized at the active zone of presynaptic nerve terminals." The Journal of cell biology **142**(2): 499-509.
- Torres, V., L. Barra, et al. (2010). "A bicistronic lentiviral vector based on the 1D/2A sequence of foot-and-mouth disease virus expresses proteins stoichiometrically." Journal of biotechnology **146**(3): 138-142.
- Torri Tarelli, F., M. Bossi, et al. (1992). "Synapsin I partially dissociates from synaptic vesicles during exocytosis induced by electrical stimulation." Neuron **9**(6): 1143-1153.
- Varoqueaux, F., A. Sigler, et al. (2002). "Total arrest of spontaneous and evoked synaptic transmission but normal synaptogenesis in the absence of Munc13-mediated vesicle priming." Proc Natl Acad Sci U S A **99**(13): 9037-9042.
- Varoqueaux, F., M. S. Sons, et al. (2005). "Aberrant morphology and residual transmitter release at the Munc13-deficient mouse neuromuscular synapse." Mol Cell Biol **25**(14): 5973-5984.
- Varshavsky, A. (2005). "Regulated protein degradation." Trends in biochemical sciences **30**(6): 283-286.
- Verhage, M., A. S. Maia, et al. (2000). "Synaptic assembly of the brain in the absence of neurotransmitter secretion." Science **287**(5454): 864-869.
- Wagh, D. A., T. M. Rasse, et al. (2006). "Bruchpilot, a protein with homology to ELKS/CAST, is required for structural integrity and function of synaptic active zones in Drosophila." Neuron **49**(6): 833-844.
- Waites, C. L., A. M. Craig, et al. (2005). "Mechanisms of vertebrate synaptogenesis." Annual review of neuroscience **28**: 251-274.
- Waites, C. L. and C. C. Garner (2011). "Presynaptic function in health and disease." Trends in neurosciences **34**(6): 326-337.
- Waites, C. L., S. A. Leal-Ortiz, et al. (2011). "Piccolo regulates the dynamic assembly of presynaptic f-actin." The Journal of neuroscience : the official journal of the Society for Neuroscience **31**(40): 14250-14263.
- Waites, C. L., C. G. Specht, et al. (2009). "Synaptic SAP97 isoforms regulate AMPA receptor dynamics and access to presynaptic glutamate." The Journal of neuroscience : the official journal of the Society for Neuroscience **29**(14): 4332-4345.
- Wang, X., B. Hu, et al. (2009). "A protein interaction node at the neurotransmitter release site: domains of Aczonin/Piccolo, Bassoon, CAST, and rim converge on the N-terminal domain of Munc13-1." The Journal of neuroscience : the official journal of the Society for Neuroscience **29**(40): 12584-12596.
- Wang, X., M. Kibschull, et al. (1999). "Aczonin, a 550-kD putative scaffolding protein of presynaptic active zones, shares homology regions with Rim and Bassoon and binds profilin." The Journal of cell biology **147**(1): 151-162.
- Wang, Y., X. Liu, et al. (2002). "A family of RIM-binding proteins regulated by alternative splicing: Implications for the genesis of synaptic active zones." Proceedings of the National Academy of Sciences of the United States of America **99**(22): 14464-14469.
- Wang, Y., M. Okamoto, et al. (1997). "Rim is a putative Rab3 effector in regulating synaptic-vesicle fusion." Nature **388**(6642): 593-598.
- Wang, Y., S. Sugita, et al. (2000). "The RIM/NIM family of neuronal C2 domain proteins. Interactions with Rab3 and a new class of Src homology 3 domain proteins." The Journal of biological chemistry **275**(26): 20033-20044.
- Wang, Z. W. (2008). "Regulation of synaptic transmission by presynaptic CaMKII and BK channels." Molecular neurobiology **38**(2): 153-166.
- Weimer, R. M., E. O. Gracheva, et al. (2006). "UNC-13 and UNC-10/rim localize synaptic vesicles to specific membrane domains." The Journal of neuroscience : the official journal of the Society for Neuroscience **26**(31): 8040-8047.
- Weimer, R. M. and J. E. Richmond (2005). "Synaptic vesicle docking: a putative role for the Munc18/Sec1 protein family." Current topics in developmental biology **65**: 83-113.

- Wendholt, D., C. Spilker, et al. (2006). "ProSAP-interacting protein 1 (ProSAPiP1), a novel protein of the postsynaptic density that links the spine-associated Rap-Gap (SPAR) to the scaffolding protein ProSAP2/Shank3." *The Journal of biological chemistry* **281**(19): 13805-13816.
- Wheeler, T. C., L. S. Chin, et al. (2002). "Regulation of synaptophysin degradation by mammalian homologues of seven in absentia." *The Journal of biological chemistry* **277**(12): 10273-10282.
- Willeumier, K., S. M. Pulst, et al. (2006). "Proteasome inhibition triggers activity-dependent increase in the size of the recycling vesicle pool in cultured hippocampal neurons." *The Journal of neuroscience : the official journal of the Society for Neuroscience* **26**(44): 11333-11341.
- Xu, W. (2011). "PSD-95-like membrane associated guanylate kinases (PSD-MAGUKs) and synaptic plasticity." *Current opinion in neurobiology* **21**(2): 306-312.
- Yao, I., Y. Sugiura, et al. (2008). "In situ proteomics with imaging mass spectrometry and principal component analysis in the Scrapper-knockout mouse brain." *Proteomics* **8**(18): 3692-3701.
- Yao, I., H. Takagi, et al. (2007). "SCRAPPER-dependent ubiquitination of active zone protein RIM1 regulates synaptic vesicle release." *Cell* **130**(5): 943-957.
- Yi, J. J. and M. D. Ehlers (2005). "Ubiquitin and protein turnover in synapse function." *Neuron* **47**(5): 629-632.
- Zennou, V., F. Mammano, et al. (1998). "Loss of viral fitness associated with multiple Gag and Gag-Pol processing defects in human immunodeficiency virus type 1 variants selected for resistance to protease inhibitors in vivo." *Journal of virology* **72**(4): 3300-3306.
- Zennou, V., C. Petit, et al. (2000). "HIV-1 genome nuclear import is mediated by a central DNA flap." *Cell* **101**(2): 173-185.
- Zhai, R., G. Olias, et al. (2000). "Temporal appearance of the presynaptic cytomatrix protein bassoon during synaptogenesis." *Molecular and cellular neurosciences* **15**(5): 417-428.
- Zhai, R. G., H. Vardinon-Friedman, et al. (2001). "Assembling the presynaptic active zone: a characterization of an active one precursor vesicle." *Neuron* **29**(1): 131-143.
- Zhang, W. and D. L. Benson (2001). "Stages of synapse development defined by dependence on F-actin." *The Journal of neuroscience : the official journal of the Society for Neuroscience* **21**(14): 5169-5181.
- Zhao, S., D. Studer, et al. (2012). "Structural plasticity of hippocampal mossy fiber synapses as revealed by high-pressure freezing." *The Journal of comparative neurology*.
- Zhen, M., X. Huang, et al. (2000). "Regulation of presynaptic terminal organization by *C. elegans* RPM-1, a putative guanine nucleotide exchanger with a RING-H2 finger domain." *Neuron* **26**(2): 331-343.
- Zhen, M. and Y. Jin (2004). "Presynaptic terminal differentiation: transport and assembly." *Current opinion in neurobiology* **14**(3): 280-287.
- Ziff, E. B. (1997). "Enlightening the postsynaptic density." *Neuron* **19**(6): 1163-1174.
- Ziv, N. E. and C. C. Garner (2004). "Cellular and molecular mechanisms of presynaptic assembly." *Nature reviews. Neuroscience* **5**(5): 385-399.
- Zufferey, R., J. E. Donello, et al. (1999). "Woodchuck hepatitis virus posttranscriptional regulatory element enhances expression of transgenes delivered by retroviral vectors." *Journal of virology* **73**(4): 2886-2892.

7. Abbreviations

°C	<i>Degree Celsius</i>
aa	<i>Amino acid</i>
<i>Abp1</i>	<i>Actin binding protein 1</i>
AD	<i>“Anno Domini,” which is Latin for “in the year of our Lord.”</i>
<i>Amp</i>	<i>Ampicillin</i>
AMPA	<i>Alpha-amino-3-hydroxy-5-methyl-4-isoxazolepropionic acid</i>
ATP	<i>Adenosine triphosphate</i>
AZ	<i>Active Zone</i>
BC	<i>Before Christ</i>
BD	<i>Binding domain</i>
BDNF	<i>Brain-derived neurotrophic factor,</i>
<i>Bicine</i>	<i>N,N-bis-(2-hydroxyethyl)-glycine</i>
<i>Bp</i>	<i>Base pair</i>
BRP	<i>Bruchpilot</i>
<i>Bsn</i>	<i>Bassoon</i>
<i>C-terminal</i>	<i>Carboxy-terminal</i>
<i>C. elegans</i>	<i>Caenorhabditis elegans</i>
C2	<i>Calcium/phospholipid binding domains</i>
Ca ²⁺	<i>Calcium ion</i>
CaMKII	<i>Ca²⁺/calmodulin-dependent protein kinases II</i>
cAMP	<i>Cyclic adenosine monophosphate</i>
cAMP-GEFII	<i>cAMP-guanidine nucleotide exchange factor II</i>
CAST	<i>CAZ-associated structural protein</i>
CAZ	<i>Cytomatrix at the active zone</i>
CC	<i>Coiled coil</i>
cDNA	<i>Complementary DNA</i>
CDS	<i>Coding sequence</i>
Cl ⁻	<i>Chloride ion</i>
CoIP	<i>Coimmunoprecipitation</i>
COS-7	<i>African green monkey cell line</i>
CtBP	<i>C-terminal binding protein</i>
DAT	<i>Dopamine transporter</i>
DIV	<i>Days in vitro</i>
DMEM	<i>Dulbecco’s Modified Eagle Medium</i>
DMSO	<i>Dimethyl sulfoxide</i>
DNA	<i>Deoxyribonucleic acid</i>
DNase	<i>Deoxyribonuclease</i>
dNTPs	<i>Deoxyribonucleotide triphosphate</i>
DTT	<i>Dithiothreitol</i>
<i>E.coli</i>	<i>Escherichia coli</i>
E3	<i>Ubiquitin ligase</i>
ECL	<i>Enhanced chemiluminescence</i>
EDTA	<i>Ethylenediamine-N,N,N',N'-tetraacetic acid</i>
EGFP	<i>Enhanced green fluorescent protein</i>
EGTA	<i>Ethylene glycol-bis(2-aminoethylether)-N,N,N',N'-tetraacetic acid</i>
EM	<i>Electron microscopy</i>
ERC	<i>ELKS/Rab6-interacting protein 2/CAST</i>
EYFP	<i>Enhanced YFP</i>
<i>F-actin</i>	<i>Filamentous actin</i>
FBS	<i>Fetal Bovine Serum</i>
Fig.	<i>Figure</i>
g	<i>Gram</i>
<i>G-Actin</i>	<i>Globular-actin</i>
GABA	<i>γ-aminobutyric-acid</i>
GIT	<i>G protein-coupled receptor kinase interacting ArfGAP 1</i>
GK	<i>Guanylate kinase-like domain</i>
h	<i>Hour</i>
HBSS	<i>Hank’s Balanced salts</i>
HEK293	<i>Human Embryonic Kidney cells clone 293</i>
HEPES	<i>4-(2-hydroxyethyl)-1-piperazineethanesulfonic acid</i>

<i>Hz</i>	<i>Herz</i>
<i>IF</i>	<i>Immunofluorescence</i>
<i>IP</i>	<i>Immunoprecipitation</i>
<i>IPSC</i>	<i>Inhibitory postsynaptic currents</i>
<i>IWA</i>	<i>Unique COOH-terminal amino acid motif from CAST</i>
K^+	<i>Potassium ion</i>
<i>kb</i>	<i>Kilo base pair</i>
<i>kDa</i>	<i>Kilo Dalton</i>
<i>LAR</i>	<i>Transmembrane protein-tyrosine-phosphatases</i>
<i>LB</i>	<i>Luria- Broth</i>
<i>Liprin</i>	<i>LIP related protein</i>
<i>LV</i>	<i>Lentivirus vector FU(tag)W</i>
<i>M</i>	<i>Molar</i>
<i>MAGUK</i>	<i>Membrane-associated guanylate kinases</i>
<i>MALS</i>	<i>The vertebrate homologs of C. elegans lin-7;</i>
<i>MAP2</i>	<i>Microtubule associated protein 2</i>
<i>METH</i>	<i>Methamphetamine</i>
<i>mg</i>	<i>Milligram</i>
<i>min</i>	<i>Minutes</i>
<i>Mint1</i>	<i>The vertebrate form of C. elegans lin-10</i>
<i>ml</i>	<i>Millilitre</i>
<i>mM</i>	<i>Millimolar</i>
<i>mRFP</i>	<i>Monomeric red fluorescence protein</i>
<i>mRNA</i>	<i>Messenger ribonucleic acid</i>
<i>ms</i>	<i>Mouse</i>
<i>Munc13</i>	<i>Mammalian homologue of UNC13</i>
<i>mut</i>	<i>Mutant</i>
<i>N-terminal</i>	<i>Amino-terminal</i>
Na^+	<i>Sodium ion</i>
<i>NAc</i>	<i>Nucleus accumbens</i>
<i>nm</i>	<i>Nanometer</i>
<i>NMDA</i>	<i>N-methyl-D-aspartic acid</i>
<i>NMDAR</i>	<i>NMDA Receptor</i>
<i>NMJ</i>	<i>Neuromuscular junction</i>
<i>PAGE</i>	<i>Polyacrylamide gel electrophoresis</i>
<i>PBH domain</i>	<i>Piccolo-Bassoon homology domain</i>
<i>PBS</i>	<i>Phosphate buffered saline</i>
<i>Pclo</i>	<i>Piccolo</i>
<i>PCR</i>	<i>Polymerase chain reaction</i>
<i>PDZ</i>	<i>PSD-95/Dlg/ZO-1</i>
<i>PFA</i>	<i>Paraformaldehyde</i>
<i>PKA</i>	<i>Protein kinase A</i>
<i>PKC</i>	<i>Protein kinase C</i>
<i>Pr</i>	<i>Probability release</i>
<i>PRD</i>	<i>Proline-rich domain</i>
<i>preLTP</i>	<i>Presynaptic forms of long-term potentiation</i>
<i>PSD</i>	<i>Postsynaptic density</i>
<i>PTV</i>	<i>Piccolo-Bassoon transport vesicle</i>
<i>PVDF</i>	<i>Polyvinylidene fluoride</i>
<i>Rab 3 protein</i>	<i>Ras-related protein 3</i>
<i>Rb</i>	<i>Rabbit</i>
<i>Rim</i>	<i>Rab3 interacting molecule</i>
<i>RIMBP</i>	<i>Rim binding protein</i>
<i>RNA</i>	<i>Ribonucleic acid</i>
<i>RNAi</i>	<i>Ribonucleic Acid interference</i>
<i>RRP</i>	<i>Ready releasable pool</i>
<i>RT</i>	<i>Room temperature</i>
<i>s</i>	<i>Second</i>
<i>SDS-PAGE</i>	<i>Sodium dodecyl sulfate polyacrylamide gel electrophoresis</i>
<i>SH3 domain</i>	<i>Src-homology 3 domain</i>
<i>SNAP</i>	<i>(Soluble NSF (N-ethylmaleimide-sensitive factor) Attachment Protein)</i>
<i>SNAP-25</i>	<i>Synaptosome-associated protein 25 kDa</i>
<i>SNARE</i>	<i>Soluble N-ethyl-maleimide-sensitive fusion protein attachment protein receptors</i>

Abbreviations

<i>SV</i>	<i>Synaptic vesicle</i>
<i>Syn</i>	<i>Synapsin.</i>
<i>Syph</i>	<i>Synaptophysin</i>
<i>TAE</i>	<i>Tris-Acetate-EDTA</i>
<i>Taq</i>	<i>Thermus aquaticus</i>
<i>TBE</i>	<i>Tris-Borate-EDTA</i>
<i>Tris/HCl</i>	<i>Tris(hydroxymethyl)-aminomethanhydrochloride</i>
<i>TX-100</i>	<i>Triton X-100</i>
<i>U</i>	<i>Unit</i>
<i>UNC13</i>	<i>Uncoordinated movement 13</i>
<i>UV</i>	<i>Ultraviolet</i>
<i>VAMP 2</i>	<i>Vesicle Associated Membrane Protein 2</i>
<i>Veli</i>	<i>The vertebrate homologs of C. elegans lin-7;</i>
<i>VGCC</i>	<i>N- and P/Q-type voltage gated Ca(2+) channels</i>
<i>WB</i>	<i>Western blot</i>
<i>YFP</i>	<i>Yellow Fluorescent Protein</i>
<i>ZF</i>	<i>Zinc finger</i>
Δ	<i>Deletion</i>
λ	<i>Wavelength</i>
μg	<i>Microgram</i>
μl	<i>Microlitre</i>
μm	<i>Micrometer</i>

8. Curriculum Vitae

Name: Sergio
 Family Name: Leal-Ortiz
 Date of Birth: October 11, 1973
 Place of Birth: Rio Bueno (Chile)
 Nationality: Chilean
 Parents: Sergio Leal
 Isabel Ortiz

EDUCATION

2009-2012 Doctoral Thesis, Leibniz Institute for Neurobiology, Otto-von-Guericke Universität Magdeburg, Otto-von-Guericke Universität Magdeburg, Magdeburg, Germany
 Sept 2009-
 Oct 2009 Neurobiology Training, Leibniz Institute for Neurobiology, Otto-von-Guericke Universität Magdeburg, Otto-von-Guericke Universität Magdeburg, Magdeburg, Germany
 2001 Bachelor of Science in Biochemistry, Austral University of Chile.

RESEARCH EXPERIENCE

2009-Present *Senior Research Associate and General Laboratory Manager*, Department of Psychiatry and Behavioral Sciences, Stanford University, Stanford, CA.
 Research: Molecular and synaptic mechanisms of synaptic vesicle membrane recycling during synapse degeneration.
 Supervisor: Dr. Craig Garner
 2002-2009 *Research Associate and Laboratory Manager*, Department of Psychiatry and Behavioral Sciences, Stanford University, Stanford, CA.
 Research: Defining the molecular and synaptic mechanisms underlying cognitive impairment in neurodevelopmental disorders.
 Supervisor: Dr. Craig Garner
 2001-2002 *Research Assistant*, Department of Neurobiology, University of Alabama at Birmingham.
 Research: Cellular mechanism of nascent synapse formation in autism.
 Supervisor: Dr. Craig Garner
 2000-2001 *Research Assistant*, Department of Biology, Universidad Nacional Andrés Bello, Santiago, Chile
 Research: Regulation of the expression of rRNAs during the acclimatization of the fish *Cyprinus carpio*
 Supervisor: Dr. Maria Ines Vera
 1999-2000 *Academic Teaching Assistant*, Department of Biology, Universidad Nacional Andrés Bello, Santiago, Chile.
 Taught laboratory practical courses in Neurophysiology, Neuroanatomy, Neurobiology, Cellular Biology and Biology.
 1998-2000 Undergraduate thesis, Department of Biochemistry, Austral University of Chile, Valdivia, Chile.
 Thesis: Quantification of the seasonal transcription of the subunit β drive protein quinasa CK2 in the fish *Cyprinus carpio*
 Advisor: Dr. Maria Ines Vera

- 1998 Internship, Department of Chemistry, Universidad de Chile, Santiago, Chile and Department of Chemistry, Universidad Nacional Andrés Bello, Santiago, Chile.
Research focus: Natural product extraction from *Usnea barbata* lichen from the XI region of Chile.
Mentor: Dr. Ramiro Arratia

PUBLICATIONS:

- Waites CL, **Leal-Ortiz SA**, Okerlund N, Dalke H, Fejtova A, Altmann WD, Gundelfinger ED, Garner CC (2013) Bassoon and Piccolo maintain synapse integrity by regulating protein ubiquitination and degradation. *EMBO J* doi: 10.1038/emboj.2013.27
- Maas C, Torres VI, Altmann WD, **Leal-Ortiz S**, Wagh D, Terry-Lorenzo RT, Fejtova A, Gundelfinger ED, Ziv NE, and Garner CC (2012) Formation of golgi-derived active zone precursor vesicles. *J Neurosci* 32:11095-11108.
- Waites CL, **Leal-Ortiz SA**, Andlauer TF, Sigrist SJ, Garner CC (2011) Piccolo regulates the dynamic assembly of presynaptic F-actin. *J Neurosci* 31:14250-14263.
- Hua Z, **Leal-Ortiz S**, Foss SM, Waites CL, Garner CC, Voglmaier SM, Edwards RH (2011) v-SNARE composition distinguishes synaptic vesicle pools. *Neuron* 71:474-487.
- Li D, Specht CG, Waites CL, Butler-Munro C, **Leal-Ortiz S**, Foote JW, Genoux D, Garner CC, Montgomery JM (2011) SAP97 directs NMDA receptor spine targeting and synaptic plasticity. *J Physiol* 589:4491-4510.
- Torres V, Barra L, Garces F, Ordenes K, **Leal-Ortiz S**, Garner CC, Fernandez F, Zamorano P (2010) A bicistronic lentiviral vector based on the 1D/2A sequence of foot-and-mouth disease virus expresses proteins stoichiometrically. *J Biotechnol* 146:138-142.
- Lucido AL, Suarez Sanchez F, Thostrup P, Kwiatkowski AV, **Leal-Ortiz S**, Gopalakrishnan G, Liazoghli D, Belkaid W, Lennox RB, Grutter P, Garner CC, Colman DR (2009) Rapid assembly of functional presynaptic boutons triggered by adhesive contacts. *J Neurosci* 29:12449-12466.
- Waites CL, Specht CG, Hartel K, **Leal-Ortiz S**, Genoux D, Li D, Drisdell RC, Jeyifous O, Cheyne JE, Green WN, Montgomery JM, Garner CC (2009) Synaptic SAP97 isoforms regulate AMPA receptor dynamics and access to presynaptic glutamate. *J Neurosci* 29:4332-4345.
- Leal-Ortiz S**, Waites CL, Terry-Lorenzo R, Zamorano P, Gundelfinger ED, Garner CC (2008) Piccolo modulation of Synapsin1a dynamics regulates synaptic vesicle exocytosis. *J Cell Biol* 181:831-846.
- Sabio G, Reuver S, Feijoo C, Hasegawa M, Thomas GM, Centeno F, Kuhlendahl S, **Leal-Ortiz S**, Goedert M, Garner C, Cuenda A (2004) Stress- and mitogen-induced phosphorylation of the synapse-associated protein SAP90/PSD-95 by activation of SAPK3/p38gamma and ERK1/ERK2. *Biochem J* 380:19-30.
- Sarmiento J, **Leal S**, Quezada C, Kausel G, Figueroa J, Ines Vera M, Krauskopf M (2000) Environmental acclimatization of the carp modulates the transcription of beta-actin. *J Cell Biochem* 80:223-228.
- Vera MI, Kausel G, Barrera R, **Leal S**, Figueroa J, Quezada C (2000) Seasonal adaptation modulates the expression of the protein kinase CK2 beta subunit gene in the carp. *Biochem Biophys Res Commun* 271:735-740.